Transport in Open Quantum Systems

Dos Santos Ferreira, Joao

How to cite

DOS SANTOS FERREIRA, Joao. Transport in Open Quantum Systems. Doctoral Thesis, 2023. doi: 10.13097/archive-ouverte/unige:174625

This publication URL: https://archive-ouverte.unige.ch/unige:174625
Publication DOI: 10.13097/archive-ouverte/unige:174625

UNIVERSITÉ DE GENÈVE
Section de Physique
Département de la matière condensée

FACULTÉ DES SCIENCES
Dr. Michele Filippone
Professeur Thierry Giamarchi

Transport in open quantum systems

THÈSE

présenté à la Faculté des Sciences de l'Université de Genève
pour obtenir le grade de docteur ès Sciences, mention Physique

par

João S. Ferreira
de
Vila do Conde (Portugal)

Thèse n° Thesis-number

GENÈVE
Atelier d'impression ReproMail
2013

Dedicado ao meu avõ João,
Doutor Honoris Causa da Universidade da Vida.

Acknowledgements

'Cause it's a long road to wisdom but it's a short one to being ignored

- Flowers in your head, The Lumineers

A few years back, I have come across the excellent speech of Arnold Schwarzenegger about him not being the *self-made* man people think he is. As I write this section, I clearly see that I, too, am not the self-made man I always thought I was. Every person who crossed my path in the past years has played a role in shaping my Ph.D. journey. My gratitude to them is boundless.

My deepest acknowledgment goes to my family, in particular, my parents. They have always stayed by my side and, in their concerned but loving way, have supported me in every decision I ever took. Thank you, family.

I want to thank my Sunshine for illuminating my life from the shadows I fell during my journey. Your support in every project I undertake is inspiring and a true testament to the amazing person you are. Thank you for sharing a life with me, Gi.

I don't think I could have completed this Ph.D. without the support of my friends: the ones I left at the point of origin (Carolina, Luís, Nuno, Ricardo, ...), the ones that boarded the plane with me (António, Ricardo, Tomás, André, ...) and those I found at my destination (Michael, Julia, the Grape Gang, Lorentzo, Nirvana, Julian, ...). Making friends in Switzerland is difficult, but I was lucky to find a home in the 14 Gang (Lucia, Andreas, Ludovica, Florian, Ralph, and Saška) and worked very hard to build a strong Ph.D. community so that no new Ph.D. has to feel alone anymore. Thank you all.

I want to thank my advisors and collaborators for helping me grow as a person and scientist. Thank you, Michele, for having the patience and willingness to always explain the situation, what I did right or wrong, and how to improve. I know how hard it is to argue with me, but you never gave up and always looked out for my interests above all. Thierry, you showed me that a good scientist can and should strive to be a kind human being first and foremost. Thank you for creating such a welcoming and positive research environment. I must also thank my adoptive

advisor Tony, who far too many times, has taken the role of teacher, life coach, friend, and confidant. I am proud to have shared with you the best scientific moment of my short research career. During the years, I had countless discussions with all the Lunch Time group members, whom I thank as well. A special thank you is due to Christophe and Louk who always had the door open for every random question that popped into my mind. Finally, I wish to thank the members of the jury for taking the time to read and evaluate my work.

An appreciation is due to my sponsor, the Swiss National Science Foundation for financing my studies (FNS/SNF Ambizione Grant No. PZ00P2 174038) and the Cogito Foundation for supporting my science communication endeavors (Grant No. 22-110-P).

My path at UNIGE is over, but with such a long list of acknowledgments, I can only be excited about what the future holds.

Résumé en français

Dans cette thèse, j'ai étudié les propriétés de transport des systèmes hors équilibre. Nous avons réalisé cet objectif en employant une combinaison de techniques analytiques et numériques pour examiner les systèmes fermioniques influencés par des interactions unitaires ou dissipation. Cette dernière peut être décrite exactement grâce à une solution exacte de toutes les fonctions de corrélation à deux points, que nous explorons pour trouver des expressions exactes non-perturbatives des courants de particules et de chaleur. Ces expressions nous permettent de décrire de nouvelles méthodes pour extraire du travail et de la chaleur des dispositifs quantiques bruités, de formuler une nouvelle théorie effective pour les systèmes diffusifs, et de proposer une interprétation semi-classique de ces systèmes. Dans le domaine des interactions unitaires, nous découvrons de nouveaux régimes de transport qui précèdent l'apparition de la diffusion dans les modèles où l'intégrabilité est rompue.

Abstract

In this thesis, I study the transport properties of driven out-of-equilibrium systems. This goal is achieved by employing a combination of analytic and numerical techniques to investigate low-dimensional fermionic chains affected by unitary interactions or dissipation. The latter allows for an exact solution of any two-point correlation functions, which we explore to find exact non-perturbative expressions for the driven particle and heat currents. These expressions enable us to describe novel ways to extract work and heat from noisy quantum devices, formulate a new effective theory for diffusive systems and propose a semi-classical interpretation of these systems. Within the realm of unitary interactions, we discover new transport regimes that precede the onset of diffusion in integrability-broken models.

Contents

CHAPTER 1

Introduction

Out-of-equilibrium systems are ubiquitous across a wide range of scales and scientific disciplines. They encompass a diversity of phenomena ranging from the subatomic scale [1], to human behavior [2], all the way up to the very fate of the universe itself [3,4]. Condensed matter is no exception. Yet, for a long time, the field of solid-state physics was dominated by equilibrium and quasi-equilibrium descriptions. The reason why thermal ensembles suffice to describe structural and electronic properties of most materials in nature [5,6] is simple. The typical time resolution of traditional electronic probes such as STM, ARPES, XPS, or n-terminal probes [7] is much larger than the typical thermalization time of electrons, i.e. for most experimental purposes electrons *are* in thermal equilibrium.

However, recent developments in femtosecond lasers allow now for direct observation of electronic relaxation processes [8, 9], opening up new venues for ultrafast pump-and-probe experiments [10]. In parallel, new quantum simulation platforms such as trapped ions [11] or ultra-cold atoms [12–14] open the possibility of simulating almost isolated systems whose relaxation dynamics are orders of magnitude slower than solid-state setups [15]. We can now probe long-lived pre-thermal states [16], new relaxation dynamics [17], or even the absence of thermalization [18]. These new tools have reinvigorated interest in out-of-equilibrium dynamics, particularly in the field of quantum many-body physics.

While the precise dynamics of quantum many-body systems are often intractable, local observables in chaotic quantum systems follow a universal behaviour [19, 20]. From a typical initial state, they quickly reach an expectation value consistent with a local equilibrium ensemble characterized by spatial-varying thermodynamic vari-

ables. Over extended periods, hydrodynamic processes, such as diffusion, relax the system to a global equilibrium state with vanishing spatial fluctuations. Diffusion is characterized by the spread of globally conserved quantities like energy, charge, spin, or mass, as dictated by Fick's law [21, 22]

$$J_q = -D_q \nabla q \ , \tag{1.1}$$

where the diffusion constant D_q relates the charge current density J_q to a superimposed charge gradient ∇q.

In this thesis, we utilize out-of-equilibrium techniques to tackle a longstanding issue in quantum many-body physics: **understanding how diffusion emerges in quantum systems**. The intuition is that interactions among components or external degrees of freedom induce elastic and inelastic scattering processes responsible for the aforementioned relaxation and emergence of diffusion. In principle, the exchange of momentum and energy is responsible for Eq. (1.1), but a rigorous derivation in quantum systems is still lacking.

One significant challenge is the apparent incongruity between a classical equation (1.1), often derived in the context of irreversible processes [23], and the reversible dynamics obtained from a unitary theory such as quantum mechanics. Multiple reasons contribute to this conundrum. First, not all interactions necessarily lead to the emergence of diffusive behavior, a notion formalized in the field of quantum integrability [24]. Second, most available analytic tools can only study transport in limiting cases, e.g. weak/strong couplings [25, 26], close to equilibrium [27], or weak quantum fluctuations [28], making it complicated to acquire a complete view of how emergent phenomena like diffusion can come to be.

To overcome this challenge, it is beneficial to find diffusive models that support a fully analytic treatment. Coupling the system to incoherent baths offers a promising avenue, for which some transport results are already available. The quantum symmetric simple exclusion process model [29] or the dephasing model [30, 31] are such cases, with the latter solved by Bethe ansatz upon mapping to the imaginary Hubbard model [32]. However, these solutions are on a case-by-case basis and often complex, making it difficult to acquire a broader picture.

In this work, we explore a manifestation of dissipative transport generated by Quantum Stochastic Hamiltonians (QSHs) of the form

$$H_{\text{st}} = \sqrt{\gamma} \sum_{\{Q\}} \left(Q \xi_t^q + Q^\dagger \xi_t^{q*} \right) \ , \tag{1.2}$$

where $\{Q = \sum_{ij} c_i^\dagger q_{ij} c_j\}$ is a set of quadratic operators composed of a single-particle creation and an annihilation operator, $\{\xi_t^q\}$ a set of complex Gaussian white noises with strength γ, zero average $\mathbb{E}[\xi_t] = 0$, and variance $\mathbb{E}\left[\xi_t^q \xi_{t'}^{q'*}\right] = \delta_{q,q'}\delta(t-t')$. The time-averaged dynamics of Eq. (1.2) mimics the presence of an

external environment interacting with a free system, as shown in Sec. 2.4. Akin to the difficulties introduced by spatial disorder in Anderson localization, the randomness (disorder) in time also makes QSHs challenging models. For each noise configuration, the time evolution is quadratic and Gaussian but the averaged evolution has non-Gaussian correlations [33, 34]. However, unlike unitary interactions in many-body systems, the QSHs encode an exact, non-perturbative solution for all two-point correlation functions, even in out-of-equilibrium scenarios. The existence of such a solution is demonstrated in full generality in this thesis, and used to analytically obtain closed expressions for the currents, without the limitations of previous methods. It provides a clear interpretation of elastic and inelastic scattering processes present in QSHs and motivates us to devise new theoretical frameworks for diffusion, which may extend to interacting Hamiltonians. The thesis is organized as follows.

1.1 Structure of the thesis

This work is divided into 4 chapters, with Chapter 1 devoted to the Introduction. In Chapter 2, we introduce the technical framework and all the concepts necessary to understand the work developed in this thesis. We begin with Sections 2.1 and 2.2, introducing the Lindblad equation and driven open systems. Section 2.3 is dedicated to the introduction of Keldysh formalism in the context of open systems. Subsequently, we discuss QSHs and derive the expression of the associated self-energy in Sec. 2.4. Sec. 2.5 discusses the inclusion of reservoirs in our driving protocol and Sec. 2.6 derives the generic expression for the current when coupling to thermal reservoirs. The chapter concludes with an introduction to tensor network concepts and time-evolved block decimation in Sec. 2.7.

Chapter 3 encompasses the contributions I made during my Ph.D. to answer the overarching question of this thesis: how do scattering processes trigger the emergence of diffusion in quantum systems? A full answer remains out of reach, but each section presents an incremental step toward that direction. The sections are intentionally arranged out of chronological sequence. Instead, they are reorganized from the simplest to the most intricate setup, mirroring the progression a novice reader would follow when learning about the topic. We start from local QSHs (Sec. 3.1), progressing to extensive QSHs (Sec. 3.2 and 3.3) and, finally, studying extensive unitary interactions (Sec. 3.4). Each section focuses on a different work published during my Ph.D. with an introduction to frame it within the thesis and standardize notations.

Section 3.1 is based on Ref. [P1] and discusses driven quantum systems in the presence of a local QSH. We identify non-reciprocal effects in the particle and heat current and exploit them to create quantum machines operating as engines or refrigerators.

Section 3.2 is based on Ref. [P2] and discusses the emergence of diffusive transport

in extensive QSHs. We formulate a new effective theory of diffusive transport, the $1/N$ *expansion*, that successfully predicts the emergence of Fick's law and some bulk properties, such as the diffusion constant.

Section 3.3 is based on Ref. [P3] and presents a simple, semi-classical interpretation of the scattering processes present in QSHs. This picture is capable of qualitatively predicting the behavior of some transport quantities not captured by the $1/N$ expansion, such as the conductance.

Section 3.4 is based on Ref. [P4] and discusses transport in models with nearest and next-to-nearest neighbor interactions. We find evidence of a parametrically large *quasi-ballistic* regime that presets the onset of diffusion.

Chapter 4 is dedicated to the discussion of the work presented, focusing on potential future research directions and unexplored territories. The Appendices provide additional technical details to Chapter 2 and 3.

CHAPTER 2

Methods and Techniques

Intuition suggests that interactions play a pivotal role in the emergence of diffusion in quantum many-body systems, primarily because they often lead to inelastic scattering processes. As highlighted in the introductory section, the interactions between the system and external degrees of freedom can be of special interest. Unlike unitary interactions among the components of the system, we are going to show that they support an analytical treatment of transport phenomena. This consideration goes beyond mere practicality; in experiments the presence of an environment is ubiquitous.

2.1 Lindblad master equation

However, in most situations, we are not interested in the state of the environment and only wish to study the effective dynamics of the system without having to keep track of its environment. In other words, we wish to focus on the reduced density matrix of the system ρ. It can be obtained from the total density matrix of the environment plus system, ρ_{all}, by tracing out the degrees of freedom associated with the environment E:

$$\rho(t) = \text{tr}_E \left[\rho_{\text{all}}(t)\right] \ . \tag{2.1}$$

The time-evolution of the reduced matrix should be generated by a linear superoperator, $\mathcal{L}$, that maps a reduced density matrix to another reduced density matrix. We employ the prefix *super-* to denote a linear operator that acts in the vector space of operators similarly to how typical operators act on the Hilbert space of quantum

states. $\mathcal{L}$ should be a linear operator but does not need to be unitary since the system exchanges information with the environment. If the information transferred to the environment returns and influences the state of the system at a later time, the time-evolution becomes non-local in time, i.e. there exists *memory effects*. Handling memory effects is extremely challenging and most methods that exist to treat non-local time evolutions often sacrifice some key property of density matrices [35], such as positive-semidefiniteness, $\rho \geq 0$, unitarity of the trace, $\mathrm{tr}[\rho(t)] = 1$, or hermiticity, $\rho = \rho^\dagger$. However, in the limit where the characteristic decay time of bath correlations is much shorter than the typical relaxation time of the system, the time evolution becomes approximately local, and memory effects vanish. This is called the Markovian limit and the most general Markovian evolution is given by the Gorini-Kossakowski-Sudarshan-Lindblad quantum master equation, also called the Lindblad equation [36, 37] ($\hbar = e = c = k_B = 1$)

$$\partial_t \rho = \mathcal{L}(\rho) = -i[H, \rho] + \sum_\alpha \gamma_\alpha \left(L_\alpha \rho L_\alpha^\dagger - \frac{1}{2} \left\{ L_\alpha^\dagger L_\alpha, \rho \right\} \right) . \tag{2.2}$$

The Liouvillian or Lindbladian super-operator $\mathcal{L}$ is composed of two terms, the unitary evolution determined by the Hamiltonian operator H and the term responsible for the non-unitary dynamics composed of jump operators L_α acting with a positive rate γ_α. The time evolution of Eq. (2.2) is local in time and the density matrix always remains hermitian, semi-positive definitive, and of trace one at all times.

The Lindblad equation is widely employed to describe the dynamics of open quantum systems. It arises naturally in various contexts, most notably in scenarios involving weak coupling with external reservoirs where the absence of memory effects is ensured by the Born, Markov, and secular approximation [38]. This is the case for optical systems, where a clear separation of time scales between the bath and the system is present and memory effects can be safely discarded. Relevant to this thesis, the Lindblad equation can also characterize the average evolution of stochastic processes in the Hilbert space of the system, in which case we say that the process represents a possible unraveling of Eq. (2.2). In Sec. 2.4.1, we prove how the average evolution of the QSHs in Eq. (1.2) evolves according to the Lindblad equation (2.2).

Formal solution of the Lindblad equation

The formal solution of Eq. (2.2) is given by

$$\rho(t) = \mathbb{T} e^{\int_0^t ds \mathcal{L}} \rho(0) , \tag{2.3}$$

where $\mathbb{T}$ is the time-order operator. For the case of time-independent Lindbladians, the solution (2.3) reduces to $\rho(t) = e^{\mathcal{L}t}\rho(0)$. In the presence of generic relaxation processes, the density matrix is expected to converge to a non-equilibrium steady-state (NESS) in the infinite time limit, $\lim_{t\to\infty} \rho(t) = \rho_{\mathrm{NESS}}$. In this work, we only

work with systems with a unique NESS for any initial condition, $\rho(0)$. In general, the NESS does not have to be unique, in which case the final state is determined by the initial density matrix.

To compute expectation values of a given operator X, $\langle X(t)\rangle = \mathrm{tr}(X\rho(t))$, it is useful to introduce the adjoint Lindblad super-operator $\mathcal{L}^\dagger$ defined from $\mathcal{L}$ as

$$\mathrm{tr}\left[X\mathcal{L}(Y)\right] = \mathrm{tr}\left[\mathcal{L}^\dagger(Y)X\right] \ ,$$

where X, Y are arbitrary operators. It follows from the cyclic properties of the trace that for time-independent Liouvillians:

$$\mathcal{L}^\dagger(X) = i[H,X] + \sum_\alpha \gamma_\alpha \left(L_\alpha^\dagger X L_\alpha - \frac{1}{2}\left\{L_\alpha^\dagger L_\alpha, X\right\}\right) \ . \tag{2.4}$$

In line with the unitary case, the adjoint Lindbladian serves as the generator of the time evolution of the operator X within the Heisenberg picture:

$$\partial_t X(t) = \mathcal{L}^\dagger(X(t)) \ . \tag{2.5}$$

To evaluate the product of two operators in Heisenberg's picture, as in Sec. 2.3, it is essential to carefully evolve the density matrix to the time at which the operator acts

$$\mathrm{tr}\left[X(t)\rho Y(t')\right] = \begin{cases} \mathrm{tr}\left[X e^{(t-t')\mathcal{L}}\left(\rho(t')Y\right)\right] & t > t' \\ \mathrm{tr}\left[e^{(t'-t)\mathcal{L}}\left(X\rho(t)\right)Y\right] & t' > t \end{cases} \ . \tag{2.6}$$

2.2 Boundary-driven systems

In this work, we leverage out-of-equilibrium techniques to better understand the transport properties of diffusive systems described by Eq. (2.2). Various methods can be employed to probe the nature of charge or heat transport in quasi-one-dimensional setups, among which boundary-driving [26]. The idea behind boundary-driving is to drive the system away from equilibrium by coupling it to biased reservoirs at each end [39, 40], as schematically depicted in Fig. 2.1.

The nature of the bias depends on the properties being studied, and in this work, we primarily focus on biases in chemical potential, temperature, or spin (denoted as a generic charge q). When a bias is present, the system experiences a directional flow of charges as it attempts to compensate for the imbalance between left and right, $q_L - q_R$. By fixing the thermodynamic state of the reservoirs, and assuming them to be infinite, the system will inevitably relax to a NESS where the charge flow has been stabilized. Steady-states generated by such boundary-driven protocols are particularly useful for studying the transport properties of the system, as they can be

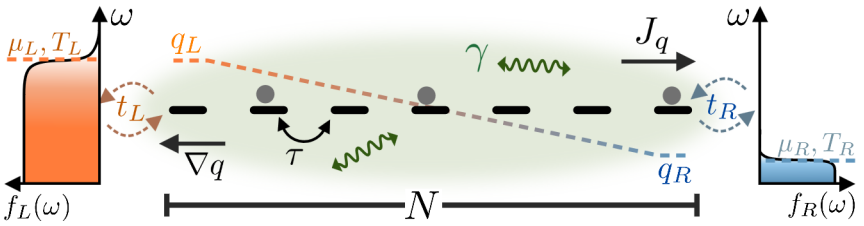

Figure 2.1: Illustrative scheme of a 1-dimensional fermionic chain undergoing a quantum stochastic evolution controlled by the rate γ and coupled to two non-interacting reservoirs at each end through the coupling matrices t_L and t_R. The reservoirs are taken in equilibrium with a fixed chemical potential μ and temperature T and impose a charge imbalance from left (q_L) to right (q_R). For diffusive systems, the bias generates an uniform charge gradient ∇q, depicted as a dashed line, and a diffusive charge current to the right, J_q. The distance between reservoirs is always N.

tuned to target specific transport phenomena. We focus on the transport of locally conserved charges that satisfy the continuity equation

$$\partial_t q = -\nabla J_q + s_q \ , \tag{2.7}$$

where, J_q is the local current operator associated with the charge q, and s_q is a source term, possibly describing the influence of reservoirs but not limited to it.

The expectation value of the current operator evaluated in the NESS, J_q, provides key insights into the transport properties of the system. Consider Drude's semi-classical interpretation of transport [41, 42] of a local charge propagating ballistically with a well-defined velocity v_q until, after a mean scattering length N^*, it scatters and changes velocity. When the scattering length is much larger than the distance between reservoirs, $N \ll N^*$, charges exiting a reservoir will always propagate coherently into the opposite reservoir (regardless of the distance) and so the current must be independent of the distance, $J_q \propto (q_L - q_R) v_q N^0$. However, when the scattering length becomes comparable to or smaller than the system length, charges will scatter multiple times leading to a finite resistivity of the material. In such cases, the system exhibits diffusive behavior with a uniform charge gradient $\nabla q \propto (q_L - q_R)/N$, see Fig. 7 of Ref. [P4] for an example of diffusive gradients in magnetization transport. The current satisfies Fick's law (1.1), $J_q \propto D_q/N$, with the diffusion constant proportional to the mean free path $D_q \sim N^*$. Is it now known that quantum systems display different universal classes of dynamical behavior at long length and time scales [43], each characterized by a distinct scaling exponent of N. The dependence of the current with the system size is thus an excellent indicator of different transport regimes and one that we can explore easily in boundary-driven setups [26, 44]. In fact, there is a whole zoo of transport regimes characterized by different scalings of the current with the system size, e.g. localized $J_q \propto e^{-N}$ [45]

and sub-diffusive or super-diffusive $J_q \propto 1/N^{\upsilon}$ ($\upsilon > 1$ or $\upsilon < 1$) [24].

Boundary-driven protocols are not the only possible way to extract the relevant transport coefficients, particularly in the weak driving/bias limit. Within the context of linear response theory, the Kubo formula [27] is widely used to compute the conductivity σ_q which relates the current J_q to the gradient in potential energy U_q as $J_q = -\sigma_q \nabla U_q$. In frequency space, the conductivity is given by

$$\sigma_q(\omega) = \lim_{t' \to \infty} \lim_{N \to \infty} \int_0^{t'} dt \int_0^{\beta} d\lambda \frac{e^{i\omega t}}{N} \left\langle J_q J_q(t + i\lambda) \right\rangle_{\beta} , \tag{2.8}$$

where the current-current correlation function is evaluated on a thermal ensemble with an inverse temperature β in the infinite size limit. Because Eq. (2.8) is evaluated in equilibrium, it circumvents the need to attach external reservoirs which modify the current in a non-universal way. However, calculating current-current correlations at different times or frequencies requires substantial numerical and analytical efforts. Numerical evaluation of Eq. (2.8) requires simulating large systems for long-times [46], while analytic calculations with field theory can diverge and may need to be renormalized [47]. Moreover, the Kubo formula is limited to linear response, making it unsuitable for studying systems far from equilibrium, as discussed in this thesis.

For diffusive systems close to equilibrium, the current driven by an imposed bias at the boundary $J_{\text{diffusion}} = -D_q \nabla q$ is exactly compensated by an opposite drift current $J_{\text{drift}} = -\sigma_q(0) \nabla U_q$ such that the diffusion constant is directly related to the DC conductivity via the Einstein relation $\sigma_q(0) = -D_q \partial_q U_q$. In other words, inducing a bias at the boundaries (boundary driving protocol) mimics the presence of a potential gradient (Kubo formula) up to finite system sizes corrections [48, 49]. These two techniques are the most common but not the only possibility to study transport, with notable mentions including memory function formalism [50, 51], semi-classical Boltzmann equations [52], local quench protocols [53] or the more recent influence matrix [54].

2.2.1 Limitations of Lindblad driving

There are different ways to simulate the biased reservoirs used in boundary-driving, a possibility is to employ jump operators. In Sec. 3.4, we use a combination of injection and loss jump operators to impose a spin imbalance at the boundaries of a one-dimensional spin-chain. However, as we now motivate, this procedure has some limitations.

Consider as an example the set of jump operators, $L_+ = \sqrt{\gamma_+} c^\dagger$ and $L_- = \sqrt{\gamma_-} c$, acting on a single site with the Hamiltonian $H = \epsilon c^\dagger c$, where $c^\dagger, c$ are the creation and anihilation fermionic operators with anti-commutation relations $\{c^\dagger, c\} = 1$, see Fig. 2.2. The steady-state occupation of the site, $n = c^\dagger c$ can be determined from the adjoint equation (2.4)

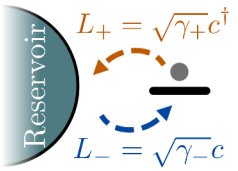

Figure 2.2: Schematic representation of a single dot coupled to an external reservoir described by an injection and loss jump operators with rate γ_+ and γ_-, respectively. The steady-state occupation of the dot is determined by the ratio γ_-/γ_+ which can be tuned to impose a local thermal state.

$$\partial_t n = 0 = i[H, n] + \gamma_+ \left(cnc^\dagger - \frac{1}{2}\left\{cc^\dagger, n\right\} \right) + \gamma_- \left(c^\dagger nc - \frac{1}{2}\left\{c^\dagger c, n\right\} \right) , \tag{2.9}$$

whose solution is simply $n = \frac{\gamma_+}{\gamma_+ + \gamma_-}$. By choosing the injection and loss rates accordingly, $\gamma_-/\gamma_+ = e^{\frac{\epsilon-\mu}{T}}$, the reached steady-state satisfies the Fermi distribution with a given chemical potential μ and temperature T. Reaching a thermal state with Lindblad injectors on a single-site system is somewhat trivial since there is only one degree of freedom. However, simulating the presence of thermal continuum reservoirs in extensive interacting systems using Lindblad injectors is a complicated task. Obtaining the Lindblad injectors whose steady-state is the Gibbs ensemble of the full system requires diagonalizing the full Hamiltonian which is as hard as the problem itself. There have been proposals to use local injectors at the edges that are optimized to target a local Gibbs state [44, 55]. Unfortunately, because they do not target the exact Gibbs state of the full system, they always inject some residual heat into the system. This is not a problem if we are interested in high-temperature transport, such as in Sec. 3.4, but to study dynamics at lower temperatures we need something else.

An ideal formalism should be capable of fully including the presence of generic thermal reservoirs as well as any bulk inelastic processes that may be described by Lindblad jump operators. Fortunately, Keldysh's field theory is well-suited to handle out-of-equilibrium dynamics generated by Lindblad jump operators while simultaneously incorporating the presence of non-interacting reservoirs.

2.3 Keldysh field theory

In equilibrium systems, quantum field theory (QFT) offers one of the most powerful tools to compute correlations in the ground state of interacting Hamiltonians. The

fundamental assumption is that the ground state $|GS\rangle$ of an interacting theory can be obtained from the ground state of its free theory $|0\rangle$ by adiabatically switching on interactions. Furthermore, after measuring any quantity of interest, one assumes that adiabatically turning off the interactions will recover the ground state of the free theory [52].

However, the fundamental assumptions of equilibrium QFT may not hold in non-equilibrium scenarios where some form of driving is present. Generally, it is not guaranteed that adiabatically turning off any driving will return the system to its initial state. As a result, a non-equilibrium formulation of the theory becomes necessary. The history of non-equilibrium field theory features parallel contributions from Schwinger, Konstantinov, Perel and Kadanoff [56–58], but Keldysh was the one who devised the modern formulation [59], thus we often refer to out-of-equilibrium field theory as Keldysh formalism.

In the subsequent discussion, we will not adhere to the conventional introduction of the Keldysh formalism [60], as it is formulated in terms of the unitary evolution operator, rendering it unpractical for describing dynamics governed by a Lindblad equation (2.2). Instead, we formulate the Keldysh action directly in the context of quantum master equations [61,62]. As we only deal with fermionic systems in Ch. 3, we only introduce the field theory for fermionic systems but extensions to bosonic setups can be found in Ref. [61].

2.3.1 Derivation of Keldysh path integral

Keldysh field theory re-writes the out-of-equilibrium partition function of the system, $\mathcal{Z} = \mathrm{tr}[\rho(t)]$, as a path integral over the possible evolutions weighted by the Keldysh action S

$$\mathcal{Z} = \mathrm{tr}[\rho(t)] = \int \mathcal{D}[\bar{\psi}, \psi] e^{iS} \, . \tag{2.10}$$

Since we are working with fermionic systems, the fields $\{\psi, \bar{\psi}\}$ satisfy the Grassmann algebra, which we review in App. A. In the following derivation, we first note that the trace of the density matrix must be preserved by the time evolution and so Eq. (2.10) is nothing but a very complicated formulation of identity, i.e. $\mathcal{Z} = 1$ at all times. However, similarly to equilibrium field theory, the path integral formulation allows easy computation of expectation values through functional derivatives of the partition function with respect to source fields, F,

$$\langle X \rangle = \mathrm{tr}[X\rho] = \lim_{F \to 0} \frac{\delta}{\delta F} \int \mathcal{D}[\bar{\psi}, \psi] e^{iS + X[\bar{\psi}, \psi]F} \, . \tag{2.11}$$

To derive the Keldysh action, we first recall that the time evolution of ρ is generated by the Liouvillian super-operator $\rho(t) = e^{(t-t_0)\mathcal{L}}\rho(t_0)$ (2.3). By discretizing the time evolution into M small intervals of size $\Delta t = (t - t_0)/M$, we can apply the Trotter decomposition [63, 64] to obtain

$$\rho(t) = e^{(t-t_0)\mathcal{L}}\rho(t_0) = \lim_{M\to\infty}\left(\mathbb{I} + \Delta t\mathcal{L}\right)^M \rho(t_0)\ . \tag{2.12}$$

Our goal is to recast $\mathrm{tr}[\rho(t)]$ as a functional integral, so we express the density matrix at each time step $t_n = n\Delta t$ in terms of the fermionic coherent basis by inserting identity closure relations, $\mathbb{I} = \int d\bar{\psi}d\psi e^{-\bar{\psi}\psi}\left|\psi\right\rangle\left\langle\psi\right|$, to the left and right of the density matrix (see App. A)

$$\rho(t_n) = \int \underbrace{d\bar{\psi}_n^+ d\psi_n^+ d\bar{\psi}_n^- d\psi_n^-}_{\mathcal{D}[\psi_n,\bar{\psi}_n]} e^{-\bar{\psi}_n^+\psi_n^+ - \bar{\psi}_n^-\psi_n^-}\left|\psi_n^+\right\rangle\left\langle\psi_n^+\right|\rho(t_n)\left|-\psi_n^-\right\rangle\left\langle-\psi_n^-\right|\ , \tag{2.13}$$

with $\psi, \bar{\psi}$ the eigenvalues of fermionic creation and annihilation operators and $\left|\psi\right\rangle, \left\langle\psi\right|$ the corresponding eigenvectors, see App. A. Since the Lindblad superoperator acts differently on the left and right of the density matrix ρ, the field variables to the left and right are distinct and denoted by superscripts $+$ and $-$, respectively. The arbitrary minus sign in the $-$ contour aligns with the functional definition of the trace in Eq. (A.7) and aids in verifying that the time evolution preserves the trace.

Next, we observe that the density matrix at time t_{n+1} satisfies the recursive relation:

$$\begin{aligned}\left\langle\psi_{n+1}^+\right|\rho(t_{n+1})\left|-\psi_{n+1}^-\right\rangle = \int \mathcal{D}[\bar{\psi}_n,\psi_n] e^{-\bar{\psi}_n^+\psi_n^+ - \bar{\psi}_n^-\psi_n^-}\left\langle\psi_n^+\right|\rho(t_n)\left|-\psi_n^-\right\rangle \times \\ \left\langle\psi_{n+1}^+\right|\left(1+\Delta t\mathcal{L}\right)\left[\left|\psi_n^+\right\rangle\left\langle-\psi_n^-\right|\right]\left|-\psi_{n+1}^-\right\rangle\ ,\end{aligned} \tag{2.14}$$

up to a correction of order Δt^2 that we discard. The matrix elements in Eq. (2.14) can be evaluated using Eqs. (A.5) and (A.8) of Appendix A to obtain

$$\left\langle\psi_{n+1}^+\right|\left|\psi_n^+\right\rangle\left\langle-\psi_n^-\right|\left|-\psi_{n+1}^-\right\rangle = e^{\bar{\psi}_{n+1}^+\psi_n^+ + \bar{\psi}_n^-\psi_{n+1}^-}\ , \tag{2.15}$$

and

$$\begin{aligned}\left\langle\psi_{n+1}^+\right|\mathcal{L}\left[\left|\psi_n^+\right\rangle\left\langle-\psi_n^-\right|\right]\left|-\psi_{n+1}^-\right\rangle = &-i\left\langle\psi_{n+1}^+\right|H\left|\psi_n^+\right\rangle\left\langle-\psi_n^-\right|\left|-\psi_{n+1}^-\right\rangle \\ &+ i\left\langle\psi_{n+1}^+\right|\left|\psi_n^+\right\rangle\left\langle-\psi_n^-\right|H\left|-\psi_{n+1}^-\right\rangle \\ &+ \sum\gamma_\alpha\Big[\left\langle\psi_{n+1}^+\right|L_\alpha\left|\psi_n^+\right\rangle\left\langle-\psi_n^-\right|L_\alpha^\dagger\left|-\psi_{n+1}^-\right\rangle \\ &- \frac{\gamma_\alpha}{2}\left\langle\psi_{n+1}^+\right|L_\alpha^\dagger L_\alpha\left|\psi_n^+\right\rangle\left\langle-\psi_n^-\right|\left|-\psi_{n+1}^-\right\rangle \\ &- \frac{\gamma_\alpha}{2}\left\langle\psi_{n+1}^+\right|\left|\psi_n^+\right\rangle\left\langle-\psi_n^-\right|L_\alpha^\dagger L_\alpha\left|-\psi_{n+1}^-\right\rangle\Big]\ ,\end{aligned} \tag{2.16}$$

where all the operators are assumed to have previously been individually normal ordered [1]. The meaning of the expectation value $\langle\psi| L_\alpha^\dagger L_\alpha |\psi\rangle$ will be clarified later but for now we can define the field representation of $\mathcal{L}$ as

$$\mathcal{L}[\bar{\psi}_{n+1}^+, \psi_n^+| - \bar{\psi}_n^-, -\psi_{n+1}^-] := \frac{\langle\psi_{n+1}^+| \mathcal{L}[|\psi_n^+\rangle\langle -\psi_n^-|] |-\psi_{n+1}^-\rangle}{e^{\bar{\psi}_{n+1}^+\psi_n^+ + \bar{\psi}_n^-\psi_{n+1}^-}} . \tag{2.17}$$

Replacing back the final expression into Eq. (2.14), we can write the trotterized version of the action

$$\begin{aligned}\langle\psi_{n+1}^+| \rho(t_{n+1}) |-\psi_{n+1}^-\rangle \\ = \int \mathcal{D}[\psi_n, \bar{\psi}_n] e^{\Delta_t\left(\partial_t[\bar{\psi}_n^+]\psi_n^+ + \bar{\psi}_n^- \partial_t[\psi_n^-] + \mathcal{L}[\bar{\psi}_{n+1}^+, \psi_n^+| - \bar{\psi}_n^-, -\psi_{n+1}^-]\right)} \\ \langle\psi_n^+| \rho(t_n) |-\psi_n^-\rangle\end{aligned} \tag{2.18}$$

where we introduced the continuous notation $\partial_t\psi_n = \frac{\psi_{n+1}-\psi_n}{\Delta t}$. Finally, we construct the action by iterating Eq. (2.18) from the initial time t_0 to the final time t and take the continuous limit $M \to \infty$ while ignoring all terms of order Δt^2 and higher. The expression of the partition function reads

$$\mathcal{Z} = \int \mathcal{D}[\bar{\psi}, \psi] e^{iS} \langle\psi^+(t_0)| \rho(t_0) |-\psi^-(t_0)\rangle , \tag{2.19}$$

where $\mathcal{D}[\bar{\psi}, \psi] = \lim_{M\to\infty} \prod_{n=0}^M d\bar{\psi}_n^+ d\psi_n^+ d\bar{\psi}_n^- d\psi_n^-$ and the action

$$S = \int_0^t dt \left[\bar{\psi}^+(t) i\partial_t \psi^+(t) - \bar{\psi}^-(t) i\partial_t \psi^-(t) - i\mathcal{L}[\psi^+, \psi^-]\right] , \tag{2.20}$$

where we take the continuum $\psi_t \to \psi(t)$ and field representation of $\mathcal{L}$ reads

$$\begin{aligned}\mathcal{L}[\psi^+, \psi^-] = -i\left([H]_t^+ - [H]_t^-\right) \\ + \sum_\alpha \gamma_\alpha \left([L_\alpha^\dagger]_t^- [L_\alpha]_t^+ - \frac{1}{2}[L_\alpha^\dagger L_\alpha]_t^+ - \frac{1}{2}[L_\alpha^\dagger L_\alpha]_t^-\right) .\end{aligned} \tag{2.21}$$

For a single generic operator $X = c_i^\dagger c_j^\dagger \cdots c_{i'} c_{j'} \cdots$, the notation $[X]_t^\pm$ is obtained by replacing the creation and annihilation operators with the field variables, $[X]_t^\pm = \bar{\psi}_i^\pm(t)\bar{\psi}_j^\pm(t)\cdots\psi_{i'}^\pm(t)\psi_{j'}^\pm(t)\cdots$. We point out the exchange in the term

[1] Normal ordering is the re-organization of creation and annihilation operators such that all creation operators are left of the annihilation ones. Individually each H, L_α and $L_\alpha^\dagger$ must be normal ordered but not the product $L_\alpha L_\alpha^\dagger$, see discussion following Eq. (2.20).

$[L_\alpha^\dagger]_t^-[L_\alpha]_t^+$, done to account for the minus sign that emerges in the case of linear jump operators. Unfortunately, the product $[L_\alpha^\dagger L_\alpha]_t^\pm$ is an ill-defined operation in QFT and must be handled with care.

Let us illustrate this problem with the action of a single dot undergoing dephasing, represented by a single jump operator $L = c^\dagger c$. The naïve but incorrect way to write part of the action (2.20) associated with the dephasing, S_γ, would be

$$S_\gamma = -i\gamma \int_0^t dt \left[\bar{\psi}^+(t)\psi^+(t)\bar{\psi}^-(t)\psi^-(t) - \bar{\psi}^+(t)\psi^+(t) - \bar{\psi}^-(t)\psi^-(t)\right] , \tag{2.22}$$

where we assumed $[L^\dagger L]_t^\pm = [c^\dagger c c^\dagger c]_t^\pm \to [c^\dagger c]_t^\pm = \bar{\psi}^\pm(t)\psi^\pm(t)$. The action (2.22) is unphysical because it does not respect the $\mathcal{Z} = 1$ condition. An easy way to see this is to check that the action does not vanish if the indices $\pm$ are dropped [60], i.e. $S(\psi^+ \to \psi, \psi^- \to \psi) \to 0$ such that in this limit $\mathcal{Z} = e^{i0} = 1$. The reason is that the partition function is a functional representation of the trace, and as such it must satisfy the cyclic property

$$\text{tr}\,[X\rho] = \text{tr}\,[\rho X] \ . \tag{2.23}$$

The two sides of Eq. (2.23) have different but equivalent functional representations mapping to X^+ and X^-, for left and right respectively. Therefore, any action that respects this cyclic property must vanish when $\pm$ superscripts are dropped.

A solution to correctly evaluate $[L^\dagger L]_t^\pm$ is to introduce a time-ordering ordering of the jump operators. In Sec. 2.4.1, we explicitly compute the action associated with the QSHs (one of the possible unravelings of the Lindblad equation) and find that the correct ordering is given by

$$\begin{aligned} S = \lim_{\delta\to 0} \int_0^t dt \Big[&\bar{\psi}^+(t) i\partial \psi_t(t)^+ - \bar{\psi}^-(t) i\partial_t \psi^-(t) - [H]_t^+ + [H]_t^- \\ &- i\sum_\alpha \frac{\gamma_\alpha}{2} \left([L_\alpha^\dagger]_t^- [L_\alpha]_{t+\delta}^+ + [L_\alpha^\dagger]_t^- [L_\alpha]_{t-\delta}^+ - [L_\alpha^\dagger]_t^+ [L_\alpha]_{t-\delta}^+ - [L_\alpha^\dagger]_t^- [L_\alpha]_{t+\delta}^- \right) \Big] , \end{aligned} \tag{2.24}$$

where δ is an infinitesimal time step and all the operator's time indexes can be dropped for the case of time-independent Liouvillians. Equation (2.24) is also valid for the bosonic case, as used in App. (B). With this prescription, the corrected action of the dephasing reads

$$\begin{aligned} S_\gamma = &i\frac{\gamma}{2} \int_0^t dt \left[\bar{\psi}^+(t)\psi^+(t)\bar{\psi}^+(t)\psi^+(t) + \bar{\psi}^-(t)\psi^-(t)\bar{\psi}^-(t)\psi^-(t)\right] \\ &- i\gamma \int_0^t dt \bar{\psi}^-(t)\psi^-(t)\bar{\psi}^+(t)\psi^+(t) , \end{aligned} \tag{2.25}$$

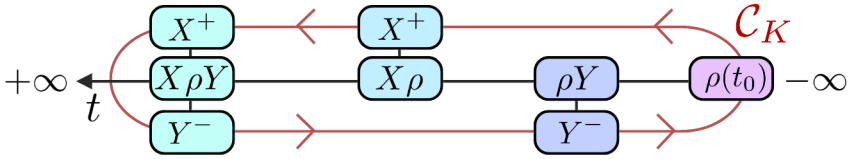

Figure 2.3: Sketch of Keldysh's contour and the functional representations of different super-operators that act left and right of the density matrix. The $+$ branch is time-ordered while the $-$ branch is anti-time ordered.

which correctly vanishes when $\psi^{\pm} \to \psi$.

To obtain the steady-state limit, we consider that the evolution occurs between $t = -\infty$ and $t = +\infty$ and, assuming the NESS to be unique, the final state cannot depend on the initial condition and so $\langle \psi^+(t_0)| \, \rho(t_0) \, |-\psi^-(t_0)\rangle$ can safely be dropped. As discussed in the next chapter, the type of Liouvillians we are interested in are time-independent so we will often work in frequency space $\psi(t) = \int \frac{d\omega}{2\pi} e^{-i\omega t} \psi(\omega)$.

2.3.2 Keldysh contour

The time-ordered integral in the action is a closed integral over the Keldysh contour, $\mathcal{C}_K$, which is composed of two branches connecting the initial density matrix $\rho(t_0)$ to the density matrix at time t. In the steady-state limit, the contour can be seen as connecting $t = -\infty$ to $t = \infty$ as shown in Fig. 2.3. The notation $\pm$ used to label the field variables anticipates the time-ordering of the contour $\mathbb{T}_K$. Along $\mathcal{C}_K$, operators acting on the $+$ or forward branch are ordered along the real time-direction (they are time-ordered) and occur before the operators acting on the $-$ or backward branch which goes opposite to the time direction (they are anti-time ordered).

The expectation value of any arbitrary correlation function can now be computed by evaluating its operators in the Keldysh contour and recalling Eq. (2.13). As an example, consider we wish to evaluate the expectation $\langle \mathcal{E}_1(t_1)\mathcal{E}_0(t_0)\rangle$ corresponding to performing two quantum maps $\mathcal{E}_0(\circ) = L_0 \circ L_0^\dagger$ and $\mathcal{E}_1(\circ) = L_1 \circ L_1^\dagger$ at time t_0 and $t_1 > t_0$ respectively. In Keldysh field theory, one of the possible functional representations of this expectation value would be the 4-point correlation function $\left\langle L^+_{1,t_1} L^+_{0,t_0} L^{\dagger -}_{0,t_0} L^{\dagger -}_{1,t_1} \right\rangle$.

2.3.3 Green's functions

In this work, we are mostly interested in single-particle observables evaluated on the steady-state, such as the current. They can always be written as combinations of the

four possible single-particle Green's functions:

$$\begin{aligned}
\mathcal{G}_{ij}^{++}(t) &= -i\left\langle \mathbb{T}_K \psi_i^+(t)\psi_j^+(0)\right\rangle = \theta(t)\mathcal{G}_{ij}^{-+}(t) + \theta(-t)\mathcal{G}_{ij}^{+-}(t)\,, \\
\mathcal{G}_{ij}^{--}(t) &= -i\left\langle \mathbb{T}_K \psi_i^-(t)\psi_j^-(0)\right\rangle = \theta(-t)\mathcal{G}_{ij}^{-+}(t) + \theta(t)\mathcal{G}_{ij}^{+-}(t)\,, \\
\mathcal{G}_{ij}^{+-}(t) &= -i\left\langle \mathbb{T}_K \psi_i^+(t)\psi_j^-(0)\right\rangle = i\left\langle c_i^\dagger(0)c_j(t)\right\rangle\,, \\
\mathcal{G}_{ij}^{-+}(t) &= -i\left\langle \mathbb{T}_K \psi_i^-(t)\psi_j^+(0)\right\rangle = -i\left\langle c_i(t)c_j^\dagger(0)\right\rangle\,,
\end{aligned} \tag{2.26}$$

where the Heisenberg representation should be understood in the sense of Eq. (2.6), and we made use of the fact that only the time difference matters when the product of operators at different times is evaluated in the NESS. We use g to denote the Green's functions of non-interacting systems in which case the action reads

$$S = \int dt dt' \begin{pmatrix} \bar\psi^+ & \bar\psi^- \end{pmatrix}(t) \begin{pmatrix} g^{++} & g^{-+} \\ g^{+-} & g^{--} \end{pmatrix}^{-1}(t-t') \begin{pmatrix} \psi^1 \\ \psi^2 \end{pmatrix}(t')\,. \tag{2.27}$$

While natural, the representation in terms of $\pm$ contours carries redundant information since

$$\mathcal{G}^{+-}(t) + \mathcal{G}^{-+}(t) = \mathcal{G}^{++}(t) + \mathcal{G}^{--}(t). \tag{2.28}$$

To fix this redundancy, we can perform a change of basis introduced by Larkin and Ovchinnikov [65]

$$\begin{aligned}
\begin{pmatrix} \psi^+ \\ \psi^- \end{pmatrix} &= \frac{1}{\sqrt{2}} \begin{pmatrix} 1 & 1 \\ 1 & -1 \end{pmatrix} \begin{pmatrix} \psi^1 \\ \psi^2 \end{pmatrix}\,, \\
\begin{pmatrix} \bar\psi^+ \\ \bar\psi^- \end{pmatrix} &= \frac{1}{\sqrt{2}} \begin{pmatrix} 1 & 1 \\ -1 & 1 \end{pmatrix} \begin{pmatrix} \bar\psi^1 \\ \bar\psi^2 \end{pmatrix}\,,
\end{aligned} \tag{2.29}$$

where fields and barred fields rotate differently. In this new basis the Keldysh action (2.27) can be re-written as

$$S = \int dt dt' \begin{pmatrix} \bar\psi^1 & \bar\psi^2 \end{pmatrix}(t) \begin{pmatrix} g^R & g^K \\ 0 & g^A \end{pmatrix}^{-1}(t-t') \begin{pmatrix} \psi^1 \\ \psi^2 \end{pmatrix}(t')\,, \tag{2.30}$$

where R stands for retarded, A for advanced and K for Keldysh component of the non-interacting Green's matrix $\boldsymbol{g}$. In general, the full Green's matrix reads

$$\boldsymbol{\mathcal{G}}(t,t') = \begin{pmatrix} \mathcal{G}^R & \mathcal{G}^K \\ 0 & \mathcal{G}^A \end{pmatrix}(t,t') = -i \begin{pmatrix} \left\langle \psi^1(t)\bar\psi^1(t')\right\rangle & \left\langle \psi^1(t)\bar\psi^2(t')\right\rangle \\ \left\langle \psi^2(t)\bar\psi^1(t')\right\rangle & \left\langle \psi^2(t)\bar\psi^2(t')\right\rangle \end{pmatrix}. \tag{2.31}$$

The lower-left corner of Eq. (2.31) vanishes identically in the Larkin-Ovchinnikov rotation, a consequence of the cyclic property of the trace as discussed

in Sec. 2.3.1. The previous rule stated that the action must vanish when $\psi^{\pm} \to \psi, \bar{\psi}^{\pm} \to \bar{\psi}$ which, in the rotated basis, corresponds to setting $\psi^2 \to 0, \bar{\psi}^1 \to 0$. In this case, only the lower-left corner of Eq. (2.31) remains and must be identically zero.

Retarded and Advanced component

The retarded and advanced components are related to the single-particle response functions of the system

$$\mathcal{G}^R_{ij}(t) = -i\theta(t) \left\langle \left\{ c_i(t), c_j^\dagger(0) \right\} \right\rangle , \tag{2.32}$$

$$\mathcal{G}^A_{ij}(t) = i\theta(-t) \left\langle \left\{ c_i(t), c_j^\dagger(0) \right\} \right\rangle . \tag{2.33}$$

They probe the response of the system to a single-particle excitation at later (retarded) or earlier (advanced) times. Evaluated at time $t = 0$ the fermionic anti-commutation relations $\{c_i, c_j^\dagger\} = \delta_{ij}$ and $\theta(0) = 1/2$ impose that the retarded and advanced components satisfy

$$\mathcal{G}^R(t=0) + \mathcal{G}^A(t=0) = 0 , \qquad \mathcal{G}^R(t=0) - \mathcal{G}^A(t=0) = -i . \tag{2.34}$$

The retarded and advanced components are related via hermitian conjugation in frequency space as:

$$\mathcal{G}^R(\omega) = \mathcal{G}^{A\dagger}(\omega), \tag{2.35}$$

and for free systems, they take the simple form $\mathcal{G}^{R/A}(\omega) = (\omega \mathbb{I} - H \pm i0^+)^{-1}$. We introduced the prescription 0^+ to preserve the causality of the functions. From now on, we will drop the ω argument whenever possible.

Keldysh component

On the other hand, the Keldysh component

$$\mathcal{G}^K_{ij}(t) = -i\langle [c_i(t), c_j^\dagger(0)] \rangle, \tag{2.36}$$

determines the connection between occupation and fluctuations (both thermal and quantum). It also measures how much the evolution on the $+$ contour differs from the $-$ contour. In equilibrium physics, the Keldysh component is fixed by the retarded and advanced components of Green's function via the fluctuation-dissipation relation

$$\mathcal{G}^K = (1 - 2f_{\text{eq}}) \left(\mathcal{G}^R - \mathcal{G}^A \right) = -2\pi i \, (1 - 2f_{\text{eq}}) \, \mathcal{A} , \tag{2.37}$$

where $\mathcal{A} = \frac{i}{2\pi}(\mathcal{G}^R - \mathcal{G}^A)$ is the spectral function. $f(\omega)$ is the equilibrium distribution function, which for fermionic systems is $f_{\text{eq}}(\omega) = \left(\exp\left(\frac{\omega - \mu}{T}\right) + 1 \right)^{-1}$, where

μ and T are the chemical potential and temperature of the system. We note that Eq. (2.37) is a matrix equation and that, in thermal equilibrium, it must be valid for all the degrees of freedom on any basis. Out-of-equilibrium, the Keldysh component is independent of the retarded and advanced components, but Eq. (2.37) is still often used to define local equilibrium properties [60]. The idea is to define the local distribution function

$$f_i^{\text{local}} := \frac{1}{2}\left(\frac{\mathcal{G}_{ii}^K}{\mathcal{G}_{ii}^R - \mathcal{G}_{ii}^A} - 1\right) , \tag{2.38}$$

which, even for out-of-equilibrium setups, can resemble a thermal distribution function with an effective temperature and chemical potential, e.g. see Ref. [66] or Ref. [P3]. In general, the Keldysh function is anti-hermitian $\mathcal{G}^K = -\mathcal{G}^{K\dagger}$ and the diagonal components relate to the occupation number, $n_i = \frac{1-i\mathcal{G}_{ii}^K}{2}$, while the off-diagonal terms pertain to the system's currents.

2.4 Quantum Stochastic Hamiltonians

Keldysh field theory provides the natural language to discuss out-of-equilibrium phenomena, in particular, to investigate the different transport regimes in driven setups. In this work, our end goal is to comprehend the emergence of diffusive transport in interacting quantum systems. However, at the field theory level, interactions enter as quartic operators in the action

$$H_{\text{int}} = n_i n_j \to S_{\text{int}} \propto \bar{\psi}_i \psi_i \bar{\psi}_j \psi_j , \tag{2.39}$$

whose integrals cannot be easily computed. Fortunately, there exists a large class of *quadratic* time-dependent Hamiltonians that may also display diffusion while allowing for analytic tractability [34]. They take the form of quadratic quantum stochastic Hamiltonians (QSH)

$$H_{\text{st}} = \sqrt{\gamma} \sum_{\{Q\}} \left(Q \xi_t^q + Q^\dagger \xi_t^{q*}\right) , \tag{2.40}$$

where the sum is over the list $\{Q\}$ of quadratic operators, $Q = \sum_{ij} c_i^\dagger q_{ij} c_j$. The variables ξ_t^q are complex Gaussian white noises with zero average, $\mathbb{E}\left[\xi_t\right] = 0$, and delta-correlated in time, $\mathbb{E}\left[\xi_t^q \xi_{t'}^{q'*}\right] = \delta_{q,q'}\delta(t-t')$ and $\mathbb{E}\left[\xi_t^q \xi_{t'}^{q'}\right] = 0$. γ is the noise rate and the average $\mathbb{E}\left[\circ\right]$ is taken over all the noise configurations.

The class of Hamiltonians represented in equation (2.40) is connected to a variety of well-studied stochastic models, such as dephasing and symmetric simple exclusion processes. These models have been the subject of extensive research in both classical and quantum regimes [67–70] and some serve as prototypical models for diffusive physics. At random instants in time, Q connects site i and j via the matrix element q_{ij}. Intuitively, if Q is a sufficiently spatially local matrix, H_{st} couples

and mixes different momentum and energy sectors, inducing an inelastic scattering process that leads to diffusion.

2.4.1 Connection to Lindblad dynamics

In fact, the link to dissipative processes is deeper. For each random realization of the noise, the evolution under the QSH remains unitary albeit stochastic, but the average evolution over different noise configurations is described by a non-unitary Lindblad equation. To prove this, we write down the quadratic action of the QSH

$$S_{\rm st} = -\sqrt{\gamma}\sum_{\{Q\}}\int dt\,\begin{pmatrix}\bar\psi^1 & \bar\psi^2\end{pmatrix}\begin{pmatrix} q\xi_t^q + q^\dagger\xi_t^{q*} & 0 \\ 0 & q\xi_t^q + q^\dagger\xi_t^{q*}\end{pmatrix}\begin{pmatrix}\psi^1 \\ \psi^2\end{pmatrix}\,, \tag{2.41}$$

and average it over all the disorder realizations using Gaussian integrals to obtain the quartic action

$$\begin{aligned}\mathbb{E}\left[e^{iS_{\rm st}}\right] &= \int D[\xi_t^*,\xi_t]e^{iS_{\rm st}}e^{-\int dt\sum_{\{Q\}}\xi_t^q\xi_t^{q*}/2} \\ &= \exp\left[-\gamma\int dt\sum_{\{Q\}}q_{ij}q^*_{j'i'}\left(\bar\psi_i^1\psi_j^1+\bar\psi_i^2\psi_j^2\right)(t)\left(\bar\psi_{i'}^1\psi_{j'}^1+\bar\psi_{i'}^2\psi_{j'}^2\right)(t)\right]\,.\end{aligned} \tag{2.42}$$

Notice that each pair of field variables is evaluated at a time t, obeying the prescription of Eq. (2.25). The action (2.42) is the same action originating from the time-evolution

$$\begin{aligned}\partial_t\rho &= -i\left[H,\rho\right]+\gamma\sum_{\{Q\}}\left(Q\rho Q^\dagger + Q^\dagger\rho Q - \frac{1}{2}\left\{QQ^\dagger+Q^\dagger Q,\rho\right\}\right) \\ &= -i\left[H,\rho\right]+\frac{\gamma}{2}\sum_{\{Q\}}\left(\left[Q,\left[\rho,Q^\dagger\right]\right]+\left[Q^\dagger,\left[\rho,Q\right]\right]\right)\,,\end{aligned} \tag{2.43}$$

generated by two jump terms $L_1 = Q$ and $L_2 = Q^\dagger$ (acting with the same strength γ) when following the procedure outlined in Sec. 2.3.1.

In other words, the QSH is one of the possible unravelings of the Lindblad equation (2.43), see Fig. 2.4. In this work, we will consider two other possible unravellings: coupling to infinite temperature baths discussed in App. B and continuous measurement processes discussed in App. C. Each unraveling provides a unique insight into the problem and will be used accordingly[2]. One ought to note that QSHs

[2]For this reason, in the rest of this work we use the words noise rate, measurement rate, monitoring rate, and dissipation strength as synonyms.

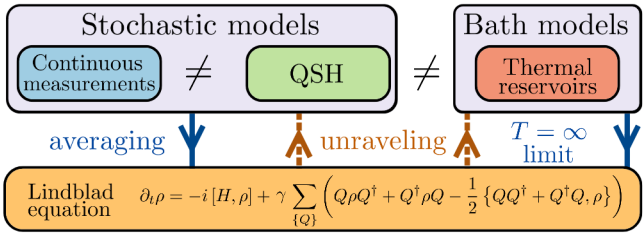

Figure 2.4: Schematic representation of the three different unravelings discussed in the thesis. The stochastic models recover the Lindblad equation when averaging over the noisy degrees of freedom whereas the unraveling with thermal reservoirs becomes valid only in the $T = \infty$ limit, see App. C and B.

of the type (2.40) only map to symmetric dissipative processes, and cannot describe asymmetric models such as asymmetric quantum simple exclusion processes [71].

From the second line of Eq. (2.43), the commutator structure implies that the equations of motion for quadratic operators close:

$$\begin{aligned}\partial_t c_n^\dagger c_{n'} &= \gamma \left([c^\dagger q]_n [q^\dagger c]_{n'} + [c^\dagger q^\dagger]_n [qc]_{n'} \right) \\ &\quad - \frac{\gamma}{2} \left(c_n^\dagger [q^\dagger q c]_{n'} + c_n^\dagger [q q^\dagger c]_{n'} + [c^\dagger q q^\dagger]_n c_{n'} + [c^\dagger q^\dagger q]_n c_{n'} \right) , \end{aligned} \tag{2.44}$$

where we assumed $H = 0$ and used the vector notation $c = (c_1, ..., c_n)^T, c^\dagger = (c_1^\dagger, ..., c_n^\dagger)$. This statement underpins previous analytic solutions [31, 66] that rely on Lindblad injectors to drive a steady-state current but cannot easily be extended to thermal reservoirs in the continuum limit. Considering the continuum limit requires solving an infinite number of equations of motion which is a difficult task. This is why we chose to work in Keldysh formalism using the QSH unraveling instead of the Lindblad equation. The former is explicitly quadratic and it allows a closed expression for any averaged two-point correlation functions even in the presence of continuum reservoirs, as we will now discuss.

2.4.2 Self-energy of QSHs

The goal of this section is to find an analytic expression for the Green function of a generic non-interacting system, described by a quadratic action S_0, in the presence of a QSH. The QSH of Eq. (2.40) enters in the Green's function as a contribution to the irreducible self-energy $\boldsymbol{\Sigma}$. The self-energy matrix has the same tridiagonal and causal structure as $\boldsymbol{\mathcal{G}}$

$$\boldsymbol{\Sigma} = \begin{pmatrix} \Sigma^R & \Sigma^K \\ 0 & \Sigma^A \end{pmatrix} , \tag{2.45}$$

and it is related to the Green's matrix via the Dyson equation

$$\boldsymbol{\mathcal{G}}^{-1} = \boldsymbol{g}^{-1} - \boldsymbol{\Sigma} \,, \tag{2.46}$$

where $\boldsymbol{g}$ is the Green's matrix of the non-interacting theory. In the diagrammatic representation, Eq. (2.46) reads

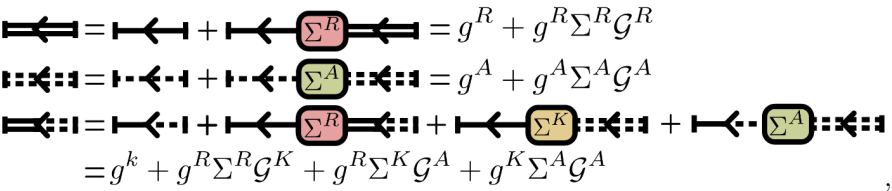

, (2.47)

where we represent Green's function of the unperturbed theory $\boldsymbol{g}$ as single-line arrows going from t' to t,

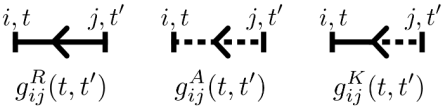

, (2.48)

and delegate double lines for the full Green's functions. The time direction is from right to left. Note that a full line can never become dashed since the term $\langle \psi^2 \bar{\psi}^1 \rangle$ is forbidden in the action. To find the Green's matrix, we start by considering the retarded component and then proceed to the solution of the Keldysh component.

Retarded component

To find the expression of $\mathcal{G}^R$, we first expand the retarded Green's function as a perturbation in the QSH

$$\begin{aligned}
\mathcal{G}^R_{ij}(t,t') &= -i \left\langle \psi^1_i(t) \bar{\psi}^1_j(t') \right\rangle \\
&= -i \int \mathcal{D}[\psi,\bar{\psi}] \psi^1_i(t) \bar{\psi}^1_j(t') e^{i(S_0+S_{\text{st}})} \\
&= -i \sum_{n=0}^{\infty} \frac{i^n}{n!} \int \mathcal{D}[\psi,\bar{\psi}] \psi^1_i(t) \bar{\psi}^1_j(t') S^n_{\text{st}} e^{iS_0} \,.
\end{aligned} \tag{2.49}$$

Since the unperturbed action S_0 is quadratic, we can use Wick's theorem to pairwise contract the fields and evaluate Eq. (2.49). To do these contractions, it is practical to resort to the diagrammatic representation. The action associated with the QSH is composed of four vertices,

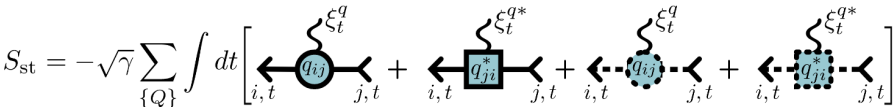

(2.50)

labeled as retarded and advanced vertices, respectively for the full and dashed circles and squares. The noise is represented by a wiggly line with indexes q and t. Note that the retarded vertices only connect full lines to full lines (related to the fields ψ^1 and $\bar{\psi}^1$) and the advanced vertices connect dashed lines to dashed lines (related to ψ^2 and $\bar{\psi}^2$).

Since all the diagrams that contribute to $\mathcal{G}^R$ must begin and end with a full line, any connected diagram in the expansion (2.49) that includes dashed vertices will forcibly include a dashed-to-full line, $\langle\psi^2\bar{\psi}^1\rangle$, and thus be zero. Still, the expansion (2.49) includes many non-zero diagrams such as

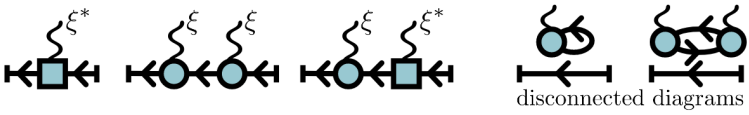

. (2.51)

In the Keldysh formalism, the sum of all disconnected diagrams cancels exactly and can be safely ignored. This leaves only the class of diagrams where the noise enters sequentially, e.g. the first three diagrams in Eq. (2.51). So far the diagrammatic expansion includes the full stochastic evolution, but we are only interested in the average evolution $\mathbb{E}\left[\mathcal{G}^R\right]$. In diagrammatic language, taking the average corresponds to the contraction rules

(2.52)

and so, in Eq. (2.51), only the diagrams with an equal number of noise terms ξ^q and conjugates ξ^{q*} remain, e.g. the third diagram in (2.51). The expansion of the retarded component then reads

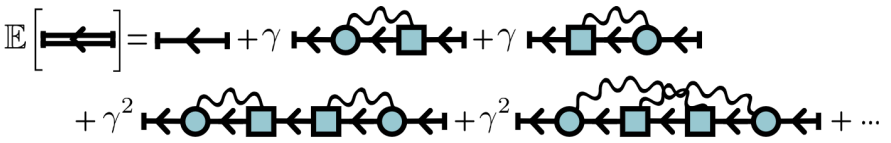

.

(2.53)

The prefactor $n!$ vanishes since, at the n^{th} order in the expansion, $n!$ diagrams contribute and give the same expression upon swapping dummy indices. For diagrams with an even number of vertices, the sign is always positive since an even number of exchanges of fermionic fields is required.

The next step to obtain the Green's function is to prove that all the diagrams with crossing wiggly lines, e.g. the last diagram in Eq. (2.53), violate causality and must vanish. To do so, it is enough to explicitly contract any two crossing lines

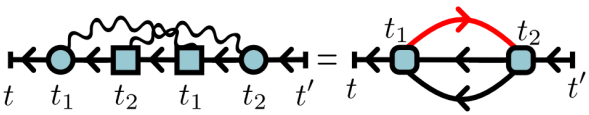

$$\propto \int dt_1 dt_2 \, \theta(t_2 - t_1)\theta(t_1 - t_2)... = 0 \quad , \tag{2.54}$$

where $t_{1,2}$ are integration variables. We note that even if each retarded propagator is dressed by other noise vertices, the proof still holds. The causal structure of the retarded propagators implies that $t \geq t_1 \geq t_2 \geq t'$. After the contraction, the retarded propagator in Eq. (2.54) is proportional to $\theta(t_2 - t_1)$ whereas the others are proportional to $\theta(t_1 - t_2)$. The only possibility left is $t_1 = t_2$, which has an integration measure of zero, and the proof is complete.

Now that we have all the non-zero diagrams of the retarded and advanced [3] components at any order in the expansion, we must re-sum them to find the expression for the irreducible self-energy of the noise $\Sigma_\gamma^{R/A}$. Without the crossing diagrams, the series is only composed of the so-called rainbow diagrams, which can be re-summed to obtain

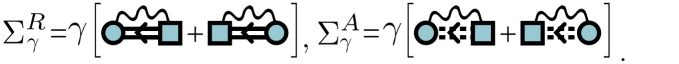

(2.55)

Keldysh component

At any arbitrary order in the expansion of the Keldysh Green's function, $\mathcal{G}^K$, there can only be a single bare Keldysh propagator. Having two or more Keldysh propagators would again imply the existence of a null propagator $\langle \psi^2 \bar{\psi}^1 \rangle = 0$, e.g. the red propagator in the expansion

[3] The proof for the retarded component extends directly to the advanced component with the only difference that now the causality relations are inverted.

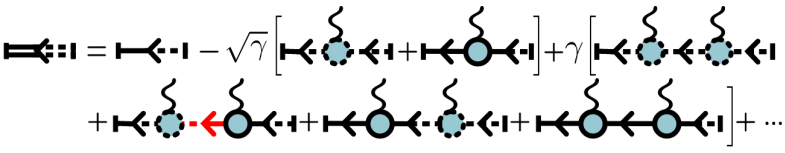

. (2.56)

There are three different types of crossing diagrams, depending on the position of the Keldysh component

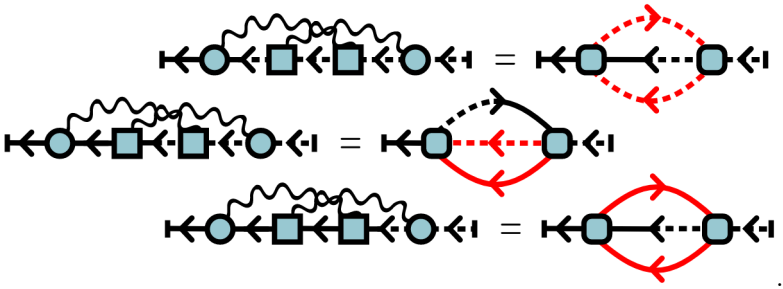

. (2.57)

Yet, after contractions, there are always two propagators with opposite causal structures (highlighted in red) leading to the vanishing of the crossing diagrams.

Similar to the retarded case, all the rainbow diagrams can be resumed to find

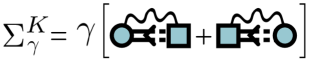

. (2.58)

Final expression

The formal expression for the retarded, advanced, and Keldysh component of the self-energy of the noise is

$$\Sigma_\gamma^{R/A/K}(t,t') = \gamma\delta(t-t')\sum_{\{Q\}}\left[q\mathcal{G}^{R/A/K}(t,t)q^\dagger + q^\dagger\mathcal{G}^{R/A/K}(t,t)q\right] . \quad (2.59)$$

The time locality of $\mathbf{\Sigma}_\gamma$ is a direct consequence of the noise being delta-correlated in time. Note that the expression of $\mathbf{\Sigma}_\gamma$ is non-perturbative as it involves the resummation of an infinite number of diagrams. This resummation scheme is often known as the self-consistent Born approximation [7], which, in the case of this class of QSH, is exact.

2.4.3 Evaluation of the Green's matrix

Once the analytic, albeit self-consistent, solution of the self-energy is available, we can find a closed expression for the Green's matrix by solving the Dyson equation,

$$\begin{pmatrix} \mathcal{G}^R & \mathcal{G}^K \\ 0 & \mathcal{G}^A \end{pmatrix} = \begin{pmatrix} \left([\boldsymbol{g}^{-1}]^R - \Sigma^R\right)^{-1} & -\mathcal{G}^R\left([\boldsymbol{g}^{-1}]^K - \Sigma^K\right)\mathcal{G}^A \\ 0 & \left([\boldsymbol{g}^{-1}]^A - \Sigma^A\right)^{-1} \end{pmatrix} , \quad (2.60)$$

in parallel with Eq. (2.59). The retarded and advanced components are particularly simple to solve since, at the same time, $\mathcal{G}^{R/A}(t,t) = \mp i\theta(0)\mathbb{I} = \mp\frac{i}{2}\mathbb{I}$ and so

$$\Sigma_\gamma^{R/A}(\omega) = \mp\frac{i\gamma}{2}\left(qq^\dagger + q^\dagger q\right) . \quad (2.61)$$

On the other hand, the self-consistent equation for the Keldysh component can be solved by integrating over all frequencies $\int \frac{d\omega}{2\pi}$ such that, in both sides of the equation, the Keldysh component evaluated at the same time $\mathcal{G}^K(t,t)$ emerges

$$\mathcal{G}^K(t,t) = -\int \frac{d\omega}{2\pi}\mathcal{G}^R\left([\boldsymbol{g}^{-1}]^K - \gamma\sum_{\{Q\}}\left[q\mathcal{G}^K(t,t)q^\dagger + q^\dagger\mathcal{G}^K(t,t)q\right]\right)\mathcal{G}^A . \quad (2.62)$$

In the worst-case scenario, this requires computing the order of N^2 integrals but, if only the diagonal terms are concerned, it can be sufficient to compute only N integrals.

2.5 Thermal reservoirs in Keldysh formalism

So far, we have discussed how to incorporate the presence of QSH in the action but, to characterize their driven properties, we need to also incorporate the presence of non-interacting reservoirs at the boundaries, see Sec. 2.2.

Consider a non-interacting fermionic reservoir, r, with the Hamiltonian $H_r = \sum_k \epsilon_{r,k} a^\dagger_{r,k} a_{r,k}$ already in the diagonal basis labeled by k. The reservoir is coupled to the system through the generic coupling $H_{c,r} = \sum_{k,r,i} t_{r,ki} a^\dagger_{r,k} c_i + h.c.$ which does not commute with the reservoir's total particle number or energy [72]. t_r is the coupling matrix which connects the last sites of the system to the eigenstates of the reservoir r, see Fig. 2.5. We assume the reservoirs to be in thermal equilibrium (2.37) with a chemical potential μ_r and a temperature T_r such that the Green's functions read

$$\begin{aligned} g^{R/A}_{r,kk'}(\omega) &= \frac{\delta_{kk'}}{\omega - \epsilon_k \pm i0^+} , \\ g^K_{r,kk'}(\omega) &= -2\pi i\delta(\omega - \epsilon_k)\tanh\left(\frac{\omega - \mu_r}{2T_r}\right) . \end{aligned} \quad (2.63)$$

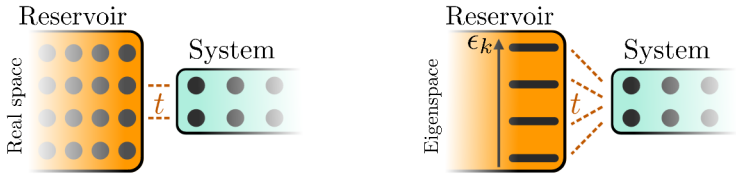

Figure 2.5: Schematic representation of the coupling matrix t of the boundary driving protocol used in this thesis. In real space (left) only the reservoir's final sites connect to the system's edge. For practical reasons, in the calculations, we use the rotated eigenbasis (right) where the edge sites may connect to all eigenstates.

Since the reservoir is non-interacting, we can integrate at the level of the action the fields $\phi_{r,k}, \bar{\phi}_{r,k}$ associated with $a_{r,k}, a^\dagger_{r,k}$ to find its contribution to the self-energy Σ_r,

$$\begin{aligned}\mathcal{Z} = \int D[\bar{\psi},\psi,\bar{\phi},\phi] \exp\Big[iS_{\text{sys}} - i\int \frac{d\omega}{2\pi} \begin{pmatrix}\bar{\phi}^1_r & \bar{\phi}^2_r\end{pmatrix} \begin{pmatrix} t_r & 0 \\ 0 & t_r\end{pmatrix} \begin{pmatrix}\psi^1 \\ \psi^2\end{pmatrix} \\ - \begin{pmatrix}\bar{\psi}^1 & \bar{\psi}^2\end{pmatrix} \begin{pmatrix} t^\dagger_r & 0 \\ 0 & t^\dagger_r\end{pmatrix} \begin{pmatrix}\phi^1_r \\ \phi^2_r\end{pmatrix} + \begin{pmatrix}\bar{\phi}^1_r & \bar{\phi}^2_r\end{pmatrix}_r \boldsymbol{g}^{-1}_r \begin{pmatrix}\phi^1_r \\ \phi^2_r\end{pmatrix} \Big] \\ = \int D[\bar{\psi},\psi] \exp\left[iS_{\text{sys}} - i\int \frac{d\omega}{2\pi} \begin{pmatrix}\bar{\psi}^1 & \bar{\psi}^2\end{pmatrix} \begin{pmatrix} t^\dagger_r & 0 \\ 0 & t^\dagger_r\end{pmatrix} \boldsymbol{g}_r \begin{pmatrix} t_r & 0 \\ 0 & t_r\end{pmatrix} \begin{pmatrix}\psi^1 \\ \psi^2\end{pmatrix} \right].\end{aligned} \tag{2.64}$$

where we use the vector notation $\bar{\phi}_r = (..., \bar{\phi}_{r,k}, ...)$, $\bar{\psi} = (..., \bar{\psi}_i, ...)$, $\phi_r = (..., \phi_{r,k}, ...)^T$ and $\psi = (..., \psi_i, ...)^T$.

The self-energy associated with the reservoir r thus reads

$$\Sigma^{R/A/K}_r = t^\dagger_r g^{R/A/K}_r t_r \ , \tag{2.65}$$

and, as long as multiple reservoirs do not couple to each other, the total contribution to the self-energy is the sum of each reservoir's contribution $\Sigma = \sum_r \Sigma_r$.

The self-energy Σ_r encodes all the information about excitations that enter the reservoir and may re-enter the system at an arbitrarily later time. The retarded component Σ^R_r is related to the hybridization matrix $\Gamma_r(\omega)$ via

$$\begin{aligned}\Sigma^R_{r,ij}(\omega) &= \sum_k \frac{t^*_{r,ki} t_{r,kj}}{\omega - \epsilon_{r,k} + i0^+} \\ &= \pi^{-1} \int d\omega' \frac{\Gamma_{r,ij}(\omega')}{\omega - \omega' + i0^+} \\ &= \int d\omega' \mathcal{P} \frac{\Gamma_{r,ij}(\omega')/\pi}{\omega - \omega'} - i\Gamma_{r,ij}(\omega) \ ,\end{aligned} \tag{2.66}$$

with $\mathcal{P}$ the principal part, and

$$\Gamma_{r,ij}(\omega) = \pi \sum_k t^*_{ki} t_{kj} \delta(\omega - \epsilon_{r,k}) \ . \tag{2.67}$$

Since the baths are assumed in thermal equilibrium, the Keldysh component of $\mathbf{\Sigma}$ also satisfies the equilibrium relation $\Sigma^K_r(\omega) = -i\,(1 - 2f_{\text{eq}}(\omega))\,\Gamma_r(\omega)$.

2.5.1 Wide-band limit

The hybridization matrix is closely related to the density of states $\nu_r(\omega) = \sum_k \delta(\omega - \epsilon_{r,k})$ of the bath and, as it depends on $\epsilon_{r,k}$, it encodes information about the band structure of the reservoir. However, to simplify calculations, e.g. Sec. 3.2, it is common to take the wide-band limit where $\Gamma_r(\omega)$ becomes frequency-independent. In this limit, the couplings are assumed to couple uniformly to the bath $t_{r,ki} \to t_{r,i}$ and the density of states to be constant $\nu(\omega) \to \nu$

$$\Gamma_{r,ij}(\omega) \to \pi t_{r,i} t_{r,j} \sum_k \delta(\omega - \epsilon_k) \to \pi t_i t_j \nu = \Gamma_{r,ij} \ , \tag{2.68}$$

such that the real part of the self-energy vanishes and $\Sigma^R_r = -i\Gamma_r$. In experiments, taking the wide-band limit is justified when, in the energy window where the transport processes occur, the dispersion of the bath is approximately linear as in the case of optical systems or metals.

Having a frequency-independent hybridization implies that the hybridization is delta-correlated in time. However, note that the wide-band limit is not equivalent to using a Lindblad injector, e.g. Eq. (2.9), since the self-energy still has non-trivial frequency dependence entering in the Keldysh component via the distribution function $f_{eq}(\omega)$.

2.5.2 Markovian limit

In this section, we show how to take the Markovian limit of reservoirs and recover a Lindblad driving without explicitly taking the weak coupling limit or the Born approximation (which assumes that the system does not modify the structure of the bath). It is enough to consider an infinite chemical potential μ and infinite temperature T with a constant ratio μ/T [73], provided that the spectrum of the system is bounded. In this case, the Fermi function flattens and the self-energy no longer depends on the frequency

$$\mathbf{\Sigma} = -i \begin{pmatrix} \Gamma_r & 2\tanh\left(\frac{\mu_r}{2T_r}\right)\Gamma_r \\ 0 & -\Gamma_r \end{pmatrix} \ . \tag{2.69}$$

If the reservoirs are coupled to the system via a single site, then Eq. (2.69) is equivalent to the particle injection and loss discussed in Eq. (2.9). The connection can be seen at the level of the action

$$\begin{aligned} S &= -i\frac{\gamma_+}{2}\int\frac{d\omega}{2\pi}\left(2\psi_r^-\bar{\psi}_r^+ - \psi_r^+\bar{\psi}_r^+ - \psi_r^-\bar{\psi}_r^-\right) \\ &\quad - i\frac{\gamma_-}{2}\int\frac{d\omega}{2\pi}\left(2\bar{\psi}_r^-\psi_r^+ - \bar{\psi}_r^+\psi_r^+ - \bar{\psi}_r^-\psi_r^-\right) \\ &= \int\frac{d\omega}{2\pi}\begin{pmatrix}\bar{\psi}^1 & \bar{\psi}^2\end{pmatrix}\begin{pmatrix}\frac{i}{2}(\gamma_+ + \gamma_-) & -i(\gamma_+ - \gamma_-) \\ 0 & -\frac{i}{2}(\gamma_+ + \gamma_-)\end{pmatrix}\begin{pmatrix}\psi^1 \\ \psi^2\end{pmatrix} . \end{aligned} \tag{2.70}$$

By identifying $\gamma_+ = 2\Gamma_r(e^{\frac{\epsilon-\mu_r}{T_r}}+1)^{-1} = 2\Gamma_r - \gamma_-$, thus establishing the $\mu, T \to \infty$ limit as equivalent to the Markovian limit of thermal reservoirs [73]. A more generic equivalence between the Markovian limit and the $\mu, T \to \infty$ limit is established in App. B for bosonic baths.

2.6 Currents in interacting regions

The key objects of this thesis are the currents induced by the presence of reservoirs, which we use to probe different transport regimes. To compute them, one cannot resort to standard scattering theory as it implies that all the scattering processes present in the system are elastic, which is not true for the noise discussed in Sec. 2.4. Time-dependent scattering theory could present a viable alternative, but analytic insight is only available in the limit of a large number of scattering channels [74, 75]. A useful formalism to compute currents through interacting regions was introduced in parallel by Meir and Wingreen in their seminal paper [76] and Pastawski [77]. It is formulated in terms of Green's functions of the system and can easily be adapted to the case of noise-induced interactions since it only assumes the baths to be non-interacting.

2.6.1 Derivation of the particle and heat currents

The expression for the steady-state particle current, $\frac{d\langle N_r\rangle}{dt}$, and heat current, $\frac{d\langle H_r - \mu_r N_r\rangle}{dt}$, flowing from the system into a reservoir r is given by:

$$
\begin{aligned}
J_r^\zeta &= i\sum_k (\epsilon_{r,k}-\mu)^\zeta \left\langle \left[H_c, a_{r,k}^\dagger a_{r,k}\right]\right\rangle \\
&= i\sum_{k,i} (\epsilon_{r,k}-\mu)^\zeta \left\langle t_{r,ki} a_{r,k}^\dagger c_i - t_{r,ki}^* c_i^\dagger a_{r,k}\right\rangle \\
&= \frac{1}{2}\sum_{k,i} (\epsilon_{r,k}-\mu)^\zeta \left(t_{r,ki}\mathcal{G}_{r,ik}^K(t,t) - t_{r,ki}^*\mathcal{G}_{r,ki}^K(t,t)\right) \ ,
\end{aligned}
$$

where $\zeta = 0$ corresponds to the particle current and $\zeta = 1$ to the heat current. The same-time Keldysh Green's function between reservoir and system satisfies $\mathcal{G}_{r,ik}^K(t,t) = 2i\langle a_{r,k}^\dagger c_i\rangle$.

Performing the diagrammatic expansion of the cross correlation functions, $\mathcal{G}_{r,ik}^K = -\mathcal{G}_{r,ki}^{K*}$, in the tunnel amplitudes $t_{r,ki}$, one finds that they can be exactly factorized as

$$
\begin{aligned}
\mathcal{G}_{r,jk}^K(\omega) &= -\left(\mathcal{G}^R(\omega)t_r^\dagger g_r^K(\omega) + \mathcal{G}^K(\omega)t_r^\dagger g_r^A(\omega)\right)_{jk} \ , \\
\mathcal{G}_{r,kj}^K(\omega) &= -\left(g_r^K(\omega)t_r\mathcal{G}^A(\omega) + g_r^R(\omega)t_r\mathcal{G}^K(\omega)\right)_{kj} \ .
\end{aligned} \tag{2.71}
$$

which, introducing back into the current, gives

$$
\begin{aligned}
J_r^\zeta = -\int \frac{d\omega}{4\pi}\sum_{k,i}(\epsilon_k-\mu)^\zeta \big[& t_{r,ki}\left(\mathcal{G}^R(\omega)t_r^\dagger g_r^K(\omega) + \mathcal{G}^K(\omega)t^\dagger g_r^A(\omega)\right)_{ik} \\
& - \left(g_r^K(\omega)t_r\mathcal{G}^A(\omega) + g_r^R(\omega)t\mathcal{G}^K(\omega)\right)_{ki} t_{r,ik}^\dagger\big] \ .
\end{aligned} \tag{2.72}
$$

Recalling the definition of the self-energy $\Sigma_r^{R/A/K} = t^\dagger g_r^{R/A/K} t$, the expression of the current can be manipulated to obtain

$$
J_r^\zeta = -\int \frac{d\omega}{4\pi}(\omega-\mu)^\zeta \mathrm{tr}\left[(\mathcal{G}^R-\mathcal{G}^A)\Sigma_r^K - \mathcal{G}^K(\Sigma_r^R-\Sigma_r^A)\right] \ , \tag{2.73}
$$

where we used Eq. (2.63) to replace $\int d\omega\epsilon_k g_{kk'}^K(\omega) = \int d\omega\omega g_{kk'}^K(\omega)$. The final expression can be obtained by replacing $\Sigma_r^R - \Sigma_r^A = -2i\Gamma_r$, $\mathcal{G}^R - \mathcal{G}^A = \mathcal{G}^R(\Sigma^R - \Sigma^A)\mathcal{G}^A$ and $\mathcal{G}^K = \mathcal{G}^R\Sigma^K\mathcal{G}^A$, to find

$$
\begin{aligned}
J_r^\zeta &= -i\int \frac{d\omega}{2\pi}(\omega-\mu)^\zeta \mathrm{tr}\left[\Gamma_r\mathcal{G}^K - (1-2f_r)\Gamma_r(\mathcal{G}^R-\mathcal{G}^A)\right] \\
&= -i\int \frac{d\omega}{2\pi}(\omega-\mu)^\zeta \mathrm{tr}\left[\Gamma_r\mathcal{G}^R\left(\Sigma^K - (1-2f_r)(\Sigma^R-\Sigma^A)\right)\mathcal{G}^A\right] \ .
\end{aligned} \tag{2.74}
$$

Equation (2.74) is the Meir-Wingreen equation for any interacting system coupled to an arbitrary number of reservoirs. In the absence of interactions, $\mathbf{\Sigma} = \sum_r \mathbf{\Sigma}_r$, and assuming only two reservoirs, r and $\bar{r}$, Equation (2.74) immediately reduces to the Landauer-Büttiker [78] expression for the current

$$J^{\zeta}_{\mathrm{LB}} = \int \frac{d\omega}{2\pi} (\omega - \mu)^{\zeta} (f_r - f_{\bar{r}}) \mathcal{T} \,, \tag{2.75}$$

where $\mathcal{T}(\omega) = \mathrm{tr}[4\Gamma_r(\omega)\mathcal{G}^R(\omega)\Gamma_{\bar{r}}(\omega)\mathcal{G}^A(\omega)]$ is the transmission probability of a scattering state with energy ω.

2.6.2 Application to QSHs

For the case of QSHs coupled to only two reservoirs, r and $\bar{r}$, the self-energy has 3 contributions $\mathbf{\Sigma} = \mathbf{\Sigma}_r + \mathbf{\Sigma}_{\bar{r}} + \mathbf{\Sigma}_{\gamma}$ as discussed previously. Substituting the explicit expression of $\mathbf{\Sigma}$ in Eq. (2.74), we find:

$$J^{\zeta}_{r} = \underbrace{J^{\zeta}_{\mathrm{LB}}}_{\text{elastic}} + \underbrace{\frac{\gamma}{\pi} \int d\omega \; (\omega - \mu_r)^{\zeta} \, \mathrm{tr} \left[\Gamma_r \mathcal{G}^R \left[q \left(\mathcal{D} - f_r \mathbb{I} \right) q^{\dagger} + q^{\dagger} \left(\mathcal{D} - f_r \mathbb{I} \right) q \right] \mathcal{G}^A \right]}_{\text{inelastic}} \,, \tag{2.76}$$

where $\mathcal{D}_{ij} = \left\langle c^{\dagger}_j c_i \right\rangle = \frac{1 - i\mathcal{G}^K_{ij}(t,t)}{2}$ is the same-time correlation matrix. The elastic term matches Landauer-Büttiker expression (2.75) with the key difference that $\boldsymbol{\mathcal{G}}$ is the full Green's function in the presence of the noise, and so $\mathcal{T}$ does not necessarily integrate to one as in the non-interacting case. The inelastic term underpins most of the new physics explored in the following chapters.

The self-consistent nature of the self-energy is now encoded into $\mathcal{D}$, which needs to be found self-consistently through

$$\mathcal{D} = \int \frac{d\omega}{2\pi} \mathcal{G}^R(\omega) \left[2 \sum_r f_r(\omega) \Gamma_r(\omega) + \gamma (q \mathcal{D} q^{\dagger} + q^{\dagger} \mathcal{D} q) \right] \mathcal{G}^A(\omega) \,, \tag{2.77}$$

which can be obtained directly from Eq. (2.62).

Example of a single dot coupled to a reservoir

We finish this section by discussing an application of Eq. (2.76) to a single level coupled to a single reservoir in the wide-band limit. This is a specific but solvable case of the generic impurity model discussed in Sec. 3.1. The level evolves under the stochastic evolution of $Q = c^{\dagger} c = Q^{\dagger}$ which, in average, corresponds to the

single-site dephasing model. The retarded self-energy is simply $\Sigma^R = -i(\Gamma_r + \gamma)$ and the solution for the occupation of the level reads

$$\mathcal{D} = \langle c^\dagger c \rangle = -\int d\omega \underbrace{\frac{1}{\pi} \frac{\mathrm{Im}\Sigma^R}{(\omega - \epsilon)^2 + (\mathrm{Im}\Sigma^R)^2}}_{\mathcal{A}(\omega)} f_r(\omega) \ , \tag{2.78}$$

where $\mathcal{A} = -\pi^{-1}\mathrm{Im}\mathcal{G}^R$ is the spectral function of the level and ϵ the energy of the level. This is the only non-trivial example where the expression for $\mathcal{D}$ resembles the equilibrium expression, $\mathcal{D} = \int d\omega \mathcal{A}(\omega) f_r(\omega)$, with the small modification that the rate broadens the spectral function of the level. In this example, the particle current flowing to the reservoir is identically zero as expected, $J_r^0 = \gamma \int d\omega \mathcal{A}(\mathcal{D} - f_r) = \gamma(\mathcal{D} - \int d\omega \mathcal{A} f_r) = 0$. Since, in the wide-band limit, the integrand in the heat current diverges, it is practical to introduce a large cut-off energy $\int d\omega = \int_{-\Lambda}^{\Lambda} d\omega$. In this case, there is always heat flowing from the dot to the reservoir, $J_r^1 = -\gamma \int d\omega \, (\omega - \epsilon) \, \mathcal{A} f_r \propto \log \Lambda > 0$, just as if the QSH acted as an additional infinite temperature reservoir. This is in agreement with the unraveling in App. B where the QSH can be understood as coupling the system to two infinite temperature reservoirs. The logarithmic divergence is an artifact of the wide-band limit. Because the hybridization matrix does not decay for large energies, the noise is capable of coupling the system to arbitrarily energetic eigenmodes of the reservoir and the energy flow diverges.

2.7 Tensor networks

For most systems, a closed non-perturbative expression for the self-energy is not known, and perturbative methods can fail at characterizing the thermodynamic properties of diffusive systems. This is the case for integrable Hamiltonians in 1-dimension such as those explored in Ref. [P4], e.g. truncating the self-energy at any order in the Kubo formula predicts a finite resistivity despite transport being ballistic [79]. In such cases, one must resort to tensor-based numerical methods [80–82]. Before we proceed, it is useful to switch to the language of spins which in 1D can be mapped to fermions via the Jordan-Wigner transformation [83]:

$$\begin{aligned} \sigma_j^+ &= \sigma_j^x + i\sigma_j^y = e^{-i\pi \sum_k^{j-1} c_k^\dagger c_k} c_j^\dagger \ , \\ \sigma_j^- &= \sigma_j^x - i\sigma_j^y = e^{i\pi \sum_k^{j-1} c_k^\dagger c_k} c_j \ , \\ \sigma_j^z &= 2c_j^\dagger c_j - 1 \ . \end{aligned} \tag{2.79}$$

The main reason is that numerically implementing the fermionic anticommutation relations requires keeping track of the order of operations and signs, which leads to

an overhead in the code. The transformation allows us to work directly with spin systems that satisfy the local commutation relations $[\sigma^i, \sigma^j] = 2i\epsilon_{ijk}\sigma^k$ and are faster to implement.

In 1D and quasi-1D setups, a powerful concept to compute steady-state properties is matrix product states (MPSs) which we now discuss briefly. For a deeper review of the subject, I recommend Ref. [84–86].

2.7.1 Matrix Product States

Consider a Hilbert space composed of N degrees of freedom with dimension h, such that the Hilbert space has dimension h^N. The basic idea behind an MPS is to rewrite a vector $|\psi\rangle$ of the Hilbert space in the computational basis $|s_1 s_2 ... s_N\rangle$ with $s_i = \{1, ..., h\}$ as a product of N tensors:

$$|\psi\rangle = \sum_{\{i,s\}} (A_1)^{s_1}_{i_1} (A_2)^{s_2}_{i_1 i_2} ... (A_N)^{s_{N-1}}_{i_{N-1}} |s_1 s_2 ... s_N\rangle \ . \tag{2.80}$$

Each tensor $(A_n)^i_{jk}$ has 3 indexes with dimensions $\dim(i, j, k) = (\chi, h, \chi)$ where d the physical dimension and χ is called the bond dimension [4]. The bond dimension caps the maximum bi-partite entanglement entropy

$$\mathcal{S} = -\mathrm{tr}_L \left[\rho_L \log \rho_L\right] = -\mathrm{tr}_R \left[\rho_R \log \rho_R\right] \leq 2 \log \chi \tag{2.81}$$

which encodes how correlated the sites left (L) of a cut in the chain are correlated to the sites to the right (R). The reduced density matrix of a pure quantum state $|\psi\rangle$ is the density matrix of a mixed state defined on the subsystem, $\rho_{L/R} = \mathrm{tr}_{R/L}[|\psi\rangle \langle\psi|]$. A bond dimension $\chi = 1$ defines the class of product states that has zero entanglement, while a larger bond dimension allows capturing increasingly more entangled states. In the limit $\chi = h^N$, the MPS can describe any state in the Hilbert space. For a fixed bond dimension, the number of parameters of an MPS scales polynomially with the degrees of freedom, in opposition to the exponential scaling of quantum states, making them very attractive for numerical simulations.

The underlying hope of using an MPS, and extensions thereafter, is that the states we are interested in describing are well captured by an MPS with a low bond dimension. This is the case for states that satisfy the area law [87] characterized by a scaling $\mathcal{S} \propto \log N^{d-1}$ where d in the number of physical dimensions of the system, e.g. ground states of gapped Hamiltonians [88] or even excited states of many-body localized Hamiltonians [89]. In the realm of out-of-equilibrium physics, matrix product ansatzes can also capture a variety of important steady-states of driven high-temperature systems. In this case, it is common to represent density matrices as

[4] The tensors at the left and right edge have dimensions $1 \times h \times \chi$ and $\chi \times h \times 1$ respectively.

matrix product density operators (MPDO) [90]

$$\rho = \sum_{\{i,s,s'\}} (M_1)^{s_1 s'_1}_{i_1} (M_2)^{s_2 s'_2}_{i_1 i_2} ... (M_N)^{s_N s'_N}_{i_{N-1}} \left|s_1 s_2 ... s_N\right\rangle \left\langle s'_1 s'_2 ... s'_N\right| \ , \tag{2.82}$$

where now M are 4-dimensional tensors. Such MPDO representation does not allow us to directly implement some of the tensorial algorithms widely available to quantum states. However, we can always use the vectorization map to represent a density matrix as an MPS

$$\rho = \sum \rho_{ij} \left|i\right\rangle \left\langle j\right| \rightarrow \left\|\rho\right\rangle = \rho_{ij} \left|i\right\rangle \otimes \left|j\right\rangle \ , \tag{2.83}$$

which re-organizes column-by-column the elements of ρ into a vector, $\left\|\rho\right\rangle$. The double bracket notation is used to represent vectorized matrices. The vectorized space has dimension h^{2N}, and for the case of $h = 2$, a suitable basis choice is the set of Pauli matrices with the identity $\left\{\left\|\sigma^0 = \mathbb{I}\right\rangle, \left\|\sigma^x\right\rangle, \left\|\sigma^y\right\rangle, \left\|\sigma^z\right\rangle\right\}$. Diagrammatically, it is useful to represent the MPS of the density matrix as

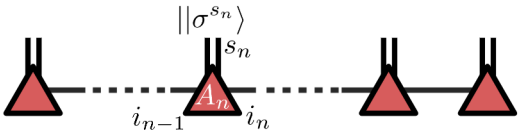

, (2.84)

where the double lines indicate the squaring of the physical dimension due to the vectorization. The choice of the A tensors has a gauge freedom which we can see by introducing an identity closure relation between any A tensors and redefining them accordingly, $A_1 A_2 \rightarrow (A_1 X)(X^{-1} A_2) \rightarrow \tilde{A}_1 \tilde{A}_2$. It is always possible to define an orthogonality center of the MPS where the all the tensors to the left of the center are left-orthogonalized $A^s_{ij} A^{*s}_{ij'} = \delta_{jj'}$, and those to the right are right-orthogonalized $A^s_{ij} A^{*s}_{i'j} = \delta_{ii'}$, in which we say the MPS is in a mixed canonical form represented as

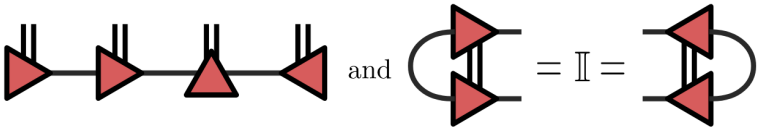

. (2.85)

The canonical form can be easily obtained from sequential singular value decompositions (SVD). A generic tensor with indices $M_{\alpha\beta_1 ... \beta_n} = M_{\alpha(\beta)}$ can always be factorized in the SVD form

$M_{\alpha(\beta)} =$  $= U_{\alpha j} \mathbf{\Lambda}_{jj} V^\dagger_{j(\beta)} =$ 

, (2.86)

where U and V are unitary tensors, i.e., $UU^\dagger = \mathbb{I}$ and $VV^\dagger = \mathbb{I}$, and Λ is a diagonal matrix with non-negative components. Consecutive application of SVD to a MPS, e.g. from the leftmost to the rightmost site, provides an efficient way to orthogonalize any state. We point to Ref. [84, 91] for an excellent and more in-depth discussion about MPS and how to orthogonalize them.

In the case of quantum states, the entries of Λ are related to Schmidt coefficients and can be used to compute the entanglement entropy. For states with low entanglement, the values of Λ follow an exponential distribution, so truncating the SVD to only the χ largest values of Λ provides a natural way to minimize errors. A similar situation occurs with the density matrix except that the quantity of interest is now the operator entanglement entropy (OE) [5] which can also be low for certain steady-states of simple models [92]. The infinite temperature state is a trivial example $\rho = \mathbb{I}/2^N$, which has an exact bond dimension $\chi = 1$ in the vectorized space. Another example is the steady-state of a boundary-driven XX chain [31] that can be written as an MPS with $\chi = 4$. In general, the time dependence of the OE when driving the system out of equilibrium is an ongoing research effort. However, results [93] suggest that, in diffusive systems, the OE is characterized by fast growth and decay (entanglement barrier) followed by slow logarithmic growth for later times. Capturing the precise dynamics during the initial entanglement barrier is a complicated task for numeric methods which often limit the maximum possible bond dimension. However, if we are only interested in the NESS, any deviation from the exact dynamics at short times is expected to become irrelevant at long times, provided that the NESS is unique and well approximated by an MPS with a computationally accessible bond dimension.

2.7.2 Time-Evolved Block Decimation

In recent years, a variety of methods have emerged that explore the tensorial nature of MPSs to compute non-equilibrium time evolution or steady-state properties. Among the methods adapted from ground-state physics, there is time-evolved block decimation (TEBD) [82, 88, 94]. It performs real-time dynamics efficiently by decomposing the evolution in M small time steps and ensuring that, at every time step in the evolution, the density matrix keeps a fixed, maximum, bond dimension.

The first step in the algorithm is to perform a Suzuki-Trotter splitting [95] of the Liouvillian operator for a small time step Δt. There exists an infinity of possible splitting schemes with distinct advantages and disadvantages. A good scheme has to have the appropriate balance between computational time and scaling of errors and may depend on the application. In the work [P4], we introduce a new scheme that combined the fast symmetric-conjugate third-order scheme [96] with an extra second-order composition to further increase precision

[5] The expression for the OE is obtained from the entanglement entropy $\mathcal{S}$ by replacing the quantum state $|\psi\rangle$ with the vectorized density matrix $\|\rho\rangle$.

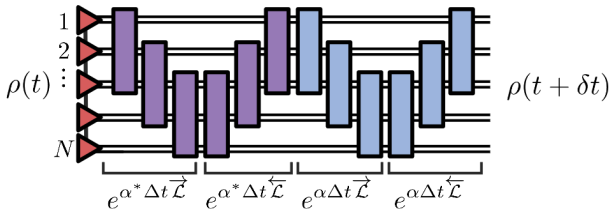

Figure 2.6: A single time step evolution in the splitting scheme of Eq. (2.87) where each term $\mathcal{L}_n$ is a 3-site gate. The last half of the gates (blue) are weighted by a factor α and the first half (purple) by the conjugate α^*. The gates are applied in sequence to always preserve the orthogonality center of the MPS

$$e^{\mathcal{L}t} \approx \left(e^{\mathcal{L}\Delta t}\right)^M \approx \left(e^{\alpha\Delta t\overleftarrow{\mathcal{L}}} e^{\alpha\Delta t\overrightarrow{\mathcal{L}}} e^{\alpha^*\Delta t\overleftarrow{\mathcal{L}}} e^{\alpha^*\Delta t\overrightarrow{\mathcal{L}}}\right)^M , \tag{2.87}$$

where $\alpha = \frac{1}{4} - i\frac{\sqrt{3}}{12}$ is a complex increment and $t = M\Delta t$. In Eq. (2.87), we decompose the Liouvillian in a sum of N local terms in real space $\mathcal{L} = \sum_n^N \mathcal{L}_n$ where the arrows indicate the order to which apply those terms, $e^{\overrightarrow{\mathcal{L}}\Delta t} = e^{\mathcal{L}_N\Delta t}...e^{\mathcal{L}_1\Delta t}$ for a right sweep, and $e^{\overleftarrow{\mathcal{L}}\Delta t} = e^{\mathcal{L}_1\Delta t}...e^{\mathcal{L}_N\Delta t}$ for a left sweep. In Fig. 2.6, we depict diagrammatically a time step in this scheme, where 3-site gates act in sequence to evolve the state from t to $t + \Delta t$. The use of a sweeping protocol ensures that at all times, the orthogonality center of the MPS remains well-defined even when $e^{\mathcal{L}_N\Delta t}$ is not unitary [91]. In the vectorized space, a super-operator acting left and right of the density matrix has a simple matrix representation

$$\mathcal{L}(\rho) = L\rho R \rightarrow L \otimes R^T \, \|\rho\rangle , \tag{2.88}$$

which can easily be exponentiated to obtain the gate $e^{\mathcal{L}\delta t}$.

The next step in the algorithm is to apply each gate efficiently while keeping the bond dimension fixed. For a 3-site gate, the steps schematically follow

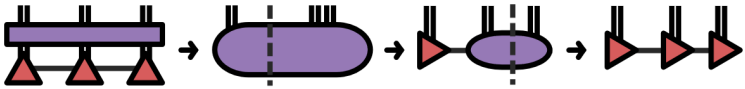

. (2.89)

After applying the gate to the affected MPS tensors, we contract all the internal indices to create a new tensor with three indices. Then, we perform two SVD decompositions to return the state to its MPS form, indicated by the dashed lines in Eq. (2.89). The direction of the SVDs follows the direction of the sweep, in this case from left to right. The SVDs only require a fixed number of operations, of order

$h^4 \times \chi^3$ for 2-site gates and $h^{10} \times \chi^3$ for 3-site gates and so the full algorithm scales polynomial as $Nh^4 \times \chi^3$ or $Nh^{10} \times \chi^3$, respectively for 2 and 3 sites gates.

We can use TEBD to find the steady-state by evolving any initial state for a sufficiently long time such that the observables of interest are sufficiently converged, provided that the NESS is unique. Empirically, we found that the fastest convergence times occur for states close to identity, which we typically take as the initial state. There exists a panoply of open-source libraries to implement tensor methods, but at the time, there was no openly available code to perform TEBD on open systems that implemented a 3-site gate needed in [P4]. For this reason, we created an extra library [97] for the well-known ITensor code [98] that included these features. Below, we showcase a snippet of the code that performs the double SVD step of Eq. (2.89).

```
#psi is the MPS representing the density matrix
#AA is the tensor obtained after applying a 3-site gate
auto AA=psi(i1)*psi(i2)*psi(i3)*g->gate();
[...]

#First SVD starting from the leftmost site i1
auto [U,S,V] = svd(AA,inds(psi(i1)),args);
if(args.getBool("DoNormalize",false))
    S *= 1./itensor::norm(S);

auto ulink=commonIndex(U,S);
auto iset=IndexSet(ulink,siteIndex(psi,i2));

#Second SVD
auto [U2,S2,V2] = svd(S*V,iset,args);
if(args.getBool("DoNormalize",false))
    S2 *= 1./itensor::norm(S2);

#Re-index of the tensor's indexes
psi.set(i1,U);
psi.set(i2,U2);
psi.set(i3,S2*V2);
```

TEBD is particularly useful in boundary-driving protocols that use Lindblad injectors as reservoirs, as in the case of Sec. 3.4. There are different reasons for this. First, the time-local nature of the Lindblad equation makes it easier to implement numerically because each time-step only depends on the state at that time and no memory about the past is required. Then, as discussed in Sec. 2.2.1, Lindblad injectors

tend to heat the system close to an infinite temperature state which has a low operator entanglement entropy, making it easier to describe with a low bond-dimension MPS.

CHAPTER 3

Published works

After establishing the foundational theoretical framework for this thesis in Chapter 2, we now advance towards our primary goal: understanding the role of inelastic scattering in quantum transport and how it can lead to diffusion. To this end, we structure this chapter in incremental steps, each based on a published paper presented alongside an extensive introduction to situate the work within the context of this thesis. The terminology used in these introductions aligns with the rest of the thesis but may differ slightly from the published work. We use the notation $[\![\circ]\!]$ to reference equations and figures from the published paper that follows each introduction.

We start by exploring quantum stochastic Hamiltonians (QSHs) which we have proven capable of supporting an analytic solution for two-point correlation functions. It is critical to recognize within the formal solution (2.76), which transport processes are driven by noise and how they can lead to diffusive behavior. As a first step, we study in Sec. 3.1 the impact of continuously measuring a finite, non-extensive region of the system with an observable $\mathcal{O}$, which is equivalent to considering a single noise term $\{Q\} = \{\mathcal{O} = \mathcal{O}^\dagger\}$, recall App. C. Specifically, we confine our exploration to QSHs acting on a maximum of two sites since they support interpretable, closed-form formulas for the currents. We are capable of identifying step-by-step how the energy fluctuations provided by the QSH induce elastic and inelastic scattering processes. Consequently, we establish the conditions where these systems can be utilized to build quantum machines capable of providing electrical work or extracting heat.

The local nature of the noise, while analytically tractable, does not lead to the emergence of diffusion and Fick's law. So, in Sec. 3.2, we investigate extensive

QSHs as prototypical models for quantum diffusion. We examine different types of QSHs, all of which display emergent diffusive behavior for large systems, prompting the nomenclature of Quantum Stochastic Resistors. In the large system size limit, at a coarse-grain level, we find that the action becomes almost Gaussian, up to corrections in the inverse system size, N. We use this discovery to propose a new theory to describe quantum diffusive systems: the $1/N$ expansion. This enables us to successfully capture key transport quantities, including diffusive constants and even some ballistic-to-diffusive transitions in the presence of long-range noise

Similarly to local noises, we would also like to have an intuitive picture of diffusive processes and how it emerges step-by-step in extensive QSHs. Diffusion, being an inherently classical phenomenon, hints at the existence of a semi-classical interpretation of transport, which we offer in Sec. 3.3. This semi-classical picture involves a single particle propagating ballistically amid random reset events, providing a qualitative explanation for the conductance profile when the system is driven at low temperatures.

The concluding Sec. 3.4 focuses on a different mechanism for diffusion induced by unitary interaction terms in the Hamiltonian. We examine the relationship between integrable and non-integrable interactions, with only the latter leading to the onset of diffusion. The competition between these two terms gives rise to an intermediate transport regime where ballistic transport is renormalized due to the influence of the interactions.

3.1 Non-reciprocal effects in the stochastic impurity problem

In this first work, we explore the role of QSHs in the context of quantum impurity problems. Akin to the better-known interacting counterparts [99, 100], we focus on geometries where a local region is in contact with a continuum of states (left and right reservoirs) and is undergoing a stochastic evolution, see examples in Fig. 3.1a and 3.1b. Due to the mapping established in App. C, these setups equally describe the average evolution of a continuous measurement process, which is non-unitary and difficult to solve analytically. There has been a growing interest in better understanding the thermodynamic aspects of measurements [101–104] and their capacity of extracting work/heat to create efficient quantum machines [40, 105–108]. This excitement is shared by Professor Mannhart who is currently exploring such realizations in solid-state setups [109, 110] and challenged us to understand how the elastic and inelastic processes in QSHs can be used toward this goal.

The main result of the paper concerns the derivation of a generic expression for the particle and heat current, under continuous measurement of a single quadratic observable $\mathcal{O} = \mathcal{O}^\dagger$,

$$J_r^\zeta = \frac{2}{\pi}\int d\omega \underbrace{(\omega-\mu_r)^\zeta\,(f_{\bar{r}}-f_r)\,\mathrm{tr}\left[\Gamma_r\mathcal{G}^R\Gamma_{\bar{r}}\mathcal{G}^A\right]}_{\text{elastic}} + \frac{2\gamma}{\pi}\int d\omega \underbrace{(\omega-\mu_r)^\zeta\,\mathrm{tr}\left[\Gamma_r\mathcal{G}^R\mathcal{O}\,(\mathcal{D}-f_r\mathbb{I})\,\mathcal{O}\mathcal{G}^A\right]}_{\text{inelastic}}. \tag{3.1}$$

This expression is a specific example of Eq. (2.76) when we consider only a single operator $\{Q\} = \{\mathcal{O}\}$. To avoid memory effects and simplify calculations, traditional investigations of similar setups are restricted to limiting regimes, such as weak coupling to the reservoirs [105, 111] or assuming local Markovian reservoirs [112, 113]. Our solution for the average currents goes beyond those approximations as it is non-perturbative in both the measurement rate γ and the coupling to the reservoirs. This allows us to explore previously unattainable parameter regimes, where all the relevant energy scales in the system are comparable.

The expression (3.1) reveals an elastic and inelastic contribution, with the former already discussed in Sec. 2.6.2. The inelastic component has a non-monotonous dependence on the measurement rate γ: growing linearly in γ for weak measurements (note the prefactor γ) before decaying slowly as the inverse rate $1/\gamma$ for fast measurements (in this limit $[\mathcal{G}^{R/A}]^{-1} = \omega\mathbb{I} - \Sigma_r - \Sigma_{\bar{r}} + i\gamma q^2 \sim \gamma$). This implies that the current peaks at the typical energy scale of the setup, see Fig. 3.1c. While the existence of a peak has been observed in similar setups [114–116], our solution allows its non-perturbative characterization in the presence of generic thermal reservoirs and any parameters of the system.

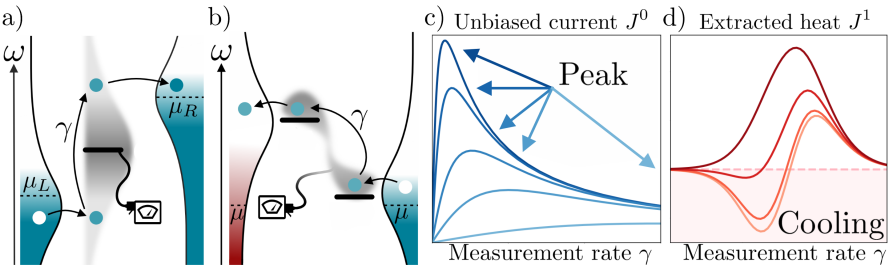

Figure 3.1: Adaptation from Figs. ⟦1,2⟧ of the paper. a) Schematic view of a single-site quantum engine powered by local measurements of the occupation number. b) Schematic view of a two-site quantum refrigerator powered by measurements of the cross-correlations between sites. In a) and b), the inelastic processes providing energy to the particles are depicted by arrows. c) Characteristic increase and decrease of the unbiased particle current with the measurement rate. Different curves represent different parameters of the model with an increasing typical energy (from dark to light blue). d) In the pink region, the heat is extracted from the cold reservoir to the hot through a quantum measurement cooling mechanism. Different curves represent different parameters of the model.

Unlike the elastic component, we find that the inelastic contribution of the particle current does not vanish in the case of unbiased reservoirs, $\mu_L = \mu_R$ and $T_L = T_R$, provided that the setup breaks particle-hole *and* mirror symmetry. These conditions for a finite unbiased current are the same found for thermoelectric currents [117] where, instead of the noise, the current is driven by a third reservoir at a higher temperature. This follows the understanding that QSHs can be recast as the coupling to infinite temperature reservoirs, see unraveling in App. B. The fact that a finite unbiased current exists implies that we can always drive a current opposite to a bias, thus creating a quantum machine capable of extracting work or heat [118]. In the second part of the paper, we discuss two examples of such machines.

The first case study addresses a single dot undergoing the continuous measurement of its occupation number. The measurement drives a particle flow between reservoirs, see Fig. 3.1a. The setup is simple enough that the inelastic processes driving the current ⟦7⟧ can be understood step-by-step:

- A particle from the Fermi-sea of a reservoir tunnels into the dot,
- The noise then induces random fluctuation in the energy of the particle,
- The particle escapes to the opposite reservoir when the energy is above the Fermi energy of the reservoir.

If a load is placed between the two reservoirs, the current generated by the inelastic processes can be used to power a quantum engine, with the extracted work given

by $\mathcal{P} = (\mu_R - \mu_L)J_R^0$. In Fig. [[1d]] we test this operating regime and find that the optimal performances occur when the rate γ is comparable to the typical energy scale of the system, a regime not available to most perturbative methods.

The second application aims to create a quantum refrigerator using quantum measurement cooling [119], where the measurement is used to transfer heat from the cold to the hot reservoir, see Fig. 3.1b. The minimal requirement to operate as a refrigerator is to have a finite heat flow when both reservoirs share the same temperature and chemical potential. Despite performing numerical tests on different parameters of the single-site setup in Fig. 3.1a, we were unable to identify a regime where a single dot could operate as a refrigerator; in all instances, heat persistently flowed toward both reservoirs. Inspired by the cooling-by-heating setups [120, 121], we consider the minimal example of two uncoupled dots undergoing continuous measurement of the cross-correlations. From the QSH perspective, it corresponds to a fluctuating hopping term that drives an inelastic heat current between reservoirs, see Eq. [[9]]. Again, we are capable of identifying all the steps present in the inelastic heat current, which now include the contribution of particles exiting and re-entering the same reservoir with a different energy. We identify and characterize the conditions for this system to operate as a refrigerator and once again find optimal performances in previously unattainable parameter regimes. An exciting application of these results would be to use measurements to cool cold-atom setups with minimal particle loss.

This work provides an intuitive understanding of the inelastic processes present in local QSHs, which we will employ in the next sections. As an open question, we would like to better understand how our results extend to the case of other impurity problems out of equilibrium, especially in the presence of interactions.

Exact description of transport and non-reciprocity in monitored quantum devices

João Ferreira,[1] Tony Jin,[1,2] Jochen Mannhart,[3] Thierry Giamarchi,[1] and Michele Filippone[4]
[1]*Department of Quantum Matter Physics, École de Physique University of Geneva*
[2]*Pritzker School of Molecular Engineering, University of Chicago, Chicago, Illinois 60637, USA*
[3]*Max Planck Institute for Solid State Research, Heisenbergstr. 1, 70569 Stuttgart, Germany and*
[4]*IRIG-MEM-L_Sim, Univ. Grenoble Alpes, CEA, Grenoble INP, Grenoble 38000, France.*

We study non-interacting fermionic systems undergoing continuous monitoring and driven by biased reservoirs. Averaging over the measurement outcomes, we derive exact formulas for the particle and heat flows in the system. We show that these currents feature competing elastic and inelastic components, which depend non-trivially on the monitoring strength γ. We highlight that monitor-induced inelastic processes lead to non-reciprocal currents, allowing to extract work from measurements without active feedback control. We illustrate our formalism with two distinct monitoring schemes providing measurement-induced power or cooling. Optimal performances are found for values of the monitoring strength γ which are hard to address with perturbative approaches.

Introduction – Non-unitary dynamics in quantum systems stems from interactions with the environment [1–4], which induce dissipation and usually suppress quantum coherence [5, 6]. Nonetheless, non-unitary evolution caused by engineered dissipation [7–11] or measurements [12, 13] can stabilize target quantum states, many-body correlations [14–23] and exotic entanglement dynamics [24–31].

Of particular interest are the effects of non-unitarity on quantum transport. Environment-assisted processes can drive currents in coherent systems [32–42] and the impact of losses [41, 43–51] is investigated in quantum simulators [22, 23, 37, 40]. Work extraction from dissipative environments [52, 53] or active monitoring [54–61] may use quantum effects at the nanoscale to break the operational limits imposed by classical thermodynamics [62].

Quantum devices are usually driven by thermodynamic baths, whose large number of degrees of freedom challenges exact numerical [63] and analytical [64–67] approaches, especially to capture the long-time or stationary dynamics of monitored or open settings. Local master equation approaches, based on weak coupling assumptions, may miss interesting effects [68] or imply apparent violations of the second law of thermodynamics [69–72].

In this work, we derive exact formulas for the particle and heat currents driven by continuous monitoring of a single-particle observable $\mathcal{O}$ and biased reservoirs in free fermion systems. We exploit an exact self-consistent Born scheme for 2-point correlation functions [73, 74] and rely on a generalized Meir-Wingreen's approach [49, 75] to account for biased reservoirs. Our main result is formula (5), which offers a simple and exact tool to address novel quantum transport phenomena in coherent systems under continuous monitoring.

We provide two illustrations of our approach showing monitor-assisted non-reciprocal effects in quantum systems. We consider first the continuous monitoring of a single level (Fig. 1). Under generic assumptions, we find that monitoring triggers a non-reciprocal current between reservoirs without external bias, and thus generates power. We then show that monitoring cross-correlations between two sites (Fig. 2) enables quantum measurement cooling [76]. For both cases, we highlight non-trivial dependencies on the measurement strength γ, showcased by peaks of performances in regimes which are not encompassed by perturbative approaches. We also stress that the measurement-based engines described here do not rely on feedback-loops or Maxwell's demons [54–61].

Derivation of monitored currents – For simplicity, we consider 2-terminal setups [77] described by Hamiltonians of form $\mathcal{H} = \mathcal{H}_{\rm res} + \mathcal{H}_{\rm T} + \mathcal{H}_{\rm sys}$. Left and right ($r = L/R$) reservoirs are ruled by $\mathcal{H}_{\rm res} = \sum_{r,k} \varepsilon_{r,k} c^\dagger_{r,k} c_{r,k}$, where $c_{k,r}$ annihilates fermions of the reservoir r in mode k of energy $\varepsilon_{r,k}$. Both reservoirs are in thermal equilibrium, with chemical potential μ_r, temperature T_r, and mode occupation obeying Fermi's distribution $f_r(\varepsilon) = [e^{(\varepsilon-\mu_r)/T_r}+1]^{-1}$. Free fermions in the system are described by $\mathcal{H}_{\rm sys} = \sum_{i,j} d^\dagger_i h_{ij} d_j$, where h_{ij} is a single-particle Hamiltonian with labels i, j referring to internal degrees of freedom (orbitals, spin…). The coupling between system and reservoirs reads $\mathcal{H}_{\rm T} = \sum_{r,k,i} t_{r,ki} c^\dagger_{r,k} d_i + {\rm H.c.}$, where $t_{r,ki}$ are tunnel amplitudes.

When an observable of the system $\mathcal{O}$ is continuously monitored with strength γ, the averaged dynamics of the system density matrix ρ obeys Lindblad's equation $\partial_t \rho = -i[\mathcal{H},\rho] + \mathcal{D}[\rho]$, where ($\hbar = e = k_{\rm B} = 1$) [78–80]

$$\mathcal{D}[\rho] = \gamma \left(2\mathcal{O}\rho\mathcal{O} - \left\{\mathcal{O}^2, \rho\right\}\right) . \tag{1}$$

We are interested in the particle ($\zeta = 0$) and heat ($\zeta = 1$) currents flowing into a reservoir r, which read

$$J^\zeta_r = i \sum_{k,i} (\varepsilon_{r,k} - \mu_r)^\zeta \left[t^*_{r,ki} \langle d^\dagger_i c_{r,k}\rangle - t_{r,ki} \langle c^\dagger_{r,k} d_i \rangle \right] . \tag{2}$$

When single-particle observables $\mathcal{O} = \sum_{ij} d^\dagger_i O_{ij} d_j$ are monitored, calculating Eq. (2) becomes a difficult task, since Eq. (1) is non-quadratic. Even though, for quadratic Hamiltonians, correlation functions obey closed systems of equations [81–83], efficient numerical calculations can

be performed only for finite systems [74, 84, 85]. We show now that analytical solutions can be obtained with infinite reservoirs thanks to the validity of the self-consistent Born scheme for 2-point correlation functions, extensively discussed in Refs. [73, 74] and in the Supplemental Material (SM) [86].

We consider the retarded, advanced, and Keldysh Green's functions: $\mathcal{G}^R_{ij}(t,t') = -i\theta(t-t')\langle\{d_i(t), d_j^\dagger(t')\}\rangle$, $\mathcal{G}^A_{ij}(t,t') = [\mathcal{G}^R_{ji}(t',t)]^*$ and $\mathcal{G}^K_{ij}(t,t') = -i\langle[d_i(t), d_j^\dagger(t')]\rangle$, that we collect in the matrix $\boldsymbol{\mathcal{G}} = \left(\begin{smallmatrix} \mathcal{G}^R & \mathcal{G}^K \\ 0 & \mathcal{G}^A \end{smallmatrix}\right)$ [87]. The matrix $\boldsymbol{\mathcal{G}}$ obeys Dyson's equation $\boldsymbol{\mathcal{G}}^{-1} = \boldsymbol{\mathcal{G}}_0^{-1} - \boldsymbol{\Sigma}$, where $\boldsymbol{\mathcal{G}}_0$ is the Green's function of the isolated system ($t_{r,ki} = \gamma = 0$) and $\boldsymbol{\Sigma}$ is the self-energy, encoding the effects of reservoirs and monitoring. The contribution of the reservoir r to $\boldsymbol{\Sigma}$ is obtained by integration of the modes $c_{r,k}$. In frequency space, $\boldsymbol{\Sigma}_{r,ij}(\omega) = \sum_k t^*_{r,ki} t_{r,kj} \boldsymbol{\mathcal{C}}_{r,k}(\omega)$, where $\boldsymbol{\mathcal{C}}_{r,k}$ is the Green's functions of the reservoir. Particle exchange with the system is described by the hybridization matrix $\Gamma_r(\omega) = [\Sigma^A_r(\omega) - \Sigma^R_r(\omega)]/2$ [88]. The Keldysh component $\Sigma^K_r(\omega) = -2i\Gamma_r(\omega)\tanh[(\omega-\mu_r)/2T_r]$ carries information about the equilibrium state of the reservoirs.

Monitoring contributes to the self-energy following the self-consistent Born scheme [73, 74], which involves the full Green's matrix $\boldsymbol{\mathcal{G}}$, including baths and monitoring:

$$\boldsymbol{\Sigma}^\gamma_{ij}(\omega) = 2\gamma \sum_{pq} O_{ip} \boldsymbol{\mathcal{G}}_{pq}(t,t) O_{qj} \,. \tag{3}$$

To derive the retarded and advanced components of $\boldsymbol{\Sigma}^\gamma$, we exploit the prescription $\mathcal{G}^{R/A}_{ij}(t,t) = \mp i\delta_{ij}/2$ [87], and obtain $[\mathcal{G}^{R/A}]^{-1}_{ij}(\omega) = \omega - h_{ij} - \sum_r \Sigma^{R/A}_{r,ij}(\omega) \pm i\gamma \sum_p O_{ip}O_{pj}$. In this expression, monitoring appears as a frequency-independent life-time $\gamma\sum_p O_{ip}O_{pj}$, in analogy with single-particle gains or losses [37, 40, 41, 47–51].

The difference between monitoring and losses appears in the Keldysh component of Eq. (3). Inserting $\mathcal{G}^K_{ij}(t,t) = 2i\langle d_j^\dagger d_i\rangle - i\delta_{ij}$ [89] and inverting the Dyson equation, one finds a self-consistent equation for the correlation matrix $\mathcal{D}_{ij} = \langle d_j^\dagger d_i\rangle$

$$\mathcal{D} = \int \frac{d\omega}{\pi} \mathcal{G}^R(\omega) \left[\sum_r f_r(\omega)\Gamma_r(\omega) + \gamma O\mathcal{D}O \right] \mathcal{G}^A(\omega) \,. \tag{4}$$

The solution of Eq. (4) completes the full derivation of the Green's function $\boldsymbol{\mathcal{G}}$. The knowledge of $\boldsymbol{\mathcal{G}}$ is sufficient to derive currents [49, 75]. After straightforward algebra, detailed in the SM [86], we find closed, exact and non-perturbative expressions for the particle and heat currents:

$$J^\zeta_r = \frac{2}{\pi}\int d\omega \underbrace{(\omega-\mu_r)^\zeta (f_{\bar r} - f_r)\,\mathrm{tr}\left[\Gamma_r \mathcal{G}^R \Gamma_{\bar r} \mathcal{G}^A\right]}_{\text{elastic}} + \gamma\frac{2}{\pi}\int d\omega \underbrace{(\omega-\mu_r)^\zeta\,\mathrm{tr}\left[\Gamma_r \mathcal{G}^R O\left(\mathcal{D} - f_r \mathbb{1}\right) O \mathcal{G}^A\right]}_{\text{inelastic}} \,. \tag{5}$$

with $\bar r = R$ if $r = L$ and viceversa. This expression is the main result of our work. It allows us to draw general conclusions on monitor-assisted transport and, combined with Eq. (4), can be directly applied to all settings described by Lindbladians of the form (1).

Equation (5) appears as a sum of two distinct terms. The first term reproduces the Landauer-Büttiker formula for currents in non-interacting systems [88, 90]. It describes the energy-preserving transfer of particles between reservoirs at energy ω with transmission probability $\mathcal{T}(\omega) = 4\mathrm{tr}\left[\Gamma_r \mathcal{G}^R \Gamma_{\bar r} \mathcal{G}^A\right]$. As $\mathcal{T}(\omega)$ depends on $\mathcal{G}^{R/A}$, where measurements only contribute to reducing life-times, monitoring affects elastic transport exactly as single-particle gains or losses [37, 40, 41, 47–51].

The second term in Eq. (5) is controlled by monitoring. The implicit dependence of the correlation matrix $\mathcal{D}$ on additional energy integrals, see Eq. (4), indicates that measurements inelastically add or subtract energy to particles in the system. A rough inspection of Eq. (5) shows that the inelastic contribution has a peak as function of the observation rate γ, interpolating between a linear growth for small γ and a γ^{-1} decay in the strong measurement limit, as $\mathcal{G}^{R/A} \propto \gamma^{-1}$ for $\gamma \to \infty$, see Figs. 1b-2c. Position and strength of this maximum depend on the details of the problem, but it is generally expected for values of γ comparable to the spectral width of the system and its coupling strength to the baths. These maxima are out of reach in perturbative approaches. Importantly, the inelastic current is not directly proportional to $f_L - f_R$, and can thus be finite even without a bias. This mechanism describes the generation of non-reciprocal currents from measurement and can be exploited for work generation.

We provide below explicit illustrations of these considerations on two different monitor-assisted devices.

Monitored density engine – We first consider a monitored setting, sketched in Fig. 1, where a single level of energy ε_d, described by the Hamiltonian $\mathcal{H}_{\rm sys} = \varepsilon_d\, d^\dagger d$, evolves under the continuous measurement of its occupation, associated with the operator $\mathcal{O} = n = d^\dagger d$. Solving Eq. (4) gives the occupation of the level

$$\langle n\rangle = \frac{\int d\omega\, \mathcal{A}(\omega)[f_L(\omega)P_L(\omega) + f_R(\omega)P_R(\omega)]}{\int d\omega\, \mathcal{A}(\omega)[P_L(\omega) + P_R(\omega)]} \,, \tag{6}$$

where $\mathcal{A}(\omega) = -\mathrm{Im}[\mathcal{G}^R_{dd}(\omega)]/\pi = \frac{1}{\pi}\frac{\Gamma_L+\Gamma_R+\gamma}{|\omega-\varepsilon_d-\Sigma_L-\Sigma_R+i\gamma|^2}$ is the spectral function of the level. We have introduced the quantity $P_r(\omega) = \Gamma_r/[\Gamma_{\rm L} + \Gamma_{\rm R} + \gamma]$, which highlights the non-equilibrium effects of monitoring. For instance, in the unbiased case ($f_{L,R} = f$), the absence of dephasing ($\gamma = 0$) is needed to recover $P_R + P_L = 1$ and the standard equilibrium expression $\langle n\rangle_{\rm eq} = \int d\omega\, \mathcal{A}(\omega) f(\omega)$ [91]. Injecting Eq. (6) in Eq. (5), we obtain the particle current

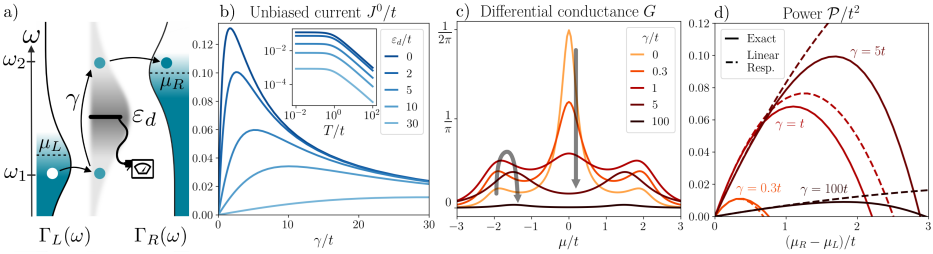

Figure 1. a) Monitored level of energy ε_d, coupled to left and right reservoirs with asymmetric hybridization functions $\Gamma_L(\omega) \neq \Gamma_R(\omega)$. The level occupation is measured with strength γ, providing the inelastic mechanism promoting particles from energy ω_1 to ω_2 and inducing a current against the bias (arrows). The blue-shaded areas correspond to the finite-temperature Fermi distributions of the reservoirs. For all plots, we use the two-filter model discussed in the main text, with $\varepsilon_R = 1.48t = -\varepsilon_L$, $\Delta = 0.55t$, which we found to maximize the unbiased particle current at $\mu_{L,R} = T_{L,R} = 0$. b) Peaked structure of the unbiased particle current as a function of the measurement strength γ for varying ε_d. Inset: The unbiased current decays monotonously for increasing temperatures ($\gamma = 1$). c) Differential conductance G as a function of the chemical potential μ at $T = 0$ for increasing γ. The measurement suppresses the resonance associated to the single level and favors those from the filters, as highlighted by arrows. d) Electric power as function of a symmetric bias $\mu_R - \mu_L$ around $\mu = 0$, for different values of γ. Dashed lines correspond to linear response calculations.

$J^0 = J^0_R = -J^0_L$ flowing through the system

$$J^0 = 2\int d\omega \mathcal{A} \frac{\Gamma_L\Gamma_R}{\Gamma_L+\Gamma_R+\gamma}\left(f_L - f_R\right) \qquad (7)$$
$$+ \frac{2\gamma}{\int d\omega \mathcal{A}\left(P_L+P_R\right)} \int d\omega d\omega' \mathcal{A}\,\mathcal{A}' P_L P'_R \left(f_L - f'_R\right),$$

where we omit all frequency dependency for compactness and use the shorthand notation $f' = f(\omega')$.

The first term reproduces the well-known expression of the current flowing through a Breit-Wigner resonance [92, 93], with an additional suppression controlled by the monitoring rate γ.

The inspection of the inelastic term in Eq. (7) directly shows that even without bias ($\mu_{L,R} = \mu$, $T_{R,L} = T$), monitoring can trigger the flow of a finite, non-reciprocal current through the system. This non-reciprocal current is finite provided that at least one of the hybridization functions $\Gamma_{L/R}$ depends on energy, and that mirror and particle-hole symmetry are simultaneously broken [94–96]. Such conditions are satisfied when $\Gamma_L \neq \Gamma_R$ and at least one function among $\mathcal{A}$ or $\Gamma_{L/R}$ is not symmetric around the chemical potential μ. The mechanism generating this current is sketched in Fig. 1a: electrons at energy ω_1 are emitted from one reservoir onto the level and the measurement provides the energy for the electron to exit into an empty state of the other reservoir at energy ω_2. The fact that the injection and emission rates depend asymmetrically on energy allows the generation of the current. The emergence of a non-reciprocal current can be also understood based on the fact that averaging over the measurement outcomes is equivalent, in this specific case, to coupling the system to an infinite-temperature bosonic bath (see SM [86]), which induces a thermoelectric flow in the system if mirror and particle-hole symmetry are broken [97–99].

Figure 1b shows that the inelastic current displays the aforementioned peak as a function of the measurement strength γ at zero bias $\delta\mu = \mu_L - \mu_R = 0$. For all numerical applications, we consider a minimal model where the level is coupled to two metallic reservoirs via two energy filters of energy $\varepsilon_{L/R}$. In this case, $\Sigma^R_r(\omega) = t^2/(\omega - \varepsilon_r + i\Delta)$, where t is the level-filter tunnel coupling and Δ the hybridization constant of the filter with the reservoirs, see SM [86]. The resulting hybridization function $\Gamma_r(\omega) = -\mathrm{Im}\Sigma^R_r(\omega)$ is peaked around ε_r, as sketched in Fig. 1a. We have found the maximum non-reciprocal current for $\gamma \simeq t$ – that is out of weak coupling ($\gamma \gg t$) – when $\varepsilon_d = 0$ and when mirror and particle-hole symmetry are broken by antisymmetric reservoirs with $\varepsilon_L = -\varepsilon_R$. The peak roughly follows ε_d and is suppressed by finite temperatures, see inset of Fig. 1b. Similar non-reciprocal effects and peaks were also discussed, from a real-time perspective, in Refs. [38, 39].

Figure 1c shows the differential conductance $G = \partial J^0/\partial\delta\mu|_{\delta\mu=0}$ for the same system. G also features elastic and inelastic contributions [100, 101], scaling differently with γ. For small rates, the elastic term dominates, showing as many peaks as resonances in the system – three in the application of Fig. 1. Because of the fact that only the central level is monitored, increasing γ strongly suppresses its associated resonance, while spectral weight is transferred to the filters (arrows in Fig. 1c). Consequently, for intermediate monitoring strengths $\gamma \simeq t$, the conductance actually increases out of resonance ($\mu \neq 0$), before being also suppressed in the $\gamma \gg t$ limit.

The fact that monitoring generates currents at zero

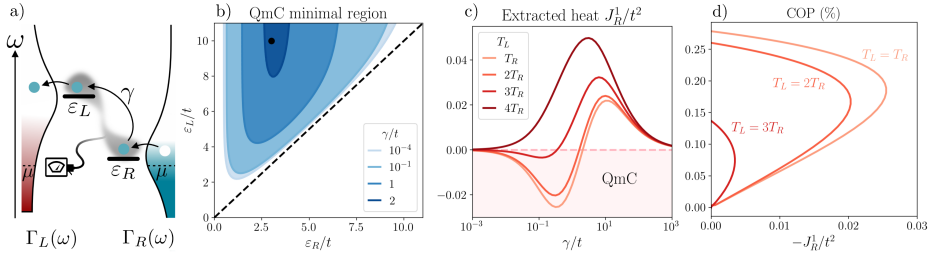

Figure 2. a) Two-level system under continuous monitoring of its cross-correlations, coupled to a left (hot) and right (cold) reservoir. For applications, we consider the same filters as in Fig. 1, aligned with the levels $\varepsilon_{L/R}$. b) Parameter region where a reservoir at a temperature $T_R = t$ can be cooled by measurement for different values of γ and $\Delta = 0.5t$. The range of parameters for which quantum measurement cooling is possible reduces by increasing γ. The black dot corresponds to $\varepsilon_L = 10t$ and $\varepsilon_R = 3t$, where panels (c) and (d) are derived. c) Heat flowing into the right reservoirs for increasing temperature bias $T_L > T_R$. Quantum measurement cooling (QmC) occurs in the colored region and below some critical temperature bias. d) Parametric plot of the coefficient of performance (COP) of QmC. Curves are obtained by varying the measurement strength γ.

bias, implies that they can flow against externally imposed biases to generate work. We consider here the generated power $\mathcal{P} = \delta\mu \cdot J^0$ and show the importance of non-perturbative and out-of-equilibrium effects on this quantity. In linear response, $J^0 \simeq J^0|_{\delta\mu=0} - \delta\mu\, G$, and the power has a parabolic dependence on $\delta\mu$, with a maximum $\mathcal{P}_{\max} = J^0|^2_{\delta\mu=0}/2G$ and a change of sign at the stopping voltage $\delta\mu_{\rm stop} = J^0|_{\delta\mu=0}/G$. Figure 1d shows that the maximum power generation is found for monitoring of strength $\gamma > t$, that is out of the weak coupling regime. Moreover, we find that non-equilibrium effects associated to strongly biased reservoirs cannot be neglected. They can be exactly derived via Eq. (7), and the dashed lines in Fig. 1d clearly show that linear-response greatly overestimates $\mathcal{P}_{\max}$ and $\delta\mu_{\rm stop}$ when $\gamma \simeq t$.

Quantum measurement cooling – We consider two independent sites $H_{\rm sys} = \varepsilon_L d_L^\dagger d_L + \varepsilon_R d_R^\dagger d_R$ that are coupled via the monitoring process, $O_{ij} = \delta_{iL}\delta_{jR} + \delta_{iR}\delta_{jL}$, see Fig. 2a. This process can be in principle realized by adding an interferometer measuring cross-correlations between the two sites [102, 103]. Also in this case, we rely on Eq. (4) to find the occupation of the levels $\langle n_r\rangle = \langle d_r^\dagger d_r\rangle$

$$\langle n_r\rangle = \frac{\int d\omega \big[f_{\bar r} P_{\bar r}\mathcal{A}_{\bar r} + \big(1 - \int d\omega' P'_{\bar r}\mathcal{A}'_{\bar r}\big) f_r P_r \mathcal{A}_r\big]}{\sum_{r'}\int d\omega P_{r'}\mathcal{A}_{r'} - \prod_{r'}\int d\omega P_{r'}\mathcal{A}_{r'}}\,, \quad (8)$$

with modified notation $P_r = \Gamma_r/(\Gamma_r + \gamma)$ and spectral functions $\mathcal{A}_r(\omega) = -{\rm Im}\mathcal{G}^R_{rr}/\pi = \frac{1}{\pi}\frac{\Gamma_r+\gamma}{|\omega-\varepsilon_r-\Sigma_r+i\gamma|^2}$.

Because of the absence of coherent hopping between sites, $\mathcal{G}^{R/A}_{LR} = 0$ and only the inelastic component of the currents in Eq. (5) is finite, for which the knowledge of Eq. (8) is needed. We are interested in exact expressions for quantum measurement cooling (QmC) [76], we thus consider the heat current flowing in the right reservoir

$$J^1_R = \frac{2\gamma}{\mathcal{N}}\int d\omega d\omega' (\omega-\mu_R)\mathcal{A}_R P_R \Big[\mathcal{A}'_L P'_L\,(f'_L - f_R) + \Big(1 - \int d\omega''\mathcal{A}''_L P''_L\Big)\mathcal{A}'_R P'_R\,(f'_R - f_R)\Big]\,, \quad (9)$$

where $\mathcal{N}$ is the denominator appearing in Eq. (8). To get physical insight on the physical requirements for QmC and the multiple processes described by Eq. (9), we first inspect the $\gamma \to 0$ limit. To leading order in γ, one can approximate $P_r = 1$ and only the first term in Eq. (9) remains. It can be cast in the compact form

$$J^1_R = 2\gamma\int d\omega\,(\omega-\mu_R)\mathcal{A}_R(\omega)\big[\langle n_L\rangle - f_R(\omega)\big]\,. \quad (10)$$

If we further approximate the spectral function by $\mathcal{A}_R(\omega) = \delta(\omega - \varepsilon_R)$, we get $J^1_R = 2\gamma(\varepsilon_R - \mu_R)(\langle n_L\rangle - \langle n_R\rangle)$. This expression makes explicit that the heat flow in the right reservoir is controlled by the position of the right level with respect to the chemical potential and the difference of occupation with respect to the left level. The condition for cooling the right reservoir is $J^1_R < 0$. In the absence of bias, such condition requires $\mu_R \lesseqgtr \varepsilon_R$ and $\varepsilon_L \lesseqgtr \varepsilon_R$, as sketched in Fig. 2a. Analogous conditions were found to achieve cooling by heating [104, 105], where the role of measurement is played by a third hot reservoir. The second term in Eq. (9) acts at order γ^2 and describes the reinjection of heat in the right reservoir by particles hopping back and forth to the left level via the monitoring process.

In Figure 2, we explore QmC and its performances also for strong temperature biases and large values of γ. For numerical applications, we consider $\mu_{L/R} = 0$ and take the same hybridization functions $\Gamma_r(\omega)$ than in the previous section, with peaks aligned with ε_r. Figure 2b shows

the regions where QmC occurs, in the absence of bias and for increasing monitoring strength γ. QmC indeed occurs when $\varepsilon_L \lesseqgtr \varepsilon_R \lesseqgtr 0$. Nonetheless, the parameter region for QmC shrinks the larger the monitoring strength γ, reflecting the fact that more heat is injected in both reservoirs the stronger the measurement process is. Fig. 2c shows the behavior of J_R^1 for increasing temperature biases as function of γ. Exactly as the non-reciprocal current discussed in the previous section (Fig. 1b), the heat current shows a peak for $\gamma \approx t$. However, increasing the temperature bias leads to a change of sign of the heat current, signaling that the left reservoir is hot enough to heat the right one.

We conclude this study by discussing the efficiency of this process, which is characterized by the coefficient of performance, $COP = |J_R^1/(J_R^1 + J_L^1)|$, which measures how much heat can be extracted from monitoring [106]. We depict the COP in Fig. 2d as a parametric plot on the rate γ. For fixed temperatures in the reservoirs, the maximum COP is found near the critical measurement strength γ at which the heat flow changes sign in Fig. 2c. This monitoring strength is also of order t and is not encompassed by the weak coupling limit.

Conclusions – We have derived exact and analytic expressions for the particle and heat currents flowing in a large class of monitored systems. These formulas were applied to investigate power harvesting and cooling assisted by measurements. In particular, we have found current peaks as a function of the measurement strength γ out of the weak-coupling limit (Figs. 1b-2c). These peaks are clear features that could favor their observation in experiments. Our results can be readily generalized to different monitored setups and pave the way to the investigation of unexplored regimes which are not captured by standard, perturbative approaches. We have shown that these regimes are important, as they manifest the best performances in terms of power generation and quantum measurement cooling.

On a more fundamental level, we have provided exact expressions for quantum transport in the presence of non-elastic effects caused by monitoring. It would be of great interest to establish in the future whether formulas like Eq. (5) also apply for interacting quantum impurity models driven out of equilibrium, and/or for systems coupled to bosonic baths at finite or even zero temperature [42, 107–110].

Acknowledgments – We are grateful to Christophe Berthod, Daniel Braak, Géraldine Haack, Manuel Houzet, Rafael Sánchez, Kyrylo Snizhko, Clemens Winkelmann and Robert Whitney for helpful comments and discussions. This work has been supported by the Swiss National Science Foundation under Division II under grant 200020-188687. J.S.F. and M.F. acknowledge support from the FNS/SNF Ambizione Grant No. PZ00P2_174038. M. F. acknowledges support from EPiQ ANR-22-PETQ-0007 part of Plan France 2030.

[1] R. P. Feynman and F. Vernon Jr, Annals of physics **281**, 547 (2000).
[2] A. Caldeira and A. Leggett, Physica A: Statistical Mechanics and its Applications **121**, 587 (1983).
[3] C. Gardiner and P. Zoller, *Quantum noise: a handbook of Markovian and non-Markovian quantum stochastic methods with applications to quantum optics* (Springer Science, 2004).
[4] A. A. Clerk, M. H. Devoret, S. M. Girvin, F. Marquardt, and R. J. Schoelkopf, Rev. Mod. Phys. **82**, 1155 (2010).
[5] D. F. Walls and G. J. Milburn, Phys. Rev. A **31**, 2403 (1985).
[6] W. H. Zurek, Rev. Mod. Phys. **75**, 715 (2003).
[7] J. F. Poyatos, J. I. Cirac, and P. Zoller, Phys. Rev. Lett. **77**, 4728 (1996).
[8] M. Müller, S. Diehl, G. Pupillo, and P. Zoller, Advances in Atomic Molecular and Optical Physics **61**, 1 (2012).
[9] A. Grimm, N. E. Frattini, S. Puri, S. O. Mundhada, S. Touzard, M. Mirrahimi, S. M. Girvin, S. Shankar, and M. H. Devoret, Nature **584**, 205 (2020).
[10] R. Lescanne, M. Villiers, T. Peronnin, A. Sarlette, M. Delbecq, B. Huard, T. Kontos, M. Mirrahimi, and Z. Leghtas, Nature Physics **16**, 509 (2020).
[11] D. Poletti, J.-S. Bernier, A. Georges, and C. Kollath, Phys. Rev. Lett. **109**, 045302 (2012).
[12] D. Gottesman, Ph. D. thesis, CalTech (1997), quant-ph/9705052.
[13] A. Calderbank, E. Rains, P. Shor, and N. Sloane, IEEE Transactions on Information Theory **44** (1998).
[14] G. Barontini, R. Labouvie, F. Stubenrauch, A. Vogler, V. Guarrera, and H. Ott, Phys. Rev. Lett. **110**, 035302 (2013).
[15] H. P. Lüschen, P. Bordia, S. S. Hodgman, M. Schreiber, S. Sarkar, A. J. Daley, M. H. Fischer, E. Altman, I. Bloch, and U. Schneider, Phys. Rev. X **7**, 011034 (2017).
[16] T. Tomita, S. Nakajima, I. Danshita, Y. Takasu, and Y. Takahashi, Science advances **3**, e1701513 (2017).
[17] M. Fitzpatrick, N. M. Sundaresan, A. C. Y. Li, J. Koch, and A. A. Houck, Phys. Rev. X **7**, 011016 (2017).
[18] R. Ma, B. Saxberg, C. Owens, N. Leung, Y. Lu, J. Simon, and D. I. Schuster, Nature **566**, 51 (2019).
[19] K. Yamamoto, M. Nakagawa, N. Tsuji, M. Ueda, and N. Kawakami, Phys. Rev. Lett. **127**, 055301 (2021).
[20] N. Dogra, M. Landini, K. Kroeger, L. Hruby, T. Donner, and T. Esslinger, Science **366**, 1496 (2019).
[21] F. Ferri, R. Rosa-Medina, F. Finger, N. Dogra, M. Soriente, O. Zilberberg, T. Donner, and T. Esslinger, Phys. Rev. X **11**, 041046 (2021).
[22] N. Syassen, D. M. Bauer, M. Lettner, T. Volz, D. Dietze, J. J. Garcia-Ripoll, J. I. Cirac, G. Rempe, and S. Durr, Science **320**, 1329 (2008).
[23] K. Sponselee, L. Freystatzky, B. Abeln, M. Diem, B. Hundt, A. Kochanke, T. Ponath, B. Santra, L. Mathey, K. Sengstock, and C. Becker, Quantum Science and Technology **4**, 014002 (2018).
[24] B. Skinner, J. Ruhman, and A. Nahum, Phys. Rev. X **9**, 031009 (2019).
[25] Y. Li, X. Chen, and M. P. A. Fisher, Phys. Rev. B **98**, 205136 (2018).
[26] S. Choi, Y. Bao, X.-L. Qi, and E. Altman, Phys. Rev.

Lett. **125**, 030505 (2020).
[27] M. J. Gullans and D. A. Huse, Phys. Rev. X **10**, 041020 (2020).
[28] O. Alberton, M. Buchhold, and S. Diehl, Phys. Rev. Lett. **126**, 170602 (2021).
[29] T. Müller, S. Diehl, and M. Buchhold, Physical Review Letters **128**, 010605 (2022).
[30] J. C. Hoke, M. Ippoliti, D. Abanin, R. Acharya, M. Ansmann, F. Arute, K. Arya, A. Asfaw, J. Atalaya, J. C. Bardin, *et al.*, arXiv:2303.04792 (2023).
[31] I. Poboiko, P. Pöpperl, I. V. Gornyi, and A. D. Mirlin, arXiv:2304.03138.
[32] M. B. Plenio and S. F. Huelga, New Journal of Physics **10**, 113019 (2008).
[33] P. Rebentrost, M. Mohseni, I. Kassal, S. Lloyd, and A. Aspuru-Guzik, New Journal of Physics **11**, 033003 (2009).
[34] F. Caruso, S. F. Huelga, and M. B. Plenio, Phys. Rev. Lett. **105**, 190501 (2010).
[35] S. Viciani, M. Lima, M. Bellini, and F. Caruso, Phys. Rev. Lett. **115**, 083601 (2015).
[36] C. Maier, T. Brydges, P. Jurcevic, N. Trautmann, C. Hempel, B. P. Lanyon, P. Hauke, R. Blatt, and C. F. Roos, Phys. Rev. Lett. **122**, 050501 (2019).
[37] L. Corman, P. Fabritius, S. Häusler, J. Mohan, L. H. Dogra, D. Husmann, M. Lebrat, and T. Esslinger, Phys. Rev. A **100**, 053605 (2019).
[38] P. Bredol, Phys. Rev. B **103**, 035404 (2021).
[39] P. Bredol, H. Boschker, D. Braak, and J. Mannhart, Phys. Rev. B **104**, 115413 (2021).
[40] M.-Z. Huang, J. Mohan, A.-M. Visuri, P. Fabritius, M. Talebi, S. Wili, S. Uchino, T. Giamarchi, and T. Esslinger, Phys. Rev. Lett. **130**, 200404 (2023).
[41] A.-M. Visuri, T. Giamarchi, and C. Kollath, Physical Review Letters **129**, 056802 (2022).
[42] O. Entin-Wohlman, Y. Imry, and A. Aharony, Phys. Rev. B **70**, 075301 (2004).
[43] D. Rossini, A. Ghermaoui, M. B. Aguilera, R. Vatré, R. Bouganne, J. Beugnon, F. Gerbier, and L. Mazza, Phys. Rev. A **103**, L060201 (2021).
[44] M. Nakagawa, N. Tsuji, N. Kawakami, and M. Ueda, Phys. Rev. Lett. **124**, 147203 (2020).
[45] L. Rosso, D. Rossini, A. Biella, and L. Mazza, Phys. Rev. A **104**, 053305 (2021).
[46] G. Mazza and M. Schirò, Phys. Rev. A **107**, L051301 (2023).
[47] A.-M. Visuri, T. Giamarchi, and C. Kollath, Phys. Rev. Res. **5**, 013195 (2023).
[48] A.-M. Visuri, J. Mohan, S. Uchino, M.-Z. Huang, T. Esslinger, and T. Giamarchi, arXiv:2304.00928.
[49] T. Jin, M. Filippone, and T. Giamarchi, Phys. Rev. B **102**, 205131 (2020).
[50] H. Fröml, A. Chiocchetta, C. Kollath, and S. Diehl, Phys. Rev. Lett. **122**, 040402 (2019).
[51] T. Müller, M. Gievers, H. Fröml, S. Diehl, and A. Chiocchetta, Phys. Rev. B **104**, 155431 (2021).
[52] F. Giazotto, T. T. Heikkilä, A. Luukanen, A. M. Savin, and J. P. Pekola, Rev. Mod. Phys. **78**, 217 (2006).
[53] G. Benenti, G. Casati, K. Saito, and R. S. Whitney, Physics Reports **694**, 1 (2017).
[54] C. Elouard, D. Herrera-Martí, B. Huard, and A. Auffèves, Physical Review Letters **118**, 260603 (2017).
[55] C. Elouard and A. N. Jordan, Phys. Rev. Lett. **120**, 260601 (2018).
[56] M. Naghiloo, J. J. Alonso, A. Romito, E. Lutz, and K. W. Murch, Phys. Rev. Lett. **121**, 030604 (2018).
[57] L. Bresque, P. A. Camati, S. Rogers, K. Murch, A. N. Jordan, and A. Auffèves, Phys. Rev. Lett. **126**, 120605 (2021).
[58] J. Stevens, D. Szombati, M. Maffei, C. Elouard, R. Assouly, N. Cottet, R. Dassonneville, Q. Ficheux, S. Zeppetzauer, A. Bienfait, A. N. Jordan, A. Auffèves, and B. Huard, Phys. Rev. Lett. **129**, 110601 (2022).
[59] X. Linpeng, L. Bresque, M. Maffei, A. N. Jordan, A. Auffèves, and K. W. Murch, Phys. Rev. Lett. **128**, 220506 (2022).
[60] K. Liu, M. Nakagawa, and M. Ueda, arXiv:2303.08326 (2023).
[61] B. Annby-Andersson, F. Bakhshinezhad, D. Bhattacharyya, G. D. Sousa, C. Jarzynski, P. Samuelsson, and P. P. Potts, Physical Review Letters **129**, 050401 (2022).
[62] S. Ryu, R. López, L. Serra, and D. Sánchez, Nature Communications **13** (2022).
[63] A. J. Daley, Advances in Physics **63**, 77 (2014).
[64] T. Prosen, New Journal of Physics **10**, 043026 (2008).
[65] M. Žnidarič, Journal of Statistical Mechanics: Theory and Experiment **2010**, L05002 (2010).
[66] L. M. Sieberer, M. Buchhold, and S. Diehl, Reports on Progress in Physics **79**, 096001 (2016).
[67] M. V. Medvedyeva, F. H. L. Essler, and T. Prosen, Phys. Rev. Lett. **117**, 137202 (2016).
[68] P. Strasberg, G. Schaller, T. L. Schmidt, and M. Esposito, Phys. Rev. B **97**, 205405 (2018).
[69] R. S. Whitney, arXiv:2304.03106 (2023).
[70] A. Levy and R. Kosloff, EPL (Europhysics Letters) **107**, 20004 (2014).
[71] P. P. Hofer, M. Perarnau-Llobet, L. D. M. Miranda, G. Haack, R. Silva, J. B. Brask, and N. Brunner, New Journal of Physics **19**, 123037 (2017).
[72] T. Novotný, Europhysics Letters (EPL) **59**, 648 (2002).
[73] P. E. Dolgirev, J. Marino, D. Sels, and E. Demler, Phys. Rev. B **102**, 100301 (2020).
[74] T. Jin, J. S. Ferreira, M. Filippone, and T. Giamarchi, Physical Review Research **4**, 013109 (2022).
[75] Y. Meir and N. S. Wingreen, Physical Review Letters **68**, 2512 (1992).
[76] L. Buffoni, A. Solfanelli, P. Verrucchi, A. Cuccoli, and M. Campisi, Phys. Rev. Lett. **122**, 070603 (2019).
[77] Generalizations with more terminals and internal degrees of freedom (*e.g.* spin) are straightforward.
[78] J. Dalibard, Y. Castin, and K. Molmer, Phys. Rev. Lett. **68**, 580 (1992).
[79] K. Jacobs and D. A. Steck, Contemporary Physics **47**, 279 (2006).
[80] X. Cao, A. Tilloy, and A. D. Luca, SciPost Phys. **7**, 024 (2019).
[81] H. Haken and G. Strobl, Zeitschrift für Physik A Hadrons and nuclei **262**, 135 (1973).
[82] D. Bernard, T. Jin, and O. Shpielberg, EPL (Europhysics Letters) **121**, 60006 (2018).
[83] D. Bernard and T. Jin, Phys. Rev. Lett. **123**, 080601 (2019).
[84] X. Turkeshi and M. Schiró, Phys. Rev. B **104**, 144301 (2021).
[85] X. Turkeshi, L. Piroli, and M. Schiró, arXiv:2306.09893.

[86] See the Supplemental Material for technical details and additional information.

[87] A. Kamenev, *Field Theory of Non-Equilibrium Systems* (Cambridge University Press, 2011).

[88] S. Datta, *Electronic Transport in Mesoscopic Systems* (Cambridge University Press, 1995).

[89] As we consider the stationary regime, $\langle d_j^\dagger(t) d_i(t)\rangle$ does not depend on time.

[90] R. Landauer, IBM Journal of Research and Development **1**, 223 (1957).

[91] Remarkably, it is also possible to have $\langle n\rangle = \langle n\rangle_{\rm eq}$ with $\gamma \neq 0$, provided that both the hybridization functions Γ_r do not depend on frequency, which is also a condition to suppress the non-reciprocal current.

[92] G. Breit and E. Wigner, Phys. Rev. **49**, 519 (1936).

[93] M. Buttiker, IBM Journal of Research and Development **32**, 63 (1988).

[94] R. Sánchez and M. Büttiker, Phys. Rev. B **83**, 085428 (2011).

[95] R. Sánchez, H. Thierschmann, and L. W. Molenkamp, New Journal of Physics **19**, 113040 (2017).

[96] G. Rosselló, R. López, and R. Sánchez, Phys. Rev. B **95**, 235404 (2017).

[97] F. Mazza, R. Bosisio, G. Benenti, V. Giovannetti, R. Fazio, and F. Taddei, New Journal of Physics **16**, 085001 (2014).

[98] B. Sothmann, R. Sánchez, and A. N. Jordan, Nanotechnology **26**, 032001 (2014).

[99] G. Fleury, C. Gorini, and R. Sánchez, Applied Physics Letters **119**, 043101 (2021).

[100] H. M. Pastawski, Phys. Rev. B **44**, 6329 (1991).

[101] H. M. Pastawski, Phys. Rev. B **46**, 4053 (1992).

[102] M. J. Gullans and D. A. Huse, Physical Review X **9**, 021007 (2019).

[103] L. Hruza and D. Bernard, Phys. Rev. X **13**, 011045 (2023).

[104] B. Cleuren, B. Rutten, and C. Van den Broeck, Phys. Rev. Lett. **108**, 120603 (2012).

[105] A. Mari and J. Eisert, Phys. Rev. Lett. **108**, 120602 (2012).

[106] H. B. Callen, *Thermodynamics and an Introduction to Thermostatistics* (American Association of Physics Teachers, 1998).

[107] L. I. Glazman and R. I. Shekhter, Soviet Journal of Experimental and Theoretical Physics **67**, 163 (1988).

[108] N. S. Wingreen, K. W. Jacobsen, and J. W. Wilkins, Physical Review Letters **61**, 1396 (1988).

[109] A.-P. Jauho, N. S. Wingreen, and Y. Meir, Phys. Rev. B **50**, 5528 (1994).

[110] D. Braak and J. Mannhart, Foundations of Physics **50**, 1509 (2020).

[111] B. Oksendal, *Stochastic Differential Equations* (Springer Berlin Heidelberg, 2003).

[112] A. I. Larkin and Y. N. Ovchinnikov, Zhurnal Eksperimentalnoi i Teoreticheskoi Fiziki **73**, 299 (1977).

Supplemental Material of "Exact description of transport and non-reciprocity in monitored quantum devices"

In this Supplemental Material, we recall how averaging over the results of weak measurements of an operator $\mathcal{O}$ leads to the Lindblad dynamics described by Eq. (1) in the main text. We then derive explicitly the contributions to the self-energy $\mathbf{\Sigma}$ coming from non-interacting reservoirs with energy filters, used for numerical applications in the main text, and, in particular, from monitoring – Eq. (3) in the main text. We provide details about the derivation of the self-consistent formula for the correlation matrix $\mathcal{D}$ – Eq. (4) in the main text – and the exact expressions for the particle and heat currents – Eq. (5) in the main text. We then establish the equivalence between the Lindblad dynamics induced by averaged measurements of the operator $\mathcal{O}$ and the coupling of the operator $\mathcal{O}$ to a bosonic bath at infinite temperature and large chemical potential.

LINDBLAD DYNAMICS INDUCED IN AVERAGE BY CONTINUOUS MONITORING

Continuous weak monitoring

In this section, we briefly discuss how the Lindbladian in Eq. (1) of the main text originates from an evolution under continuous measurement of the operator $\mathcal{O} = \sum_{ij} d_i^\dagger O_{ij} d_j$ with $O_{ij}^* = O_{ji}$. The associated monitored dynamics of the quantum state is described by a stochastic Schrödinger equation. Taking the Itō prescription, the infinitesimal increment of the wave-function $d|\psi_t\rangle = |\psi_{t+dt}\rangle - |\psi_t\rangle$ obeys [79]

$$d\,|\psi_t\rangle = \left[-i\mathcal{H} - \gamma\left(\mathcal{O} - \langle\mathcal{O}\rangle_t\right)^2\right]|\psi_t\rangle\,dt + \sqrt{2\gamma}\left(\mathcal{O} - \langle\mathcal{O}\rangle_t\right)|\psi_t\rangle\,dB_t\,, \tag{S1}$$

where $\mathcal{H}$ is the Hamiltonian of the system, $\langle\mathcal{O}\rangle_t = \langle\psi_t|\mathcal{O}|\psi_t\rangle$ and γ is the measurement strength. The quantity dB_t is the increment of a stochastic Wiener process B_t, which, according to Itō rules [111], behaves in average as $\mathbb{E}[dB_t] = 0$ and $dB_t^2 = dt$. The equation ruling the dynamics of the mean density matrix $\rho_t = \mathbb{E}\left[|\psi_t\rangle\langle\psi_t|\right]$ is then obtained by averaging over all measurement outcomes and over the noise realizations B_t. It satisfies the differential equation

$$\begin{aligned} d\rho_t &= \mathbb{E}\left[(d\,|\psi_t\rangle)\langle\psi_t| + |\psi_t\rangle\,(d\,\langle\psi_t|) + (d\,|\psi_t\rangle)(d\,\langle\psi_t|)\right] && \text{(S2)}\\ &= \mathbb{E}\left[-i[\mathcal{H}, |\psi_t\rangle\langle\psi_t|]dt - \gamma[\mathcal{O}, [\mathcal{O}, |\psi_t\rangle\langle\psi_t|]]dt + \sqrt{2\gamma}\{\mathcal{O} - \langle\mathcal{O}\rangle_t, |\psi_t\rangle\langle\psi_t|\}dB_t\right] && \text{(S3)}\\ &= -i[\mathcal{H}, \rho_t]dt - \gamma[\mathcal{O}, [\mathcal{O}, \rho_t]]dt\,, && \text{(S4)} \end{aligned}$$

where we have neglected all terms of order $dB_t dt$ and dt^2 and used the Itō rules $dB_t^2 = dt$ and $\mathbb{E}[dB_t] = 0$.

Importantly, we see that the second term in Equation S4 involves a double commutator, which reproduces the Lindblad form $\mathcal{D}[\rho] = \gamma(2\mathcal{O}\rho\mathcal{O} - \{\mathcal{O}^2, \rho\})$, see also Eq. (1) in the main text. Since we consider observables $\mathcal{O}$ and Hamiltonians $\mathcal{H}$ that are quadratic in the creation and annihilation operators, on average, the contribution of the measurements to the evolution equation of n-point correlators close on themselves.

We illustrate this last point on the two-point function $G_{k,l}(t) = \langle d_k d_l^\dagger\rangle_t = \mathrm{tr}[\rho_t d_k d_l^\dagger]$. If we suppose a quadratic Hamiltonian of the form $\mathcal{H} = \sum_{i,j} d_i^\dagger h_{ij} d_j$, thanks to the cyclic properties of the trace, one finds that the time evolution of the correlation function G is ruled by the differential equation

$$\frac{d}{dt}G_{k,l}(t) = \frac{d}{dt}\langle d_k d_l^\dagger\rangle_t = i\langle[\mathcal{H}, d_k d_l^\dagger]\rangle_t - \gamma\langle[\mathcal{O}, [\mathcal{O}, d_k d_l^\dagger]]\rangle_t\,. \tag{S5}$$

Since both the operators $\mathcal{H}$ and $\mathcal{O}$ are quadratic in the creation and annihilation operators d and $d^\dagger$, the commutators also generate quadratic operators. As a consequence, one can write down a closed system of equations for the elements of the correlation matrix G:

$$\frac{d}{dt}G(t) = -i[h, G(t)] - \gamma[O, [O, G(t)]]. \tag{S6}$$

Such considerations extend to any n-point correlation function.

Equivalence to averaged evolution of a quantum stochastic Hamiltonian

Alternatively, the averaged evolution equation (S4) can also be generated by the quantum stochastic Hamiltonian (QSH):

$$d\mathcal{H}_t = \sqrt{2\gamma} O dB_t, \tag{S7}$$

where B_t is the same Wiener process as above. The infinitesimal evolution of the wave-function is unitary and reads

$$|\psi_{t+dt}\rangle = e^{-i\mathcal{H}dt - id\mathcal{H}_t}|\psi_t\rangle \qquad \Longrightarrow \qquad d|\psi_t\rangle = -i(\mathcal{H}+d\mathcal{H}_t)dt|\psi_t\rangle - \gamma\mathcal{O}^2 dt|\psi_t\rangle\,, \tag{S8}$$

where we have again discarded terms of order $dB_t dt$ and dt^2 and applied $dB_t^2 = dt$. The infinitesimal evolution generated by this term on the density matrix $\rho_t = \mathbb{E}\left[|\psi_t\rangle\langle\psi_t|\right]$ reads

$$d\rho_t = -i[\mathcal{H},\rho_t]dt - \frac{1}{2}[d\mathcal{H}_t,[d\mathcal{H}_t,\rho_t]] = -i[\mathcal{H},\rho_t]dt - \gamma[\mathcal{O},[\mathcal{O},\rho_t]]dt, \tag{S9}$$

where we have again made use of the fact that $\mathbb{E}[dB_t] = 0$ and which coincides with Eq. (S4).

If we are only interested in the average evolution of the density matrix, it is advantageous to use the unraveling in terms of QSHs. Indeed, for this procedure, the evolution at the stochastic level is both unitary and quadratic in fermionic creation and annihilation operators, meaning that Gaussian states are preserved under evolution. Additionally, the equations of motion remain linear at the stochastic level - differently from the monitored case.

Note however that, despite these advantages, the inclusion of thermal baths with finite memory time is still challenging, as it will render the equations of motion non-local in time. An additional powerful property of QSHs for that matter is that, at the field theory level, the self-consistent Born approximate (SCBA) is *exact* for QSHs [49, 73]. This allows to express all observables of interest in a closed-form even in the presence of thermal baths as we will discuss in Section .

SELF-ENERGY OF THE SYSTEM: RESERVOIRS AND MONITORING CONTRIBUTIONS

We recall that we consider density matrices ρ evolving according to the Lindblad equation

$$\partial_t\rho = -i\left[\mathcal{H},\ \rho\right] + \gamma\left(2\mathcal{O}\rho\mathcal{O} - \{\mathcal{O}^2,\rho\}\right)\,, \tag{S10}$$

where $\mathcal{O} = \sum_{ij} d_i^\dagger O_{ij} d_j$ is the monitored single particle operator. The Hamiltonian describes a system tunnel coupled to reservoirs in the generic form $\mathcal{H} = \mathcal{H}_{\rm res} + \mathcal{H}_{\rm T} + \mathcal{H}_{\rm sys}$, with

$$\mathcal{H} = \underbrace{\sum_{k,r=L,R}\varepsilon_{r,k}c_{r,k}^\dagger c_{r,k}}_{\text{Reservoir}} + \underbrace{\sum_{k,i,r=L/R}\left[t_{r,ki}c_{r,k}^\dagger d_i + t_{r,ki}^* d_i^\dagger c_{r,k}\right]}_{\text{Tunnel Coupling}} + \underbrace{\sum_{i,j} d_i^\dagger h_{ij} d_j}_{\text{System}}\,, \tag{S11}$$

where $c_{r,k}$ destroys electrons in the mode k of the left ($r=L$) or right ($r=R$) reservoir and $\{d_i^\dagger, d_i\}$ forms a complete, ortho-normal set of single-electron creation and annihilation operators acting on the system.

To derive the self-energies associated to reservoirs and monitoring, we rely on the Keldysh path-integral formalism [87], which can be extended to dissipative systems [66]. In this formalism, the partition function of the system $\mathcal{Z} = \mathrm{tr}[\rho(t)]$ is expressed in the form

$$\mathcal{Z} = \int \mathcal{D}\left[\bar{c},c,\bar{d},d\right] e^{i\mathcal{S}\left[\bar{c},c,\bar{d},d\right]}\,, \tag{S12}$$

where $\left[\bar{c},c,\bar{d},d\right]$ is a set of Grassmann variables on the Keldysh contour corresponding to the creation and annihilation operators in Eq. (S11). The action $\mathcal{S}$ corresponding to Eq. (S10) has a unitary and a dissipative component $\mathcal{S} = \mathcal{S}_U + \mathcal{S}_D$. We adopt Larkin-Ovchinnikov's convention [112] for generic Grassman variables ψ

$$\psi^1 = \frac{\psi^+ + \psi^-}{\sqrt{2}}\,, \qquad \psi^2 = \frac{\psi^+ - \psi^-}{\sqrt{2}}\,, \qquad \bar{\psi}^1 = \frac{\bar{\psi}^+ - \bar{\psi}^-}{\sqrt{2}}\,, \qquad \bar{\psi}^2 = \frac{\bar{\psi}^+ + \bar{\psi}^-}{\sqrt{2}}\,. \tag{S13}$$

In this convention, the unitary action corresponding to the Hamiltonian (S11) reads, in frequency space,

$$\mathcal{S}_U = \int \frac{d\omega}{2\pi} \left[\sum_{k,r} \bar{c}_{r,k}(\omega) \boldsymbol{\mathcal{C}}^{-1}_{r,k}(\omega) c_{r,k}(\omega) - \sum_{r,ki} \left[t_{r,ki}\, \bar{c}_{r,k}(\omega) \cdot d_i(\omega) + t^*_{r,ki}\, \bar{d}_i(\omega) \cdot c_{r,k}(\omega) \right] + \sum_{ij} \bar{d}_i(\omega) \boldsymbol{\mathcal{G}}^{-1}_{0,ij}(\omega) d_j(\omega) \right], \tag{S14}$$

where we used the shorthand vector notation $\bar{c} = (\bar{c}^1 \quad \bar{c}^2)$, $c = (c^1 \quad c^2)^T$ and analogous for d and $\bar{d}$. The Green's functions have a retarded, advanced and Keldysh component

$$\boldsymbol{\mathcal{G}} = \begin{pmatrix} \mathcal{G}^R & \mathcal{G}^K \\ 0 & \mathcal{G}^A \end{pmatrix}. \tag{S15}$$

In the case of the action (S14), the inverse of the Green's function of the reservoirs and system read, respectively,

$$\boldsymbol{\mathcal{C}}^{-1}_{r,k}(\omega) = \begin{bmatrix} \omega - \varepsilon_{r,k} + i0^+ & 2i\pi 0^+ \tanh\left[\frac{\omega-\mu_r}{2T_r}\right] \\ 0 & \omega - \varepsilon_{r,k} - i0^+ \end{bmatrix}, \qquad \boldsymbol{\mathcal{G}}^{-1}_{0,ij}(\omega) = \begin{bmatrix} \omega - h_{ij} + i0^+ & 0 \\ 0 & \omega - h_{ij} - i0^+ \end{bmatrix}, \tag{S16}$$

where the infinitesimal Keldysh component of $\boldsymbol{\mathcal{G}}_0$ can be safely ignored, being regularized by the integration of the reservoirs, see Section .

The dissipative contribution of the action is instead diagonal in time and reads

$$\mathcal{S}_D = i\gamma \int dt \sum_{ijkl} O_{ij} O_{kl} \left[\bar{d}^1_i(t) d^1_j(t) \bar{d}^1_k(t) d^1_l(t) + 2\bar{d}^1_i(t) d^1_j(t) \bar{d}^2_k(t) d^2_l(t) + \bar{d}^2_i(t) d^2_j(t) \bar{d}^2_k(t) d^2_l(t) \right]. \tag{S17}$$

This action can be derived by averaging over the quantum stochastic unitary dynamics, see Section .

Both the presence of reservoirs and monitoring modify the Green's functions of the system $\boldsymbol{\mathcal{G}}$ through a self-energy $\boldsymbol{\Sigma}$, according to the Dyson equation

$$\boldsymbol{\mathcal{G}} = \left[\boldsymbol{\mathcal{G}}_0^{-1} - \boldsymbol{\Sigma} \right]^{-1}. \tag{S18}$$

We proceed with the calculation of such contributions below.

Self-energy with generic reservoirs and explicit expression with energy filters

The contribution to the self-energy due to the presence of reservoirs, $\boldsymbol{\Sigma}_{L/R}$, can be obtained by Gaussian integration of the reservoirs, namely of the fields $c_{r,k}$ and $\bar{c}_{r,k}$ in the action (S14). Completing the square in Eq. (S14), one finds the self-energy associated to generic reservoirs reported in the main text

$$\boldsymbol{\Sigma}_{r,ij}(\omega) = \sum_k t^*_{r,ki} t_{r,kj} \boldsymbol{\mathcal{C}}_{r,k}(\omega) = \sum_k t^*_{r,ki} t_{r,kj} \begin{bmatrix} \frac{1}{\omega - \varepsilon_{r,k} + i0^+} & -2i\pi\delta(\omega - \varepsilon_{r,k}) \tanh\left(\frac{\omega-\mu_r}{2T_r}\right) \\ 0 & \frac{1}{\omega - \varepsilon_{r,k} - i0^+} \end{bmatrix}. \tag{S19}$$

We derive an explicit expression of this self-energy for the numerical applications used in the main text. The simplest way to obtain an explicit form of a frequency-dependent hybridization function $\Gamma_r(\omega)$ consists in considering the reservoirs as a lead with a constant density of states ν_0, which is coupled to the system via an energy filter of energy ε_r, see sketches in Fig. S1. We also neglect all energy dependence of the tunnel amplitudes. The Hamiltonians describing this situation, and which are used for the two numerical applications in the main text, read

$$\mathcal{H}_1 = \sum_{r,k} \left[\varepsilon_{r,k} c^\dagger_{r,k} c_{r,k} + \tau \left(c^\dagger_{r,k} c_r + c^\dagger_r c_{r,k} \right) \right] + \sum_r \varepsilon_r c^\dagger_r c_r + t \sum_r \left[c^\dagger_r d + d^\dagger c_r \right] + \varepsilon_d d^\dagger d\,, \tag{S20}$$

$$\mathcal{H}_2 = \sum_{r,k} \left[\varepsilon_{r,k} c^\dagger_{r,k} c_{r,k} + \tau \left(c^\dagger_{r,k} c_r + c^\dagger_r c_{r,k} \right) \right] + t \sum_r \left[c^\dagger_r d_r + d^\dagger_r c_r \right] + \sum_r \varepsilon_r \left[c^\dagger_r c_r + d^\dagger_r d_r \right], \tag{S21}$$

where the operators c_r and $c^\dagger_r$ act on the filters and where we have also made explicit, in $\mathcal{H}_2$, that filters and levels have the same energy ε_r. This is the assumption used in the numerical applications of the main text in the context of quantum measurement cooling, but it is not necessary at all for the following discussion.

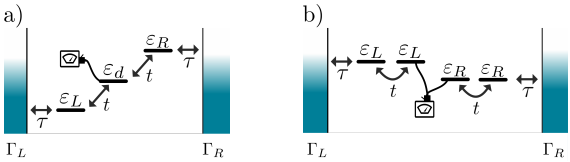

Figure S1. Schematic representation of the systems described by the Hamiltonians (S20) and (S21), used for numerical applications concerning a) Monitored density engine and b) Quantum measurement cooling in the main text, respectively. Each reservoir is tunnel coupled to a single level through a constant tunnel coupling τ. These levels act as energy filters, which are in turn coupled to the system via a tunneling strength t.

Switching back to the field theory language, we proceed now with the integration of all the fields $(c, \bar{c})$, associated with the reservoirs. We start with those with labels (r, k), corresponding to a metallic lead with a constant density of states ν_0. Focusing on the case of $\mathcal{H}_1$ in Eq. (S20), their integration leads to a self-energy contribution of the form (S19) to the energy-filters $(c_r, \bar{c}_r)$, which leads to a Keldysh action of the form

$$\mathcal{S}_1 = \int \frac{d\omega}{2\pi} \left\{ \sum_r \bar{c}_r(\omega) \begin{bmatrix} \omega - \varepsilon_r + i\Delta & 2i\Delta \tanh\left(\frac{\omega-\mu_r}{2T_r}\right) \\ 0 & \omega - \varepsilon_r - i\Delta \end{bmatrix} c_r(\omega) \right.$$
$$\left. -t \sum_r \left[\bar{c}_r(\omega) \cdot d(\omega) + \bar{d}(\omega) \cdot c_r(\omega) \right] + \bar{d}(\omega) \begin{bmatrix} \omega - \varepsilon_d & 0 \\ 0 & \omega - \varepsilon_d \end{bmatrix} d(\omega) \right\}, \quad \text{(S22)}$$

where $\Delta = \pi\nu_0\tau^2$ is the standard expression of the hybridization constant for a single level coupled to a metallic reservoir with a constant density of states in the wide-band limit. The action corresponding to $\mathcal{H}_2$ in Eq. (S21) is analogous. Notice also that the Keldysh component of the inverse Green's function in the first term of Eq. (S22) is now finite and we can send the infinitesimal term in the Keldysh component of the last term of Eq. (S22) safely to zero. The Gaussian integration of the filters $(c_r, \bar{c}_r)$ leads to the final form of the self-energy used for the numerical applications in the main text, namely

$$\Sigma_r(\omega) = \begin{bmatrix} \frac{t^2}{\omega - \varepsilon_r + i\Delta} & -2i\Gamma_r(\omega) \tanh\left(\frac{\omega-\mu_r}{2T_r}\right) \\ 0 & \frac{t^2}{\omega - \varepsilon_r - i\Delta} \end{bmatrix}, \quad \text{(S23)}$$

where we have also introduced the hybridization function

$$\Gamma_r(\omega) = \frac{\Sigma_r^A(\omega) - \Sigma_r^R(\omega)}{2} = -\mathrm{Im}\Sigma_r^R(\omega) = \frac{t^2\Delta}{(\omega - \varepsilon_r)^2 + \Delta^2}, \quad \text{(S24)}$$

which has the Lorentzian shape sketched in Figs. 1a and 2a of the main text.

Validity of the self-consistent Born scheme for the monitoring contribution to the self-energy

The action (S17), associated to the monitoring of the observable $\mathcal{O}$ averaged over the measurement outcomes, is a quartic action in the Grassmann fields and thus cannot be integrated using Gaussian integrals. However, it is possible to derive an exact expression of the self-energy according to the self-consistent Born scheme, Eq. (3) in the main text. The idea is to rely on the unraveling procedure corresponding to Eq. (S7). The corresponding action reads

$$\mathcal{S}_{\mathrm{QSH}} = -\sum_{i,j} \int dt \sqrt{2\gamma} O_{ij} \left[\bar{d}_i^1(t) d_j^1(t) + \bar{d}_i^2(t) d_j^2(t) \right] \xi(t). \quad \text{(S25)}$$

One can readily verify that performing the Gaussian noise average with moments $\mathbb{E}[\xi(t)] = 0$ and $\mathbb{E}[\xi(t)\xi(t')] = \delta(t-t')$ directly leads to the dissipative action (S17)

$$\mathbb{E}[e^{i\mathcal{S}_{\mathrm{sto}}}] = \int D[\xi] e^{i\mathcal{S}_{\mathrm{sto}} - \int dt \xi^2(t)/2} = e^{i\mathcal{S}_{\mathcal{D}}}. \quad \text{(S26)}$$

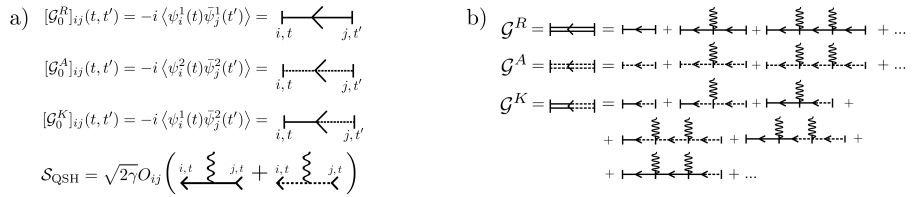

Figure S2. a) Diagrammatic representation of the bare retarded, advanced and Keldysh Green functions and of the vertex associated to the quantum stochastic action (S25). Full lines represent the retarded propagator, dashed lines the advanced one, and mixed lines the Keldysh propagator. b) Diagrammatic expansion of the retarded, advanced and Keldysh propagators. At a given order n in the expansion, only one diagram contributes to the retarded/advanced self-energy, whereas the Keldysh component has $n+1$ diagrammatic contributions, corresponding to the insertion of the Keldysh bare component at different times.

Figure S3. a) Diagrammatic representation of the averaging over the noise realizations. The fact that the noise is Gaussian and δ-correlated in time is represented by connecting two wiggly lines, which are then contracted to a single point in time. b) Example of a crossing diagram for the Keldysh component. The red lines highlight the part of the diagram violating the causality structure, as it features two retarded components with opposite directions in time. This diagram thus vanishes and can be discarded.

The unraveling corresponding to Eq. (S25) thus corresponds to a Hubbard-Stratonovich transformation, where the action becomes quadratic in terms of the Grassmann variables at the price of introducing the time-dependent noise $\xi(t)$. However, the fact that the *averaged* noise is δ-correlated in time allows a dramatic simplification of the diagrammatic expansion of the single-particle correlation functions in terms of the measurement strength γ.

Consider the diagrammatic representation of the Green's function in Fig. S2a. The vertex corresponding to Eq. (S25) only connects solid lines with solid ones and dashed lines with dashed ones. As a consequence, in the diagrammatic expansion of the retarded (advanced) propagators only retarded (advanced) propagators appear. For the Keldysh component, one can switch only once from dashed to solid lines through the insertion of a Keldysh propagator, see Fig. S2b.

Averaging over noise realizations corresponds diagrammatically to imposing an equal time index when connecting wiggly lines, see Fig. S3a. The key insight is that after noise-averaging the diagrams, those with crossing wiggly lines do not contribute to the action. In Fig. S3b, we show an example of a diagram with crossing wiggly lines arising from the diagrammatic expansion of the Keldysh component. In that example, after averaging, two retarded propagators run in opposite time directions. As a consequence, this diagram involves the multiplication of two retarded functions with opposite time-dependence, which equals zero. Similar considerations apply for all crossing diagrams, and we redirect the interested reader to Refs. [73, 74] for the complete demonstration. Since the crossing diagrams vanish, the Born non-crossing approximation is exact, and all the remaining non-crossing diagrams can be exactly re-summed, leading to the self-consistent equation for the self-energy

$$\mathbf{\Sigma}^{\gamma}_{ij}(t,t') = 2\gamma\delta(t-t')\sum_{pq} O_{ip}\boldsymbol{\mathcal{G}}_{pq}(t,t)O_{qj}\,, \tag{S27}$$

which corresponds to Eq. (3) in the main text.

DERIVATION OF THE SELF-CONSISTENT EQ. (4) IN THE MAIN TEXT

The way to solve the self-consistent equation (S27) for its retarded and advanced components is given in the main text. We provide here additional details concerning the solution of its Keldysh component leading to Eq. (4) in the main text. We first recall that the total self-energy includes the contributions from the reservoirs. It has thus the

form $\Sigma^K = \Sigma^K_R + \Sigma^K_L + 2\gamma O\mathcal{G}^K\mathcal{O}$, with $\Sigma^K_{L/R}$ given in Eq. (S23). We then rely on the fact that $\mathcal{G}^K = \mathcal{G}^R\Sigma^K\mathcal{G}^A$ to derive, in time representation,

$$\mathcal{G}^K(t,t) = -2i\int\frac{d\omega}{2\pi}\mathcal{G}^R(\omega)\left[\sum_{r=L/R}(1-2f_r(\omega))\Gamma_r(\omega)\right]\mathcal{G}^A(\omega) + 2\gamma\int\frac{d\omega}{2\pi}\mathcal{G}^R(\omega)O\mathcal{G}^K(t,t)O\mathcal{G}^A(\omega)\,. \tag{S28}$$

Relying on the identities

$$\mathcal{G}^R - \mathcal{G}^A = \mathcal{G}^R(\Sigma^R - \Sigma^A)\mathcal{G}^A = -2i\mathcal{G}^R\big(\Gamma_L + \Gamma_R + \gamma\mathcal{O}^2\big)\mathcal{G}^A\,, \qquad \mathcal{D}_{ij} = \langle d^\dagger_j d_i\rangle = \frac{\delta_{ij} - i\mathcal{G}^K_{ij}(t,t)}{2}\,, \tag{S29}$$

we can apply the property

$$i\int\frac{d\omega}{2\pi}[\mathcal{G}^R(\omega) - \mathcal{G}^A(\omega)] = \mathbb{1}\,, \tag{S30}$$

to derive a self-consistent equation for the correlation matrix $\mathcal{D}$, namely

$$\mathcal{D} = \int\frac{d\omega}{\pi}\mathcal{G}^R(\omega)\left[\sum_{r=L/R}f_r(\omega)\Gamma_r(\omega) + \gamma O\mathcal{D}O\right]\mathcal{G}^A(\omega)\,, \tag{S31}$$

which corresponds to Eq. (4) in the main text. Equations of this type can be solved by vectorization or by direct substitution, for a few site systems.

FORMULA FOR CURRENTS IN MONITORED SYSTEMS – EQ. (5) OF THE MAIN TEXT

In the presence of interactions or dissipation, the Landauer-Büttiker expressions [88, 90] for elastic transport are no longer applicable and several extensions have been derived [75, 101]. We follow here the approach of Meir and Wingreen [49, 75] and show how it can be used to derive Eq. (5) of the main text. We start by considering the particle ($\zeta = 0$) and heat ($\zeta = 1$) currents flowing into the reservoir r – Eq. (2) in the main text

$$J^\zeta_r = i\sum_{k,i}(\varepsilon_{r,k} - \mu_r)^\zeta\left[t^*_{r,ki}\langle d^\dagger_i c_{r,k}\rangle - t_{r,ki}\langle c^\dagger_{r,k}d_i\rangle\right] = \sum_{k,i}\int\frac{d\omega}{4\pi}(\varepsilon_{r,k} - \mu_r)^\zeta\left[t^*_{r,ki}\mathcal{G}^K_{rk,i}(\omega) - t_{r,ki}\mathcal{G}^K_{i,rk}(\omega)\right]\,, \tag{S32}$$

where we have introduced the Keldysh correlation functions $\mathcal{G}^K_{i,kr}(t,t') = -i\langle[d_i(t), c^\dagger_{r,k}(t')]\rangle$ and $\mathcal{G}^K_{kr,i}(t,t') = -i\langle[c_{r,k}(t), d^\dagger_i(t')]\rangle$. By performing the diagrammatic expansion of these correlation functions in the tunnel amplitudes $t_{r,ki}$, one finds that they can be factorized as

$$\mathcal{G}^K_{rk,i}(\omega) = \mathcal{C}^R_{r,k}(\omega)\sum_j t_{r,kj}\mathcal{G}^K_{j,i}(\omega) + \mathcal{C}^K_{r,k}(\omega)\sum_j t_{r,kj}\mathcal{G}^A_{j,i}(\omega)\,, \tag{S33}$$

$$\mathcal{G}^K_{i,rk}(\omega) = \mathcal{C}^A_{r,k}(\omega)\sum_j t^*_{r,kj}\mathcal{G}^K_{i,j}(\omega) + \mathcal{C}^K_{r,k}(\omega)\sum_j t^*_{r,kj}\mathcal{G}^R_{i,j}(\omega)\,, \tag{S34}$$

where the correlation functions $\boldsymbol{\mathcal{C}}_{r,k}(\omega)$ are the correlation functions of the *isolated* reservoirs given in Eq. (S16), whereas the correlation functions $\boldsymbol{\mathcal{G}}$ are the full Green's functions of the system *including both reservoirs and monitoring*. By inserting Eqs. (S33-S34) into Eq. (S32), we then derive the expression

$$J^\zeta_r = \sum_{k,i,j}\int\frac{d\omega}{4\pi}(\varepsilon_{r,k} - \mu_r)^\zeta\, t_{r,ki}t^*_{r,kj}\Big[\Big(\mathcal{C}^R_{r,k}(\omega) - \mathcal{C}^A_{r,k}(\omega)\Big)\mathcal{G}^K_{i,j}(\omega) + \mathcal{C}^K_{r,k}(\omega)\Big(\mathcal{G}^A_{i,j}(\omega) - \mathcal{G}^R_{i,j}(\omega)\Big)\Big]\,. \tag{S35}$$

Exploiting the fact that $\mathcal{C}^R_{r,k}(\omega) - \mathcal{C}^A_{r,k}(\omega) = -2\pi i\delta(\omega - \varepsilon_{r,k})$ and that $\mathcal{C}^K_{r,k}(\omega) = -2\pi i\delta(\omega - \varepsilon_{r,k})\tanh[(\omega - \mu_r)/2T_r]$ we obtain:

$$J^\zeta_r = -i\int\frac{d\omega}{2\pi}(\omega - \mu_r)^\zeta\,\mathrm{tr}\Big[\Gamma_r(\omega)\mathcal{G}^K(\omega) + (1 - 2f_r(\omega))\Gamma_r(\omega)\Big(\mathcal{G}^A(\omega) - \mathcal{G}^R(\omega)\Big)\Big]\,, \tag{S36}$$

where we have introduced the generalized hybridization function $\Gamma_{r,ij}(\omega) = \pi \sum_k t_{r,ki} t^*_{r,kj} \delta(\omega - \varepsilon_{r,k})$. Note that although Eq. (S24) corresponds to the particular case of a reservoir composed of a metallic lead tunnel coupled to an energy filter the relation $\Gamma_r(\omega) = [\Sigma_r^A(\omega) - \Sigma_r^R(\omega)]/2$ is always valid.

The formula (S36) also applies to the monitored systems described by the Liouvillian dynamics (S10). Injecting the exact expressions Eqs. (S28-S29), we derive Eq. (5) in the main text, namely

$$J_r^\zeta = \frac{2}{\pi} \int d\omega \underbrace{(\omega - \mu_r)^\zeta \, (f_{\bar{r}} - f_r) \, \mathrm{tr}\left[\Gamma_r \mathcal{G}^R \Gamma_{\bar{r}} \mathcal{G}^A\right]}_{\text{elastic}} + \gamma \frac{2}{\pi} \int d\omega \underbrace{(\omega - \mu_r)^\zeta \, \mathrm{tr}\left[\Gamma_r \mathcal{G}^R O \left(\mathcal{D} - f_r \mathbb{1}\right) O \mathcal{G}^A\right]}_{\text{inelastic}} . \tag{S37}$$

LINDBLAD DYNAMICS INDUCED BY A BOSONIC BATH AT LARGE TEMPERATURE AND CHEMICAL POTENTIAL

In this section, we show how the Lindblad dynamics of Eq. (1) in the main text can also describe the situation where a bosonic bath of large temperature and chemical potential is coupled to the monitored operator $\mathcal{O}$. This situation is described by a Hamiltonian of the form, $\mathcal{H} = \sum_k \varepsilon_k b_k^\dagger b_k + \tau \sum_k (b_k + b_k^\dagger)\mathcal{O}$, with the operator $\mathcal{O}$ being hermitian and quadatic $\mathcal{O} = \sum_{ij} d_i^\dagger O_{ij} d_j$, and where the operators b_k and $b_k^\dagger$ annihilate and create bosons of energy ε_k in the bath. To derive the Keldysh action associated to this Hamiltonian, we follow the standard convention defining rotated classical and quantum bosonic fields in the Keldysh action [87]

$$b^c = \frac{b^+ + b^-}{\sqrt{2}} , \qquad\qquad b^q = \frac{b^+ - b^-}{\sqrt{2}} , \tag{S38}$$

which also applies for the complex counterparts, at variance from the Grassman fermionic variables, see Eq. (S13). The resulting action reads

$$\begin{aligned} \mathcal{S}_{\text{boson bath}} = \sum_k \int dt dt' \left[\begin{array}{cc} \bar{b}_k^c & \bar{b}_k^q \end{array}\right]_t [\boldsymbol{\mathcal{B}}_k(t-t')]^{-1} \left[\begin{array}{c} b_k^c \\ b_k^q \end{array}\right]_{t'} - \\ \tau \sum_{k,i,j} O_{i,j} \int dt \left[\frac{\bar{b}_k^c + b_k^c}{\sqrt{2}} (\bar{d}_i^1 d_j^1 + \bar{d}_i^2 d_j^2) + \frac{\bar{b}_k^q + b_k^q}{\sqrt{2}} (\bar{d}_i^1 d_j^2 + \bar{d}_i^2 d_j^1)\right] , \end{aligned} \tag{S39}$$

where $\boldsymbol{\mathcal{B}}_k$ is the Green's matrix of the isolated ($\tau = 0$) bosonic bath, which in frequency space reads

$$\boldsymbol{\mathcal{B}}_k(\omega) = \begin{bmatrix} \mathcal{B}_k^K(\omega) & \mathcal{B}_k^R(\omega) \\ \mathcal{B}_k^A(\omega) & 0 \end{bmatrix} = \begin{bmatrix} -2i\pi\delta(\omega - \varepsilon_k) \coth\left(\frac{\omega - \mu_B}{2T_B}\right) & \frac{1}{\omega - \varepsilon_k + i0^+} \\ \frac{1}{\omega - \varepsilon_k - i0^+} & 0 \end{bmatrix} , \tag{S40}$$

where μ_B and T_B are the chemical potential and the temperature of the bosonic bath respectively. The bosonic degrees of freedom of the action (S39) can be integrated using a Gaussian integral to obtain

$$\begin{aligned} \mathcal{S}'_{\text{boson bath}} &= -\frac{\tau^2}{2} \sum_{k,i,j,k,l} O_{ij} O_{kl} \int dt dt' \left[\begin{array}{cc} \bar{d}_i^1 d_j^1 + \bar{d}_i^2 d_j^2 & \bar{d}_i^1 d_j^2 + \bar{d}_i^2 d_j^1 \end{array}\right]_t \boldsymbol{\mathcal{B}}_k(t-t') \left[\begin{array}{c} \bar{d}_k^1 d_l^1 + \bar{d}_k^2 d_l^2 \\ \bar{d}_k^1 d_l^2 + \bar{d}_k^2 d_l^1 \end{array}\right]_{t'} \\ &= -\frac{\tau^2}{2} \sum_{k,i,j,k,l} O_{ij} O_{kl} \int dt dt' \Big\{ \left(\bar{d}_i^1 d_j^1 + \bar{d}_i^2 d_j^2\right)_t \mathcal{B}_k^K(t-t') \left(\bar{d}_k^1 d_l^1 + \bar{d}_k^2 d_l^2\right)_{t'} + \\ &\qquad \left(\bar{d}_i^1 d_j^1 + \bar{d}_i^2 d_j^2\right)_t \left[\mathcal{B}_k^R(t-t') + \mathcal{B}_k^A(t'-t)\right] \left(\bar{d}_k^1 d_l^2 + \bar{d}_k^2 d_l^1\right)_{t'} \Big\} . \end{aligned} \tag{S41}$$

We want to find the conditions for which this action maps onto the action (S17), corresponding to the Lindbladian in Eq. (S10). For this, the last term in Eq. (S41) must vanish and $\sum_k \mathcal{B}_k^K(t-t')$ is proportional to a δ-function in time, or, equivalently, its Fourier transform does not depend on frequency. The last term in Eq. (S41) is proportional to

$$\begin{aligned} \sum_k \left[\mathcal{B}_k^R(t-t') + \mathcal{B}_k^A(t'-t)\right] &= -i\theta(t-t') \sum_k \left[e^{-i\varepsilon_k(t-t')} - e^{i\varepsilon_k(t-t')}\right] \\ &= -i\theta(t-t') \int d\omega \, \nu(\omega) \left[e^{-i\omega(t-t')} - e^{i\omega(t-t')}\right] , \end{aligned} \tag{S42}$$

where we have introduced the density of states of the bosonic bath $\nu(\omega)$. If this density of states is constant, the contribution (S42) vanishes as well as the last term in Eq. (S41).

The k-integration of the Keldysh component gives instead

$$\sum_k \mathcal{B}^K(t) = -i \int d\omega\, \nu(\omega) \coth\left(\frac{\omega - \mu_B}{2T_B}\right) e^{-i\omega t}\,, \tag{S43}$$

which would equal $\sum_k \mathcal{B}^K(t) \simeq 2\pi i \coth(\mu_B/2T_B)\delta(t)$, if we can neglect the energy dependence of the density of states $\nu(\omega)$ and of the cotangent in the integration. Assuming negative chemical potential, one finds the action (S17) by making the identification

$$\gamma = \pi\tau^2 \coth\left(\frac{|\mu_B|}{2T_B}\right)\,. \tag{S44}$$

The above approximations can be justified in the limit where the density of states of the bosonic bath is constant for energies comparable to the spectral width of the fermionic system to which the bosonic bath is coupled to, and in the limit where μ_B and T_B are much larger than the spectral width of the fermionic system. Similar arguments were used to derive loss and gain terms in the Lindblad form by allowing the system to exchange particles with a fermionic reservoir with a much larger temperature and chemical potential [49].

3.2 Hydrodynamic description of diffusive QSHs

As motivated in the introduction, the question of diffusion revolves around the appearance of Fick's law (1.1), a classical hydrodynamic equation appearing in a quantum context. It suggests that diffusive systems support an effective hydrodynamic description characterized by a single transport parameter, the diffusion constant D. Such an effective theory describes the dynamics at a coarse-grain length scale (hydrodynamic length), whose unit cell encodes a large number of microscopic degrees of freedom. This concept forms the rationale behind quantum generalized hydrodynamics which, with significant success [28, 122, 123], presumes such a scale's existence. However, finding a procedure capable of predicting the effective hydrodynamic theory starting from the microscopic model remains an open question.

In this work, we propose the $1/N$ expansion as a (potentially generic) procedure to establish such an effective hydrodynamic theory for diffusive systems. The main idea is to find *the* effective action, $\tilde{S}$, that captures all relevant properties of the system in the $N \to \infty$ limit, and then compute transport quantities perturbatively as $1/N$ corrections to it.

To obtain the effective action is not enough to expand it in the system's parameters, e.g. hopping or coupling. Instead, one must first scale the system to the thermodynamic limit and then perform a coarse-graining scheme to extract $\tilde{S}$, see Fig. 3.2a. In Eq. ⟦8⟧, we propose a real-space coarse-graining procedure that groups together a sites to form a single cell of the new coarse-grained lattice. Both the scaling and coarse-grain are done at a fixed interaction/noise strength which requires evaluating the Green's function in non-perturbative regimes, a difficult task for generic interacting models. However, the exact solution of the QSHs allows us to benchmark this procedure against our class of QSHs with excellent results.

At a coarse-grain level and for infinite systems $N = \infty$, we expect the action to be exactly Gaussian and composed of uncoupled cells in local thermal equilibrium. Each cell is characterized by a local chemical potential $\tilde{\mu}$, temperature $\tilde{T}$, and self-energy $\tilde{\Sigma}$, see Eq. ⟦9,10⟧, with the latter encoding the relaxation processes inside the cell. This ansatz aligns with the intuition that in this limit the current vanishes, $J^0 \sim N^{-1} \to 0$, and the expectation that quantum diffusive systems support a finite correlation length where thermalization occurs (similar to classical systems [68, 124, 125]). Since the effective action $\tilde{S}$ predicts zero particle flow, the diffusive transport must originate from the finite size corrections to the action, which scale as $1/N$. We conjecture that these $1/N$ corrections include all the action components that do not commute with the local particle number, such as, but not limited, to hopping terms. Consequently, the diffusive particle current can be calculated as a perturbation in these terms, Eq. ⟦11⟧. indices are nice.

It is our hope that the $1/N$ expansion can be shown to work in the context of interacting systems, but doing so requires performing the coarse-grain procedure in an already notoriously difficult problem. Extensive QSHs offer an ideal testing ground

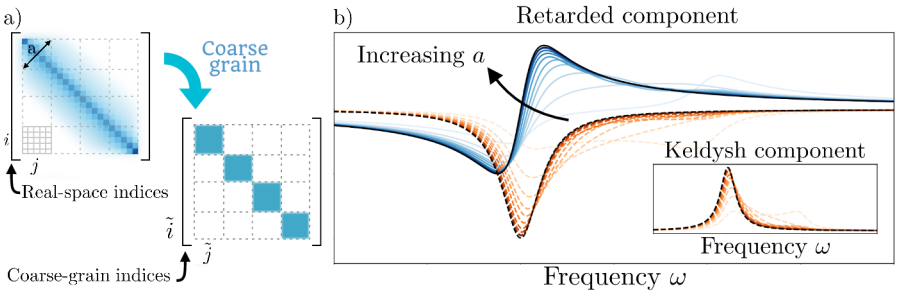

Figure 3.2: Adaptation from Fig. [[2,10]] of the paper. a) Schematic view of the coarse-graining procedure where a sites in the microscopic model are grouped to create a new cell in the coarse-grained lattice. In the thermodynamic limit, the cells become uncoupled and in local thermal equilibrium. b) Example of the coarse-grain scheme in the dephasing model. As more sites are included in the coarse-grain cell (light to dark colors), the effective Green's functions converge to the ansatz of Eq. ⟦8,9⟧ plotted as full and dashed lines.

for our theory, as they exhibit diffusive physics while allowing for a simple numerical solution to the Green's functions, see App. D for numerical considerations. In this work, we test the $1/N$ expansion against three extensive QSHs with different spacial noise correlations, dedicating the bulk of our efforts to the dephasing model. In this thesis's notation, the dephasing model corresponds to the QSH composed of N local occupation operators acting with the same rate, $\{Q\} = \{c_1^\dagger c_1, ..., c_N^\dagger c_N\}$. We consider symmetric reservoirs in the wide-band limit (2.68) but at finite temperature, where the inelastic current does not have the unbiased contribution discussed in Sec. 3.1.

The driven dephasing model is a prototypical model of diffusion, even supporting an analytic solution in terms of MPS [31] when assuming Lindblad reservoirs. Moreover, through the unravellings already introduced in App. B and C, it can also be understood as coupling the chain to either N independent bosonic reservoirs or N independent measurement apparatus [69, 126], as explored in Sec. 3.3. We wish to use the $1/N$ expansion to predict the emergence of Fick's law in QSHs and obtain an expression for the diffusion constant from the microscopic parameters. To obtain the effective action $\tilde{S}$, we directly carry out the coarse-graining procedure for increasingly larger coarse-graining cells, observing how the Green's function in the effective lattice evolves, see Fig. 3.2b. At some point, the off-diagonal elements of $\mathcal{G}$ converge to zero, while the diagonal terms converge towards Eq. ⟦9,10⟧, indicating that we reached the hydrodynamic scale. Afterward, we can extract the parameters of effective theory parameters via a direct fit. For all QSHs under study, see Fig. ⟦7⟧, we find that $\tilde{\Sigma}(\omega) = -2\tau + i\gamma$ and $\tilde{\mu}, \tilde{T} = \infty$ with a finite ratio $\tilde{\mu}/\tilde{T}$ determined by the local occupancy of the chain. The system is thus locally in an infinite temper-

ature state [66], as expected from the unraveling of Sec. B. Having obtained $\tilde{S}$, the effective parameters can be inserted into the perturbative calculation of the current. We find that, at the coarse-grain level, the current satisfies Fick's law with the correct diffusion constant for all the model's parameters, see Eq. ⟦51⟧. We replicated the same procedure for other QSHs and once again found Fick's law with the correct diffusion constant for every parameter, motivating the nomenclature of quantum stochastic resistors.

Surprisingly, the $1/N$ expansion's applicability extends beyond diffusive systems. Another model under consideration is the long-range noise

$$\{Q\} \propto \left\{ \frac{c_i^\dagger c_j}{|i-j|^\alpha} \right\}_{i=1,j>i}^{N}, \tag{3.2}$$

which, by changing the power-law exponent α, exhibits a unconventional ballistic-to-diffusive transition in the thermodynamic limit at a critical value α_c which depends on γ ($\alpha_c \leq 3$ for $\gamma \geq 0$). Across the transition, Fick's law still holds but the diffusion constant diverges with the system size for $\alpha \leq \alpha_c$. In the Lindblad driving limit, the $1/N$ expansion is capable of predicting the correct diffusion constant (and divergence thereafter) for any α, as well as the correct scaling coefficients. It is not clear why the $1/N$ expansion can predict the existence of a ballistic regime. It might relate to the fact that the system is never coherent, and the ballistic nature is a consequence that, in the $\alpha \to 0$ limit, every site in the chain is equally but incoherently coupled to every other site.

The $1/N$ expansion is naturally suitable to compute bulk properties, e.g. the diffusion constant, but cannot compute contact properties, e.g. the conductance $G = \lim_{\mu_L - \mu_R \to 0} J^0/(\mu_L - \mu_R)$, which depend on the details of the reservoirs, see Fig. ⟦9⟧. In Sec. 3.3, we address this deficiency by introducing a semi-classical description of diffusive transport.

Lastly, we hope that the $1/N$ expansion can be extended to interacting systems with minimal modifications to the coarse-graining procedure. If this is the case, we might be able to find a procedure to compute the effective self-energy directly from the microscopic theory.

Exact description of quantum stochastic models as quantum resistors

Tony Jin [1], João S. Ferreira [1], Michele Filippone [1,2] and Thierry Giamarchi [1]
[1]*Department of Quantum Matter Physics, Ecole de Physique University of Geneva, Quai Ernest-Ansermet 24, CH-1211 Geneva 4, Switzerland*
[2]*Université Grenoble Alpes, CEA, IRIG-MEM-L_Sim, F-38000 Grenoble, France*

(Received 28 June 2021; accepted 14 December 2021; published 11 February 2022)

We study the transport properties of generic out-of-equilibrium quantum systems connected to fermionic reservoirs. We develop a perturbation scheme in the inverse system size, named $1/N$ expansion, to study a large class of out of equilibrium diffusive/ohmic systems. The bare theory is described by a Gaussian action corresponding to a set of independent two level systems at equilibrium. This allows a simple and compact derivation of the diffusive current as a first-order pertubative term. In addition, we obtain exact solutions for a large class of quantum stochastic Hamiltonians (QSHs) with time and space dependent noise, using a self-consistent Born diagrammatic method in the Keldysh representation. We show that these QSHs exhibit diffusive regimes, which are encoded in the Keldysh component of the single particle Green's function. The exact solution for these QSHs models confirms the validity of our system size expansion ansatz, and its efficiency in capturing the transport properties. We consider in particular three fermionic models: (i) a model with local dephasing, (ii) the quantum simple symmetric exclusion process model, and (iii) a model with long-range stochastic hopping. For (i) and (ii) we compute the full temperature and dephasing dependence of the conductance of the system, both for two- and four-points measurements. Our solution gives access to the regime of finite temperature of the reservoirs, which could not be obtained by previous approaches. For (iii), we unveil a ballistic-to-diffusive transition governed by the range and the nature (quantum or classical) of the hopping. As a byproduct, our approach equally describes the mean behavior of quantum systems under continuous measurement.

DOI: 10.1103/PhysRevResearch.4.013109

I. INTRODUCTION

Diffusion is the transport phenomenon most commonly encountered in nature. It implies that globally conserved quantities such as energy, charge, spin, or mass spread uniformly all over the system according to Fick/Ohm's law

$$J = -D\nabla n, \tag{1}$$

where the diffusion constant D relates the current density J to a superimposed density gradient ∇n.

Despite its ubiquity, understanding the emergence of classical diffusive phenomena from underlying quantum mechanical principles is highly nontrivial. Early works based on field theory and perturbative methods [1,2] pointed out the possibility that interactions do not necessarily lead to diffusion at finite temperature, a question addressed then more rigorously by using the concepts of integrability [3]. These questions have then fueled many exciting discoveries in low-dimensional interacting systems [4]. A notable example is the ballistic-to-diffusive transition in quantum integrable *XXZ* spin chains [5–10], which also exhibit a superdiffusive point in the Kardar-Parisi-Zhang universality class [9,11–14]. These discoveries have motivated the generalized hydrodynamical descriptions of integrable systems [15,16], providing an elegant path to the question of diffusion at finite temperature [17], and paving the way to the description of diffusive phenomena based on perturbative approaches [18–23].

The out-of-equilibrium driving protocol illustrated in Fig. 1, where a system is coupled to external dissipative baths, has been crucial to unveil and characterize such exotic transport phenomena [6,7,24,25]. It allows to study disordered systems [26–28], uncover novel integrable structures [6,29], and show diffusive transport [30–35]. These open quantum systems [36–38], are described within the Lindblad formalism [39,40], which is actively employed to investigate the exotic dynamics induced by nontrivial interactions with external degrees of freedom, such as lattice vibrations, quantum measurements [41–46], dephasing [47–52], losses [53–57], coupling to a lightfield [58–60], and environmental engineering [61].

This research activity is also motivating ongoing experiments, where recent progress in space- and time-resolved techniques is applied to directly observe emergent diffusive and exotic dynamics in various quantum systems, including cold atoms [58,62–65], spin chains [66–71], and solid-state [72–74]. In this context, theoretical predictions are usually made case-by-case, with strong constraints on geometries and driving protocols [75]. Thus, devising versatile tools to solve generic quantum models that show diffusion becomes crucial to understand emerging classical Ohmic transport.

In this paper, we develop a novel approach to characterize the bulk transport properties of quantum resistors, which we show to be *exact* and *systematic* for a wide class of quantum stochastic Hamiltonians (QSHs). Our starting point is the Meir-Wingreen's formula [76,77] (MW), which expresses the current J of a system driven at its boundaries, see Fig. 1, in terms of single-particle Green's functions. We show that, for Ohmic systems, the MW formula supports an expansion of the current in terms of the inverse of the system size N. We illustrate how to perform practically this $1/N$ expansion, which reveals efficient to derive the diffusive current and the diffusion constant: we assume that, in the $N \to \infty$ limit, diffusive lattices admit a simple description in terms of independently equilibrated sites and demonstrate that a well-chosen perturbation theory over this trivial state leads to the desired $1/N$ expansion.

We provide a comprehensive demonstration of the validity of our approach in the context of QSHs. Relying on diagrammatic methods and out-of-equilibrium field theory [78], we show that single-particle Green's functions of QSHs can be exactly and systematically derived relying on the self-consistent Born approximation (SCBA)—a generalization of previous results derived for a dephasing impurity in a thermal bath [49]. Equipped with this exact solution, and relying on MW formula, we explicitly derive the dissipative current flowing in the system and show that the Keldysh component of the single particle Green's function encodes the Ohmic suppression of the current. Then, we explicitly derive the asymptotically equilibrated state by "coarse-graining" of single-particle Green's functions and validate our procedure to perform the $1/N$ expansion.

We illustrate the effectiveness and versatility of our approach for three different QSHs of current interest: (i) the dephasing model [29–31,79,80]; (ii) the quantum symmetric simple exclusion process (QSSEP) [34,81–85]; and (iii) models with stochastic long range hopping [45,86]. The case studies (i) and (ii) illustrate the effectiveness of our approach, providing simple derivations of the current J and of the diffusion constant D, in alternative to approaches relying on matrix-product state [30,31,79], integrability [29], or other case-by-case solutions [32,34]. Additionally, we address previously unexplored regimes, by exactly solving the out-of-equilibrium problem with fermion reservoirs at arbitrary temperatures and chemical potentials. Our approach also allows to access two-times correlators in the stationary state, which were not described by previous studies. For case (iii), we show instead the ability of our approach to predict novel and nontrivial transport phenomena, namely a displacement of the ballistic-to-diffusive transition induced by coherent nearest-neighbor tunneling in one-dimensional chains. A byproduct of our analysis is that all the results presented here apply also for system under continuous measurement, which are currently attracting a lot of interest in the context of measurement induced phase transition [41,43,45,86].

Our paper is structured as follows. Section II describes how the MW formula is a good starting point to build a systematic expansion of the current in terms of the inverse system size N. Section III presents QSH and shows the exactitude of SCBA for the computation of single-particle self-energies. Section IV shows how our formalism allows to fully compute the transport properties of the dephasing model, the QSSEP, and the long-range model. Section V is dedicated to our conclusions and the discussion of the future research perspectives opened by our work.

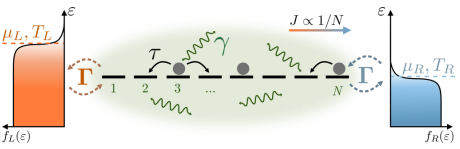

FIG. 1. A stationary current J flows in a one-dimensional lattice when connected to left (L) and right (R) fermionic reservoirs, described by Fermi distributions $f(\varepsilon)$ with different temperatures T or chemical potentials μ. The wiggly lines denote dissipative degrees of freedom acting on the system with rate γ. For a fixed difference of chemical potential $\delta\mu = \mu_L - \mu_R$, dissipative terms are normally responsible for the Ohmic suppression of the current, $J \propto 1/N$.

II. RESISTIVE SCALING IN FINITE-SIZE BOUNDARY DRIVEN SYSTEMS AND PERTURBATIVE APPROACH

In this section, we introduce generic tools aimed at studying diffusive transport in boundary-driven setups like those of Fig. 1. For these setups, the current is given by the MW formula [76]. In the simplified (yet rather general) situation, where the reservoirs have a constant density of states and the tunnel exchange of particles does not depend on energy, the MW formula reads (we assume $e = \hbar = k_B = 1$):

$$J = i \int \frac{d\omega}{2\pi} \mathrm{Tr}\Big\{ \frac{1}{2}(\Gamma_L - \Gamma_R) G^{\mathcal{K}} + \times \Big[\Big(f_L - \frac{1}{2}\Big)\Gamma_L - \Big(f_R - \frac{1}{2}\Big)\Gamma_R \Big] \big(G^{\mathcal{R}} - G^{\mathcal{A}}\big) \Big\}, \quad (2)$$

where $f_{L(R)}(\omega) = [e^{(\omega - \mu_{L(R)})/T_{L(R)}} + 1]^{-1}$ are the Fermi distributions associated to the left and right reservoir with chemical potentials $\mu_{L(R)}$ and temperatures $T_{L(R)}$. $G^{\mathcal{R}/\mathcal{A}/\mathcal{K}}$ are the retarded ($\mathcal{R}$), advanced ($\mathcal{A}$), and Keldysh ($\mathcal{K}$) components of the single-particle Green's functions of the system. They are defined in time representation as $G^{\mathcal{R}}_{j,k}(t-t') = -i\theta(t-t')\langle\{c_j(t), c_k^\dagger(t')\}\rangle$, $G^{\mathcal{A}}_{j,k}(t-t') = [G^{\mathcal{R}}_{j,k}(t'-t)]^*$ and $G^{\mathcal{K}}_{j,k}(t-t') = -i\langle[c_j(t), c_k^\dagger(t')]\rangle$, where the (curly)square brackets indicate (anti)commutation [87]. c_j is the annihilation operator of a spinless fermion at site j. The $\Gamma_{L(R)}$ matrices describe system-reservoirs couplings.

Our aim is to establish a systematic procedure to compute diffusive current for large systems. The starting point will be the state of the system in the thermodynamic limit ($N \to \infty$). By identifying in the MW formula (2) the terms leading to Fick's law (1), we motivate the simple structure of the problem for an infinite system size. In resistive systems, a fixed difference of density $\Delta n := n_1 - n_N$ at the edges of the system enforces the $1/N$ suppression of the current ($J \propto \nabla n \propto \Delta n/N$). It is thus natural to perform a perturbative $1/N$ expansion of the current on the $N \to \infty$ state. We conjecture a possible perturbation scheme and show its validity in the context of QSHs.

Without loss of generality, we focus on discrete $1D$ lattice systems of size N [88]. In this case, the $\Gamma_{L(R)}$ matrices in Eq. (2) acquire a simple form in position space: $[\Gamma_{L(R)}]_{j,k} = \Gamma\delta_{j,1(N)}\delta_{j,k}$. We also express the local densities in terms of Green's functions, namely, $2n_j = 2\langle c_j^\dagger c_j\rangle = 1 - i\int d\omega\, G^{\mathcal{K}}_{j,j}(\omega)/(2\pi)$, which also implies $2i\Delta n = G^{\mathcal{K}}_{1,1}(t=0) - G^{\mathcal{K}}_{N,N}(t=0) = \Delta G^{\mathcal{K}}$. The MW formula then acquires the more compact form:

$$J = \Gamma\int d\omega[f_L(\omega)\mathcal{A}_L(\omega) - f_R(\omega)\mathcal{A}_R(\omega)] - \Gamma\Delta n, \quad (3)$$

where we have introduced the local spectral densities $\mathcal{A}_{L(R)}(\omega) = -\frac{1}{\pi}\mathrm{Im}[G^{\mathcal{R}}_{1,1(N,N)}(\omega)]$ and made use of the fact that $\int d\omega\mathcal{A}_{L(R)}(\omega) = 1$.

The local spectral densities $\mathcal{A}_{L(R)}(\omega)$ exponentially converge in the thermodynamic limit $N\to\infty$. This feature is generally expected and is illustrated in Fig. 8 for different classes of QSHs. This observation allows to establish that the $1/N$ scaling, proper to diffusive currents, must entirely arise from Δn in (3). The possibility to ignore the size-dependence of the first term of (3) imposes strong constraints on the $1/N$ expansion of the difference of density Δn in diffusive systems. If we write this expansion as

$$2i\Delta n = \Delta G^{\mathcal{K}} = \Delta G^{(\infty)} + \frac{1}{N}\Delta G' + \ldots, \quad (4)$$

one notices immediately that the leading term $\Delta G^{(\infty)}$ has to compensate the first one in (3), implying

$$\frac{\Delta G^{(\infty)}}{2i} = \int d\omega[f_L(\omega)\mathcal{A}_{1,1}(\omega) - f_R(\omega)\mathcal{A}_{N,N}(\omega)]. \quad (5)$$

A sufficient but not necessary condition fulfilling this relation is obtained by imposing at each boundary:

$$\int\frac{d\omega}{2\pi}G^{\mathcal{K}(\infty)}_{L(R)}(\omega) = -i\int d\omega\tanh\left(\frac{\omega-\mu_{L(R)}}{2T_{L(R)}}\right)\mathcal{A}_{L(R)}(\omega), \quad (6)$$

which will turn out to be satisfied for QSHs. These relations have a simple and interesting interpretation. In the infinite size limit, the flowing current is zero and thus the stationary value of the densities at the boundary can be computed by supposing that they fulfill a *fluctuation-dissipation* relation or equivalently, that these sites are at equilibrium with the neighboring reservoirs.

Reinjecting (4) in the MW formula gives the current

$$J = i\frac{\Gamma}{2N}\Delta G' \quad (7)$$

and as expected, we get the $1/N$ diffusive scaling. This relation tells us that the information about the diffusion constant is hidden in the $1/N$ correction to the density profile, which can be in general a nontrivial quantity to compute. However, we will see in the following that there is a shorter path to access it via the use of an infinite system size perturbation theory.

The main idea of the $1/N$ perturbation is to find an effective simple theory that captures the relevant properties of the system in the $N\to\infty$ limit. From there, transport quantities are computed *perturbatively* on top of this limit theory. To determine this effective theory, we conjecture that there is a typical length a beyond which two points of the systems can be considered to be statistically independent. Thus, by coarse-graining the theory over cells of size a, each cell becomes uncoupled and in local equilibrium, see Fig. 2.

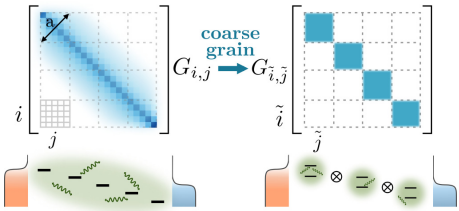

FIG. 2. Cartoon picture of the coarse-graining procedure. On the left, spacial correlations in the infinite size limit are depicted. These decay exponentially as a function of the distance and are nonzero only within a finite length a. By coarse-graining the theory over this typical length, we obtain an effective theory (right) consisting of an ensemble of uncoupled sites with a finite self-energy at equilibrium.

The reasons motivating such factorization are twofold. First, the current is suppressed as $1/N$ in the large system size limit, so the infinite size theory should predict a null stationary current. Second, factorization of stationary correlations has actually been demonstrated for a certain number of diffusive toy models, most notably in the context of large deviations and macroscopic fluctuation theory [34,81,89,90]. For instance, it is known that the nth connected correlation functions of physical observables, such as density, generically behaves as $N^{-(n-1)}$. Thus, it is natural to assume that for $N\to\infty$, correlations must be exponentially decaying over a length a. We will show explicitly that in all of the examples studied, this factorization in the coarse-grained theory will turn out to be true and provide an analytic estimation for a in Appendix F.

We now put these assumptions on formal grounds. Let $\tilde{j}$ and $\tilde{k}$ be the spatial indices of the coarse-grained theory

$$G^{\mathcal{R}/\mathcal{A}/\mathcal{K}}_{\tilde{j},\tilde{k}} := \frac{1}{a}\sum_{m,n=0}^{a-1}G^{\mathcal{R}/\mathcal{A}/\mathcal{K}}_{\tilde{j}a+m,\tilde{k}a+n}. \quad (8)$$

The relation between the different components $\mathcal{R}$, $\mathcal{A}$, and $\mathcal{K}$ of the single particle Green's functions are assumed to describe uncoupled sites at equilibrium with a local self-energy $\Sigma_{\tilde{j}}$ [78]. These conditions require then local fluctuation-dissipation relations of the form

$$G^{\mathcal{K}(\infty)}_{\tilde{j},\tilde{k}}(\omega) = \delta_{\tilde{j},\tilde{k}}\tanh\left(\frac{\omega-\mu_{\tilde{j}}}{2T_{\tilde{j}}}\right)[G^{\mathcal{R}}_{\tilde{j},\tilde{j}}(\omega) - G^{\mathcal{A}}_{\tilde{j},\tilde{j}}(\omega)], \quad (9)$$

with retarded and advanced Green's functions, which are diagonal in the coarse-grained space representation

$$G^{\mathcal{R}(A)}_{\tilde{j},\tilde{k}}(\omega) = \frac{\delta_{\tilde{j},\tilde{k}}}{\omega - \omega^0_{\tilde{j}} \pm \Sigma_{\tilde{j}}(\omega)}. \quad (10)$$

These relations fix entirely the stationary property of the system in the infinite size limit. The specification of the free parameters $\mu_{\tilde{j}}$, $T_{\tilde{j}}$, $\omega^0_{\tilde{j}}$ and $\Sigma_{\tilde{j}}$ have to be done accordingly to the model under consideration. We will see that they take a simple form for QSHs, namely the self-energy $\Sigma_{\tilde{j}}$ is frequency

independent and the $\mu_{\tilde{j}}, T_{\tilde{j}} \gg \omega$ limit can be taken taken in Eq. (9), as expected in the Markovian limit of the dissipative process [77].

To get the current, one needs to go one step further and understand which terms have to be expanded. The thermodynamic equilibrated theory does not exhibit transport, thus should be left invariant by the part of the Hamiltonian that commutes with the conserved quantity, for us the local particle density. It is then natural to conjecture that the perturbative term for the current is given by the dynamical part of the theory, that is, the part of the Hamiltonian $\hat{H}_{\rm dyn}$, which does not commute with the local density. Thus, we conjecture that, at order $1/N$, the current is given by

$$J = \langle \hat{J}\hat{H}_{\rm dyn}\rangle_{\infty}, \tag{11}$$

where the $\langle\rangle_{\infty}$ means the expectation value must be taken with respect to the infinite system size theory. This formula has the remarkable advantage that its computational complexity is very low since the coarse-grained theory is Gaussian. We remark that the $1/N$ expansion presented here is *not* a standard expansion in the hopping amplitude τ, since the latter has an exponentially large degenerate manifold of states at $\tau = 0$.

In Sec. IV, we show explicitly how these ideas unfold for QSHs, by comparing computations done from the $1/N$ theory with the one obtained from the exact solution that we present in the following Section Sec. III. Understanding to which extent and under which conditions Eqs. (9,10) and (11) can be applied is one of the very challenging direction of study, in particular in the context of interacting quantum systems without bulk dissipative terms.

III. VALIDITY OF THE SELF-CONSISTENT BORN APPROXIMATION FOR QUANTUM STOCHASTIC HAMILTONIANS

In this section, we present a class of quantum stochastic models and associated Liouvillians (12), that describe either stochastic local dephasing or stochastic jumps of fermionic particles on a graph. The random processes are defined by a quantum Markov equation also known as a Lindblad equation. We will show explicitly two ways, exemplified by Eqs. (15) and (A1), to associate an underlying quantum stochastic model to such Lindblad equation, a process known as *unraveling* or *dilatation* [91–93]. Of particular interest for us is the description in terms of quantum stochastic Hamiltonians (QSHs) (15). It provides a way to resum exactly the perturbative series associated to the stochastic noise, which coincides with the self-consistent Born approximation (SCBA) for single particle Green's functions. This method was originally devised for the particular case of a single-site dephaser in Ref. [49] and we extend it here to more general situations. We will show in Section IV that, relying on SCBA, we can derive the diffusive transport properties of these models and show the validity of the assumptions underpinning the perturbative $1/N$ expansion presented in Sec. II.

Consider a graph made of discrete points, each corresponding to a site. To such graph we associate a Markovian process where spinless fermions on a given site can jump to any other site only if the target site is empty, see Fig. 3. We define $\gamma_{ij} \geqslant 0$ as the probability rate associated to the process of a fermion jumping from i to j and $\gamma_{ji} = \gamma_{ij}$ the reverse process. The generator of such process is given by the Liouvillian, which acts on the density matrix ρ of the system:

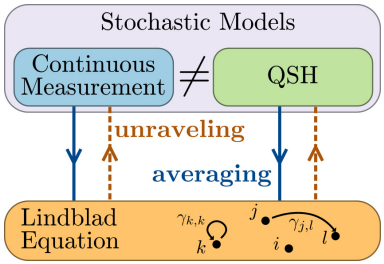

FIG. 3. Schematic representation of our random process. The orange box represents the Lindblad equation (12), which describes random quantum jumps between sites connected by an arrow. An arrow leaving and arriving at the same site represents a local dephasing. To a given Lindblad equation, we can associate multiple stochastic process (blue and green boxes), a process called *unraveling* (orange dashed lines). The Lindblad equation is recovered by averaging over the noisy degrees of freedom (full blue lines). We show that the unraveling in terms of quantum stochastic Hamiltonian (QSH) is particularly useful for the diagrammatic expansion of the theory.

$$\mathcal{L}(\rho) = \sum_{i,j} \gamma_{i,j}(2c_j^{\dagger}c_i\rho c_i^{\dagger}c_j - \{c_i^{\dagger}c_j c_j^{\dagger}c_i, \rho\}). \tag{12}$$

The total evolution of the density matrix ρ is in general given by

$$\frac{d}{dt}\rho = \mathcal{L}_0(\rho) + \mathcal{L}(\rho), \tag{13}$$

where $\mathcal{L}_0$ generates what we call the *free evolution*, in the sense that $\mathcal{L}_0$ is quadratic in the fermion operators c_i and the related spectrum and propagators can be efficiently computed with Wick's theorem [94,95]. Such Liouvillians can generally describe single-particle Hamiltonians or dissipative processes (coherent hopping, losses,...). We will consider $\mathcal{L}(\rho)$ as a perturbation on top of this theory.

There exists a general procedure to see $\mathcal{L}(\rho)$ as the emergent *averaged* dynamics of an underlying microscopic stochastic, yet Hamiltonian, process. Lifting $\mathcal{L}(\rho)$ to this stochastic process is known as *unraveling* and there is not a unique way of doing so, see Fig. 3. The stochastic Hamiltonian can be treated as a perturbation in field theory, which requires the summation of an infinite series. Our strategy is to pick the relevant stochastic theory for which there exists a simple way to reorganize the summation and then take the average in order to get the mean evolution.

We now proceed to present the unraveled theory. Let dH_t be the stochastic Hamiltonian increment, generating the evolution, which is defined by

$$|\psi_{t+dt}\rangle = e^{-idH_t}|\psi_t\rangle. \tag{14}$$

We work in the Itō prescription and consider stochastic Hamiltonians of the form

$$dH_t = \sum_{i,j} \sqrt{2\gamma_{i,j}} c_j^\dagger c_i dW_t^{i,j}. \tag{15}$$

$W_t^{i,j}$ describes a complex noise and we adopt the convention that $W_t^{ij*} = W_t^{j,i}$. The corresponding Itō rules are summed up by

$$dW_t^{i,j} dW_t^{k,l} = \delta_{i,l}\delta_{k,j} dt. \tag{16}$$

Using the Itō rules to average over the noise degrees of freedom one recovers the Liouvillian (12).

Finally, an other point we would like to emphasize concerns the connection to systems evolving under continuous measurements. Indeed, another way to unravel (12) is to see it as the average evolution with respect to the measurement outcomes of a system for which the variables $c_j^\dagger c_i + c_i^\dagger c_j$ and $i(c_i^\dagger c_j - c_j^\dagger c_i)$ are continuously monitored and independently measured with rate $\gamma_{i,j}$ [91]. Although the physics is radically different at the level of a single realisation of the noise, on average it gives the same result than the prescription (15). Hence, all the results that will be presented for the mean behavior of our class of stochastic Hamiltonians also describe the mean behavior of systems subject to continuous measurements. The unraveling procedure corresponding to continuous measurements is described in detail in Appendix A.

A. Self-energy

We show now that the perturbation theory in the stochastic Hamiltonian (15) can be fully resummed, leading to exact results for single particle Green's functions. To perform this task, we rely on the Keldysh path-integral formalism [78], which describes the dynamics of the system through its action S. The presence of dissipative effects can be naturally included in S using Lindblad formalism [96]. The action gives the Keldysh partition function $\mathcal{Z} = \mathrm{tr}(\rho_t)$

$$\mathcal{Z} = \int \mathcal{D}[\psi^\pm, \bar\psi^\pm] e^{iS[\psi^\pm, \bar\psi^\pm]}. \tag{17}$$

where $\psi = (\psi^+, \psi^-)$ are Grassmann variables defined respectively on the positive and negative Keldysh time contours $\mathcal{C}_\pm$. We follow the Larkin-Ovchinnikov's convention [97], in which the Keldysh action S_0 corresponding to the free-evolution $\mathcal{L}_0$ is expressed in terms of the inverse Green's function $\boldsymbol{G}^{-1}$. namely,

$$\mathcal{S}_0 = \sum_{i,j} \int \frac{d\omega}{2\pi} (\bar\psi^1, \quad \bar\psi^2)_i [\boldsymbol{G}^{-1}]_{i,j} \begin{pmatrix} \psi^1 \\ \psi^2 \end{pmatrix}_j. \tag{18}$$

All variables in the integral (18) are implicitly assumed to depend on a single frequency ω, which coincides with the assumption of stationary behavior, valid for our class of problems. The inverse Green's function $\boldsymbol{G}^{-1}$ is itself expressed in terms of the retarded, advanced and Keldysh green functions $G^{\mathcal{R}/A/K}$, defined in Sec. II:

$$[\boldsymbol{G}^{-1}] = \begin{pmatrix} G^{\mathcal{R}} & G^{\mathcal{K}} \\ 0 & G^{\mathcal{A}} \end{pmatrix}^{-1} \tag{19}$$

$$[G_0^{\mathcal{R}}]_{i,j}(t',t) = -i \left\langle \psi_i^1(t') \bar\psi_j^1(t) \right\rangle =$$

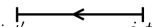

$$[G_0^{\mathcal{A}}]_{i,j}(t',t) = -i \left\langle \psi_i^2(t') \bar\psi_j^2(t) \right\rangle =$$

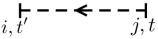

$$[G_0^{\mathcal{K}}]_{i,j}(t',t) = -i \left\langle \psi_i^1(t') \bar\psi_j^2(t) \right\rangle =$$

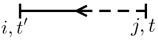

$$0 = -i \left\langle \psi_i^2(t') \bar\psi_j^1(t) \right\rangle$$

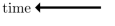

FIG. 4. Diagrammatic representation of the retarded ($\mathcal{R}$), advanced ($\mathcal{A}$) and Keldysh ($\mathcal{K}$) Green's function. Time flows from right to left.

and whose diagrammatic representations in the time domain are given in Fig. 4. The causality structure of the Keldysh Green functions is enforced by the suppression of correlators $\langle \psi^2 \bar\psi^1 \rangle = 0$. This means that a retarded propagator can never become advanced, which pictorially translates into the fact that a solid line cannot switch to a dashed one.

The action corresponding to the Liouvillian term (12) reads [96]

$$S_{\mathcal{L}} := -\int dt \sum_{i,j} \gamma_{i,j} \left(\bar\psi_{j,t}^1 \psi_{i,t}^1 \bar\psi_{i,t}^2 \psi_{j,t}^2 + \bar\psi_{i,t}^1 \psi_{j,t}^1 \bar\psi_{j,t}^2 \psi_{i,t}^2 \right). \tag{20}$$

which is a quartic action in the Grassmann fields. At the level of single particle Green's functions, the action $S_{\mathcal{L}}$ is incorporated through the self-energy $\boldsymbol{\Sigma}$, defined as the sum of all one-particle irreducible diagrams. As in equilibrium field theory, the Dyson equation relates the full propagator to the bare propagator and the self-energies $\boldsymbol{\Sigma}$:

$$\boldsymbol{G} = \left[\boldsymbol{G}_0^{-1} - \boldsymbol{\Sigma} \right]^{-1}. \tag{21}$$

To compute the diffusive current from MW formula, $\boldsymbol{\Sigma}$ must be know to any order; an *a priori* difficult task given the quartic nature of the action (20). Instead, rewriting the action at the stochastic level allows us to exactly derive the self-energy $\boldsymbol{\Sigma}$ and solve this problem. In the field-theory language, the unraveling procedure exemplified by Eq. (15) leads to the equivalent action

$$S_{\mathrm{sto}} = -\sum_{i,j} \int \sqrt{2\gamma_{i,j}} \left(\bar\psi_{j,t}^1 \psi_{i,t}^1 + \bar\psi_{j,t}^2 \psi_{i,t}^2 \right) dW_t^{i,j}, \tag{22}$$

where S_{sto} is related to $S_{\mathcal{L}}$ by the average $\mathbb{E}[]$ over the noise degrees of freedom:

$$\mathbb{E}[e^{iS_{\mathrm{sto}}}] = e^{iS_{\mathcal{L}}}. \tag{23}$$

In formal terms, this transformation is reminiscent of a Hubbard-Stratonovich transformation where the action becomes quadratic in terms of the Grassmann variables. Note that the complexity encoded in Eq. (20) is preserved by the consequent introduction of the space and time dependent noise $dW_t^{i,j}$. However, the noise correlations imposed by Itō's rules (16) allow a dramatic simplification of the diagrammatic expansion in $\gamma_{i,j}$ of the Green functions within the stochastic formulation. Such simplified structure does

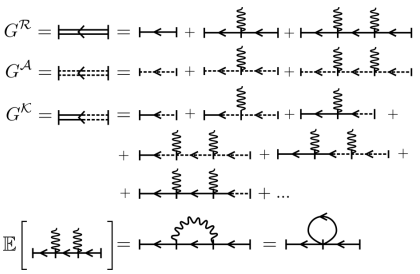

FIG. 5. Perturbative series in the Keldysh formalism for our class of stochastic models. Average quantities are obtained by contracting pairs of wiggly lines together. Here a wiggly line represents either $dW_t^{i,j}$ or its complex conjugated pair for simplicity. The formulation of the theory in terms of QSH allows for a simple writing of the perturbative expansion.

not manifestly appear when working with the Lindbladian (averaged) formulation of the problem (20) (see Fig. 14 in Appendix B).

The resummation works as follows. In Fig. 5, we show the diagrammatic expansion of (21) up to second order in the stochastic noise $\gamma_{i,j}$. The wiggly lines represent $dW_t^{i,j}$. Since we are interested in the mean behavior, we have to take the average over the noise degrees of freedom. This amounts to contract wiggly lines pair by pair. From the Itō rules (16), we see that upon contraction, a wiggly line forces the two vertices it connects to have the same time and position, as illustrated in Fig. 5.

The important consequence is that all the diagrams, which present a *crossing* of the wiggly lines vanish because of the causal structure of the Keldysh's Green function, namely that $G^{\mathcal{R}}(t,t')$ is nonzero only for $t > t'$ and conversely for $G^{\mathcal{A}}$. For a detailed proof of this statement, see Appendix B. In particular, the constraints of avoided wiggly lines establishes the validity of the self-consistent Born approximation (SCBA) for the self-energy of single particle Green's function and generalize the approach presented in Ref. [49]. SCBA allows a simple and compact derivation of all components as exemplified by the diagrammatic representation in Fig. 6. Namely, we have that in position space

$$\boldsymbol{\Sigma}_{i,j}(t,t') = \delta_{i,j}\delta(t,t')\sum_k \gamma_{i,k}\boldsymbol{G}_{k,k}(t,t). \tag{24}$$

For the retarded and advanced components, this relation takes a particularly simple form since $G^{\mathcal{R}(\mathcal{A})}_{j,k}(t,t) = \mp\frac{i}{2}\delta_{j,k}$

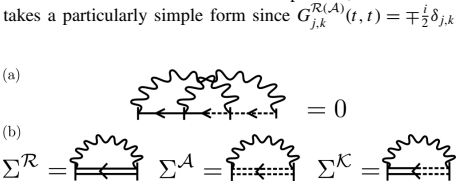

FIG. 6. (a) Noncrossing rule for the contraction of wiggly lines. (b) Self-energies for the different Keldysh components.

in position space. Note that this simple expression is only valid when the two time indices are taken to be equal and comes entirely from the causal structure of the Green's functions in the Keldysh formalism. One way to see this is to evaluate the step function $\theta(t-t')$ for the retarded and advanced Green's functions from the discrete version of the path integral presented in 9.2 of [80]. To get the Keldysh component $G^{\mathcal{K}}$, one has to solve the self-consistent Dyson equation:

$$\boldsymbol{G}^{\mathcal{K}} = -\boldsymbol{G}^{\mathcal{R}}\left(\left[\boldsymbol{G}_0^{-1}\right]^{\mathcal{K}} - \boldsymbol{\Sigma}^{\mathcal{K}}\right)\boldsymbol{G}^{\mathcal{A}}, \tag{25}$$

which is a problem whose complexity only scales polynomially with the number of degrees of freedom in the system (such as the system size N of the setup in Fig. 1). This solves the problem entirely at the level of single-particle correlation functions. Remark that this applies to any model as long as the bare theory respects a Wick's theorem and its propagators are known. It allows a systematic study of quantum systems in the presence of external noisy degrees of freedom.

This ability to calculate the Keldysh Green's function is crucial to give an exact description of out-of-equilibrium transport in dissipative systems, as we are going to show in the next section.

IV. APPLICATIONS

We now proceed to employ the self-consistent approach to showcase our $1/N$ expansion, presented in Sec. II, against a large class of QSHs that display diffusive transport.

The action describing the out-of-equilibrium setting represented in Fig. 1 has the form

$$S = S_{\mathrm{Bd}} + S_0 + S_{\mathrm{sto}}. \tag{26}$$

The first term in the action, S_{Bd}, describes the exchange coupling with gapless noninteracting fermionic reservoirs of chemical potential $\mu_{L,R}$ and temperature $T_{L,R}$. The corresponding action, under the assumptions discussed in Sec. II, was derived for instance in Ref. [77]:

$$S_{\mathrm{Bd}} = i\Gamma\sum_{a=L,R}\int\frac{d\omega}{2\pi}\bar{\psi}_a\begin{bmatrix}1 & 2\tanh\left(\frac{\omega-\mu_a}{2T_a}\right)\\ 0 & -1\end{bmatrix}\psi_a, \tag{27}$$

where ψ_a is a shorthand notation for (ψ_a^1, ψ_a^2), L designates site 1 and R designates site N. The action S_0 is the quadratic action related to the intrinsic dynamics of the system, which can describe various situations from coherent dynamics to single-particle dissipative gains and losses [77]. In this paper, we will focus on one-dimensional nearest-neighbour coherent bulk hopping, which is described by the standard Hamiltonian,

$$H_\tau := \tau\sum_{j=1}^{N-1}(c_j^\dagger c_{j+1} + c_{j+1}^\dagger c_j), \tag{28}$$

with τ the hopping amplitude. The corresponding action reads

$$S_0 = -i\tau\sum_j\int\frac{d\omega}{2\pi}\left(\bar{\psi}_j^1\psi_{j+1}^1 + \bar{\psi}_j^2\psi_{j+1}^2 + \mathrm{c.c}\right). \tag{29}$$

The free propagators are directly derived from the previous expressions of the action and read

$$\left[G_0^{-1}\right]^{\mathcal{R}(\mathcal{A})}_{j,k}(\omega) = \delta_{j,k}[\omega \pm i\Gamma(\delta_{j,1} + \delta_{j,N})] + \tau(\delta_{j,k+1} + \delta_{j,k-1}), \tag{30}$$

$$\left[G_0^{-1}\right]^{\mathcal{K}}_{j,k}(\omega) = 2i\Gamma\delta_{j,k}\sum_{a=L,R}\delta_{j,a}\tanh\left(\frac{\omega-\mu_a}{2T_a}\right). \tag{31}$$

Notice that the reservoirs act, through the hybridization constant Γ, as natural regulators of the imaginary components of the noninteracting problem [78].

Finally S_{sto} is the action corresponding to the QSH (22). As explained in the previous section, the demonstrated validity of SCBA for the Dyson equation (25) allows to derive exact expressions for the self-energies (24), and thus for the propagators of the full theory. Such solution allows to fully determine the transport properties of the system through MW formula (3). As shown in Sec. III, Eq. (24) implies a particularly simple form for the advanced and retarded components of the self-energy:

$$\Sigma^{\mathcal{R}(\mathcal{A})}_{i,j} = \mp i\delta_{i,j}\delta(t,t')\sum_l \frac{\gamma_{i,l}}{2}. \tag{32}$$

Importantly, in the geometry of Fig. 1, we can derive a compact and explicit expression of (25) for the diagonal terms $G^{\mathcal{K}}(t,t)$

$$\vec{G}^{\mathcal{K}} = (\mathbb{I} - M)^{-1}\cdot\vec{V} \tag{33}$$

where we introduced the N-dimensional vectors

$$\vec{G}^{\mathcal{K}}_j = G^{\mathcal{K}}_{j,j}(t,t), \tag{34}$$

$$\vec{V}_j = \frac{2\Gamma}{i}\sum_{a\in\{L,R\}}\int\frac{d\omega}{2\pi}G^{\mathcal{R}}_{j,a}G^{\mathcal{A}}_{a,j}\tanh\left(\frac{\omega-\mu_a}{2T_a}\right), \tag{35}$$

and M is an $N\times N$ matrix with elements

$$M_{j,k} = \sum_l \gamma_{k,l}\int\frac{d\omega}{2\pi}G^R_{j,l}G^A_{l,j}. \tag{36}$$

Notice that only $G^{\mathcal{K}}$ carries information about the biased reservoirs, as can be seen from (35). The first term in (3) depends exclusively on spectral functions, which are readily derived from Eqs. (30) and (32), while Eq. (33) sets, through Eq. (4), the expression of the density differences at the edges Δn.

Note that our analysis shows that the matrix M (36) is the key object encoding information about diffusion and it appears exclusively in the Keldysh component of the single-particle Green's function (33). A convenient way to understand this is to consider systems with single-particle gains and losses that do not display Ohmic $1/N$ suppression of the current. It was shown in Ref. [77] that, while (32) remains valid in those systems, the matrix M in (33) becomes 0 for these systems and the current saturates to a size-independent value. Thus, having a finite-lifetime in the retarded and advanced Green's function is not sufficient to get diffusive transport. The imaginary contribution to the retarded/advanced self-energy, such as the one in (32), has the interpretation of a lifetime for the free single-particle excitations of the system, yet it is the Keldysh component of the self-energy that describes the consequences of dissipative scattering on the transport properties of the system. When $M \neq 0$, Eq. (36) gives us a linear profile for the density profile, which eventually leads to a $1/N$ diffusive contribution for the current as discussed in the Sec. II.

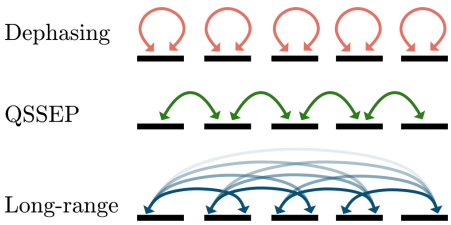

FIG. 7. Particular 1D discrete cases that will be of interest. Only the noise contribution is presented in this figure. In the dephasing model, all the sites are paired with themselves. For the QSSEP, the pairs are between nearest neighbours. In the long-range model, a given point is linked to all the rest of the lattice with a coupling decaying as power law.

These considerations are those underpinning our general discussion about diffusive transport in Sec. II. We now turn to the case-by-case study of the specific QSHs depicted in Fig. 7. As said in Sec. I, we will focus on three one-dimensional models: the dephasing model, the quantum symmetric simple exclusion process (QSSEP), and models with stochastic long-range hopping. For the dephasing model, every single point on the lattice is coupled with itself by the noise. For the QSSEP, the noise couples each point with its neighbours. For the long-range, a given point is paired to all the rest of the lattice with a power-law decay as a function of the distance. These processes are illustrated for all three models in Fig. 7 and we will give more details about their physical motivations in the related sections.

Without loss of generality, in the oncoming analysis of the current J, we focus on a linear response regime in the chemical potential bias. We set an identical temperature for both reservoirs $T_L = T_R = T$ and $\mu_L \to \mu + \delta\mu$, $\mu_R \to \mu - \delta\mu$. We expand Eq. (3) in $\delta\mu$. One thus obtains, to linear order in $\delta\mu$:

$$J = \Gamma\frac{\delta\mu}{2T}\int d\omega\frac{1}{\cosh^2\left(\frac{\omega-\mu}{2T}\right)}\left[\mathcal{A}(\omega) - \frac{\Gamma}{2\pi}\Delta^{\mathcal{K}}(\omega)\right]. \tag{37}$$

where $\mathcal{A}(\omega)$ is the edge spectral function, which coincides with $\mathcal{A}_{L/R}(\omega)$, because of the mirror symmetry of the class of QSHs that we will consider. The second term can be expressed in the form

$$\Delta^{\mathcal{K}}(\omega) = \left[\frac{1}{\mathbb{I}-M}\cdot\vec{W}(\omega)\right]_1 - \left[\frac{1}{\mathbb{I}-M}\cdot\vec{W}(\omega)\right]_N, \tag{38}$$

in which $\vec{W}$ is an N dimensional vector whose components are given by $\vec{W}_j(\omega) = G^{\mathcal{R}}_{j,1}(\omega)G^{\mathcal{A}}_{1,j}(\omega) - G^{\mathcal{R}}_{j,N}(\omega)G^{\mathcal{A}}_{N,j}(\omega)$.

A. Dephasing model

The dephasing model describes fermions hopping on a 1D lattice while subject to a random on-site dephasing coming from dissipative interactions with external degrees of freedom. In the language of Sec. III, this model corresponds to the case where all the points are paired with themselves, which results in substituting the rates

$$\gamma_{i,j} \to \gamma_{\rm Dph}\delta_{i,j}, \tag{39}$$

in Eqs. (12) and (15) (see also Fig. 7). There are various limits in which this model can be derived. For instance, it can be thought as describing the effective dynamics of fermions interacting weakly with external bosonic degrees of freedom within the Born-Markov approximation [37]. In Refs. [30,31,79] it was shown, relying on matrix product operator techniques, that the dephasing model exhibits diffusive transport. Two-times correlators in the *XXZ* under dephasing was also studied in [51] and were shown to exhibit a complex relaxation scheme. For bosonic interacting systems, it was shown that the addition of an external dephasing could lead to anomalous transport [98,99]. Additionally, as discussed in Sec. III, the mean dynamics of this model coincides with the one where the occupation numbers of fermions on each site are independently and continuously monitored [44,100]. For this reason, the dephasing model has recently attracted a lot of interest as a prototypical model exhibiting a measurement rate-induced transition in the entanglement dynamics [42,43]. Finally, we note that in Ref. [29] a mapping between the dephasing model and the Fermi-Hubbard model was established. Although we will not discuss this mapping here, we stress that it implies that our method also provides the computation of exact quantities valid for equivalent systems governed by Hubbard Hamiltonians.

The stochastic Hamiltonian for the dephasing model is readily obtained from the substitution (39), namely

$$dH_t = \sqrt{2\gamma_{\rm Dph}}\sum_j \hat{n}_j dB_t^j, \tag{40}$$

where B_t denotes a real Brownian motion with Itō rule $dB_t^j dB_t^k = \delta_{j,k}dt$. The retarded and advanced self-energies are obtained from Eq. (32) and read

$$\Sigma^{\mathcal{R}(\mathcal{A})}_{j,k}(t,t') = \mp\frac{i}{2}\gamma_{\rm Dph}\delta_{j,k}\delta(t-t'). \tag{41}$$

while $G^{\mathcal{R},\mathcal{A}}$ are obtained by inversion of Eq. (30) with inclusion of the self-energy (41). These functions are symmetric and given by, for $i \leqslant j$ [77,101]:

$$G^{\mathcal{R}/\mathcal{A}}_{i,j}(\omega) = \frac{(-1)^{i+j}\tau^{j-i}B^{\mathcal{R}/\mathcal{A}}_{i-1}B^{\mathcal{R}/\mathcal{A}}_{N-j}}{\left[\omega \pm i\left(\Gamma+\frac{\gamma_{\rm Dph}}{2}\right)\right]B^{\mathcal{R}/\mathcal{A}}_{N-1} - \tau^2 B^{\mathcal{R}/\mathcal{A}}_{N-2}}, \tag{42}$$

where $B^{\mathcal{R}/\mathcal{A}}_i = [(r_+ \pm i\Gamma)r_+^i - (r_- \pm i\Gamma)r_-^i]/(r_+ - r_-)$ and $r_\pm = (\omega \pm i\frac{\gamma}{2} + \sqrt{(\omega \pm i\frac{\gamma_{\rm Dph}}{2})^2 - 4\tau^2})/2$.

The related spectral functions at the system edges $\mathcal{A}(\omega) = \mathcal{A}_{11}(\omega) = \mathcal{A}_{NN}(\omega)$ is represented in Fig. 8 for different system sizes N. It displays N peaks corresponding to the eigenspectrum of the system without dissipation. The width of the peaks is controlled nontrivially by the hybridization constant Γ and the bulk dissipation rate $\gamma_{\rm Dph}$. Plots for closely

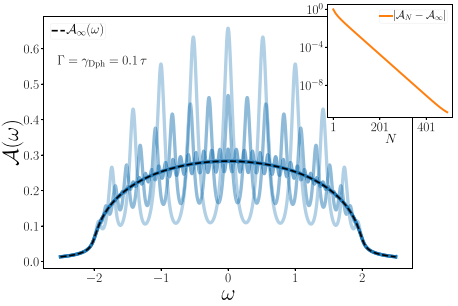

FIG. 8. Edge spectral function $\mathcal{A}(\omega)$ for the dephasing model (40) in the configuration of Fig. 1 for difference systems sizes N. Darker blue-solid lines correspond to larger systems sizes $N = 11, 21, 51, 101, 201, 501, 1001$. We consider only odd values of N, as they ensure the presence of a resonance at $\omega = 0$. The inset shows the exponential convergence of the spectral function at a fixed (odd) system size $\mathcal{A}_N = \mathcal{A}(\omega = 0)$ towards its asymptotic value $\mathcal{A}_\infty(\omega)$, obtained from Eq. (43) and corresponding to the dashed-black line in the main plot [for $N \gtrsim 100$ and the parameters reported in the plot, numerical curves overlap with $\mathcal{A}_\infty(\omega)$].

related quantities in the $\gamma_{\rm Dph} \to 0$ limit can be found in Ref. [77]. In this nondissipative limit, the height of the peaks does not decay with the system size N. On the contrary, for $\gamma_{\rm Dph} > 0$, the peaks vanish in the $N \to \infty$ limit, and the spectral function converges *exponentially* towards a smooth function $\mathcal{A}_\infty(\omega)$ as shown in the inset of Fig. 8. One can analytically derive $\mathcal{A}_\infty(\omega)$, as the retarded Green function (42) at the edges $G^{\mathcal{R}}_{1,1} = G^{\mathcal{R}}_{N,N}$ converges to

$$\lim_{N\to\infty} G^{\mathcal{R}}_{1,1}(\omega) = \frac{1}{\omega + i\left(\Gamma + \frac{\gamma_{\rm Dph}}{2}\right) - \frac{\tau^2}{r_{\mathrm{sgn}(\omega)}}}. \tag{43}$$

The exponential convergence of the edge spectral function is reproduced by all the other QSHs discussed below and verifies one of the preliminary assumptions exposed in Sec. II, identifying the density difference Δn as the term entirely responsible for the $1/N$ suppression of the dissipative current in (3).

Our approach provides an efficient way to compute the second term in (37), through an explicit derivation of the matrix M:

$$M_{j,k} = \gamma_{\rm Dph}\int \frac{d\omega}{2\pi} G^{\mathcal{R}}_{j,k} G^{\mathcal{A}}_{k,j}. \tag{44}$$

As we detail in Appendix D, the expressions (38), (42), and (44) allow the efficient derivation of the current (37) up to system sizes $N \simeq 10^{3-4}$. As a consequence, we can systematically study the expected crossover from a ballistic-to-diffusive regime expected at length scales $N^* \simeq \gamma_{\rm Dph}^{-1}$ [30]. See also Appendix E for additional details.

Two main technical advances of our approach compared to previous studies [25,30,31,79,95,102,103] consist in its ability to naturally address reservoirs with finite temperatures $T < \infty$,

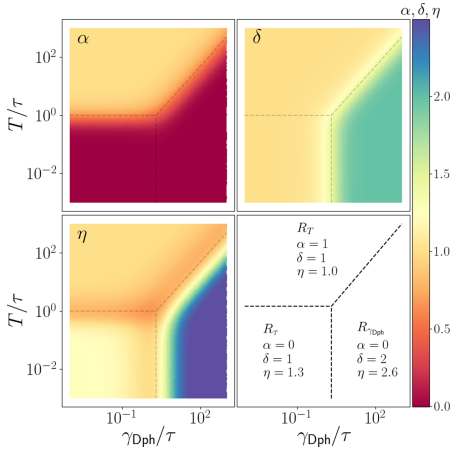

FIG. 9. Fitted parameters $(\alpha, \delta, \upsilon)$ of the rescaled conductance of the dephasing model as defined in Eq. (45). These values define different regions in the temperature - dephasing plane with different behaviors for the conductance, see Eq. (46). The dashed lines are a guide for the eyes to delimit the regions. The bottom right plot summarizes the characteristic values of each region.

accessing transport regimes left unexplored by previous studies and to access two-times correlators in the stationary state. An important consequence of our analysis is that the rescaled conductance of the system, that we define as $\mathcal{G} = NJ/\delta\mu$, has a nontrivial dependence on the temperature T and the dephasing rate $\gamma_{\rm Dph}$, namely,

$$\mathcal{G} = \lim_{N\to\infty} \frac{JN}{\delta\mu} = \frac{\eta\tau^{\alpha+\delta}}{T^{\alpha}\gamma_{\rm Dph}^{\delta}}. \tag{45}$$

In Fig. 9, we plot the coefficients (α, δ, η) across the parameter space $(T, \gamma_{\rm Dph})$. From the plot, we identify three main diffusive transport regimes $R_{\tau,T,\gamma}$, in which these coefficients are different. Note that the regions are not connected by sharp phase transitions but instead by crossovers, which appear sharp in logarithmic scale. Deep in the three regions, the rescaled conductance takes the approximate values

$$\mathcal{G} = \begin{cases} \frac{\tau^2}{T\gamma_{\rm Dph}} & T \gg \gamma_{\rm Dph}, \tau \\ \frac{2.6\tau^2}{\gamma_{\rm Dph}^2} & \gamma_{\rm Dph} \gg T, \tau \\ \frac{1.3\tau}{\gamma_{\rm Dph}} & \tau \gg \gamma_{\rm Dph}, T \end{cases}. \tag{46}$$

In previous studies carried in the $T \to \infty$ limit for the reservoirs, where they can be described as Lindblad injectors [77], the conductance $\mathcal{G}$ is assumed to be proportional to the bulk diffusion constant D [4,20]. The density profiles in the system (see Appendix E) clearly show that such interpretation cannot be extended to lower temperatures. The emergence of coherent effects between the system and its baths leads to finite-sized boundary effects, which do not allow the determination of the bulk diffusion constant through Eq. (46). To obtain the bulk diffusion constant we can use our approach to derive the density profiles *inside the system* and far away from its boundaries. We numerically verify Fick's law (1) in the bulk and find the diffusion constant to be

$$D = \frac{2\tau^2}{\gamma_{\rm Dph}}, \tag{47}$$

which is double the conductance in the $T \gg \gamma_{\rm Dph}$ limit, as expected. At variance with the rescaled conductances (46), this quantity is not affected by any boundary effect and it is in agreement with previous analytical ansatzes, valid in the infinite temperature limit [30]. The independence of the diffusion constant (47) from the temperature at the boundaries is a consequence of the stochastic dephasing (40), which locally brings the system back to an infinite temperature equilibrium state regardless of boundary conditions. We thus see on this example that our approach allows to compute both the two- and four-points measurements of the resistance. Even for diffusive systems, the distinction between the two processes can be important.

To conclude our analysis of the transport in the dephasing model, we note that the different transport regimes in (46) explicitly depend on the *stationary bias* $n_1 - n_N$, which suffers from boundary effects in some regions of the $(T, \gamma_{\rm Dph})$ parameter space. We confirm with our exact numerical solution that this is indeed the case. This interesting bias dependence is beyond the scope of the present paper and left for future studies.

1. 1/N expansion

Let us now show how the diffusion constant (47), that we obtained from our exact solution, can also be easily derived from the novel $1/N$ perturbative theory we introduced in Sec. II.

The first step is to fix the action of the infinite size theory S_∞ with the aid of the coarse graining procedure. We start by disposing the elements of $G^{\mathcal{R}/\mathcal{A}/\mathcal{K}}_{i,j}$ as a matrix and subdivide it in square cells of width a. We take the average over all the terms in the cell to obtain the effective Green function $G^{\mathcal{R}/\mathcal{A}/\mathcal{K}}_{\tilde{i},\tilde{j}}$, describing the correlations between the $\tilde{i}$ and $\tilde{j}$th cell. This procedure is illustrated in Fig. 10-(right) for the retarded Green's function and increasing cell size ($a = 1$ corresponds to no coarse graining). As the cell size increases, $G^{\mathcal{R}/\mathcal{A}/\mathcal{K}}_{\tilde{i},\tilde{j}}$ becomes a diagonal matrix with the off-diagonal terms vanishing as $1/a$ and exponentially suppressed with the distance $|\tilde{i} - \tilde{j}|$.

This explicit calculation confirms the diagonal structure of $G^{\mathcal{R}/\mathcal{A}/\mathcal{K}}$ and the reduction of the action to a sum of local commuting terms $S_\infty = \sum_{\tilde{j}} S_{\tilde{j}}$, where $S_{\tilde{j}}$ is the action associated to the $\tilde{j}$th cell. To simplify the notations, we drop the tilde indices from now on and implicitly assume that the calculations are done in the effective coarse-grained theory. The diagonal terms of $G^{\mathcal{R}}(\omega = 0)$ are depicted in Fig. 10-(left) as function of frequency with $G^{\mathcal{K}}$ shown in the inset. As a increases, the symmetry center of the functions changes to $\omega = -2\tau$ converging to the black curves depicting Eqs. (9) and (10). As mentioned before, the only free parameters that need to be fixed in the local theory are μ_j, T_j, and $\Sigma_j(\omega)$.

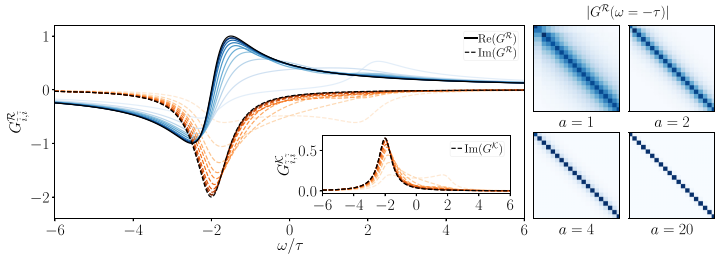

FIG. 10. Coarse-graining procedure in the dephasing model, $\gamma_{\mathrm{Dph}}=1$ for increasing size of the cell, a. Left: Real and imaginary part of the diagonal terms of $G^{\mathcal{R}}(\omega)$ for increasing cell size, $a=1,2,3,4,5,7,12,20,40,50$, respectively from light to dark. Inset: $G^{\mathcal{K}}$ component measured at one-third of the chain and $T=0.1$. Black lines depict the $1/N$ predictions obtained by inverting the matrix in Eq. (48). The symmetry around $\omega=0$ is broken as a increases. Right: Color plot of the absolute value of $G^{R}(\omega=0)$ for the first 20×20 coarse grained cells of a system with $N=2000$ sites, darker colors represent higher values.

For the dephasing model, we find that the self-energy is simply given by $i\gamma_{\mathrm{Dph}}/2$. For a single site such an imaginary term was shown [77] to coincide with the effective action of a reservoir within the limit $\mu_j, T_j\to\infty$ while keeping the ratio μ_j/T_j fixed. Let n_j be the local density at site j, $n_j=\frac{1}{2}(1-iG^{K}(t,t))$. Using $[G^{-1}]^{\mathcal{K}}=-G^{\mathcal{R}-1}G^{\mathcal{K}}G^{\mathcal{A}-1}$ and $G^{\mathcal{K}}(\omega)=-\tanh\frac{\mu_j}{T_j}(G^{\mathcal{R}}(\omega)-G^{\mathcal{A}}(\omega))$. Interestingly, at leading order in $1/N$, this relation turns out to be verified even at the microscopic level, i.e., for $a=1$. This tells us that the local equilibration condition of the infinite size theory is always true in our case. We furthermore suppose that in the coarse-grained theory, the expression of the retarded and advanced components will be given by a single-site two-level system, i.e., we suppose the following expression for $S_{\tilde{j}}$:

$$S_{\tilde{j}}=\int\frac{d\omega}{2\pi}(\bar{\psi}^1_{\tilde{j}},\bar{\psi}^2_{\tilde{j}})\begin{pmatrix}\omega+i\frac{\gamma_{\mathrm{Dph}}}{2} & -i(2n_j-1)\gamma_{\mathrm{Dph}}\\ 0 & \omega-i\frac{\gamma_{\mathrm{Dph}}}{2}\end{pmatrix}\begin{pmatrix}\psi^1_{\tilde{j}}\\ \psi^2_{\tilde{j}}\end{pmatrix}. \tag{48}$$

Where we absorbed the -2τ shift of frequencies in the integral. Expression (48) is valid in the bulk, independently from any value of μ, T at the boundaries. We check explicitly that the coarse-grained theory indeed converges towards $S_{\tilde{j}}$ as a is increased as shown in Fig. 10.

In the path integral formalism, the $1/N$ corrections to the current (11) is given by

$$J=i\langle\hat{J}_j[\bar{\psi}^+,\psi^+]S_{\mathrm{dyn}}\rangle_\infty \tag{49}$$

where $\hat{J}$ is the current operator, $\hat{J}[\bar{\psi}^+,\psi^+]$ is the evaluation of this operator in the fermionic coherent basis on the $+$ Keldysh contour, $\langle\bullet\rangle_\infty:=\int\mathcal{D}[\psi^\pm,\bar{\psi}^\pm]e^{iS_\infty}\bullet$ and S_{dyn} is the Keldysh action (29) associated to the contour integral of $\hat{H}_{\mathrm{dyn}}$ defined in (11). Here we have explicitly that $\hat{H}_{\mathrm{dyn}}=\tau\sum_j c^\dagger_j c_{j+1}+\mathrm{H.c.}$ The current operator is in this case :

$$\hat{J}_j=i\tau(c^\dagger_{j+1}c_j-c^\dagger_j c_{j+1}). \tag{50}$$

A straightforward calculation reported in Appendix C then leads to an explicit derivation of Fick's law:

$$J=-\frac{2\tau^2}{\gamma_{\mathrm{Dph}}}\nabla n_j. \tag{51}$$

where ∇ is the discrete gradient $\nabla n_j=n_{j+1}-n_j$. Equation (51), derived from the $1/N$ expansion, coincides with the exact result (47) in the whole parameter space. Such agreement validates the $1/N$ expansion as a systematic and efficient procedure to compute diffusion constants. From the computational point-of-view, note that the $1/N$ expansion did not resort to any numerical schemes and provided an exact expression of the diffusive constant, which could not be extracted explicitly from the Dyson equation (25).

B. QSSEP

In this section, we illustrate how our method can also be applied to the study of the *quantum symmetric simple exclusion process* (QSSEP) [34].

The QSSEP is a model of fermionic particles that hop on the lattice with random amplitudes, which can be thought as the quantum generalization of classical exclusion processes [90]. Classical exclusion processes have attracted a widespread interest over the last decades as they constitute statistical models with simple rules but a rich behavior that is thought to be representative of generic properties of non-equilibrium transport. It has been particularly impactful in the formulation of the macroscopic fluctuation theory (MFT) [89], which aims at understanding in a generic, thermodynamic sense, macroscopic systems driven far from equilibrium. It is hoped that the QSSEP will play a similar role in a quantum version of MFT, which is for now largely unknown.

We are interested in a model of QSSEP plus the coherent jump Hamiltonian (28) that was first studied in Ref. [32]. The case of pure QSSEP can be retrieved in the limit $\tau\to 0$. As for the dephasing model discussed in Sec. IV A, we will see that the $1/N$ expansion formalism again offers a simple route to derive the diffusive current.

As pictured in Fig. 7, the QSSEP couples nearest neighbor sites. It is derived from Eqs. (12) and (15) by taking the prescription

$$\gamma_{i,j}=\gamma_{\mathrm{QS}}\frac{\delta_{i,j+1}+\delta_{i,j-1}}{2}. \tag{52}$$

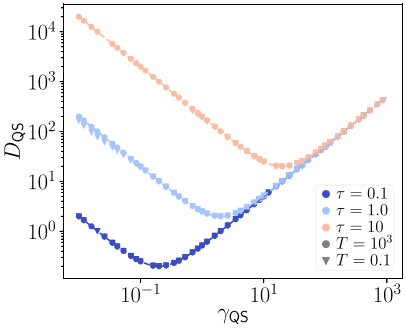

FIG. 11. Diffusion constant of the QSSEP model as a function of the noise strength γ for different hopping amplitudes τ and temperatures T. The results are independent of the latter. The dots are obtained from the MW formula (3) while dashed lines depict the results of the $1/N$ expansion (56).

The associated QSH is

$$dH_t = \sqrt{\gamma_{QS}} \sum_j \left[c_j^\dagger c_{j+1} dW_t^{j+1,j} + c_{j+1}^\dagger c_j dW_t^{j,j+1} \right]. \quad (53)$$

From Eq. (24), we get the advanced and retarded components of the self-energies:

$$\Sigma_{j,k}^{\mathcal{R}(\mathcal{A})}(t,t') = \mp \frac{i}{2} \gamma_{QS} \delta_{j,k} \delta(t,t') \left[1 - \frac{\delta_{1,j} + \delta_{j,N}}{2} \right]. \quad (54)$$

The retarded and advanced Green functions are given by inserting the bare propagators (30) and the self-energy (54) into the Dyson equation (25). These propagators can be directly derived from the ones of the dephasing model by making the substitutions $\gamma_{Dph} \to \gamma_{QS}$ and $\Gamma \to \Gamma - \gamma_{QS}/2$. As a consequence, all the considerations made for the spectral function and Fig. 8, in the dephasing model, equally apply to the QSSEP.

This is not the case for the Keldysh component, where the M matrix has the different expression [104]

$$M_{j,k} = \frac{\gamma_{QS}}{2} \int \frac{d\omega}{2\pi} \left(G_{j,k-1}^{\mathcal{R}} G_{k-1,j}^{\mathcal{A}} + G_{j,k+1}^{\mathcal{R}} G_{k+1,j}^{\mathcal{A}} \right). \quad (55)$$

Combining the above equation with (33) allows to obtain G^K and allows to compute the current from (3), or its linearized version (37). For all values of the parameter space (T, γ_{QS}) the current follows the relation (see Fig. 11)

$$J_j = -\left(\frac{\gamma_{QS}}{2} + \frac{2\tau^2}{\gamma_{QS}} \right) \nabla n_j. \quad (56)$$

which tells us that the diffusion constant is $\frac{\gamma_{QS}}{2} + \frac{2\tau^2}{\gamma_{QS}}$ in agreement with the result presented in [32]. For $\tau = 0$, this generalizes the result from [34], which was restricted to boundaries with infinite temperature and chemical potential.

1. 1/N expansion

The expression (56) for the current can also be obtained easily in the $1/N$ perturbative approach illustrated in Sec. II. The action in the infinite size limit is again of the form (48). From (54) we see that the expression of the self-energy is similar to the one of the dephasing model by simply replacing γ_{Dph} by γ_{QS} up to differences that tend to 0 in the infinite size limit. The current operator from site j to $j+1$ in the bulk is given here by

$$\hat{J}_j = \frac{\gamma_{QS}}{2} (\hat{n}_j - \hat{n}_{j+1}) + i\tau (c_{j+1}^\dagger c_j - c_j^\dagger c_{j+1}). \quad (57)$$

The first part is easily evaluated to be $-\gamma_{QS} \nabla n_j/2$ to first order in $1/N$ in the diffusive limit. For the second part, we simply need to redo the previous derivation by replacing γ_{Dph} by γ_{QS}. The term $i\tau (c_{j+1}^\dagger c_j - c_j^\dagger c_{j+1})$ then becomes $-\frac{2\tau^2}{\gamma_{QS}} (n_{j+1} - n_j)$, which yields (56).

C. Long-range Hopping

Finally we turn to the model with long-range hopping from the noise (see Fig. 7). In this model each particle can jump to any unoccupied site with a probability rate that decays with the distance as a power law of exponent α. Power laws appear naturally for instance in quantum simulation with Rydberg atoms [105–107] where they emerge because of the dipole-dipole interactions. Depending on the order of the interactions between atoms, different power laws can be reached. In the limit $\alpha \to \infty$, we get an "all-to-all" model, i.e there are random quantum jumps between all sites. These types of models have recently attracted interest as toy models to understand the interplay between quantum chaos and quantum information notably in the context of random unitary circuits [86,108].

For the long-range QSH we have

$$\gamma_{i,j} = (1 - \delta_{i,j}) \frac{\gamma_{LR}}{\mathcal{N}_\alpha |j-k|^\alpha} \quad (58)$$

and the corresponding Hamiltonian is

$$dH_t = \sum_{j \neq k} \sqrt{\frac{2\gamma_{LR}}{\mathcal{N}_\alpha |j-k|^\alpha}} c_j^\dagger c_k dW_t^{k,j}. \quad (59)$$

where $\mathcal{N}_\alpha = 2 \sum_{k=1}^{N/2} k^{-\alpha}$ is a suitable normalization condition such that $\mathcal{N}_\infty = 2$ and $\mathcal{N}_0 = N$. The limiting cases of this model are the QSSEP and "all-to-all" model, respectively $\alpha = 0$ and $\alpha \to \infty$.

For the long-range hopping the expression of the retarded(advanced) self-energy is

$$\Sigma_{j,k}^{\mathcal{R}(A)}(t,t') = \mp \delta_{j,k} \delta(t-t') \frac{i}{2} \sum_{l \neq j} \frac{\gamma_{LR}}{\mathcal{N}_\alpha |j-l|^\alpha}. \quad (60)$$

As before, injecting the bare propagators (30), (31), and (60) in (25) yields $G^{\mathcal{R}(A)}$. As illustrated in Fig. 15 in Appendix C 3, this form of the self-energy is equivalent to the one derived for the dephasing model (41), with the only difference that the effective dephasing rate γ becomes site-dependent because of the presence of boundaries connected to reservoirs. We verified that the exponential convergence of the spectral function illustrated in Fig. 8, equally applies, as expected, for this model as well.

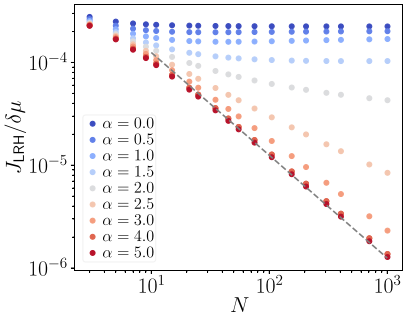

FIG. 12. Scaling of the linear response current as a function of the system size N, for varying power-law coefficients α in the long-range hopping Hamiltonian (59). The saturation of J_{LRH} to finite values, for $\alpha \ll 1$, signals a ballistic regime of transport, which contrasts with the diffusive regime observed for $\alpha \gg 1$, where J_{LRH} vanishes as N^{-1}, as highlighted by the black-dashed line.

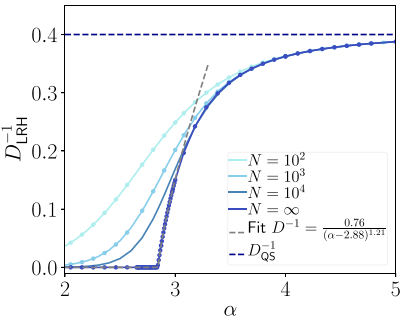

FIG. 13. Second-order phase transition in the long-range hopping of $D^{-1} = -\lim_{N\to\infty} \nabla n / J_{\mathrm{LRH}}$ as a function of α and $\gamma_{\mathrm{LR}} = 1$. Dots represent the numerical solution of (37) while full lines depict the $1/N$ expansion's predictions; both results overlap. The $N \to \infty$ limit is obtained via the fitting procedure detailed in Appendix E. The gray-dashed line highlights the divergence of the diffusion constant as $D \sim (\alpha - \alpha_c)^{1.21}$.

The M matrix is

$$M_{j,k} = \sum_{l\neq k} \int \frac{d\omega}{2\pi} G^{\mathcal{R}}_{j,l}(\omega) G^{\mathcal{A}}_{l,j}(\omega) \frac{\gamma_{\mathrm{LR}}}{\mathcal{N}_\alpha |k-l|^\alpha}, \tag{61}$$

which combined to (33) yields G^K.

In the absence of coherent hopping, there is a simple argument to conjecture a phase transition in the transport properties of the system at $\alpha = 3$. If one considers the stochastic process (59) alone, its average has a simple interpretation as a classical Markov process, where the probability for a fermion at site 0 to jump to site j during a timestep Δt, given that the target site j is empty, is $p_j := \frac{\gamma_{\mathrm{LR}}}{\mathcal{N}_\alpha |j|^\alpha} \Delta t$. For a single particle, this defines a random walk whose variance is given by $v := \sum_j p_j j^2$, which is related to the diffusion constant via $D = v/\Delta t$. This diverges at least logarithmically for $\alpha \leqslant 3$. However, note that there is no simple reasoning to understand what happens if one were to study the model with the coherent hopping term as, *a priori*, a purely classical analysis does not hold anymore.

For the numerical computations, we fix $\gamma_{\mathrm{LR}} = 1$ and $T = 1000$ but the results are independent of the latter. In Fig. 12, we show the dependence of the linear response current with the system size for different values of α. When α is small, the current saturates in the $N \to \infty$ limit, while for large values of α it decays as N^{-1}, as depicted in dashed gray line. This a signature of a ballistic-to-diffusive transition that occurs at a finite value of α.

To characterize this transition further, we look at the order parameter $D^{-1} = -\lim_{N\to\infty} \nabla n / J$. For diffusive systems, D^{-1} is the inverse of the diffusion constant and should be zero for ballistic systems. In Appendix E, we discuss the numerical fitting required to obtain D^{-1} from a finite-size scaling analysis. D^{-1} undergoes a second-order phase transition at a critical power $\alpha_c \approx 2.87$ (see the dark-blue dots in Fig. 13). When approaching the transition from the diffusive region, the diffusion constant diverges as $D \sim (\alpha - \alpha_c)^{1.21}$ (see the gray-dashed line in Fig. 13). It is quite remarkable and counterintuitive that setting $\tau \neq 0$ pushes the diffusive regime to values of $\alpha < 3$ instead of the opposite. A naive reasoning would suggest that the addition of a coherent hopping term would push the ballistic phase to values of α larger than the classical estimate ($\alpha = 3$), as a finite τ would favor the coherent propagation of single particles across the system. We observe that the opposite is surprisingly true, and we leave the exploration of this effect to future investigations.

1. 1/N expansion

For $\alpha > \alpha_c$, the $1/N$ expansion is valid and we can compute D^{-1} in the limit of infinite temperature. The action in the infinite system size is again of the form (48) and the lifetime is fixed by (60).

Unlike the previous models, there is no simple analytic expression for the diffusion constant since its derivation depends on the system size. We provide a detailed derivation of the diffusive current in Appendix C. In Fig. 13, we depict the results of the $1/N$ expansion for various system sizes (full lines) and overlap them with the numeric solution of (37) (dots). Both methods agree up to machine precision, which may be an indication that the $1/N$ perturbative approach is surprisingly exact even in the ballistic regime, $\alpha < \alpha_c$.

As already highlighted above, the interplay between transport and coherence gives rise to a rich physics in the long-range hopping model, but understanding it in depth is beyond the goals of this paper and will be addressed in a subsequent work.

V. CONCLUSION

In this paper, we provided a comprehensive analysis of the large system size properties of diffusive quantum systems driven out-of-equilibrium by boundary reservoirs. In particular, we showed that diffusive quantum systems can be

described by an effective and simple equilibrated Gaussian theory, which allows a systematic way to compute their diffusive transport properties via an expansion in the inverse system size. We illustrated the correctness of our $1/N$ expansion by comparing to exact results we obtained, using a self-consistent Born method, for a large class of quantum stochastic Hamiltonians, which show diffusive behavior. In particular, the self-consistent approach allowed us to explicitly derive the structure of the effective Gaussian theory, which consists of decoupled sites with a finite lifetime and where the effective equilibration and diffusivity is entirely encoded in the Keldysh component of local correlations.

As an illustration of the effectiveness of our approach, we computed the current in three models that have been of interest in the recent literature: the dephasing model, the QSSEP, and a model with stochastic long-range hopping. For the dephasing model and the QSSEP, we illustrated the ability of our approach to extend the study of transport to situations with boundaries at finite temperatures and arbitrary chemical potentials. This allowed us to show how dissipative processes restore effective infinite temperature behavior in the bulk and explicitly derive the effective Gaussian theory via a coarse-graining procedure. For the long-range hopping model, our analysis unveiled that coherent hopping processes trigger diffusive behavior in regimes where transport would be ballistic in the exclusive presence of stochastic long-range hopping. This counter-intuitive phenomenon is a remarkable example of the nontrivial interplay between coherent and dissipative dynamics in open quantum systems, which could be efficiently addressed based on the self-consistent approach.

The validity of the self-consistent Born approximation for our class of stochastic Hamiltonians provides in principle the solution to the noisy version of any model whose bare action is Gaussian. Our proof is not limited by stationary behavior or by the one-dimensional geometry of the problems addressed in this paper, but can be extended to time-dependent and higher dimensional problems as well. This possibility opens interesting perspectives for the investigation of phenomena in a large class of problems. Extension of our approach could be devised to study quantum asymmetric exclusion processes [109–111], spin and heat transport, the dynamics after a quench, fluctuations on top and relaxation to stationary states and their extensions to ladder geometries or with nontrivial topological structure. These settings have been for the moment largely untractable, or were solved by case by case methods, for which we provided here an unified framework.

An important issue raised by our work consists in showing whether our description equally holds and provides technical advantage for studying the emergence of resistive behavior triggered by intrinsic many-body interactions with unitary dynamics, where the breaking of integrability leads to diffusive transport [1–4,18–23]. A priori, the arguments presented in Section II apply for any quantum systems, which follows a local Fick's law and, as such, they have the potential for very broad applications. Additionally, it is commonly accepted that the phenomenology of diffusion is associated with integrability breaking and subsequent approach to thermal equilibrium [112–116]. Understanding if and how our approach can help make this link clearer is an exciting open question. In this respect, we also note that, because of the existing mapping between the Fermi-Hubbard and the dephasing model [29], the self-consistent Born approximation allows to compute exact quantities in the Fermi-Hubbard model. As far as we know, exact solutions for this model were only obtained in the framework of the Bethe ansatz and it is thus interesting that a seemingly unrelated approach allows to obtain exact quantities as well. Whether a connection exists between the two approaches and whether the exact summation allows to compute quantities out of reach of the Bethe ansatz are interesting open questions.

Note added. We also thank X. Turkeshi and M. Schir for making us aware of their work [103] before publication, where a study of the dephasing model from the point of view of Green's function has also been performed.

ACKNOWLEDGMENTS

We thank L. Mazza for useful suggestions during the writing of the manuscript. This work has been supported by the Swiss National Science Foundation under Division II. J.S.F. and M.F. acknowledge support from the FNS/SNF Ambizione Grant No. PZ00P2_174038.

APPENDIX A: UNRAVELING TO CONTINUOUS MEASUREMENT

In this Appendix, we discuss the unraveling of Eq. (12) to a quantum stochastic differential equation describing a system under continuous monitoring. In the Itō prescription the stochastic equation of motion of a quantum system subject to continuous measurement of an observable $O + O^\dagger$ at rate γ is given by [93]

$$d\rho = \mathcal{L}_0(\rho) + \frac{\gamma}{2} L_O(\rho) + \sqrt{\frac{\gamma}{2}} D_O(\rho) dB_t \tag{A1}$$

where $\mathcal{L}_0$ describes the dynamics in absence of measurement, $L_O(\rho) = (O\rho O^\dagger - \frac{1}{2}(O^\dagger O\rho + \rho O^\dagger O))$ and $D_O(\rho) = O\rho + \rho O^\dagger - \rho \mathrm{tr}(O\rho + \rho O^\dagger)$. If we assume that at each link we have two independent measurement processes 1 and 2 with the same rate $2\gamma_{i,j}$ and $O_{1,i,j} := c_j^\dagger c_i$ and $O_{2,i,j} := ic_j^\dagger c_i$. The corresponding measured observables are $O_{1,i,j} + O_{1,i,j}^\dagger = c_j^\dagger c_i + c_i^\dagger c_j$ and $O_{2,i,j} + O_{2,i,j}^\dagger = i(c_j^\dagger c_i - c_i^\dagger c_j)$, namely the so-called bond density and the current. It is straightforward to see that averaging out (A1), we get (12) again.

APPENDIX B: PROOF OF THE NONCROSSING RULE

We want to prove that for all stochastic Hamiltonians of the form given by (15), the only nonvanishing diagrams in the averaged perturbative expansion of the retarded, advanced and Keldysh Green functions are those for which there is no crossing.

This statement only relies on the causality structure of the retarded and advanced Green functions, i.e.,

$$G^{\mathcal{R}}(t,t') = 0 \text{ if } t < t', \tag{B1}$$

$$G^{\mathcal{A}}(t,t') = 0 \text{if} t > t'. \tag{B2}$$

Let $\langle \bullet \rangle_0$ denote the average with respect to a quadratic theory. First, we remark that the causality structure of a given propa-

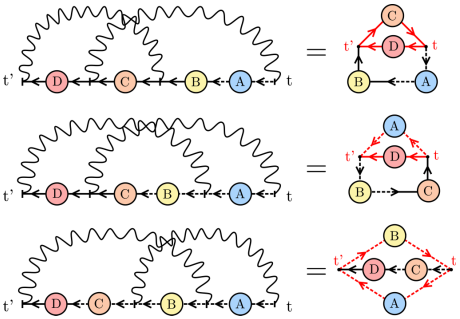

FIG. 14. All possible crossings for the Keldysh component of the Green's function with the contracted versions on the right. The red lines highlight the part of the diagram violating the causality structure and are responsible for making the diagram vanish.

gator depends only on its incoming edge and outgoing edge, and thus

$$G(t,t') := \langle \psi^1(t) f[\psi^1, \bar{\psi}^1, \psi^2, \bar{\psi}^2] \bar{\psi}^1(t') \rangle_0 = 0 \text{ for } t < t', \tag{B3}$$

$$G'(t,t') := \langle \psi^2(t) f[\psi^1, \bar{\psi}^1, \psi^2, \bar{\psi}^2] \bar{\psi}^2(t') \rangle_0 = 0 \text{ for } t > t'. \tag{B4}$$

where $f[\psi^1, \bar{\psi}^1, \psi^2, \bar{\psi}^2]$ is an arbitrary polynomial in the Grassman variables coming from the expansion of the stochastic action. This is straightforward to show starting from the action (22): starting from an incoming full (dashed) line, one cannot switch at any point to a dashed (full) line. Hence, the causality structure is preserved for each line and thus for the whole propagator. Direct inspection of these diagrams show that there cannot be any crossing when contracting the noise terms, as it would lead to a contradiction in the time-orderings. There is only a single one particle irreducible diagram made of a single loop. This establishes the noncrossing result for the retarded and advanced components.

For the Keldysh components, a case by case examination of all possible crossings that are depicted on Fig. 14 where the labels A, B, C, D denote generic product of free propagators is needed. For each one of these diagrams, there is always a subpart that shows an incompatibility (shown in red in Fig. 14) in the time orderings causing the whole diagram to vanish. This establishes the noncrossing result for the Keldysh propagator.

APPENDIX C: COMPUTATION OF THE CURRENT IN THE 1/N EXPANSION

In this Appendix, we compute the current in the dephasing, QSSEP, and long-range model using the perturbative theory in inverse system size presented in Sec. II.

1. Dephasing model

For the dephasing model, the definition of the current in the bulk from site j to $j+1$ is given by

$$\hat{J}_j = i\tau(c_{j+1}^\dagger c_j - c_j^\dagger c_{j+1}). \tag{C1}$$

The expectation value of $\hat{J}_j$ in the stationary state is given by

$$\begin{aligned} J_j(t) &:= \mathrm{tr}(\hat{J}_j \rho_t) = i\tau \langle \bar{\psi}_{j+1}^+(t)\psi_j^+(t) - \bar{\psi}_j^+(t)\psi_{j+1}^+(t) \rangle \\ &= i\frac{\tau}{2}\big\langle \big(\psi_{j+1}^1\bar{\psi}_j^1 + \psi_{j+1}^1\bar{\psi}_j^2 + \psi_{j+1}^2\bar{\psi}_j^2 \\ &\quad - \big(\psi_j^1\bar{\psi}_{j+1}^1 + \psi_j^1\bar{\psi}_{j+1}^2 + \psi_j^2\bar{\psi}_{j+1}^2\big)\big)_t \big\rangle \end{aligned} \tag{C2}$$

where we used the Larkin rotation and removed the terms $\psi^2\bar{\psi}^1$ as they are always 0 for causality reasons.

Using the action associated to the coherent jump S_τ

$$\begin{aligned} S_\tau = -\tau \int dt' \sum_j \big(&\bar{\psi}_j^1\psi_{j+1}^1 + \bar{\psi}_j^2\psi_{j+1}^2 \\ &+ \bar{\psi}_{j+1}^1\psi_j^1 + \bar{\psi}_{j+1}^2\psi_j^2\big)_{t'} \end{aligned} \tag{C3}$$

we get, from (49), to leading order in $\frac{1}{N}$:

$$\begin{aligned} J_j(t) = \frac{\tau^2}{2}\int dt' \big\langle &\big(\psi_{j+1}^1\bar{\psi}_j^1 + \psi_{j+1}^1\bar{\psi}_j^2 + \psi_{j+1}^2\bar{\psi}_j^2 \\ &- (\psi_j^1\bar{\psi}_{j+1}^1 + \psi_j^1\bar{\psi}_{j+1}^2 + \psi_j^2\bar{\psi}_{j+1}^2)\big)_t \\ &\times \big(\bar{\psi}_j^1\psi_{j+1}^1 + \bar{\psi}_j^2\psi_{j+1}^2 + \bar{\psi}_{j+1}^1\psi_j^1 + \bar{\psi}_{j+1}^2\psi_j^2\big)_{t'} \big\rangle_\infty \end{aligned} \tag{C4}$$

where $\langle\rangle_\infty$ means the average with respect to the bare action in the infinite size limit, where all the sites are uncorrelated.

Using Wick's theorem and that $\langle \psi_j^a \bar{\psi}_{j+1}^b \rangle_\infty = 0$, the previous equation greatly simplifies:

$$\begin{aligned} J_j = -\frac{\tau^2}{2}\int \frac{d\omega}{2\pi} \big(&G_{j+1,j+1}^{\mathcal{R}}(\omega) G_{j,j}^{\mathcal{K}}(\omega) \\ &+ G_{j,j}^{\mathcal{A}}(\omega) G_{j+1,j+1}^{\mathcal{K}}(\omega) \\ &- G_{j,j}^{\mathcal{R}}(\omega) G_{j+1,j+1}^{\mathcal{K}}(\omega) - G_{j+1,j+1}^{\mathcal{A}}(\omega) G_{j,j}^{\mathcal{K}}(\omega)\big) \end{aligned} \tag{C5}$$

We can now use the bare action of individual sites (in presence of the dephasing noise):

$$S_j = \int \frac{d\omega}{2\pi} (\bar{\psi}_j^1, \bar{\psi}_j^2) \begin{pmatrix} \omega + i\frac{\gamma_{\mathrm{Dph}}}{2} & -i(2n_j - 1)\gamma_{\mathrm{Dph}} \\ 0 & \omega - i\frac{\gamma_{\mathrm{Dph}}}{2} \end{pmatrix} \begin{pmatrix} \psi_j^1 \\ \psi_j^2 \end{pmatrix} \tag{C6}$$

to obtain the explicit expression of the current

$$\begin{aligned} J_j &= \tau^2 \int \frac{d\omega}{2\pi} \left(\frac{\gamma_{\mathrm{Dph}}}{(\omega^2 + (\frac{\gamma_{\mathrm{Dph}}}{2})^2)^2} \right) \frac{i\gamma_{\mathrm{Dph}}}{2} (2i(n_{j+1} - n_j)) \\ &= -\frac{2\tau^2}{\gamma_{\mathrm{Dph}}} \nabla n_j \end{aligned} \tag{C7}$$

from which we immediately read the diffusion constant $D = \frac{2\tau^2}{\gamma_{\mathrm{Dph}}}$.

2. QSSEP

For the QSSEP, the self-energy for an individual site is $\Sigma_j(\omega) = \gamma_{\mathrm{QS}} - \frac{\gamma_{\mathrm{QS}}}{2}(\delta_{j,1} + \delta_{j,N})$. The current in the bulk is

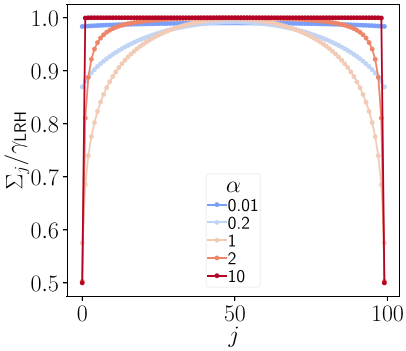

FIG. 15. Dependence on the site index j of the self-energy in the long-range model for a chain of $N = 100$ sites and different values of the exponent α of the noise, see (C13). The $\alpha \to \infty$ limit corresponds to the QSSEP.

given by

$$\hat{J}_j = \frac{\gamma_{\rm QS}}{2}(\hat{n}_j - \hat{n}_{j+1}) + i\tau(c_j^\dagger c_{j+1} - c_{j+1}^\dagger c_j) \tag{C8}$$

The first part of the current already scales like $1/N$ at order 0 in the S_τ expansion. The second term is evaluated in the same fashion as for the dephasing model. This leads to

$$J_j = -\left(\frac{\gamma_{\rm QS}}{2} + \frac{2\tau^2}{\gamma_{\rm QS}}\right)\nabla n_j + O\left(\frac{1}{N^2}\right) \tag{C9}$$

and $D = \frac{\gamma_{\rm QS}}{2} + \frac{2\tau^2}{\gamma_{\rm QS}}$.

3. Long-range hopping

For the long-range hopping model, the local current is defined from the local conservation equation of the particle number :

$$\frac{d}{dt}\hat{n}_j := \hat{J}_j^{\rm inc} - \hat{J}_j^{\rm out} \tag{C10}$$

with

$$\hat{J}_j^{\rm inc} = \sum_{k<j} \frac{\gamma_{\rm LR}}{\mathcal{N}_\alpha |k-j|^\alpha}(\hat{n}_k - \hat{n}_j) + i\tau(c_{j-1}^\dagger c_j - c_j^\dagger c_{j-1}), \tag{C11}$$

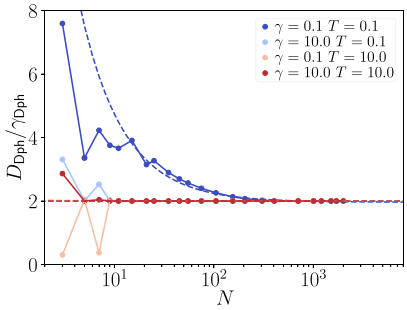

FIG. 17. Diffusion constant of the dephasing model at different (T, γ) values. In general, the diffusion constant decays with the inverse system size, which we exploit to extract the $N \to \infty$ limit from a nonlinear fit, dashed lines.

$$\hat{J}_j^{\rm out} = \sum_{k>j} \frac{\gamma_{\rm LR}}{\mathcal{N}_\alpha |k-j|^\alpha}(\hat{n}_j - \hat{n}_k) + i\tau(c_j^\dagger c_{j+1} - c_{j+1}^\dagger c_j). \tag{C12}$$

Recall the expression of the self-energy at site j (60):

$$\Sigma_j = \frac{\gamma_{\rm LR}}{2\mathcal{N}_\alpha} \sum_{k\neq j} \frac{1}{|k-j|^\alpha}. \tag{C13}$$

which is depicted in Fig. 15.

To get the current with the $1/N$ expansion, we take, as for the previous model, the 0th order term in the first term in the expression of the current and the first-order term in the second part. We obtain

$$J_j^{\rm inc} = \sum_{k<j} \frac{\gamma_{\rm LR}}{\mathcal{N}_\alpha |k-j|^\alpha}(n_k - n_j) + \frac{2\tau^2}{\Sigma_{j-1} + \Sigma_j}(n_{j-1} - n_j) \text{ for } j \in [2, N], \tag{C14}$$

$$\hat{J}_j^{\rm out} = \sum_{k>j} \frac{\gamma_{\rm LR}}{\mathcal{N}_\alpha |k-j|^\alpha}(n_j - n_k) + i\tau(n_j - n_{j+1}) \text{ for } j \in [1, N-1]. \tag{C15}$$

For simplicity, we give in this paper only the expressions for the infinite temperature and chemical potential boundary

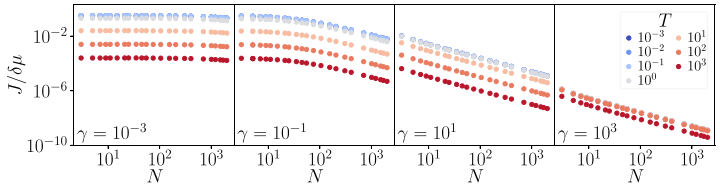

FIG. 16. Scaling of the current as a function of the system size in the dephasing model. From left to right: $\gamma = 10^{-3}, 10^{-1}, 10^{1}, 10^{3}$. As the dephasing increases, diffusion sets in at smaller system sizes. The vanishing dependence of J with the temperature indicates the crossover into the R_γ region (46).

conditions, which amount to take Lindblad injecting and extracting terms (see [77]). The current at the boundaries is then given by

$$J_1^{\text{in}} = \alpha_L(1-n_1) - \beta_L n_1, \tag{C16}$$

$$J_N^{\text{out}} = -\alpha_R(1-n_N) + \beta_R n_N. \tag{C17}$$

In the stationary state we have that $\forall j \in [1,N]$, $J_j^{\text{in}} = J_j^{\text{out}}$, which leads to the following system of linear equation to solve in order to get the density profile:

$$\mathcal{M}.\vec{n} = \vec{v} \tag{C18}$$

where $\vec{n}$ and $\vec{v}$ are N-dimensional vectors with elements n_j and $\mathcal{M}$ is an $N \times N$ matrix such that

$$\begin{aligned}\mathcal{M}_{j,k} =& \frac{\gamma_{\text{LR}}}{\mathcal{N}_\alpha |k-j|^\alpha}(1-\delta_{j,k}) \\ &+ \frac{2\tau^2}{\Sigma_j + \Sigma_{j+1}}(\delta_{k,j+1} - \delta_{j,k}(1-\delta_{j,N})) \\ &+ \frac{2\tau^2}{\Sigma_j + \Sigma_{j-1}}(\delta_{k,j-1} - \delta_{j,k}(1-\delta_{j,1})) \\ &- \delta_{j,k}\left(\sum_{k\neq j} \frac{\gamma_{\text{LR}}}{\mathcal{N}_\alpha |k-j|^\alpha}\right) \\ &- \delta_{j,k}\delta_{j,1}(\alpha_L + \beta_L) - \delta_{j,k}\delta_{j,N}(\alpha_R + \beta_R)\end{aligned} \tag{C19}$$

and

$$v_j = -\delta_{j,1}\alpha_L - \delta_{j,N}\alpha_R. \tag{C20}$$

APPENDIX D: NUMERICAL IMPLEMENTATION

In this Appendix, we present some important elements of the numerical implementation. The first step to compute any presented result is to stabilize and efficiently evaluate $G^{\mathcal{R}(\mathcal{A})}(\omega)$ at any ω. For the case of a uniform stochastic noise (e.g., free system, dephasing), a naive use of (42) would require evaluating the ratio of two polynomials of order $\mathcal{O}(N)$, a notoriously difficult task for large N using floating point arithmetics. A possible solution would be to resort to arbitrary-precision arithmetic but this would entail a heavy speed cost.

We used for the results of the present paper the fact that $G^{\mathcal{R}(\mathcal{A})}(\omega)$ can be written as a ratio of polynomials and therefore, decomposed into a product of monomials $G^{\mathcal{R}}(\omega) \sim \prod_j(\omega - z_j)/\prod_i(\omega - p_i)$. To efficiently find the zeros and poles of $G^{\mathcal{R}}$ [117], we note that the inverse of $G^{\mathcal{R}}$ is a simple tridiagonal matrix with a generic form

$$T^{-1}(\omega) = \begin{pmatrix} \omega + a_1 & b_1 & 0 & 0 \\ b_1^* & \omega + a_2 & \ddots & 0 \\ 0 & \ddots & \ddots & b_{N-1} \\ 0 & 0 & b_{N-1}^* & \omega + a_N \end{pmatrix} \tag{D1}$$

whose inverse is given by [118]

$$T_{i,j}(\omega) = \begin{cases} (-1)^{i+j} b_i \ldots b_{j-1}\theta_{i-1}\phi_{j+1}/\theta_L & i < j \\ \theta_{i-1}\phi_{j+1}/\theta_L & i = j \\ (-1)^{i+j} b_j^* \ldots b_{i-1}^* \theta_{j-1}\phi_{i+1}/\theta_L & i > j \end{cases} \tag{D2}$$

where $\theta_i = (\omega + a_i)\theta_{i-1} - |b_{i-1}|^2\theta_{i-2}$ and $\phi_i = (\omega + a_i)\phi_{i+1} - |b_i|^2\phi_{i+2}$. Therefore, computing the poles and zeros of G^R requires computing all the zeros of the sequences $\{\phi_i, \theta_i\}_{i=0}^{L+1}$, a task that can be done efficiently. If the matrix is invariant under a reflection along the anti-diagonal, it is enough to compute a single sequence instead, $\phi_i = \theta_{L+1-i}$. This is always the case in the models studied in the present paper. Since a_i does not depend on ω, ϕ_i is a polynomial of degree i with the initial conditions defined as $\phi_0 = 1$ and $\phi_1 = \omega + a_1$. One can efficiently find all the roots $\{z_k\}_{k=1}^i$ of ϕ_i using a Weierstrass-like recursive method [119,120], see Eqs. (D3) and (D4) for a second and fourth-order scheme

$$z_k^{(2)} = z_k - \frac{W_k}{\prod_{k\neq j}(z_k - z_j)} = z_k - C_k^{(2)} \tag{D3}$$

$$\begin{aligned} z_k^{(4)} &= z_k - \frac{W_k}{1 - \sum_{k\neq j} \frac{W_j}{z_k - W_k - z_j}} = z_k - C_k^{(4)} \\ W_k &= \phi_i(z_k) \end{aligned} \tag{D4}$$

where W_k is the Weierstrass weight. We chose these derivative-free schemes to avoid computing explicit derivatives that would slow down the computation. Choosing the correct initial condition is critical to the success of the scheme. To find the roots of ϕ_i, we initialize the scheme with the roots of ϕ_{i-1} plus an extra root. We empirically found that the extra root should have a random position close to the middle root (after sorting by the real part) to guarantee the best convergence. This initial choice can still fail when some roots are located very far way from the others, which occurs for example for the model QSSEP. This happens when, at some step in the iteration, two roots coalesce and $C_k^{(i)}$ diverges strongly. In order to stabilize this divergence, we introduce a damping factor κ that suppresses large corrections $z_i^{(k)} = z_i - C_i^{(k)} e^{-\max|C_i^{(k)}|/\kappa}$. κ is a purely empirically value, which we typically take as $\kappa = \max(|b|)$. The role of κ is to slow down the algorithm and allow the coalescing roots to separate. Our root-searching algorithm has thus two parts: a quick search using a second-order damped scheme, followed by a fourth-order damped scheme to precisely locate the roots. Once all the roots are recovered, we generate the new matrix $\tilde{T}$ obtained from the estimates of the roots. We consider that $\tilde{T}$ is a good estimate only when $\max|T^{-1}(0)\cdot\tilde{T}^{-1}(0)| < 10^{-10}$. With the exception of the QSSEP, we find a typical value $\max|T^{-1}(0)\cdot\tilde{T}^{-1}(0)| \sim 10^{-13}$ for any system size.

Once the poles and zeros of $G^{\mathcal{R}(\mathcal{A})}(\omega)$ are computed, we proceed to compute $G^{\mathcal{K}}$ using (33). To evaluate the M matrix, we resort to the residue theorem. If the poles of $G^{\mathcal{R}(\mathcal{A})}$ are simple poles, the sum over residues can be computed in parallel only requiring the evaluation of the monomials $\{(\omega - z_k)\}$. We note that while each monomial $(\omega - z_k)$ is of order unity, a sequential multiplication can lead to overflown errors in the limit of large N. To avoid this problem, we multiply the monomials at random. If the algorithm fails to, within machine precision, separate two roots, the residue is computed from the contour integral instead.

The last step to compute $G^{\mathcal{K}}$ and the current J, is to perform the frequency integral convoluted with $\cosh^{-2}(\frac{\omega-\mu}{2T})$. This is done by evaluating the integral using a discrete integration scheme instead of residue theorem. Since the thermal de-

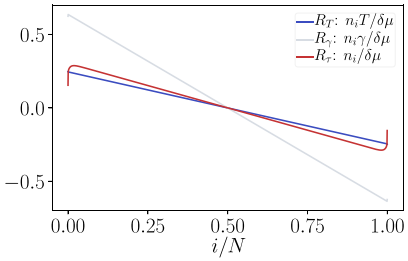

FIG. 18. Density profiles of a chain of size $N = 2000$ in the diffusive regime for the different regions $R_{\tau,\gamma,T}$ shown in Fig. 9. The breaking of Fick's law is limited to a nonextensive number of sites near the edge.

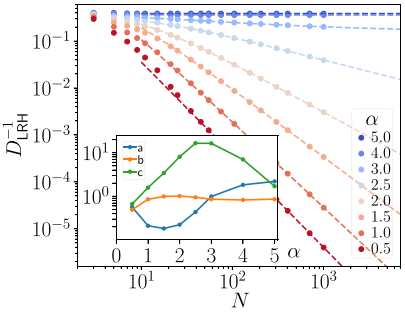

FIG. 19. Inverse of the diffusion constant in the long-range model for different powers of α. Dashed lines are fits to $D^{-1} = (aH^{(\alpha-b+1)}_{N+|c|})^{-1}$. The results of the fitting are depicted in the inset.

pendence is only encoded in the $\cosh^{-2}(\frac{\omega-\mu}{2T})$, discretizing the integral allows us deal with different (T, μ) values at no significant cost. We carefully verify that the mesh is fine enough to guarantee convergence of the integral at any (T, μ).

APPENDIX E: FINITE-SIZE SCALING

In this section, we detail the finite-size scaling analysis necessary to plot Figs. 9, 11, 13.

The presence of a dephasing term is not enough to ensure that the system behaves diffusely at any system size. Signatures of diffusive transport such as $J \sim 1/N$, only emerge at a characteristic dephasing length, $N^* \sim 1/\gamma$. At short system sizes, or short time-scales, the system behaves as if it was ballistic. In Fig. 16 we highlight this ballistic-to-diffusive transition for different values of the dephasing and temperature in the baths. At small dephasing values, one cannot reliably extract the diffusion constant by fitting a a straight line to Fig. 16. Instead, to extract the relevant information in the $N \to \infty$, we use the fact that the diffusion constant has itself a $1/N$ scaling [20] when measured in the middle of the chain. In the QSSEP and dephasing model, we use this result to perform nonlinear fits to D as shown in Fig. 17.

In this figure we plot the diffusion constant of the dephasing model as measured in the middle of the chain for increasing system sizes and different (T, μ) values. The dashed lines depict the nonlinear fit of the function $a + b/(N + c)$ with a, b, c fitting parameters. We find that most observables in these models exhibit $1/N$ corrections as discussed in [20]. The speed of convergence however depends on the point in the phase space (T, μ), with region R_τ (see Fig. 9) showing the slowest convergence. This is a consequence of the effects of the bath discussed in the main text. Deep in the τ-dominated regime, we observe the breaking of Fick's law near the edges as shown in Fig. 18.

Since this effect only occurs in a finite portion of the system close to the edges, the convergence is only slowed down. We thus evaluate D in the middle of the chain to mitigate its effects and get a better accuracy.

For the long-range model, one needs a different approach to obtain the $N \to \infty$ limit correctly, especially when close to the ballistic-diffusive transition described in the main text. A tentative form for the finite size extrapolation is provided by the solution of the diffusion equation for single particle under a random walk with long-range hopping discussed in Sec. IV C, which gives a diffusion constant $D = H^{(\alpha-2)}_L$, where $H^{(r)}_x$ is the generalized Harmonic number. We find that a fit $D^{-1} = (aH^{(\alpha-b+1)}_{N+|c|})^{-1}$, correctly captures the finite-size dependence of D^{-1} for all α values. The fitting parameters a, b, c respectively describe the amplitude, critical exponent and possible finite-size corrections. In Fig. 19, we depict D^{-1} against the result of the fit, respectively dots and dashed lines. The best fitting parameters are plotted in the inset. The quality of the fit allows us to conjecture that, at the transition point, the diffusion constant diverges logarithmically $D_{LR}(\alpha = \alpha_c) \sim H^{(1)}_N \to \log(N)$.

APPENDIX F: COARSE-GRAIN LENGTH a

In this section, we analytically estimate the coarse-grain length a from the correlation length of the dephasing model. Due to Eq. (9), it is enough to estimate a from a single Green function, in this case the retarded component. The starting point is the analytic expression of the elements $G^R_{i,j}$ in the bulk of the chain. For large systems, the boundaries become irrelevant and the good basis of the problem is the momenta basis. In k space, the self-energy takes a diagonal form

$$\Sigma^R_{k,k'} = \left(-\frac{i\gamma}{2}\right)\delta_{k,k'}. \tag{F1}$$

For the QSSEP, there are cross-diagonal terms in momentum that vanish as $1/L$ and can be safely ignored. Since both self-energy and Hamiltonian are diagonal in the momenta basis, one has

$$G^R_{k,k'} = \delta_{k,k'}\frac{1}{\omega - \epsilon_k - \Sigma_{k,k'}}, \tag{F2}$$

where $\epsilon_k = 2\tau\cos(k)$ is the eigenenergy of the bulk Hamiltonian. To find the retarded function in position space, we take

the Fourier transform with the continuum limit for k

$$G^R_{r,r'} = \int \frac{dk}{2\pi} \frac{e^{-ik(r-r')}}{\omega - 2\tau\cos k + i\gamma/2}. \tag{F3}$$

The integral can be solved using the residue theorem and, after some lengthy yet simple manipulations, we find a compact formula

$$G^R_{r,r'} = \frac{i^{|r-r'|-1}}{2\tau\cos y} e^{i\gamma|r-r'|}, \tag{F4}$$

where $y = \arcsin\frac{\omega+i\gamma/2}{2\tau}$ is a complex variable with $\mathrm{Im}(y(\omega)) > 0$. Therefore, in the dephasing model an estimate for the correlation length is given by

$$\xi = \frac{1}{\min\left(\mathrm{Im}\left(\arcsin\frac{\omega+i\gamma/2}{2\tau}\right)\right)} = \frac{1}{\mathrm{arcsinh}\frac{\gamma}{4\tau}}, \tag{F5}$$

In the limit of small dephasing γ, we have $\xi = 4\tau/\gamma$, which serves as an estimate for the coarse-grain length $a \sim \tau/\gamma$. As expected, a should be of the order of the dephasing length $N^* \sim 1/\gamma$.

[1] T. Giamarchi, Umklapp process and resistivity in one-dimensional fermion systems, Phys. Rev. B **44**, 2905 (1991).

[2] A. Rosch and N. Andrei, Conductivity of a Clean One-Dimensional Wire, Phys. Rev. Lett. **85**, 1092 (2000).

[3] X. Zotos and P. Prelovšek, Evidence for ideal insulating or conducting state in a one-dimensional integrable system, Phys. Rev. B **53**, 983 (1996).

[4] B. Bertini, F. Heidrich-Meisner, C. Karrasch, T. Prosen, R. Steinigeweg, and M. Žnidarič, Finite-temperature transport in one-dimensional quantum lattice models, Rev. Mod. Phys. **93**, 025003 (2021).

[5] X. Zotos, Finite Temperature Drude Weight of the One-Dimensional Spin- 1/2 Heisenberg Model, Phys. Rev. Lett. **82**, 1764 (1999).

[6] T. Prosen, Open *XXZ* Spin Chain: Nonequilibrium Steady State and a Strict Bound on Ballistic Transport, Phys. Rev. Lett. **106**, 217206 (2011).

[7] M. Ljubotina, M. Žnidari, and T. Prosen, Spin diffusion from an inhomogeneous quench in an integrable system, Nat. Commun. **8**, 16117 (2017).

[8] E. Ilievski, J. De Nardis, M. Medenjak, and T. Prosen, Superdiffusion in One-Dimensional Quantum Lattice Models, Phys. Rev. Lett. **121**, 230602 (2018).

[9] J. De Nardis, S. Gopalakrishnan, E. Ilievski, and R. Vasseur, Superdiffusion from Emergent Classical Solitons in Quantum Spin Chains, Phys. Rev. Lett. **125**, 070601 (2020).

[10] J. De Nardis, D. Bernard, and B. Doyon, Hydrodynamic Diffusion in Integrable Systems, Phys. Rev. Lett. **121**, 160603 (2018).

[11] M. Kardar, G. Parisi, and Y.-C. Zhang, Dynamic Scaling of Growing Interfaces, Phys. Rev. Lett. **56**, 889 (1986).

[12] T. Kriecherbauer and J. Krug, A Pedestrian view on interacting particle systems, KPZ universality and random matrices, J. Phys. A: Math. Theor. **43**, 403001 (2010).

[13] M. Ljubotina, M. Žnidarič, and T. Prosen, Kardar-Parisi-Zhang Physics in the Quantum Heisenberg Magnet, Phys. Rev. Lett. **122**, 210602 (2019).

[14] S. Gopalakrishnan and R. Vasseur, Kinetic Theory of Spin Diffusion and Superdiffusion in *XXZ* Spin Chains, Phys. Rev. Lett. **122**, 127202 (2019).

[15] O. A. Castro-Alvaredo, B. Doyon, and T. Yoshimura, Emergent Hydrodynamics in Integrable Quantum Systems Out of Equilibrium, Phys. Rev. X **6**, 041065 (2016).

[16] B. Bertini, M. Collura, J. De Nardis, and M. Fagotti, Transport in Out-of-Equilibrium *XXZ* Chains: Exact Profiles of Charges and Currents, Phys. Rev. Lett. **117**, 207201 (2016).

[17] E. Ilievski and J. De Nardis, Microscopic Origin of Ideal Conductivity in Integrable Quantum Models, Phys. Rev. Lett. **119**, 020602 (2017).

[18] J. De Nardis, D. Bernard, and B. Doyon, Diffusion in generalized hydrodynamics and quasiparticle scattering, SciPost Phys. **6**, 049 (2019).

[19] A. J. Friedman, S. Gopalakrishnan, and R. Vasseur, Diffusive hydrodynamics from integrability breaking, Phys. Rev. B **101**, 180302(R) (2020).

[20] M. Žnidarič, Nonequilibrium steady-state Kubo formula: Equality of transport coefficients, Phys. Rev. B **99**, 035143 (2019).

[21] M. Žnidarič, Weak Integrability Breaking: Chaos with Integrability Signature in Coherent Diffusion, Phys. Rev. Lett. **125**, 180605 (2020).

[22] M. Znidaric, Absence of superdiffusion in the quasiperiodic spin chain at weak integrability breaking, Phys. Rev. B **103**, 237101 (2021).

[23] J. S. Ferreira and M. Filippone, Ballistic-to-diffusive transition in spin chains with broken integrability, Phys. Rev. B **102**, 184304 (2020).

[24] M. Žnidarič, Spin Transport in a One-Dimensional Anisotropic Heisenberg Model, Phys. Rev. Lett. **106**, 220601 (2011).

[25] K. Yamanaka and T. Sasamoto, Exact solution for the Lindbladian dynamics for the open *XX* spin chain with boundary dissipation, arXiv:2104.11479.

[26] M. Žnidarič, A. Scardicchio, and V. K. Varma, Diffusive and Subdiffusive Spin Transport in the Ergodic Phase of a Many-Body Localizable System, Phys. Rev. Lett. **117**, 040601 (2016).

[27] J. J. Mendoza-Arenas, M. Žnidarič, V. K. Varma, J. Goold, S. R. Clark, and A. Scardicchio, Asymmetry in energy versus spin transport in certain interacting disordered systems, Phys. Rev. B **99**, 094435 (2019).

[28] M. Žnidarič and M. Ljubotina, Interaction instability of localization in quasiperiodic systems, Proc. Natl. Acad. Sci. USA **115**, 4595 (2018).

[29] M. V. Medvedyeva, F. H. L. Essler, and T. Prosen, Exact Bethe Ansatz Spectrum of a Tight-Binding Chain with Dephasing Noise, Phys. Rev. Lett. **117**, 137202 (2016).

[30] M. Žnidarič, Exact solution for a diffusive nonequilibrium steady state of an open quantum chain, J. Stat. Mech.: Theory Exp. (2010) L05002.

[31] M. Žnidarič, Dephasing-induced diffusive transport in the anisotropic Heisenberg model, New J. Phys. **12**, 043001 (2010).

[32] V. Eisler, Crossover between ballistic and diffusive transport: The quantum exclusion process, J. Stat. Mech.: Theory Exp. (2011) 06007.

[33] M. Bauer, D. Bernard, and T. Jin, Stochastic dissipative quantum spin chains (I) : Quantum fluctuating discrete hydrodynamics, SciPost Phys. **3**, 033 (2017).

[34] D. Bernard and T. Jin, Open Quantum Symmetric Simple Exclusion Process, Phys. Rev. Lett. **123**, 080601 (2019).

[35] A. Bastianello, J. De Nardis, and A. De Luca, Generalized hydrodynamics with dephasing noise, Phys. Rev. B **102**, 161110(R) (2020).

[36] C. Gardiner and P. Zoller, *Quantum Noise: A Handbook of Markovian and Non-Markovian Quantum Stochastic Methods with Applications to Quantum Optics*, Springer Series in Synergetics (Springer, New York, 2000).

[37] H. P. Breuer and F. Petruccione, *The Theory of Open Quantum Systems* (Oxford University Press, Oxford, 2002).

[38] H. Wichterich, M. J. Henrich, H.-P. Breuer, J. Gemmer, and M. Michel, Modeling heat transport through completely positive maps, Phys. Rev. E **76**, 031115 (2007).

[39] V. Gorini, A. Kossakowski, and E. C. G. Sudarshan, Completely positive dynamical semigroups of N-level systems, J. Math. Phys. **17**, 821 (1976).

[40] G. Lindblad, On the generators of quantum dynamical semigroups, Commun. Math. Phys. **48**, 119 (1976).

[41] B. Skinner, J. Ruhman, and A. Nahum, Measurement-Induced Phase Transitions in the Dynamics of Entanglement, Phys. Rev. X **9**, 031009 (2019).

[42] O. Alberton, M. Buchhold, and S. Diehl, Entanglement Transition in a Monitored Free-Fermion Chain: From Extended Criticality to Area Law, Phys. Rev. Lett. **126**, 170602 (2021).

[43] M. Buchhold, Y. Minoguchi, A. Altland, and S. Diehl, Effective Theory for the Measurement-Induced Phase Transition of Dirac Fermions, Phys. Rev. X **11**, 041004 (2021).

[44] X. Cao, A. Tilloy, and A. De Luca, Entanglement in a fermion chain under continuous monitoring, SciPost Phys. **7**, 024 (2019).

[45] T. Müller, S. Diehl, and M. Buchhold, Measurement-induced dark state phase transitions in long-ranged fermion systems, arXiv:2105.08076.

[46] P. Zhang, C. Liu, S.-K. Jian, and X. Chen, Universal entanglement transitions of free fermions with long-range non-unitary dynamics, arXiv:2105.08895.

[47] F. Tonielli, R. Fazio, S. Diehl, and J. Marino, Orthogonality Catastrophe in Dissipative Quantum Many-Body Systems, Phys. Rev. Lett. **122**, 040604 (2019).

[48] M. T. Mitchison, T. Fogarty, G. Guarnieri, S. Campbell, T. Busch, and J. Goold, *In Situ* Thermometry of a Cold Fermi Gas via Dephasing Impurities, Phys. Rev. Lett. **125**, 080402 (2020).

[49] P. E. Dolgirev, J. Marino, D. Sels, and E. Demler, Non-Gaussian correlations imprinted by local dephasing in fermionic wires, Phys. Rev. B **102**, 100301(R) (2020).

[50] V. Alba, Unbounded entanglement production via a dissipative impurity, SciPost Phys. **12**, 011 (2022).

[51] S. Wolff, J.-S. Bernier, D. Poletti, A. Sheikhan, and C. Kollath, Evolution of two-time correlations in dissipative quantum spin systems: Aging and hierarchical dynamics, Phys. Rev. B **100**, 165144 (2019).

[52] A. M. Lacerda, J. Goold, and G. T. Landi, Dephasing enhanced transport in boundary-driven quasiperiodic chains, Phys. Rev. B **104**, 174203 (2021).

[53] D. Roberts and A. A. Clerk, Driven-Dissipative Quantum Kerr Resonators: New Exact Solutions, Photon Blockade and Quantum Bistability, Phys. Rev. X **10**, 021022 (2020).

[54] H. Fröml, A. Chiocchetta, C. Kollath, and S. Diehl, Fluctuation-Induced Quantum Zeno Effect, Phys. Rev. Lett. **122**, 040402 (2019).

[55] D. Rossini, A. Ghermaoui, M. B. Aguilera, R. Vatré, R. Bouganne, J. Beugnon, F. Gerbier, and L. Mazza, Strong correlations in lossy one-dimensional quantum gases: From the quantum zeno effect to the generalized Gibbs ensemble, Phys. Rev. A **103**, L060201 (2021).

[56] K. Yamamoto, M. Nakagawa, K. Adachi, K. Takasan, M. Ueda, and N. Kawakami, Theory of Non-Hermitian Fermionic Superfluidity with a Complex-Valued Interaction, Phys. Rev. Lett. **123**, 123601 (2019).

[57] T. Müller, M. Gievers, H. Fröml, S. Diehl, and A. Chiocchetta, Shape effects of localized losses in quantum wires: Dissipative resonances and nonequilibrium universality, Phys. Rev. B **104**, 155431 (2021).

[58] N. Dogra, M. Landini, K. Kroeger, L. Hruby, T. Donner, and T. Esslinger, Dissipation-induced structural instability and chiral dynamics in a quantum gas, Science **366**, 1496 (2019).

[59] H. Pichler, A. J. Daley, and P. Zoller, Nonequilibrium dynamics of bosonic atoms in optical lattices: Decoherence of many-body states due to spontaneous emission, Phys. Rev. A **82**, 063605 (2010).

[60] C.-M. Halati, A. Sheikhan, H. Ritsch, and C. Kollath, Numerically Exact Treatment of Many-Body Self-Organization in a Cavity, Phys. Rev. Lett. **125**, 093604 (2020).

[61] F. Verstraete, M. M. Wolf, and J. I. Cirac, Quantum computation and quantum-state engineering driven by dissipation, Nat. Phys. **5**, 633 (2009).

[62] A. Sommer, M. Ku, G. Roati, and M. W. Zwierlein, Universal spin transport in a strongly interacting Fermi gas, Nature (London) **472**, 201 (2011).

[63] P. N. Jepsen, J. Amato-Grill, I. Dimitrova, W. W. Ho, E. Demler, and W. Ketterle, Spin transport in a tunable Heisenberg model realized with ultracold atoms, Nature (London) **588**, 403 (2020).

[64] P. N. Jepsen, W. W. Ho, J. Amato-Grill, I. Dimitrova, E. Demler, and W. Ketterle, Transverse spin dynamics in the anisotropic Heisenberg model realized with ultracold atoms, Phys. Rev. X **11**, 041054 (2021).

[65] R. Bouganne, M. B. Aguilera, A. Ghermaoui, J. Beugnon, and F. Gerbier, Anomalous decay of coherence in a dissipative many-body system, Nat. Phys. **16**, 21 (2020).

[66] M. Takigawa, N. Motoyama, H. Eisaki, and S. Uchida, Dynamics in the *S=1/2* One-Dimensional Antiferromagnet Sr_2CuO_3 via ^{63}Cu NMR, Phys. Rev. Lett. **76**, 4612 (1996).

[67] K. R. Thurber, A. W. Hunt, T. Imai, and F. C. Chou, 17*O* NMR Study of $q = 0$ Spin Excitations in a Nearly Ideal $S = 1/2$ 1D Heisenberg Antiferromagnet, Sr_2CuO_3, up to 800 K, Phys. Rev. Lett. **87**, 247202 (2001).

[68] F. L. Pratt, S. J. Blundell, T. Lancaster, C. Baines, and S. Takagi, Low-Temperature Spin Diffusion in a Highly Ideal $S = 1/2$ Heisenberg Antiferromagnetic Chain Studied by Muon Spin Relaxation, Phys. Rev. Lett. **96**, 247203 (2006).

[69] H. Maeter, A. A. Zvyagin, H. Luetkens, G. Pascua, Z. Shermadini, R. Saint-Martin, A. Revcolevschi, C. Hess, B. Büchner, and H.-H. Klauss, Low temperature ballistic spin transport in the *S= 1/2* antiferromagnetic Heisenberg chain compound $SrCuO_2$, J. Phys.: Condens. Matter **25**, 365601 (2013).

[70] A. Scheie, N. E. Sherman, M. Dupont, S. E. Nagler, M. B. Stone, G. E. Granroth, J. E. Moore, and D. A. Tennant, Detection of Kardar–Parisi–Zhang hydrodynamics in a quantum Heisenberg spin-1/2 chain, Nat. Phys. **17**, 726 (2021).

[71] C. Zu, F. Machado, B. Ye, S. Choi, B. Kobrin, T. Mittiga, S. Hsieh, P. Bhattacharyya, M. Markham, D. Twitchen *et al.*, Emergent hydrodynamics in a strongly interacting dipolar spin ensemble, Nature (London) **597**, 45 (2021).

[72] P. J. W. Moll, P. Kushwaha, N. Nandi, B. Schmidt, and A. P. Mackenzie, Evidence for hydrodynamic electron flow in $PdCoO_2$, Science **351**, 1061 (2016).

[73] L. Ella, A. Rozen, J. Birkbeck, M. Ben-Shalom, D. Perello, J. Zultak, T. Taniguchi, K. Watanabe, A. K. Geim, S. Ilani, and J. A. Sulpizio, Simultaneous voltage and current density imaging of flowing electrons in two dimensions, Nat. Nanotechnol. **14**, 480 (2019).

[74] J. A. Sulpizio, L. Ella, A. Rozen, J. Birkbeck, D. J. Perello, D. Dutta, M. Ben-Shalom, T. Taniguchi, K. Watanabe, T. Holder *et al.*, Visualizing Poiseuille flow of hydrodynamic electrons, Nature (London) **576**, 75 (2019).

[75] M. Ljubotina, D. Roy, and T. Prosen, Absence of thermalization of free systems coupled to gapped interacting reservoirs, arXiv:2106.08373.

[76] Y. Meir and N. S. Wingreen, Landauer Formula for the Current Through an Interacting Electron Region, Phys. Rev. Lett. **68**, 2512 (1992).

[77] T. Jin, M. Filippone, and T. Giamarchi, Generic transport formula for a system driven by Markovian reservoirs, Phys. Rev. B **102**, 205131 (2020).

[78] A. Kamenev, *Field Theory of Non-Equilibrium Systems* (Cambridge University Press, Cambridge, 2011), pp. 1–341.

[79] M. Žnidarič and M. Horvat, Transport in a disordered tight-binding chain with dephasing, Eur. Phys. J. B **86**, 67 (2013).

[80] C. Monthus, Dissipative random quantum spin chain with boundary-driving and bulk-dephasing: Magnetization and current statistics in the non-equilibrium-steady-state, J. Stat. Mech.: Theory Exp. (2017) 043302.

[81] M. Bauer, D. Bernard, and T. Jin, Equilibrium fluctuations in maximally noisy extended quantum systems, SciPost Phys. **6**, 45 (2019).

[82] D. Bernard and T. Jin, Solution to the quantum symmetric simple exclusion process: The continuous case, Commun. Math. Phys. **384**, 1141 (2021).

[83] D. Bernard and P. L. Doussal, Entanglement entropy growth in stochastic conformal field theory and the KPZ class, Europhys. Lett. **131**, 10007 (2020).

[84] F. H. L. Essler and L. Piroli, Integrability of one-dimensional Lindbladians from operator-space fragmentation, Phys. Rev. E **102**, 062210 (2020).

[85] D. Bernard and L. Piroli, Entanglement distribution in the quantum symmetric simple exclusion process, Phys. Rev. E **104**, 014146 (2021).

[86] A. Nahum, S. Roy, B. Skinner, and J. Ruhman, Measurement and entanglement phase transitions in all-to-all quantum circuits, on quantum trees, and in Landau-Ginsburg theory, PRX Quantum **2**, 010352 (2021).

[87] The dependence of the Green's functions on time differences $t - t'$, instead of separate times t, t' is a consequence of the fact that we consider stationary situations.

[88] The extension to different geometries and additional degrees of freedom is straightforward.

[89] L. Bertini, A. De Sole, D. Gabrielli, G. Jona-Lasinio, and C. Landim, Macroscopic fluctuation theory, Rev. Mod. Phys. **87**, 593 (2015).

[90] B. Derrida, Non-equilibrium steady states: Fluctuations and large deviations of the density and of the current, J. Stat. Mech.: Theory Exp. (2007) 07023.

[91] J. Dalibard, Y. Castin, and K. Mølmer, Wave-Function Approach to Dissipative Processes in Quantum Optics, Phys. Rev. Lett. **68**, 580 (1992).

[92] H. Carmichael, *An Open Systems Approach to Quantum Optics* (Springer, Berlin, 1993).

[93] V. P. Belavkin, Nondemolition measurements, nonlinear filtering and dynamic programming of quantum stochastic processes, in *Modeling and Control of Systems*, edited by A. Blaquiére (Springer, Berlin, 1989), pp. 245–265.

[94] T. Prosen, Third quantization: a general method to solve master equations for quadratic open Fermi systems, New J. Phys. **10**, 043026 (2008).

[95] C. Guo and D. Poletti, Solutions for bosonic and fermionic dissipative quadratic open systems, Phys. Rev. A **95**, 052107 (2017).

[96] L. M. Sieberer, M. Buchhold, and S. Diehl, Keldysh field theory for driven open quantum systems, Rep. Prog. Phys. **79**, 096001 (2016).

[97] In our conventions, Larkin-Ovchinnikov's rotation reads $\psi^{1/2} = (\psi^+ \pm \psi^-)/\sqrt{2}\, \bar{\psi}^{1/2} = (\bar{\psi}^+ \mp \bar{\psi}^-)/\sqrt{2}$ [121].

[98] D. Poletti, J.-S. Bernier, A. Georges, and C. Kollath, Interaction-Induced Impeding of Decoherence and Anomalous Diffusion, Phys. Rev. Lett. **109**, 045302 (2012).

[99] D. Poletti, P. Barmettler, A. Georges, and C. Kollath, Emergence of Glasslike Dynamics for Dissipative and Strongly Interacting Bosons, Phys. Rev. Lett. **111**, 195301 (2013).

[100] D. Bernard, T. Jin, and O. Shpielberg, Transport in quantum chains under strong monitoring, Europhys. Lett. **121**, 60006 (2018).

[101] L. S. L. Tan, Explicit inverse of tridiagonal matrix with applications in autoregressive modelling, IMA J. Appl. Math. **84**, 679 (2019).

[102] D. Karevski and T. Platini, Quantum Nonequilibrium Steady States Induced by Repeated Interactions, Phys. Rev. Lett. **102**, 207207 (2009).

[103] X. Turkeshi and M. Schiro, Diffusion and thermalization in a Boundary-Driven Dephasing Model, Phys. Rev. B **104**, 144301 (2021).

[104] In the previous expression, if an index is out of boundary, it must simply be set to 0, we donot write that explicitly to avoid cumbersome notation.

[105] H. Bernien, S. Schwartz, A. Keesling, H. Levine, A. Omran,

H. Pichler, S. Choi, A. S. Zibrov, M. Endres, M. Greiner *et al.*, Probing many-body dynamics on a 51-atom quantum simulator, Nature (London) **551**, 579 (2017).

[106] D. Bluvstein, A. Omran, H. Levine, A. Keesling, G. Semeghini, S. Ebadi, T. T. Wang, A. A. Michailidis, N. Maskara, W. W. Ho *et al.*, Controlling quantum many-body dynamics in driven Rydberg atom arrays, Science **371**, 1355 (2021).

[107] L. Henriet, L. Beguin, A. Signoles, T. Lahaye, A. Browaeys, G.-O. Reymond, and C. Jurczak, Quantum computing with neutral atoms, Quantum **4**, 327 (2020).

[108] A. Nahum, S. Vijay, and J. Haah, Operator Spreading in Random Unitary Circuits, Phys. Rev. X **8**, 021014 (2018).

[109] R. L. Hudson and K. R. Parthasarathy, Quantum Ito's formula and stochastic evolutions, Commun. Math. Phys. **93**, 301 (1984).

[110] B. Derrida, E. Domany, and D. Mukamel, An exact solution of a one-dimensional asymmetric exclusion model with open boundaries, J. Stat. Phys. **69**, 667 (1992).

[111] T. Jin, A. Krajenbrink, and D. Bernard, From Stochastic Spin Chains to Quantum Kardar-Parisi-Zhang Dynamics, Phys. Rev. Lett. **125**, 040603 (2020).

[112] J. M. Deutsch, Quantum statistical mechanics in a closed system, Phys. Rev. A **43**, 2046 (1991).

[113] M. Srednicki, The approach to thermal equilibrium in quantized chaotic systems, J. Phys. A: Math. Gen. **32**, 1163 (1999).

[114] M. Rigol, V. Dunjko, and M. Olshanii, Thermalization and its mechanism for generic isolated quantum systems, Nature (London) **452**, 854 (2008).

[115] L. D'Alessio, Y. Kafri, A. Polkovnikov, and M. Rigol, From quantum chaos and eigenstate thermalization to statistical mechanics and thermodynamics, Adv. Phys. **65**, 239 (2016).

[116] T. Kinoshita, T. Wenger, and D. S. Weiss, A quantum Newton's cradle, Nature (London) **440**, 900 (2006).

[117] The poles and zeros of $G^{\mathcal{A}}$ are the conjugate of $G^{\mathcal{R}}$.

[118] R. A. Usmani, Inversion of a tridiagonal Jacobi matrix, Linear Algebra Appl. **212**, 413 (1994).

[119] I. Gargantini and P. Henrici, Circular arithmetic and the determination of polynomial zeros, Numer. Math. **18**, 305 (1971).

[120] M. Petković and D. Milošević, Derivative free inclusion methods for polynomial zeros, Computing **75**, 71 (2005).

[121] A. I. Larkin and I. N. Ovchinnikov, Nonlinear effects during vortex motion in superconductors, Zh. Eksp. Teor. Fiz. **73**, 299 (1977).

3.3 Semi-classical picture of transport in QSHs

The success of the $1/N$ expansion suggests that, at least on a hydrodynamic scale, QSHs support a classical interpretation of transport. This inspired us to look for an effective classical model capable of explaining the emergence of diffusion and completing some of the gaps left by the $1/N$ expansion. Semi-classical models such as Boltzmann's equation [52, 127] or generalized hydrodynamics [128], are not expected to precisely capture all the correlations present in quantum many-body systems. Nevertheless, they are capable of qualitatively capturing the main transport properties. In Sec. 3.1, we already explored a semi-classical interpretation of inelastic processes in local QSHs: an incoming particle when affected by a QSH may return to the initial reservoir or be transmitted with a new energy. In this work, we extend and formalize the semi-classical picture to extensive systems undergoing dephasing. The key insight is that the dephasing model can also be unraveled as a continuous projective measurement process [129], where the densities at each site are independently measured at a rate γ, see App. C.

We propose the following semi-classical model of transport in dephased chains, see scheme in Fig. 3.3. A single particle from the Fermi sea of a reservoir enters the system and starts to propagate ballistically. Its initial velocity is determined from its initial momentum in the reservoir and the role of dephasing is to measure the occupancy at each site independently with a rate γ. After propagating for a time t, the particle is eventually *found* with a probability determined by the Poissonian distribution $p(t) = \gamma e^{-\gamma t}$. Once found, the velocity of the particle is randomly reset according to the local dispersion relation, see Eq. ⟦21⟧, and the particle resumes its ballistic propagation. This cycle continues until the particle either exits through the initial reservoir or the opposite one. The current, and consequently the conductance, is determined by the probability that a particle entering a reservoir exits from the opposite one, see Eqs. ⟦15⟧ and ⟦22⟧. This semi-classical transmission probability $\mathcal{T}$ can be computed numerically, and in the infinite size limit even analytically, using the self-consistent equation ⟦24⟧.

The semi-classical predictions were tested against the exact solution of the dephasing model and found to be surprisingly accurate[1] in some regimes, see a comparison of the conductance G for different parameters in Fig. 3.3a. In the thermodynamic limit and for small measurement rates, the semi-classical model not only correctly predicts a diffusive scaling of the current but also the correct dependence on the parameters of the model, $J^0 \sim \frac{\tau}{\gamma N}(\mu_L - \mu_R)$ for $T \gg \tau$ and $J^0 \sim \frac{\tau^2}{T\gamma N}(\mu_L - \mu_R)$ for $T \ll \tau$ with τ the hopping strength. Regrettably, the success of the semi-classical picture does not extend to the strong measurement regime where the average distance between measurements is much smaller than the lattice spacing. This is expected

[1] During subsequent work, we found a mistake of a factor of 2 unaccounted for in Ref. [P3], which makes the semi-classical picture almost match with the exact results despite being twice as big. We did not consider the possibility of not measuring the particle, which could explain why the measurement rate used in the semi-classical model should be half of the dephasing strength.

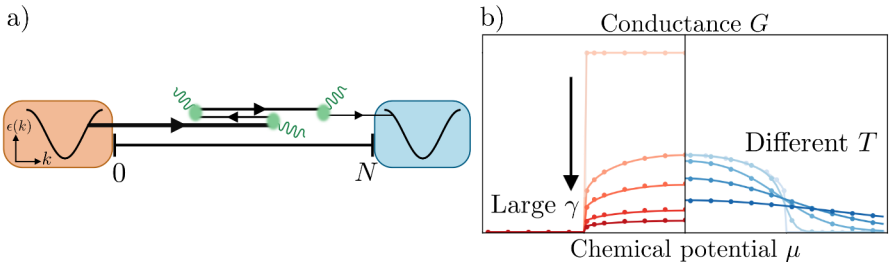

Figure 3.3: Adaptation from Figs. [[1,2]] of the paper. a) Semi-classical depiction of diffusive transport in a chain coupled to reservoirs with a cosine band dispersion. A particle exits the reservoir with a predetermined velocity and propagates ballistically until a reset event alters its velocity. This sequence repeats until the particle exits into one of the reservoirs. b) Dependence of the conductance with chemical potentials for different sizes and parameters. The semi-classical model (lines) agrees well with the exact solutions (dots).

since the semi-classical model assumes the chain to be in the continuum limit. The semi-classical picture is also capable of qualitatively explaining why the conductance tends to zero when the chemical potential is closer to the band edges, as depicted in Fig. 3.3b. A particle near the band's edge enters the system with a lower velocity and, as a consequence, it has a higher chance that a reset event will occur closer to the edge, sending it back to the initial reservoir.

The second half of this work is devoted to extending the semi-classical model beyond 1D geometries. We examine how different types of noise, possibly correlated along the transverse direction but uncorrelated longitudinally could influence transport. This was motivated by experiments investigating quantum transport in synthetic lattices [130, 131]. In these setups, the constituents of the experiment (e.g. ultracold atoms [132] or ring cavities [133, 134]) encode the longitudinal degrees of freedom, whilst the transverse ones are encapsulated in the non-spatial degrees of freedom of each constituent (e.g. internal spin or frequency state). As such, a noise acting on the physical dimension would influence all the synthetic degrees of freedom at once.

Our investigations reveal that different noises can lead to identical conductance profiles, despite resulting in markedly different steady states, see Fig. ⟦3⟧. A formal condition for two noises to exhibit identical conductance is provided in Eq. ⟦36⟧, but the motivation for this observation can be found in the semi-classical picture. A particle propagating from a reservoir, upon measurement, might change its transverse momentum or gain correlations in the transverse direction, but its longitudinal momentum will always be reset uniformly. If the reset rate remains consistent across all transverse modes, so will the longitudinal current.

We showcase how a semi-classical interpretation can be a powerful tool to understand transport in stochastic setups and perhaps other phenomena. Similar quasiparticle models have already been proposed to explain entanglement growth within the dephasing model [126, 135], but the connection with our semi-classical picture remains an open research direction.

Semiclassical theory of quantum stochastic resistors

Tony Jin [1], João Ferreira [1], Michel Bauer [2,3], Michele Filippone [4], and Thierry Giamarchi [1]

[1] *Department of Quantum Matter Physics, École de Physique University of Geneva, Quai Ernest-Ansermet 24, CH-1211 Geneva 4, Switzerland*

[2] *Université Paris-Saclay, CNRS, CEA, Institut de Physique Théorique, 91191 Gif-sur-Yvette, France*

[3] *PSL Research University, CNRS, École normale supérieure, Département de mathématiques et applications, 75005 Paris, France*

[4] *Univ. Grenoble Alpes, CEA, Grenoble INP, IRIG-MEM-L_Sim, Grenoble, France*

(Received 30 June 2022; revised 14 November 2022; accepted 13 December 2022; published 23 January 2023)

We devise a semiclassical model to describe the transport properties of low-dimensional fermionic lattices under the influence of external quantum stochastic noise. These systems behave as *quantum stochastic resistors*, where the bulk particle transport is diffusive and obeys the Ohm/Fick's law. Here, we extend previous exact studies beyond the one-dimensional limit to ladder geometries and explore different dephasing mechanisms that are relevant to different physical systems, from solid-state to cold atoms. We show how the semiclassical description is useful to explain the nontrivial dependence of the conductance of these systems on the chemical potential of the reservoirs. This description provides an intuitive and simpler interpretation of transport in quantum stochastic resistors in good quantitative agreement with the exact numerical solution. Moreover, we find that the conductance of quantum ladders is insensitive to the coherence of the dephasing process along the direction transverse to transport, despite the fact that the system reaches different stationary states.

DOI: 10.1103/PhysRevResearch.5.013033

I. INTRODUCTION

Diffusion is the most common type of transport encountered in many-body systems, both in the classical and in the quantum world. In condensed matter setups, it is observed whenever the resistance of a metallic conductor is measured. The emergence of resistive behavior is commonly attributed to the diffusive propagation of charge carriers caused by scattering with disorder, impurities or particles of the same or different nature (electrons, holes, phonons, magnons, etc.) [1]. Despite the clarity of these physical mechanisms, describing the emergence of diffusive transport from a full quantum perspective remains an open issue in theoretical physics [2–8].

In recent years, the study of open quantum systems has opened new exciting venues to understand the emergence of diffusion. The Markovian description of leads [9–16], losses [17–20] or external time-dependent noises [15,21–31] has provided valuable numerical and analytic insight into the problem. In this context, dephasing has been in the spotlight for being an analytically tractable process of physical importance. It is capable of describing the emergence of diffusion in quantum coherent systems [15,32–34], which behave as *quantum stochastic resistors* [35].

Despite these exact derivations of classical diffusive transport in the quantum realm, it remains an open question to which extent a classical description can account for the coherent transport properties and with which accuracy [36–38]. If successful, a classical description could provide additional insight on transport phenomena outside the framework of open quantum systems.

Moreover, most of the studies mentioned above are restricted to one dimension, often exploiting integrable structures in some fine tuned cases [8,22,32,39]. It is thus important to investigate the extension of exact solutions to higher dimensions and their richer behavior [40]. This understanding is also relevant to open new perspectives in the context of quantum matter simulators, where controlled dissipative dynamics is under study in both bosonic [41–43] and fermionic systems [44,45].

In this paper, we devise a semiclassical model, which accurately describes the transport properties of one-dimensional quantum stochastic resistors. We then derive a set of conditions under which the result for the 1D conductance can be extended to 2D systems. We focus on the quantum ladders geometries sketched in Fig. 1 (top), where a current is driven by a difference of chemical potential $\delta\mu$ between thermal leads. The lattice is under the influence of dephasing processes and the working principle of the semiclassical model is illustrated in Fig. 1 (bottom), in the one-dimensional limit. Semiclassically, dephasing is conceived as a stochastic reset of single particle velocities, which mimics a series of random quantum measurements of the particle position.

To characterize the transport properties of a dephased chain, we consider their conductance at a weak bias $\delta\mu$. We show that, in the presence of dephasing, the conductance is suppressed with the longitudinal extent of the system—the number of sites N in Fig. 1 (top)—revealing the emergence of bulk resistivity. We also observe that dephasing triggers a nontrivial dependence of the conductance on the chemical

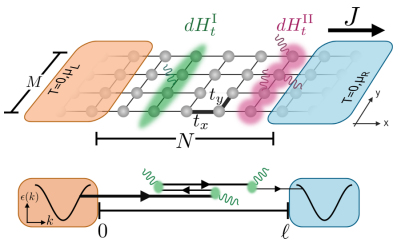

FIG. 1. (Top) Schematic representation of the system under study. An M-leg square ladder is attached at the edges to two leads prepared at the same temperature with distinct chemical potentials $\mu_{\mathrm{L,R}}$. The bias $\delta\mu$ in the chemical potential drives a particle current J that can depend on the noise. Noises differ on the spatial correlation along the y direction ranging from uniformly correlated dH_t^{I} to uncorrelated dH_t^{II}. (Bottom) Semiclassical interpretation of a 1D diffusive channel. A particle leaves a lead with a velocity determined by the band dispersion. A reset of a particle's velocity occurs at random times until it escapes to one of the leads. The distance between leads is $\ell = Na$ with a the lattice spacing.

potential μ of the reservoirs. In particular, the conductance vanishes when the chemical potential approaches the band edges, reflecting a suppression with the velocity of particles injected by the reservoirs. This dependence is absent in the ballistic case and is particularly intriguing as it is also absent in the bulk diffusion constant of the system. We show then how the semiclassical model is able to accurately reproduce the emergent μ dependence of the conductance, providing at the same time a simple physical picture connecting boundary and bulk diffusive effects.

We then extend these considerations to ladder systems. The presence of an additional degree of freedom along the y direction, transverse to the current flow along x, allows different dephasing processes. These processes can be either coherent or incoherent along the y direction, see Fig. 1 (top). The coherent case is for instance relevant to cold atom systems with a synthetic y dimension [46–49]. Even though these different noises drive the system towards totally different stationary states, we find that they carry exactly the same current. We explain this remarkable coincidence as a manifestation of the fact that the correlations of these different noises obey identical isotropy conditions, that we derive and discuss in detail.

This paper is structured as follows. In Sec. II, we discuss the Keldysh approach for the exact self-consistent derivation of currents in quantum stochastic ladder resistors. Section III introduces the semiclassical approach and illustrates its ability to reproduce exact results. Section IV discusses the extension to ladders and Sec. V discusses results and conclusions.

II. MODEL AND METHODS

We study the transport properties of spinless fermions on the discrete square lattice geometry sketched in Fig. 1 (top). We consider an infinite lattice along the longitudinal direction (x axis), with M sites in the transverse direction (y axis). The corresponding Hamiltonian reads

$$H = -\sum_{j,m}[t_x c^\dagger_{j+1,m}c_{j,m} + t_y c^\dagger_{j,m+1}c_{j,m} + \mathrm{H.c}]\,, \qquad (1)$$

where the sum over j runs between $\pm\infty$ and the second index between 1 and M. The operators $c_{j,m}$ annihilate fermions on site (j,m) and $t_{x/y}$ control the hopping amplitude along the x/y directions. We further divide the sum over the longitudinal direction into three regions: the system (S) for $j \in [1,N]$, the left (L) lead for $j<1$ and the right (R) lead for $j>N$, see Fig. 1 (top). It is useful to introduce the basis diagonalizing the transverse hopping term in Eq. (1), given by the unitary transformation $a_{j,p} = \sum_{m=1}^{M}\sqrt{\frac{2}{M+1}}\sin(\frac{\pi mp}{M+1})c_{j,m}$. This transformation uncouples the M transverse modes and the corresponding Hamiltonian reads

$$H = \sum_{j,p}[-t_x(a^\dagger_{j+1,p}a_{j,p} + \mathrm{H.c}) + \epsilon_p a^\dagger_{j,p}a_{j,p}]\,, \qquad (2)$$

with $\epsilon_p = -2t_y\cos(p\pi/(M+1))$ and $p\in[1,M]$. If the system is translational invariant along the x direction, the transverse modes have nondegenerate dispersion relations $\epsilon_{p,k} = -2t_x\cos(k)+\epsilon_p$, with $k\in[-\pi,\pi]$ the quasimomentum in the first Brillouin zone, see sketches in Fig. 3 for an illustration in the $M=2$ case. We reserve the indexes j,m for the physical sites in the x and y direction, and the indexes k,p label respectively longitudinal quasi-momenta and transverse modes.

In addition to the coherent Hamiltonian dynamics, we introduce a noise term modelled by a quantum stochastic Hamiltonian (QSH) that leads to various dephasing mechanisms that we are going to detail. The QSH is defined by the infinitesimal generator dH_t such that the total unitary operator $U(t)$ is evolved as

$$U(t+dt) = e^{-i(Hdt+dH_t)}U(t)\,. \qquad (3)$$

In this paper, we are interested in QSHs, which conserve the total particle number and lead to dephasing. They are described by

$$dH_t = \sqrt{2\gamma}\sum_{j,p,p'} a^\dagger_{j,p}a_{j,p'}dW_t^{j,p,p'}\,, \qquad (4)$$

where γ controls the overall dephasing rate and the dW_t are increments of stochastic processes defined within the Itō prescription [50]. The noise have a 0 mean, $\mathbb{E}[dW_t=0]$ and their Itō rules are defined to be

$$dW_t^{j_1,p_1,p_1'}dW_{t'}^{j_2,p_2,p_2'} = \delta_{j_1,j_2}C_{p_1,p_1',p_2,p_2'}dt \quad \text{for } t=t',$$
$$dW_t^{j_1,p_1,p_1'}dW_{t'}^{j_2,p_2,p_2'} = 0 \quad \text{for } t\neq t'. \qquad (5)$$

By construction, the noise is thus uncorrelated in time and in the longitudinal x direction, j index, but not necessarily on the transverse y direction, p index. Correlations of the noise in the y direction are taken into account by the function C, which can be adapted to describe different physical scenarios, as we are going to illustrate in the context of ladder geometries in Sec. IV. Since the dW_t commute with one another, we have $C_{p_1,p_1',p_2,p_2'} = C_{p_2,p_2',p_1,p_1'}$. Hermiticity also imposes that $dW_t^{j,p,p'} = (dW_t^{j,p',p})^*$. Qualitatively speaking, each term in

the sum of Eq. (4) describes transitions from a state indexed by p' to a state indexed by p with a random complex amplitude given by $dW_t^{j,p,p'}$. Since the Cs are arbitrary, Eq. (4) constitutes the most general way of writing noisy quadratic jump processes between different transverse propagation modes. In one dimension, discussed in Sec. III, Eq. (4) reduces to an on-site stochastic fluctuation of potential, leading to standard dephasing, see also Eqs. (13) and (14). In Sec. IV, we will specify different noise-correlations on ladders and discuss their implication on transport.

The mean evolution generated by the stochastic Hamiltonian (4), with the prescription (5), is described by the Lindblad generator acting on the reduced density matrix of the system ρ,

$$\mathcal{L}(\rho) = \gamma \sum_{j,p_1,p_2,p_1',p_2'} C_{p_1,p_1',p_2,p_2'} \big(2a^\dagger_{j,p_1} a_{j,p_1'} \rho a^\dagger_{j,p_2} a_{j,p_2'} - \{a^\dagger_{j,p_2} a_{j,p_2'} a^\dagger_{j,p_1} a_{j,p_1'}, \rho\}\big) \tag{6}$$

where $\{,\}$ denotes anticommutation; see Appendix B.

A. Keldysh approach and exact self-consistent solution of transport in quantum stochastic resistors

As we will be dealing with systems under the effect of dephasing noise and biased leads, the dynamics of the system is intrinsically out of equilibrium. The natural language to describe these systems is the Keldysh formalism [51], detailed in Appendix A. The central objects of the theory are the retarded (R), advanced (A), and Keldysh (K) components of the single-particle Green's functions $\mathcal{G}^{R/A/K}$. They are defined in time representation as $\mathcal{G}^R_{j,m;i,n}(t-t') = -i\theta(t-t')\langle\{c_{j,m}(t), c^\dagger_{i,n}(t')\}\rangle$, $\mathcal{G}^A_{j,m;i,n}(t-t') = [\mathcal{G}^R_{i,n;j,m}(t'-t)]^*$ and $\mathcal{G}^K_{j,m;i,n}(t-t') = -i\langle[c_{j,m}(t), c^\dagger_{i,n}(t')]\rangle$ [52]. By adopting the notation by Larkin and Ovchinnikov [53], these three components are collected in a unique matrix, which obeys the Dyson equation

$$\boldsymbol{\mathcal{G}} = \begin{pmatrix} \mathcal{G}^R & \mathcal{G}^K \\ 0 & \mathcal{G}^A \end{pmatrix}, \quad \boldsymbol{\mathcal{G}}^{-1} = \boldsymbol{g}^{-1} - \boldsymbol{\Sigma}, \tag{7}$$

where $\boldsymbol{g}$ corresponds to the Green's function of the system disconnected from the leads and unaffected by noise. The matrix $\boldsymbol{\Sigma}$ corresponds to the self-energy, which has the same matrix structure as $\boldsymbol{\mathcal{G}}$.

In the path integral formalism, the fermionic degrees of freedom of the leads can be integrated out. Their integration gives a contribution to the self-energy of the system $\boldsymbol{\Sigma}_{\mathrm{L/R}}$, which has nonzero components only at the system edges $j = 1, N$. The general procedure of this integration is detailed in Appendix A. To give a more explicit idea of the result of this procedure, we report here the result for the simplest one-dimensional case ($M = 1$). The edge contributions then read in frequency space

$$\begin{aligned}
\Sigma^{R/A}_{\mathrm{L},i,j} &= t_x^2 g^{R/A}_{0,0}\delta_{i,j}\delta_{i,1}, \\
\Sigma^{R/A}_{\mathrm{R},i,j} &= t_x^2 g^{R/A}_{N+1,N+1}\delta_{i,j}\delta_{i,N}, \\
\Sigma^{K}_{\mathrm{L},i,j} &= 2it_x^2 F_{\mathrm{L}} \mathrm{Im}\big(g^R_{0,0}\big)\delta_{i,j}\delta_{i,1}, \\
\Sigma^{K}_{\mathrm{R},i,j} &= 2it_x^2 F_{\mathrm{R}} \mathrm{Im}\big(g^R_{N+1,N+1}\big)\delta_{i,j}\delta_{i,N},
\end{aligned} \tag{8}$$

where $\mathrm{Im}(\cdot)$ gives the imaginary part. The retarded and advanced components of the self-energy are renormalized by the corresponding reservoir Green functions, which are calculated at the site closest to the system. See Eq. (A7) for the explicit expression of $g^{R/A}_{0,0}(\omega)$ and $g^{R/A}_{N+1,N+1}(\omega)$ in the case of leads identical to the system. The Keldysh components describe the tendency of the edges of the system to equilibrate to the attached reservoirs. The functions $F_{\mathrm{L,R}}(\omega)$ describe the state of the leads, and the self-energies obey a local equilibrium fluctuation-dissipation relation [51]. In the absence of noise, the leads are considered in thermal equilibrium with a well-defined chemical potential $\mu_{\mathrm{L,R}}$ and shared temperature T. In frequency representation, this situation is described by $F_{\mathrm{L,R}}(\omega) = \tanh[(\omega - \mu_{\mathrm{L,R}})/2T]$. The fact that the system is out of equilibrium can be read in Eq. (8) via the fact that different functions F affect the self-energy of the system at its borders.

The Keldysh formulation of the problem is advantageous because it allows to deal exactly with the dephasing dynamics caused by the presence of the noise described by Eq. (4). Despite the quartic nature of Eq. (6), the stochastic formulation of the dephasing (4) allows for a closed exact solution of the self-energy [24,34,35]. Indeed, the latter can be expressed in terms of the Green's function via the relation

$$\boldsymbol{\Sigma}_\gamma(t,t')_{(j,p_1),(j',p_2')} = \gamma\delta(t-t')\delta_{j,j'} \sum_{p_1'p_2} C_{p_1,p_1',p_2,p_2'} \boldsymbol{\mathcal{G}}_{(j,p_1')(j,p_2)}(t,t), \tag{9}$$

which, inserted in Eq. (7), has to be solved self-consistently, see Appendix B. To summarize, we derive an explicit expression of the self-energies in the Dyson equation (7), which reads

$$\boldsymbol{\mathcal{G}}^{-1} = \boldsymbol{g}^{-1} - \boldsymbol{\Sigma}_{\mathrm{L}} - \boldsymbol{\Sigma}_{\mathrm{R}} - \boldsymbol{\Sigma}_\gamma, \tag{10}$$

where the expression of $\boldsymbol{\mathcal{G}}$ is obtained numerically.

Equipped with the formal expression of the single-particle Green's functions, we can directly and exactly inspect the transport properties of quantum systems under the influence of dephasing noise. By imposing a finite bias, $\mu_{\mathrm{L/R}} = \mu \pm \frac{\delta\mu}{2}$, between the right and left leads, a uniform longitudinal current J flows through the system. By construction, the noise (4) preserves the total density $n_{j,\mathrm{tot}} = \sum_p a^\dagger_{j,p} a_{j,p}$ at a fixed position j on the x axis, i.e., $[dH_t, n_{j,\mathrm{tot}}] = 0$. Thus, the definition of the total longitudinal current operator is unchanged by the noise term, and the current can be evaluated at any site j, namely

$$\begin{aligned}
J &= it_x \sum_{m=1}^{M} \langle c^\dagger_{j+1,m} c_{j,m} - c^\dagger_{j,m} c_{j+1,m}\rangle \\
&= t_x \sum_{m=1}^{M} \mathrm{Re}\big[G^K_{j,m;j+1,m}(t=0)\big].
\end{aligned} \tag{11}$$

In the following, we will explicitly derive this expression from the exact self-consistent solution of Dyson's equation (9). Additionally, we rely on the linear expansion of Eq. (11) in the chemical potential difference $\delta\mu$ to study the conductance

of the system, which is defined as

$$G = \lim_{\delta\mu\to 0} 2\pi \frac{J}{\delta\mu}. \tag{12}$$

Notice that we rescaled the conductance by 2π in order to have the quantum of conductance equal to 1 and adopt the convention $e = k_B = \hbar = 1$. In the following sections, we devise a semiclassical model, which can capture the results from Eqs. (10), (11), and (12) in the presence of dephasing. In particular, we will inspect the conductance dependence on the chemical potential of the leads μ.

III. CONDUCTANCE OF A 1D QUANTUM STOCHASTIC RESISTOR

In this section, we focus on a strictly one-dimensional geometry to showcase the effectiveness of the semiclassical approach in describing the emergent diffusive transport properties of quantum stochastic resistors.

A. Exact derivation

We begin by deriving the dependence of the conductance G on the chemical potential of the leads μ, via the exact solution of a single chain subjected to on-site dephasing noise. In one dimension, the noise term in Eq. (4) reduces to

$$dH_t = \sqrt{2\gamma} \sum_j c_j^\dagger c_j dW_t^j, \tag{13}$$

with the corresponding Lindblad operator

$$\mathcal{L}(\rho) = \gamma \sum_j (2n_j \rho n_j - \{n_j, \rho\}). \tag{14}$$

For a QSH described by Eq. (4), the conductance of the system can be written

$$G_\gamma(\mu) = \int d\omega \frac{\mathcal{T}_\gamma(\omega)}{4T\cosh^2\left(\frac{\omega-\mu}{2T}\right)}. \tag{15}$$

Two equivalent expressions of $\mathcal{T}_\gamma(\omega)$ are derived in Appendix B, one relying on the expansion in $\delta\mu$ of Eq. (11), and the other on the expansion of the Meir-Wingreen formula as devised in Refs. [14,35]. The expression (15) for the conductance reproduces Landauer-Büttiker's formula, valid for noninteracting ballistic systems [54]. As such, $\mathcal{T}_\gamma(\omega)$ is interpreted as the transmittance of the channel at energy ω for a fixed γ, a quantity independent of the temperature T and chemical potential μ of the leads. An explicit expression of $\mathcal{T}_\gamma(\omega)$ was computed in Ref. [35] in similar settings. We stress that the extension of Landauer-Büttiker's formula (15) to dephased systems is highly nontrivial, given the fact that dephasing triggers inelastic scattering events in the conducting region.

If we consider leads, which are identical to the system, see Eq. (1), no reflection occurs at the interface and $\mathcal{T}_{\gamma=0}(\omega) = 1$ for $\omega \in [-2t_x, 2t_x]$ and 0 elsewhere. At zero temperature, this implies the usual quantized conductance $G = 1$ when the chemical potential of the leads lies within the dispersion relation of the reservoirs, $\mu \in [-2t_x, 2t_x]$ [1,55–57]; see Fig. 2.

The presence of any finite dephasing rate leads to diffusive transport in the thermodynamic limit [15,33–35,58]. In these

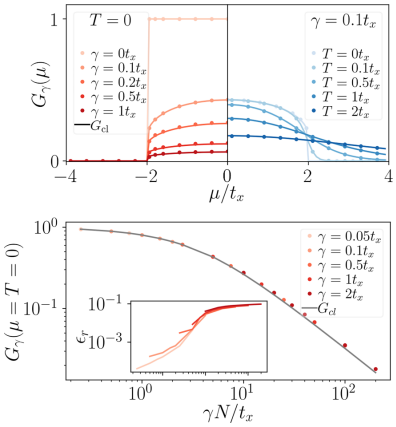

FIG. 2. (Top) Conductance as a function of chemical potential for increasing dephasing rates γ at $T = 0$ (left) and increasing temperature (right) at a fixed system size $N = 50$. The dots are derived relying on the exact quantum calculation (Sec. III A), while the dashed lines correspond to the semiclassical approximation (Sec. III B). (Bottom) Scaling of the conductance with the parameter γN when $T = 0$, $\mu = 0$. (Inset) Relative error of the semiclassical conductance at $\mu = 0$, $\epsilon_r = |G_{cl} - G_\gamma|/G_\gamma$.

studies, it was shown that the bulk transport properties are described by Fick's law

$$J = -D\nabla n, \tag{16}$$

where D is the diffusion constant and ∇n the particle density gradient along the chain. In particular, for fixed boundary conditions, Fick's law implies the $1/N$ suppression of the current with the system size and

$$D = \frac{2t_x^2}{\gamma}. \tag{17}$$

This suppression reveals the emergence of a resistive behavior, compatible with Ohm's law. This relation holds in the bulk *regardless* of the average chemical potential μ and temperature T of the biased leads. This fact can be understood as follows: at equilibrium, the effect of the noise term is to drive the system towards an infinite temperature state with a fixed number of particle [59]. Here the situation is more intricate since we are out-of-equilibrium. Nevertheless, we show numerically in Appendix D that, deep in the bulk, there exist a well-defined notion of *local equilibrium*, where the system does reach an infinite temperature state. Thus, in the bulk, the information about the energy scales of the leads is erased, and one expects that bulk transport properties, such as the diffusion constant, will be independent of the temperature and the chemical potentials of the boundaries. This point will be further emphasized in Sec. IV.

In contrast to the diffusion constant D, the conductance strongly depends on the temperature and chemical potential of the attached leads; see Fig. 2 (top) [60]. For a finite

dephasing rate γ, G_γ develops a clear dome-like dependence on the chemical potential [61] This shape persists even in the diffusive regime $N \gg t_x/\gamma$ where the conductance vanishes as $1/N$; see Fig. 2 (bottom) and Fig. 7 in Appendix C. At $T = 0$, the dome is restricted to energies within the bandwidth $[-2t_x, 2t_x]$ and the differential conductance $\partial_\mu G$ diverges whenever the chemical potential touches the edges of the band, even when $\gamma > 0$. This behavior is reminiscent of the "staircase" behavior of the conductance for noninteracting systems and $\gamma = 0$. The main difference is that for $\gamma > 0$ the conductance G is not quantized and acquires a μ dependence in the $[-2t_x, 2t_x]$ interval. As expected, increasing the temperature of the leads smears the dependence of the conductance with respect to the chemical potential, as illustrated in Fig. 2 (top).

The dome-like dependence of the conductance ultimately originates from its connection to the leads but it is independent of the microscopic details of the latter. Reservoirs with a linear band dispersion (i.e., not a cosine dispersion) would equally lead to a maximum of the conductance near the band center. Despite its usefulness, the numerical exact solution relies on relatively involved technical tools (Keldysh field theory and full diagrammatic ressummation), which somehow prevent a transparent interpretation of the phenomenology at work (e.g., the dome-shaped dependence of the conductance on μ). It is thus important to have a simpler description of transport that can simultaneously explain a constant diffusion constant, as well as the quantitative dependence of the conductance with the chemical potential.

In the next section, we show that a semiclassical model allows to build an intuitive physical explanation of the dependence of G_γ on the chemical potential and to connect it with the bulk behavior of transport.

B. Semiclassical approach

The Lindblad operator (14) can actually describe the average evolution of a system under different stochastic processes, which differ from the stochastic fluctuations of potential considered in Eq. (13). Indeed, the most natural way to devise a semiclassical description of the Lindblad dynamics of Eq. (14) is to "unravel" it to a projective measurement process, where the densities at each site are measured independently with rate γ [62,63]. Notice that for single realizations of the stochastic process, the projective dynamics fundamentally differs from the quantum stochastic dynamics described by Eq. (13). For instance, a density measurement on site j would project the system in a state with 1 or 0 particles on that site in a nonunitary fashion. On the contrary, the random potential fluctuations described by Eq. (13) are always unitary at the level of a single realization. Nevertheless, the projective and QSH dynamics coincide in average and are described by the same effective Lindblad operator (14).

In the projective case, at each time step Δt, a measurement at site j occurs with probability $\gamma\,\Delta t$. After a measurement, depending on whether the local particle number is measured to be zero or one, the density matrix is updated as follows:

$$\rho \to \rho_0 = \frac{(1-n_j)\rho(1-n_j)}{\mathrm{Tr}[\rho(1-n_j)]}, \quad \rho_1 = \frac{n_j\rho n_j}{\mathrm{Tr}[\rho n_j]}, \tag{18}$$

with respective probabilities

$$P_{\rho_0} = \mathrm{Tr}[\rho(1-n_j)], \quad P_{\rho_1} = \mathrm{Tr}[\rho n_j]. \tag{19}$$

Averaging over the possible outcomes for a small time step dt yields the average evolution of the density matrix $d\rho_t = \rho_{t+dt} - \rho_t$,

$$d\rho_t = \gamma\, dt \sum_j (2n_j\rho_t n_j - \{n_j, \rho\}), \tag{20}$$

which is equivalent to the Lindblad evolution described by Eq. (14).

This alternative point of view is the natural one to devise a semiclassical description of transport in systems affected by dephasing. If we consider a single-particle traveling through the chain, the effect of a measurement is to localize it at a given site j. When the particle is localized, it is in a superposition of all possible momentum states.

We thus propose the analogous classical model in the continuum limit: consider a single particle of initial velocity $v_0(\omega)$ coming from the left lead into the system of length $\ell = Na$, where a is the lattice spacing. Its velocity is set by its energy ω, $v_0(\omega) = \partial\epsilon_k/\partial k|_\omega$, where ϵ_k is the dispersion relation of the lead, see Fig. 1 (bottom). At a random time t, determined by the Poissonian probability distribution $p(t) = \gamma e^{-\gamma t}$, its velocity is reinitialized by drawing a momentum k sampled from a uniform probability distribution on the interval $[-\pi, \pi]$. For a dispersion relation $\epsilon_k = -2t_x\cos(k)$, the probability distribution of the velocity v reads

$$p(v) = \frac{1}{2\pi t_x\sqrt{1-\left(\frac{v}{2t_x}\right)^2}}, \quad v \in [-2t_x, 2t_x]. \tag{21}$$

Once the velocity has been reset, the process is restarted. Whenever the particle reaches one boundary located at $x = 0$ or $x = \ell$, it exits the system. The problem of computing the semiclassical transmittance $\mathcal{T}_{\mathrm{cl}}$ can be reduced to compute the probability of exiting the system by touching the right boundary. Note that this problem differs from a usual random walk, as in this case the length of the steps are not uniform in time.

Once a measurement occurs, the velocity of a particle injected by a reservoir gets totally randomized according to the probability distribution (21). Thus the object of interest becomes the probability $P(x)$ of exiting the system once a given measurement has taken place at some position $x \in [0, \ell]$. The first measurement takes place at position x and time $t = x/v_0(\omega)$ with Poissonian probability distribution $\gamma e^{-\gamma t}$. Thus, the semiclassical transmittance $\mathcal{T}_{\mathrm{cl}}$, for a particle injected from the left lead with velocity $v_0(\omega)$, is given by

$$\mathcal{T}_{\mathrm{cl}}(\omega) = \int_0^\infty P(x)\frac{\gamma}{v_0(\omega)}e^{-\gamma\frac{x}{v_0(\omega)}}dx\,. \tag{22}$$

We recall that, because of the specific dispersion of the leads under consideration, $\mathcal{T}_{\mathrm{cl}}(|\omega| > 2t_x) = 0$.

It remains to determine $P(x)$. It is useful to introduce the probability $P_v(x)$ for a particle to exit on the right when it starts at x with velocity v. The probability $P(x)$ is thus the integral of this probability over all possible velocities, $P(x) = \int dv\, p(v)P_v(x)$. As we assume that no measurement process

occurs in the leads, $P(x)$ has to fulfill the boundary conditions

$$P(x<0)=0, \quad P(x>\ell)=1. \tag{23}$$

In the system, where the measurement processes occur, $P_v(x)$ is expressed in the closed form

$$P_v(x)=\theta(v)\left[e^{-\gamma\frac{\ell-x}{v}}+\int_0^{\frac{\ell-x}{v}}dt\gamma e^{-\gamma t}P(x+vt)\right] +\theta(-v)\int_0^{-\frac{x}{v}}dt\,\gamma e^{-\gamma t}P(x+vt) \tag{24}$$

where $\theta(v)$ is the usual Heaviside step function. The first term corresponds to the probability that the particle goes through the system without the occurrence of any measurement. The second term is the probability that a right mover resets at time t multiplied by the probability to exit if the particle starts again from this position. The last term corresponds to the same process but for a left mover. By integrating over the distribution of velocities (21), we get an implicit equation for $P(x)$ for $x\in[0,\ell]$,

$$P(x)=\varphi(\ell-x)-\int_0^{\ell-x}dy\,\varphi'(y)\,P(x+y) -\int_0^{x}dy\,\varphi'(y)\,P(x-y) \tag{25}$$

where we have introduced the function

$$\varphi(y)=\int_0^\infty dv\,p(v)\,e^{-\gamma\frac{y}{v}}=\int_0^1 dx\,\frac{e^{-\frac{\gamma y}{2t_x x}}}{\pi\sqrt{1-x^2}}, \tag{26}$$

and $\varphi'(y)=\partial\varphi/\partial y$. From Eq. (25), the probability $P(x)$ can be in principle derived iteratively in the number of measurement-induced resets of velocity. This solution would consist in writing

$$P(x)=\sum_{n=0}^{\infty}P_n(x), \tag{27}$$

where $P_n(x)$ is the probability of exiting on the left after n resets starting from x. This leads to

$$P_0(x)=\varphi(\ell-x), \tag{28}$$

$$P_{n+1}(x)=-\int_0^{\ell-x}dy\,\varphi'(y)\,P_n(x+y) -\int_0^{x}dy\,\varphi'(y)\,P_n(x-y). \tag{29}$$

Nevertheless, we have found empirically that solving Eq. (25) self-consistently provides faster convergence and numerical stability [64] in comparison to the recursive solution (27). We use the derived solution in Eq. (22), to obtain the semiclassical expression of the transmittance.

Using the newly found transmittance in formula (15), we compute the associated semiclassical conductance $G_{\rm cl}$. In Fig. 2, we compare $G_{\rm cl}$ (solid lines) with the exact quantum calculation G_γ (dots) and find an excellent agreement for all chemical potentials and temperatures.

Deep in the diffusive region, $N\gg t_x/\gamma$, the semiclassical model has some deviations with respect to the quantum solution. In the inset of Fig. 2 (bottom), we depict the relative error $\epsilon_r=|G_{cl}-G_\gamma|/G_\gamma$ in the middle of the spectrum and verify it does not increase above 10%. One possible explanation for this discrepancy could be that the semiclassical model assumes that at each reset event the new momentum is drawn uniformly in the interval $[-\pi,\pi]$ and the particle has ballistic propagation at the corresponding velocity. In principle, we have to take into account the mode occupation of the fermions in the system. Indeed, the exclusion principle should prevent the particle to acquire a momentum corresponding to an already occupied mode. Taking these effects into account is, however, beyond the scope of this paper. We also stress that within this approach, we have considered leads and systems described by the same Hamiltonian in absence of dephasing. This assumption ensures that we do not need to take into account any additional reflection phenomena that might occur when the particle is transferred from the leads to the system.

The semiclassical picture provides an intuitive explanation of the conductance drop observed close to the band edges, $\mu_{\rm edge}=\pm 2t_x$. Close to these points, the velocity of incoming particles is the lowest. It is then more likely that a measurement process will occur and reset its speed, increasing its chance to backscatter into the original lead, and thus reducing the conductance. Additionally, the first measurement process resets the single-particle velocity, leading to a uniform distribution of the particle over all the accessible states. Thus, after the measurement the particle attains an infinite temperature state, which is reservoir-independent and is the one related to the bulk transport properties described by the diffusion constant (17). Remark that this picture is consistent with the fact that the diffusion constant evaluated in the bulk is independent of the boundary chemical potentials and temperatures. In conclusion, this simple semiclassical physical picture connects bulk and boundary effects on the transport properties of this system, which are revealed by the diffusion constant and the conductance respectively.

IV. DEPHASED LADDER

We now extend the result for the conductivity of a 1D system to a ladder made of M legs in the transverse direction, as described by the Hamiltonian (1), see also Fig. 1. In this section, we consider noises that are site-to-site independent along the x axis, but without a fixed structure in the y direction. Even though a natural choice is to consider noise processes, which are uncorrelated along the y direction (as we will do), considering also correlated structures is motivated from synthetic dimensions setups. These setups make use of coupling between nonspatial degrees of freedom to simulate motion along additional dimensions [46–49]. In our setup, the x direction would correspond to the physical dimension while the synthetic dimension is mapped to the transverse y direction. With this mapping, the QSH studied here could be realized from randomly oscillating potentials that are spatially resolved in the physical direction; see also Sec. V.

We recall the generic expression for the QSH Eq. (4),

$$dH_t=\sqrt{2\gamma}\sum_{j,p,p'}a^\dagger_{j,p}a_{j,p'}dW_t^{j,p,p'}, \tag{30}$$

with the covariance of the noise $dW_t^{j_1,p_1,p_1'} dW_t^{j_2,p_2,p_2'} = \delta_{j_1,j_2} C_{p_1,p_1',p_2,p_2'} dt$. Each term of the sum describes a transition from a state indexed by p' to a state indexed by p with a random complex amplitude given by $dW_t^{j,p,p'}$. It is the most general way of writing noisy quadratic jump processes between different states in the y direction.

In what follows, we will investigate the transport for different geometries of the noise by specifying the covariance tensor C.

A. Noise I

We start with the simplest case, that we label Noise I. It involves a single uniform noise acting on a given vertical section of the system, see also Fig. 1 (top). It is described by

$$C^{\mathrm{I}}_{p_1,p_2,p_1',p_2'} = \delta_{p_1,p_2}\delta_{p_2,p_1'}\delta_{p_1',p_2'}\,, \tag{31}$$

which corresponds to a QSH of the form

$$dH_t^{\mathrm{I}} = \sqrt{2\gamma}\sum_{j,m} c^\dagger_{j,m} c_{j,m} dB_t^j = \sqrt{2\gamma}\sum_{j,p} a^\dagger_{j,p} a_{j,p} dB_t^j\,, \tag{32}$$

with $\{B_t^j\}$ independent Brownian processes (recall that m indexes the spatial degrees of freedom in the y direction while p indexes the transverse modes). This kind of noise can be naturally implemented in synthetic ladders generated from internal spin degrees of freedoms of ultracold atoms [46–49]. Equation (31) would correspond to a randomly fluctuating potential that acts independently on each atom and uniformly shifts the energy levels of each spin state by $\sqrt{2\gamma}$.

The noise dH_t^{I} commutes at fixed j with the occupation number operator of every mode p, $a^\dagger_{j,p} a_{j,p}$, and therefore does not couple different modes. As a consequence, all the results that we have derived for the conductance of a 1D system can be trivially extended to the present case since the system is then equivalent to a collection of uncoupled 1D bands. The dispersion associated to each band $\epsilon_p(k)$ is the same than for the 1D case with an overall energy shift given by $\epsilon_p(\pi/2)$. Thus, the total conductance is the sum of the contribution of each mode, namely,

$$G_{\mathrm{I}}(\mu) = \sum_p G_\gamma\Big[\mu - \epsilon_p\Big(\frac{\pi}{2}\Big)\Big]\,, \tag{33}$$

where G_γ is given by Eq. (15), extensively studied in the purely 1D case.

In the absence of dephasing and at zero temperature ($\gamma = T = 0$), the conductance shows the usual staircase quantization with respect to the chemical potential. As it is shown in Fig. 3 for a two-leg ladder, the jumps in conductance take place whenever the number of bands crossed by the chemical potential changes. For a finite rate γ, the action of the dephasing noise is the same for each individual band and, as a consequence, the total conductance decays as $1/N$ for larger systems.

We stress that since Noise I does not mix the different modes, it cannot change the value of their occupation number, which is set by the chemical potential in the reservoirs. For instance, if a given mode was initially empty, it will remain so in the steady state. However, at fixed p, within *a single band*, the dephasing noise (13) drives the density matrix to a state proportional to the identity [59], which is reminiscent of the infinite temperature state discussed in the 1D case, see also Appendix D. We therefore say that Noise I is *maximally mixing* the modes k in the x direction but not mixing at all the modes p in the y direction. As a consequence, it does not drive the system to a genuine infinite temperature state, this only happens within each individual band. A picture of this stationary state for increasing chemical potentials is sketched in Fig. 3.

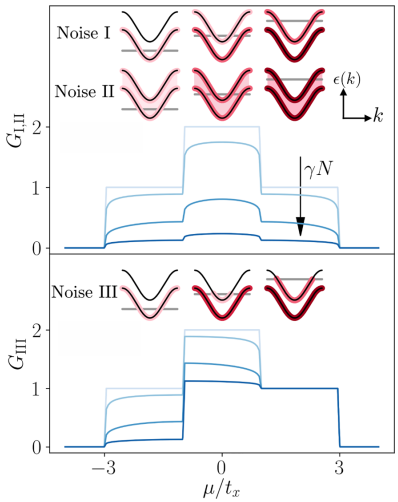

FIG. 3. Conductance profiles for different correlations of the noise (30) and increasing values of γN. For increasing shades of blue: $\gamma = 0$; $\gamma = 0.1\,t_x, N = 5$; $\gamma = 0.5\,t_x, N = 10$ and $\gamma = 0.5\,t_x, N = 50$ and $t_y = t_x$. Noise I and II share the same conductance profile, while Noise III features the coexistence of ballistic and diffusive transport, see main text. The sketches on top of the conductance plots depict the stationary state reached in the bulk. These states may or may not depend on the position of the chemical potential μ in the reservoirs (horizontal-grey lines), with respect to the dispersion relations of the different conduction modes in the system (black lines). The red halo on top of the dispersion relations indicates the occupation probability of the modes. Noise I distributes particle uniformly within each band separately, while Noise II distributes the states in all bands isotropically. Noise III is a special case, which preserves the shape of the zero temperature distribution of the reservoirs in the bulk only in the upper band.

We now show that the conductance profile illustrated in Fig. 3 is not unique to the uncorrelated Noise I (31), and also describes other types of geometries.

B. Noise II

In this section, we consider an isotropic case, where the noise is uncorrelated both in the x and y directions. In this

case, that we label Noise II, the QSH in position basis reads

$$dH_t^{\mathrm{II}} = \sqrt{2\gamma}\sum_{j,m} c^\dagger_{j,m} c_{j,m} dB_t^{j,m}, \tag{34}$$

with $dB_t^{j_1,m_1} dB_t^{j_2,m_2} = \delta_{j_1,j_2}\delta_{m_1,m_2} dt$. After performing the unitary transformation that diagonalizes the nonstochastic problem (1) in the form (2), we find the noise correlation function

$$C^{\mathrm{II}}_{\substack{p_1,p_1'\\ p_2,p_2'}} = \left(\frac{2}{M+1}\right)^2 \sum_{m=1}^{M} \prod_{\substack{a=p_1,\\ p_1',p_2,p_2'}} \sin\left(\frac{\pi a m}{M+1}\right). \tag{35}$$

Contrary to the previous case, Noise II is maximally mixing for the modes k in the x direction and for the modes p in the y direction. As a consequence, this noise drives the system to a genuine infinite temperature state in the bulk; see also sketches in Fig. 3. The mixing of the modes in the transverse direction renders the task of computing the conductance an *a priori* nontrivial one.

Nevertheless, as we show in Appendix E, for any noise satisfying the condition

$$\sum_p C_{p_1,p,p,p_2} = \mathcal{N}\delta_{p_1,p_2}, \tag{36}$$

the equations of motion of the total current J coincide to those generated by Noise I up to a renormalization of γ by a constant $\mathcal{N}$. As shown in the Appendix E, this condition corresponds $\forall p$ to $(a^\dagger_{j,p}, a_{j,p})$ being eigenvectors of the dual Lindbladian $\mathcal{L}^*$ with the same eigenvalue $\mathcal{N}$. The fact that $\mathcal{L}^*$ act the same way on the transverse modes can be seen as an isotropy condition for the noise term, i.e., this term cannot discriminate between longitudinal modes and hence, cannot change the value of the total current.

Using that $\delta_{a,a'} = \frac{2}{M+1}\sum_j \sin(\frac{\pi a j}{M+1})\sin(\frac{\pi a' j}{M+1})$, one can verify that C^{II} satisfies condition (36) with $\mathcal{N} = 1$. Thus we find that

$$G_{\mathrm{I}}(\mu) = G_{\mathrm{II}}(\mu). \tag{37}$$

This result may sound surprising as, even though Noise II drives the system towards the maximally mixed, infinite temperature state, the staircase behavior of G is preserved, i.e., there is a discontinuity of $\partial_\mu G$ every time the chemical potential touches a band.

The remarkable equality (37) can be intuitively understood within the semiclassical picture. All that matters for the conductance is the number of modes that can contribute to the current. This number is fixed by the chemical potential, which in turn controls the staircase behavior of the conductance. Once a particle has entered the system, different scattering events may switch it from one channel to the other isotropically, as expressed mathematically by the condition (36). Nevertheless, all the channels carry the current in the same fashion, since the dispersion relations of all the transverse modes coincide in quasi-momentum k, except for an irrelevant energy shift. As a consequence, the total conductance is insensitive to whether the noise is coherent (or not) along the transverse direction.

C. Noise III

Finally, we illustrate how breaking the condition (36) may lead to exotic transport. We introduce the case of Noise III, where the correlations C^{III} of Noise III are designed such that they only couple pairs of transverse modes,

$$C^{\mathrm{III}}_{p_1,p_1',p_2,p_2'} = f_{p_1,p_2}\delta_{p_1,p_2'}\delta_{p_1',p_2}, \tag{38}$$

for which

$$\sum_p C^{\mathrm{III}}_{p_1,p,p,p_2} = \delta_{p_1 p_2}\sum_p f_{p_1,p}. \tag{39}$$

This qualitatively corresponds to the case where, for any noisy process that transfers a particle from the band p_1 to p_2, there is the reverse process that transfers a particle from p_2 to p_1 with the same rate f_{p_1,p_2}.

The isotropy condition (36) is fulfilled if, for example, we impose f_{p_1,p_2} to be equal to a constant c for every (p_1, p_2) in which case we have that $\mathcal{N} = Mc$.

Breaking the isotropy condition can lead to a hybrid type of transport. For instance, let us consider the case where

$$f_{p_1,p_2} = \delta_{p_1,p_2}\theta(p - p_0), \tag{40}$$

with the convention $\theta(0) = 0$ for the Heaviside step function. This noise imposes diffusive transport to the lowest transverse modes ($p \leqslant p_0$) while the highest modes ($p > p_0$) remain ballistic. Since this noise does not couple the different transverse modes, the conductance has both ballistic and diffusive contributions,

$$G_{\mathrm{III}}(\mu) = \sum_{p\leqslant p_0} G_\gamma(\mu - \epsilon_{y,p}) + \sum_{p>p_0} G_{\gamma=0}(\mu - \epsilon_{y,p}). \tag{41}$$

We plot an example of such situation on Fig. 3 (bottom) for a two-leg ladder and $p_0 = 1$. The overall current has diffusive behavior until the chemical potential reaches the bottom of the upper band at $\mu_0 = -2t_x - 2t_y\cos(\frac{p_0\pi}{M+1})$. For $\mu \geqslant \mu_0$ the ballistic mode starts contributing and dominates the conductance in the thermodynamic limit $N \to \infty$

V. CONCLUSIONS AND PERSPECTIVES

In this paper, we have studied the current flowing through M-leg ladders subject to external dephasing noises with different correlations along the direction y transverse to transport. Starting from the purely one-dimensional case, $M = 1$, we have devised a semiclassical model to compute the conductance as a function of the chemical potential and found excellent agreement with numerical solutions obtained from exact self-consistent calculations of Dyson's equation.

Showing the effectiveness of this semiclassical model is important as it allows to build a simple and intuitive physical picture of the emergence of bulk resistive behavior in quantum stochastic resistors. As extensively discussed in the core of this paper, the bulk transport properties of these systems, such as the diffusion constant or the resistivity, are insensitive to the temperature and chemical potential of the connected reservoirs. We showed that this is not the case for their conductance and that we could rely on the semiclassical approach to bridge between boundary and bulk effects. It could be interesting to understand the deeper connections between our semiclassical

model and the quasiparticle picture recently introduced to describe entanglement growth [65,66].

The effectiveness of the semiclassical approach may also hint to a potential connection to Drude models of impurity scattering. As in Drude models, the dependence of the conductance on the chemical potential shown in Fig. 2 is somehow directly related to the inverse of the density of states of the system. Even though the semiclassical approach in our case strongly relies on the unraveling of the Lindblad operator to a measurement process, we can also understand the local dephasing as induced by a local phonon bath at infinite temperature. Whether such unraveling is possible/relevant for more generic scattering problems, also in higher dimensions, remains to be understood.

We have also shown that these nontrivial results in one dimension could be also extended to M-leg ladder systems. In particular, we have shown that the results valid in 1D could be immediately applied to the case where the noise term preserves the coherence in the vertical direction, this case being particularly relevant to systems featuring synthetic dimensions [46–49]. In this case, the total conductance is just the sum of the contributions of independent 1D channels and its diffusion constant remains unchanged.

We then demonstrated that the coherence properties of the noise along the y direction do not play a role on the conductance of a ladder system when the noise fulfills the condition (36). We also showed that breaking this condition for the correlations of the noise allows to engineer exotic transport. We gave an example (Noise III) where the longitudinal current switches between a diffusive or ballistic behavior depending on the chemical potential.

The isotropy condition (36) can be understood as the condition under which each transverse mode contributes to the total longitudinal current in the same manner. This raises the natural question of understanding what would happen if this degeneracy were to be lifted. A particularly interesting problem would be to understand the effect of density-density interactions in the transverse direction to the transport. In the two-leg ladder, numerical studies relying on DMRG techniques could be supported by the infinite system size perturbation technique recently introduced in Ref. [35].

We briefly comment on the prospect of experimental realizations. The noise discussed here is specially suitable for implementation in synthetic dimensions setups such as ultracold atoms in shaken constricted optical channels [67] or with synthetic spin dimension [46–49,68], or even photonic systems with ring resonator arrays [69,70]. In these systems, the synthetic dimension plays the role of transverse direction in our model while the physical dimension encodes the longitudinal direction. A dephasing noise in the physical dimension would thus affect in the same manner all the synthetic sites, giving a natural realization of Noise I described by Eq. (31).

ACKNOWLEDGMENTS

The authors thank Iacopo Carusotto for helpful discussions. This work has been supported by the Swiss National Science Foundation under Division II. J.S.F. and M.F. acknowledge support from the FNS/SNF Ambizione Grant No. PZ00P2_174038.

APPENDIX A: GREEN'S FUNCTION OF THE FREE SYSTEM

To compute the current operator (11), one first needs to compute the Green's function of the lead alone and of the system in presence of the leads. For simplicity, we treat here the 1D channel but generalization to M legs will be straightforward. For a single left lead, the Hamiltonian (1) can be divided as

$$H = H_{\mathrm{S}} + H_{\mathrm{L}} - t_x(c_0^\dagger c_1 + c_1^\dagger c_0). \tag{A1}$$

We suppose the lead (L) and the system (S) to be noninteracting so that $H_{\mathrm{L,S}}$ is a quadratic Hamiltonian. The associated action in the Keldysh formalism, using Larkin notation [53] for the fermionic fields,

$$\begin{aligned} S = S_{\mathrm{S}} + \int \frac{d\omega}{2\pi}([\bar\psi_{\mathrm{L}}]\boldsymbol{g}_{\mathrm{L}}^{-1}[\psi_{\mathrm{L}}]) \\ + t_x\left(\bar\psi_0^1\psi_1^1 + \bar\psi_0^2\psi_1^2 + \bar\psi_1^1\psi_0^1 + \bar\psi_1^2\psi_0^2\right) \end{aligned} \tag{A2}$$

where S_{S} is the action of the system, $[\psi_{\mathrm{L}}]$ is a vector containing all Grassman variables associated to the left lead and $\boldsymbol{g}$ is the Green's function before coupling, with the same matrix structure as $\boldsymbol{\mathcal{G}}$ in Eq. (7), $\boldsymbol{g} := \left(\begin{smallmatrix} g^R & g^K \\ 0 & g^A \end{smallmatrix}\right)$. Integrating out the lead's degrees of freedom, one finds

$$\begin{aligned} S = S_{\mathrm{S}} - \int \frac{d\omega}{2\pi}\begin{pmatrix}\bar\psi_1^1 & \bar\psi_1^2\end{pmatrix}\begin{pmatrix}\Sigma^R & \Sigma^K \\ 0 & \Sigma^A\end{pmatrix}\begin{pmatrix}\psi_1^1 \\ \psi_1^2\end{pmatrix}, \\ \Sigma^{R/A/K} = t_x^2 g_{0,0}^{R/A/K}. \end{aligned} \tag{A3}$$

For an infinite-size lead made of n discrete sites with a tight-binding Hamiltonian coinciding with Eq. (1), the spectrum is given by $\epsilon_k = -2t_x\cos(\frac{k\pi}{n+1})$, $k \in [1, n]$. The associated retarded Green's function in momentum space is given by (the tilde designates momentum space)

$$\tilde g_{k,k'}^R(\omega) = \frac{\delta_{k,k'}}{\omega + 2t_x\cos\left(\frac{k\pi}{n+1}\right) + i0^+}. \tag{A4}$$

In position space, this yields

$$\begin{aligned} g_{j,j'}^R = \frac{2}{n+1}\sum_k \sin\left(\frac{k(j+1)\pi}{n+1}\right)\sin\left(\frac{k(j'+1)\pi}{n+1}\right) \\ \times \frac{1}{\omega + 2t_x\cos\left(\frac{k\pi}{n+1}\right) + i0^+}. \end{aligned} \tag{A5}$$

We are interested in the $j = j' = 0$ term in the semi-infinite limit, i.e., we take $n \to \infty$. Introducing $p = \frac{k\pi}{n+1}$, we get

$$g_{0,0}^R = \frac{2}{\pi}\int_0^\pi dp \frac{\sin^2 p}{(\omega + 2t_x\cos p + i0^+)}, \tag{A6}$$

which can be computed by contour integral in the complex plane to be

$$g_{0,0}^R = \frac{1}{2t_x^2}(\omega + i0^+ - i\sqrt{(2t_x)^2 - (\omega + i0^+)^2}). \tag{A7}$$

The advanced component is just the complex conjugate of the retarded one. To obtain the Keldysh component, we will

suppose that the lead is at thermal equilibrium so that

$$g^K_{0,0}(\omega) = \tanh\left(\frac{\omega-\mu}{2T}\right) 2i\mathrm{Im}(g^R_{0,0}) = -\theta(2t_x-|\omega|)\frac{i}{t_x^2}\tanh\left(\frac{\omega-\mu}{2T}\right)\sqrt{(2t_x)^2-\omega^2}\,, \tag{A8}$$

which is enough to compute the Green's function of the system in presence of the leads [71]. In the absence of noise, the Green's function of the system is easily computed by noticing that the system with both leads constitutes a discrete tight-binding chain of infinite size. In this case, the Green's function in momentum space is given by

$$\tilde{\mathcal{G}}^R(p,p') = \frac{\delta(p-p')}{\omega + 2t_x\cos p + i0^+}. \tag{A9}$$

By doing the inverse Fourier transform we get it in position space

$$\mathcal{G}^R_{j,k} = \int_{-\pi}^{\pi}\frac{dp}{2\pi}\frac{e^{-ip(j-k)}}{\omega+2t_x\cos p+i0^+}\,, \tag{A10}$$

which can be again computed by contour integral to be

$$\mathcal{G}^R_{j,k} = \frac{z_+^{k-j}}{t_x(z_+-z_-)}\,, \tag{A11}$$

for $j \leqslant k$ with $z_\pm = -(\frac{\omega+i0^+}{2t_x}) \pm i\sqrt{1-(\frac{\omega+i0^+}{2t_x})^2}$. Using the symmetry property $\mathcal{G}^R_{j,k} = \mathcal{G}^R_{k,j}$ we have the full Green's function in position space.

APPENDIX B: DERIVATION OF THE EXACT SELF-CONSISTENT EQUATION AND OF THE TRANSMITTANCE OF QUANTUM STOCHASTIC RESISTORS

In this section, we summarize the derivation of the self-consistent condition (9) as obtained in previous papers [24,35]. We also explain the factorization of the current in the form of Eq. (15). We also derive the Linbdlad equation describing the dynamics of QHS averaged over the noise realizations.

1. Self-consistent equation

In full generality and to improve readability, we consider a more compact formulation of the noise than in Eq. (4), where $dH_t = \sum_{i,j}\sqrt{2\gamma}c_i^\dagger c_j dW_t^{i,j}$ and i, j are indices labeling generic lattice sites on an arbitrary lattice and $dW_t^{i,j}dW_{t'}^{k,l} = C_{ijkl}dt$ when $t = t'$ and 0 elsewhere.

The action associated to this noise reads

$$S_\gamma = -\sum_{i,j}\int\sqrt{2\gamma}\left(\bar{\psi}^1_{i,t}\psi^1_{j,t} + \bar{\psi}^2_{i,t}\psi^2_{j,t}\right)dW_t^{i,j}\,. \tag{B1}$$

We consider the diagrammatic representation of the Green's function in Fig. 4. Full lines represent the retarded propagator, dashed lines the advanced one and mixed lines the Keldysh propagator. We represent with wiggly lines the two vertex associated to the noise action (B1), one connecting only solid lines and the other only dashed ones. The first contributions

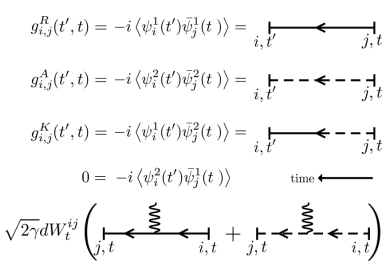

FIG. 4. Diagrammatic representation of the retarded (R), advanced (A), and Keldysh (K) Green's function. Time flows from right to left. On the bottom, we add the diagrammatic representation of the vertex provided by the action (B1), which preserves dashed and solid lines.

to the diagrams of $\mathcal{G}^{R,A,K}$ are depicted in Fig. 5. One readily realizes that in the diagrammatic expansion of the retarded (advanced) propagators only retarded (advanced) propagators appear. For the Keldysh component, one can switch only once from dashed to solid lines through the insertion of a Keldysh propagator.

The average over different noise realizations is computed using the Itō rules, which impose an equal time index when connecting wiggly lines, $dW_t dW_{t'} \neq 0 \Rightarrow t' = t$. Diagrammatically, wiggly lines merge as shown in Fig. 6. The key insight is that after noise-averaging the diagrams, those with crossing wiggly lines do not contribute to the action. In Fig. 5, we show a diagram with crossing wiggly lines arising from the diagrammatic expansion of the Keldysh component. In that example, after averaging, two retarded propagators (labeled A and B) have opposite directions. In our representation, this implies the multiplication of two retarded functions with opposite time dependence, which equals 0. Similar considerations apply for all crossing diagrams, and we direct the interested reader to Refs. [24,35] for the complete demonstration. Since the crossing diagrams vanish, the Born noncrossing approximation is exact, and all the remaining rainbow diagrams can be exactly resummed, leading to the

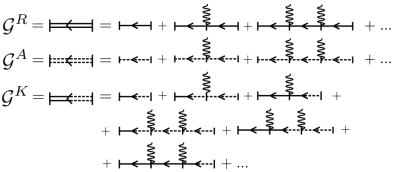

FIG. 5. Diagrammatic expansion of the retarded, advanced, and Keldysh propagators in the quantum stochastic action (B1). At a given order n in the expansion, the retarded/advanced component of the self energy only has one diagram whereas the Keldysh component has $n+1$ diagrams, corresponding to the insertion of the Keldysh bare component at different times.

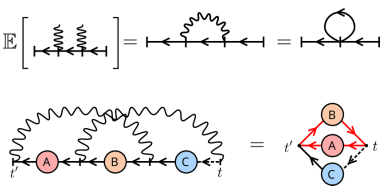

FIG. 6. Example of a crossing diagram for the Keldysh component. The red lines highlight the part of the diagram violating the causality structure and are responsible for making the diagram vanish.

following self-consistent equation for the self-energy

$$\mathbf{\Sigma}_{\gamma,ij}(t,t') = \gamma\delta(t-t')\sum_{kl} C_{iklj}\mathcal{G}_{kl}(t,t)\,, \tag{B2}$$

which is equivalent to Eq. (9) in the main text.

2. Transmittance of a quantum stochastic resistor

We derive now two explicit and equivalent expressions of the transmittance $\mathcal{T}_\gamma(\omega)$ used to derive the conductance in Eq. (15). To do this, we rely first on the Meir-Wingreen expression of the current flowing from the reservoirs to the system [14,72],

$$J = \frac{i}{2}\int\frac{d\omega}{2\pi}\mathrm{Tr}\{[\Gamma_{\mathrm{L}}(\omega)-\Gamma_{\mathrm{R}}(\omega)]\mathcal{G}^K(\omega) - [F_{\mathrm{L}}(\omega)\Gamma_{\mathrm{L}}(\omega)-F_{\mathrm{R}}(\omega)\Gamma_{\mathrm{R}}(\omega)][\mathcal{G}^R(\omega)-\mathcal{G}^A(\omega)]\}\,, \tag{B3}$$

where the trace is performed over spatial indices, $F_{\mathrm{L/R}}(\omega) = \tanh[\beta(\omega-\mu_{\mathrm{L/R}})/2]$ gives the equilibrium state of the right (R) and left (L) reservoirs, and $\Gamma_{\mathrm{L/R}}(\omega) = -\mathrm{Im}(\Sigma_{\mathrm{L/R}})/\pi$ are the frequency-dependent hybridization functions describing the coupling of the system with its left and right reservoirs. In the idealized case of Sec. III, where system and reservoirs are identical, the explicit expression of these hybridization functions can be derived from Eq. (8) and (A7), so that $\Gamma_{i,j;\mathrm{L/R}}(\omega) = \delta_{i,j}\delta_{i,1/N}\Gamma(\omega)$ in the interval $\omega\in[-2t_x,2t_x]$, with $\Gamma(\omega) = (\sqrt{4t_x^2-\omega^2})/2\pi$. Outside of the interval $\omega\in[-2t_x,2t_x]$, $\Gamma(\omega)=0$. Remind that we take $j=1$ and N as the leftmost and rightmost sites of the one-dimensional system.

We focus on the case of identical reservoirs exchanging particles with the system only at one site and that the Meir-Wingreen formula (B3) thus simplifies to

$$J = \int d\omega\Gamma(\omega)\left[\frac{i}{2}\frac{\mathcal{G}_1^K(\omega)-\mathcal{G}_N^K(\omega)}{2\pi} + \frac{F_{\mathrm{R}}(\omega)-F_{\mathrm{L}}(\omega)}{2}\mathcal{A}(\omega)\right], \tag{B4}$$

where we have introduced the shorthand notation $\mathcal{G}_i^{R/A/K} = \mathcal{G}_{ii}^{R/A/K}$ and assumed a mirror symmetric system, so that the spectral functions at the system edges, $\mathcal{A}(\omega) = \mathcal{A}_{1/N}(\omega) = -\mathrm{Im}[\mathcal{G}_{1/N}^R(\omega)]/\pi$, is the same at both edges. The above expression requires the derivation of the Keldysh Green's functions $\mathcal{G}_i^K(\omega)$, which are derived by solving the self-consistent equation

$$\mathcal{G}_{ij}^K(\omega) = -\mathcal{G}_{il}^R(\omega)\big[g^{-1,K}(\omega)-\Sigma_\gamma^K(\omega)\big]_{lm}\mathcal{G}_{mj}^A(\omega)\,, \tag{B5}$$

where we use the convention of the summation of repeated indices and where Σ_γ^K is given by the Keldysh component of Eq. (B2).

For the specific case of the on-site dephasing of Sec. III, $C_{ijkl} = \delta_{ij}\delta_{ik}\delta_{kl}$ and the self-consistent equation (B2) can be cast in the form

$$[\delta_{ij}-M_{ij}]\mathcal{G}_j^K(t,t) = D_i, \tag{B6}$$

where we have introduced the matrix and vector notations

$$M_{ij} = \gamma\int\frac{d\omega}{2\pi}\mathcal{M}_{ij}(\omega), \quad \mathcal{M}_{ij}(\omega) = \left|\mathcal{G}_{ij}^R(\omega)\right|^2, \tag{B7}$$

$$D_{ij} = -\int\frac{d\omega}{2\pi}\mathcal{G}_{ij}^R(\omega)g_{jk}^{-1,K}(\omega)\mathcal{G}_{kj}^A(\omega), \quad D_i = D_{ii}\,, \tag{B8}$$

where we also exploited the property $\mathcal{G}_{ij}^A(\omega) = [\mathcal{G}_{ji}^R(\omega)]^*$. Generalized forms of Eqs. (A3) and (A8) lead to

$$g^{-1K}(\omega) = 2\pi i[F_{\mathrm{L}}(\omega)\Gamma_{\mathrm{L}}(\omega)+F_{\mathrm{R}}(\omega)\Gamma_{\mathrm{R}}(\omega)]\,, \tag{B9}$$

which, in the specific case of Sec. III, reads

$$g_{ij}^{-1K}(\omega) = 2\pi i\delta_{ij}\Gamma(\omega)[F_{\mathrm{L}}(\omega)\delta_{i,1}+F_{\mathrm{R}}(\omega)\delta_{i,N}]\,. \tag{B10}$$

Given the explicit dependence of the above expression on the distribution functions of the reservoirs $F_{\mathrm{L/R}}$, we can now perform the expansion in linear order in the chemical potential difference $\delta\mu = \mu_{\mathrm{L}}-\mu_{\mathrm{R}}$ to obtain the transmittance. We first show the linear expansion of the Keldysh component from Eq. (B5), whose diagonal terms read

$$i\frac{\mathcal{G}_i^K(\omega)}{2\pi} = \Gamma(\omega)U_i(\omega)+\gamma\mathcal{M}_{ij}(\omega)\left[\frac{1}{\mathbb{I}-M}\right]_{jk} \times\int\frac{d\omega'}{2\pi}\Gamma(\omega')U_k(\omega'), \tag{B11}$$

$$U_i(\omega) = F(\omega)V_i(\omega) - \frac{\delta\mu}{4T\cosh^2\left(\frac{\omega-\mu}{2T}\right)}W_i(\omega)\,, \tag{B12}$$

where we introduced the N dimensional vectors $V_i(\omega) = |\mathcal{G}_{i1}^R(\omega)|^2+|\mathcal{G}_{iN}^R(\omega)|^2$, $W_i(\omega) = |\mathcal{G}_{i1}^R(\omega)|^2-|\mathcal{G}_{iN}^R(\omega)|^2$ and $F(\omega) = \tanh[(\omega-\mu)/2T]$. Thanks to the mirror symmetry of the problem in Sec. III, the first term in Eq. (B12), proportional to the equilibrium distribution function F, does not contribute to the current given by the MW formula in Eq. (B4) and can be discarded. Assuming also $\mathcal{A}(\omega) = \mathcal{A}_{\mathrm{L/R}}(\omega)$, we thus find the following compact form for the transmittance in Eq. (15)

$$\mathcal{T}_\gamma(\omega) = 2\pi\Gamma(\omega)[\mathcal{A}(\omega)-\Delta^K(\omega)] \tag{B13}$$

with

$$\Delta^K(\omega) = [P(\omega)W(\omega)]_1 - [P(\omega)W(\omega)]_N\,, \tag{B14}$$

and

$$P(\omega) = \frac{\Gamma(\omega)}{2}+\frac{\gamma}{2}\int\frac{d\omega'}{2\pi}\Gamma(\omega')\mathcal{M}(\omega')\frac{1}{\mathbb{I}-M}\,, \tag{B15}$$

with the matrix $\mathcal{M}$ defined in Eq. (B7). In the case of a reservoir with a constant density of state, $\Gamma(\omega) = \Gamma$ and expression Eq. (B13) coincides with the one derived in Ref. [35].

Despite the general character of Eq. (B13), we note that, in purely one-dimensional systems, the current in the system equals the one flowing from the reservoirs to the system. As a consequence, we can extract a different, but equivalent, expression of the transmittance from performing similar manipulations as the ones described to derive Eq. (B13), but taking the local current expression Eq. (11) as a starting point. For this, the off-diagonal elements of $\mathcal{G}^K_{ij}(t=0)$ are needed, that can be readily obtained by injecting the solution (B6) for the diagonal elements into the Dyson equation (B5). Once taking the Fourier transform one finds

$$\mathcal{G}^K_{ij}(t=0) = iD_{ij} + i\gamma \int \frac{d\omega}{2\pi} \mathcal{G}^R_{il}(\omega) \left[\frac{1}{\mathbb{I} - M}\right]_{lm} D_m \mathcal{G}^A_{lj}(\omega). \tag{B16}$$

And the expression for the transmittance can be found from expanding D in the bias. The zeroth-order term in $\delta\mu$ does not contribute to the current, since without the bias the system is mirror symmetric and the current must be zero. Replacing the linear-order term of Eq. (B16) in Eq. (11) gives

$$\mathcal{T}_\gamma(\omega) = 2\pi t_x \Gamma(\omega) \mathrm{Im}\Bigg[\mathcal{G}^R_{i1}(\omega)\mathcal{G}^A_{1,i+1}(\omega) - \mathcal{G}^R_{iN}(\omega)\mathcal{G}^A_{N,i+1}(\omega) + \gamma \left[\frac{1}{\mathbb{I} - M}\right]_{lm} W_m(\omega) \int \frac{d\omega'}{2\pi} \mathcal{G}^R_{il}(\omega')\mathcal{G}^A_{l,i+1}(\omega')\Bigg]. \tag{B17}$$

The index i originates from computing the local current at site i but since the latter does not depend on the position, neither does the transmittance.

3. Average Lindblad description of the QSH dynamics

Lastly, we show how averaging a QSH over different noise realizations maps to a Lindblad evolution. Under the quantum stochastic evolution, the density matrix evolves as follows:

$$\begin{aligned}\rho_{t+dt} &= e^{-i(Hdt + dH_t)} \rho_t e^{-i(Hdt + dH_t)} \\ &= \rho_t - i[Hdt + dH_t, \rho_t] \\ &\quad + dH_t \rho_t dH_t - \frac{1}{2}\{dH_t^2, \rho_t\} + \mathcal{O}(dt^{3/2}), \\ &\approx \rho_t - i[Hdt + dH_t, \rho_t] \\ &\quad + \gamma \sum_{ijkl} (2c_i^\dagger c_j \rho_t c_k^\dagger c_l - \{c_k^\dagger c_l c_i^\dagger c_j, \rho_t\}) C_{ijkl} dt,\end{aligned} \tag{B18}$$

where we used the Itō rules and discarded terms of higher order than dt. The Lindblad equation is obtained by taking the noise-average of Eq. (B18), which sets the term proportional to dH_t to 0 in the Itō convention,

$$\frac{d}{dt}\rho_t = -i[H, \rho_t] + \gamma \sum_{ijkl} C_{ijkl} (2c_i^\dagger c_j \rho c_k^\dagger c_l - \{c_k^\dagger c_l c_i^\dagger c_j, \rho\}). \tag{B19}$$

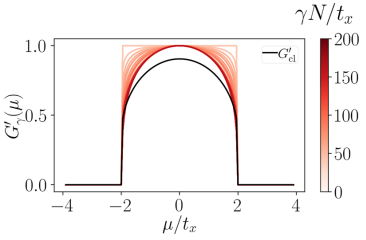

FIG. 7. Rescaled conductance profiles $G'_\gamma(\mu, N) := G_\gamma(\mu, N)/G_\gamma(0, N)$ for different values of γN with $\gamma = [0, 2]t_x$ and $N = [5, 200]$. The rescaled conductance converges in the diffusive limit $\gamma N/t_x \gg 1$ to a curve qualitatively similar to the semiclassical expectations in the same limit.

APPENDIX C: RESCALED CONDUCTANCE PROFILES

In this section, we present further numerical data on the conductance profiles in the diffusive regime. In this regime, the conductance decays with the inverse system size $G \propto 1/N$ thus, to focus on the chemical potential dependence, we depict in Fig. 7 the rescaled conductance $G'_\gamma(\mu, N) := G_\gamma(\mu, N)/G_\gamma(0, N)$ profiles for different values of γN and compare with the semiclassical rescaled value $G'_{\gamma,cl}(\mu, N) = G_{\gamma,cl}(\mu, N)/G_\gamma(0, N)$. The dependence of $G_\gamma(\mu = 0)$ on the system size N is plotted in Fig. 2. As we transition to the diffusive limit, the rescaled curves converge to a dome-like shape, which follows the qualitative dependence of the semiclassical approach, see black line for $G'_{\mathrm{cl}}(N \to \infty)$. The deviations between the exact and semiclassical approach are more significant in the center of the band but never exceed 10%.

We note that such strong dependence on the thermodynamic properties of the leads is not present in the diffusion constant and is a unique property of the conductance.

APPENDIX D: MIXING EFFECTS WITH DEPHASING NOISE

In this Appendix, we discuss the stationary state induced by dephasing noise on a one-dimensional tight-binding chain. We will qualitatively describe the out-of-equilibrium state reached by the dephased chain and show numerically on Fig. 8 that this qualitative intuition is correct. In the absence of dephasing, the whole chain will be in thermal equilibrium with a chemical potential and temperature matching the lead. Locally, it implies that the Green's functions satisfy the fluctuation dissipation relation

$$\mathcal{G}^K_{i,i}(\omega) = (1 - 2n_i(\omega))\big(\mathcal{G}^R_{i,i}(\omega) - \mathcal{G}^A_{i,i}(\omega)\big) \tag{D1}$$

with $n_i(\omega)$ the local Fermi distribution with parameters μ, T.

Beyond thermal equilibrium, we can still use Eq. (D1) as an *ad hoc* definition of $n_i(\omega)$ to characterize local deviations from equilibrium.

The presence of any dephasing rate drives the system out of equilibrium. As explained in the main text, the dephasing maximally mixes the longitudinal momentum states. Since

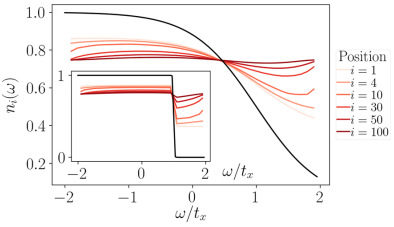

FIG. 8. Nonequilibrium local occupation distribution extracted from Eq. (D1) at different positions in a chain of $N = 200$ sites with on-site dephasing rate $\gamma = 0.05t_x$. The chain is coupled on the first and last site $i = 1, 200$ to a thermal lead with $\mu = t_x$ and $T = 0.5t_x$. The black line corresponds to the Fermi distribution of the attached reservoirs. (Inset) Same plot but the temperature of the leads is $T = 0.01t_x$.

these, in 1D, label all the eigenstates of the system the action of dephasing corresponds to heat the system to infinite temperature. However, since the dephasing terms commute with the local particle number operator, the attained steady-state preserves a well defined particle number. In other words, the local density matrix deep into a dephasing region resembles a thermal distribution with an effective μ^* and T^* such that $\mu^*, T^* \to \infty$ and μ^*/T^* tuned in such a way to have in the system the same spatial averaged particle density than the one in the attached leads.

This is clear in Fig. 8 where we plot $n_i(\omega)$ for different points in a dephasing chain coupled to a thermal lead on the left and right. By definition, the lead is in local thermal equilibrium and $n_{\mathrm{L,R}}(\omega)$ is given by the Fermi distribution, see black line. Near the lead, $n_i(\omega)$ deviates strongly from a thermal distribution indicating that the system is far from equilibrium. Deep into the chain, that is at distances from the leads larger than the scattering length ($i > t_x/\gamma$, in Fig. 8), $n(\omega)$ becomes flat as expected from a state with infinite μ, T. The exact ratio μ^*/T^* is uniquely determined from the density of the reservoirs but its exact value depends on the distribution of the system near the edges.

APPENDIX E: PROOF OF THE CONDITION (36)

In this Appendix, we give a proof of the condition Eq. (36) in the main text. The strategy is to write down the equations of motion for the total current of different noises and derive a condition under which they are equivalent (up to a factor) for different types of noise.

The action of the deterministic part H for the total current (11) evaluated at site j, is given for any site by

$$\begin{aligned}\partial_t J = i[H, J] = it_x^2 \sum_p [&(n_{j+1,p} - n_{j,p}) \\ &+ a^\dagger_{j-1,p} a_{j+1,p} - a^\dagger_{j,p} a_{j+2,p} \\ &- a^\dagger_{j+2,p} a_{j,p} + a^\dagger_{j+1,p} a_{j-1,p}] \,. \end{aligned} \tag{E1}$$

Since H is quadratic, and since it doesn't mix the different modes by construction, its further action on quadratic operators will only generate terms of the type $a^\dagger_{j+k,p} a_{j+k,p'}$. By construction, the QSH (4) conserves the total number of particles at a given position on the x axis, i.e., $[dH_t, n_{j,\mathrm{tot}}] = 0$. Then, one sufficient but not necessary condition for the equations of motion to have the same form for all protocols is that the dual action on operators $\mathcal{L}^*$ for the averaged noise does not produce any new terms, i.e., we must have for $j \neq j'$

$$\mathcal{L}^*(a^\dagger_{j,p} a_{j',p}) = -\mathcal{N} a^\dagger_{j,p} a_{j',p} \,, \tag{E2}$$

where $\mathcal{N}$ is a constant, which depends on the type of noise we are interested in. Invoking the locality of the noise operator with respect to the longitudinal direction we have that

$$\mathcal{L}^*(a^\dagger_{j,p} a_{j',p}) = \mathcal{L}^*(a^\dagger_{j,p}) a_{j',p} + a^\dagger_{j,p} \mathcal{L}^*(a_{j',p}) \,. \tag{E3}$$

So the sufficient condition (E2) can be cast into an even more restrictive one where we impose that $\forall p$, $(a^\dagger_{j,p}, a_{j,p})$ are eigenvectors of the operator $\mathcal{L}^*$.

Recall the explicit expression of $\mathcal{L}^*$

$$\begin{aligned}\mathcal{L}^*(\hat{O}) = \gamma \sum_{j, p_{1,2}, p'_{1,2}} C_{p_1,p'_1,p_2,p'_2} (&2a^\dagger_{j,p_1} a_{j,p'_1} \hat{O} a^\dagger_{j,p_2} a_{j,p'_2} \\ &- \{a^\dagger_{j,p_1} a_{j,p'_1} a^\dagger_{j,p_2} a_{j,p'_2}, \hat{O}\}) \,. \end{aligned} \tag{E4}$$

Using that $C_{p_1,p'_1,p_2,p'_2} = C_{p'_1,p_1,p'_2,p_2}$, we have that

$$\mathcal{L}^*(a^\dagger_{j,p}) = -\gamma \sum_{p_1,p'} C_{p_1,p',p',p} a^\dagger_{j,p_1} \,, \tag{E5}$$

$$\mathcal{L}^*(a_{j,p}) = -\gamma \sum_{p_1,p'} C_{p',p_1,p,p'} a_{j,p_1} \,, \tag{E6}$$

and a sufficient condition for $(a^\dagger_{j,p}, a_{j,p})$ to be eigenvectors of $\mathcal{L}^*$ is then

$$\sum_p C_{p_1,p,p,p_2} = \mathcal{N} \delta_{p_1,p_2} \,, \tag{E7}$$

which is Eq. (36) of the main text.

For the coherent Noise I, one has $\mathcal{N} = 1$ and the transport properties of a given protocol model can be deduced from those of Noise I by rescaling the coefficient $\gamma \to \mathcal{N}\gamma$.

[1] E. Akkermans and G. Montambaux, *Mesoscopic Physics of Electrons and Photons* (Cambridge University Press, Cambridge, 2007)

[2] T. Giamarchi, Umklapp process and resistivity in one-dimensional fermion systems, Phys. Rev. B **44**, 2905 (1991).

[3] A. Rosch and N. Andrei, Conductivity of a Clean One-Dimensional Wire, Phys. Rev. Lett. **85**, 1092 (2000).

[4] J. Lux, J. Müller, A. Mitra, and A. Rosch, Hydrodynamic long-time tails after a quantum quench, Phys. Rev. A **89**, 053608 (2014).

[5] M. Medenjak, K. Klobas, and T. Prosen, Diffusion in Deterministic Interacting Lattice Systems, Phys. Rev. Lett. **119**, 110603 (2017).

[6] S. Gopalakrishnan and R. Vasseur, Kinetic Theory of Spin Diffusion and Superdiffusion in *XXZ* Spin Chains, Phys. Rev. Lett. **122**, 127202 (2019).

[7] A. J. Friedman, S. Gopalakrishnan, and R. Vasseur, Diffusive hydrodynamics from integrability breaking, Phys. Rev. B **101**, 180302(R) (2020).

[8] B. Bertini, F. Heidrich-Meisner, C. Karrasch, T. Prosen, R. Steinigeweg, and M. Žnidarič, Finite-temperature transport in one-dimensional quantum lattice models, Rev. Mod. Phys. **93**, 025003 (2021).

[9] T. Prosen, Open *XXZ* Spin Chain: Nonequilibrium Steady State and a Strict Bound on Ballistic Transport, Phys. Rev. Lett. **106**, 217206 (2011).

[10] T. Prosen, Exact Nonequilibrium Steady State of a Strongly Driven Open *XXZ* Chain, Phys. Rev. Lett. **107**, 137201 (2011).

[11] D. Karevski and T. Platini, Quantum Nonequilibrium Steady States Induced By Repeated Interactions, Phys. Rev. Lett. **102**, 207207 (2009).

[12] D. Karevski, V. Popkov, and G. M. Schütz, Exact Matrix Product Solution for the Boundary-Driven Lindblad *XXZ* Chain, Phys. Rev. Lett. **110**, 047201 (2013).

[13] J. S. Ferreira and M. Filippone, Ballistic-to-diffusive transition in spin chains with broken integrability, Phys. Rev. B **102**, 184304 (2020).

[14] T. Jin, M. Filippone, and T. Giamarchi, Generic transport formula for a system driven by Markovian reservoirs, Phys. Rev. B **102**, 205131 (2020).

[15] M. Žnidarič, Exact solution for a diffusive nonequilibrium steady state of an open quantum chain, J. Stat. Mech. (2010) L05002.

[16] B. Bertini, M. Collura, J. De Nardis, and M. Fagotti, Transport in Out-Of-Equilibrium *XXZ* Chains: Exact Profiles of Charges and Currents, Phys. Rev. Lett. **117**, 207201 (2016).

[17] T. Müller, M. Gievers, H. Fröml, S. Diehl, and A. Chiocchetta, Shape effects of localized losses in quantum wires: Dissipative resonances and nonequilibrium universality, Phys. Rev. B **104**, 155431 (2021).

[18] D. Rossini, A. Ghermaoui, M. B. Aguilera, R. Vatré, R. Bouganne, J. Beugnon, F. Gerbier, and L. Mazza, Strong correlations in lossy one-dimensional quantum gases: From the quantum zeno effect to the generalized Gibbs ensemble, Phys. Rev. A **103**, L060201 (2021).

[19] V. Alba and F. Carollo, Noninteracting fermionic systems with localized losses: Exact results in the hydrodynamic limit, Phys. Rev. B **105**, 054303 (2022).

[20] A. M. Visuri, T. Giamarchi, and C. Kollath, Symmetry-Protected Transport Through a Lattice with a Local Particle Loss, Phys. Rev. Lett. **129**, 056802 (2022).

[21] M. Žnidarič, Dephasing-induced diffusive transport in the anisotropic Heisenberg model, New J. Phys. **12**, 043001 (2010).

[22] A. Bastianello, J. De Nardis, and A. De Luca, Generalized hydrodynamics with dephasing noise, Phys. Rev. B **102**, 161110(R) (2020).

[23] V. Eisler, Crossover between ballistic and diffusive transport: the quantum exclusion process, J. Stat. Mech. (2011) P06007.

[24] P. E. Dolgirev, J. Marino, D. Sels, and E. Demler, Non-Gaussian correlations imprinted by local dephasing in fermionic wires, Phys. Rev. B **102**, 100301(R) (2020).

[25] D. Wellnitz, G. Preisser, V. Alba, J. Dubail, and J. Schachenmayer, The Rise and Fall, and Slow Rise Again, of Operator Entanglement Under Dephasing, Phys. Rev. Lett. **129**, 170401 (2022).

[26] M. Bauer, D. Bernard, and T. Jin, Equilibrium fluctuations in maximally noisy extended quantum systems, SciPost Phys. **6**, 045 (2019).

[27] D. Bernard and T. Jin, Open Quantum Symmetric Simple Exclusion Process, Phys. Rev. Lett. **123**, 080601 (2019).

[28] T. Jin, A. Krajenbrink, and D. Bernard, From Stochastic Spin Chains to Quantum Kardar-Parisi-Zhang Dynamics, Phys. Rev. Lett. **125**, 040603 (2020).

[29] F. H. L. Essler and L. Piroli, Integrability of one-dimensional lindbladians from operator-space fragmentation, Phys. Rev. E **102**, 062210 (2020).

[30] D. Bernard and L. Piroli, Entanglement distribution in the quantum symmetric simple exclusion process, Phys. Rev. E **104**, 014146 (2021).

[31] D. Bernard and P. L. Doussal, Entanglement entropy growth in stochastic conformal field theory and the KPZ class, Europhys. Lett. **131**, 10007 (2020).

[32] M. V. Medvedyeva, F. H. L. Essler, and T. Prosen, Exact Bethe Ansatz Spectrum of a Tight-Binding Chain with Dephasing Noise, Phys. Rev. Lett. **117**, 137202 (2016).

[33] M. Bauer, D. Bernard, and T. Jin, Stochastic dissipative quantum spin chains (I) : Quantum fluctuating discrete hydrodynamics, SciPost Phys. **3**, 033 (2017).

[34] X. Turkeshi and M. Schiró, Diffusion and thermalization in a boundary-driven dephasing model, Phys. Rev. B **104**, 144301 (2021).

[35] T. Jin, J. S. Ferreira, M. Filippone, and T. Giamarchi, Exact description of quantum stochastic models as quantum resistors, Phys. Rev. Research **4**, 013109 (2022).

[36] J. De Nardis, S. Gopalakrishnan, E. Ilievski, and R. Vasseur, Superdiffusion from Emergent Classical Solitons in Quantum Spin Chains, Phys. Rev. Lett. **125**, 070601 (2020).

[37] C. Zu, F. Machado, B. Ye, S. Choi, B. Kobrin, T. Mittiga, S. Hsieh, P. Bhattacharyya, M. Markham, D. Twitchen, A. Jarmola *et al.*, Emergent hydrodynamics in a strongly interacting dipolar spin ensemble, Nature (London) **597**, 45 (2021).

[38] J. Wurtz, P. W. Claeys, and A. Polkovnikov, Variational Schrieffer-Wolff transformations for quantum many-body dynamics, Phys. Rev. B **101**, 014302 (2020).

[39] J. D. Nardis, D. Bernard, and B. Doyon, Diffusion in generalized hydrodynamics and quasiparticle scattering, SciPost Physics **6**, 049 (2019).

[40] R. Steinigeweg, F. Heidrich-Meisner, J. Gemmer, K. Michielsen, and H. De Raedt, Scaling of diffusion constants in the spin-1/2 XX ladder, Phys. Rev. B **90**, 094417 (2014).

[41] N. Dogra, M. Landini, K. Kroeger, L. Hruby, T. Donner, and T. Esslinger, Dissipation-induced structural instability and chiral dynamics in a quantum gas, Science **366**, 1496 (2019).

[42] F. Ferri, R. Rosa-Medina, F. Finger, N. Dogra, M. Soriente, O. Zilberberg, T. Donner, and T. Esslinger, Emerging Dissipative Phases in a Superradiant Quantum Gas with Tunable Decay, Phys. Rev. X **11**, 041046 (2021).

[43] R. Rosa-Medina, F. Ferri, F. Finger, N. Dogra, K. Kroeger, R. Lin, R. Chitra, T. Donner, and T. Esslinger, Observing Dynamical Currents in a Non-Hermitian Momentum Lattice, Phys. Rev. Lett. **128**, 143602 (2022).

[44] L. Corman, P. Fabritius, S. Häusler, J. Mohan, L. H. Dogra, D. Husmann, M. Lebrat, and T. Esslinger, Quantized conductance through a dissipative atomic point contact, Phys. Rev. A **100**, 053605 (2019).

[45] M. Lebrat, S. Häusler, P. Fabritius, D. Husmann, L. Corman, and T. Esslinger, Quantized Conductance Through a Spin-Selective Atomic Point Contact, Phys. Rev. Lett. **123**, 193605 (2019).

[46] M. Mancini, G. Pagano, G. Cappellini, L. Livi, M. Rider, J. Catani, C. Sias, P. Zoller, M. Inguscio, M. Dalmonte, and L. Fallani, Observation of chiral edge states with neutral fermions in synthetic Hall ribbons, Science **349**, 1510 (2015).

[47] D. Genkina, L. M. Aycock, H.-I. Lu, M. Lu, A. M. Pineiro, and I. Spielman, Imaging topology of Hofstadter ribbons, New J. Phys. **21**, 053021 (2019).

[48] T. Chalopin, T. Satoor, A. Evrard, V. Makhalov, J. Dalibard, R. Lopes, and S. Nascimbene, Probing chiral edge dynamics and bulk topology of a synthetic Hall system, Nat. Phys. **16**, 1017 (2020).

[49] T. W. Zhou, G. Cappellini, D. Tusi, L. Franchi, J. Parravicini, C. Repellin, S. Greschner, M. Inguscio, T. Giamarchi, M. Filippone, J. Catani, and L. Fallani, Observation of universal Hall response in strongly interacting fermions, arXiv:2205.13567.

[50] B. Øksendal, *Stochastic Differential Equations* (Springer, Berlin, 2003).

[51] A. Kamenev, *Field Theory of Non-Equilibrium Systems* (Cambridge University Press, Cambridge, 2011) pp. 1–341.

[52] The Green's functions depend on the time differences $t - t'$, instead of separate times t, t', as we consider situations where both the Hamiltonian (1) and Lindblad generator (6) do not depend explicitly on time.

[53] A. I. Larkin and I. N. Ovchinnikov, Nonlinear effects during vortex motion in superconductors, Zh. Eksp. Teor. Fiz. **73**, 299 (1977).

[54] R. Landauer, Spatial variation of currents and fields due to localized scatterers in metallic conduction, IBM J. Res. Dev. **1**, 223 (1957).

[55] S. Datta, *Electronic Transport in Mesoscopic Systems* (Cambridge University Press, Cambridge, 1997).

[56] G. B. Lesovik and I. A. Sadovskyy, Scattering matrix approach to the description of quantum electron transport, Phys. Usp. **54**, 1007 (2011).

[57] Y. V. Nazarov and Y. M. Blanter, *Quantum Transport: Introduction to Nanoscience* (Cambridge University Press, Cambridge, 2009).

[58] M. Žnidarič and M. Horvat, Transport in a disordered tight-binding chain with dephasing, Eur. Phys. J. B **86**, 67 (2013).

[59] Z. Cai and T. Barthel, Algebraic Versus Exponential Decoherence in Dissipative Many-Particle Systems, Phys. Rev. Lett. **111**, 150403 (2013).

[60] Despite the possibility to rely on Eq. (15) to calculate the conductance for $\gamma > 0$, we found more practical to perform the direct numerical calculation of the current as expressed in Eq. (11) directly in the linear regime to derive the conductance (12).

[61] The different scalings of D and G with μ, T indicate that the contact resistance between bulk and leads is extensive with the system size. Fig. 8 and previous papers [34] suggest that thermalization only occurs very deep in the bulk, supporting this hypothesis.

[62] J. Dalibard, Y. Castin, and K. Mølmer, Wave-Function Approach to Dissipative Processes in Quantum Optics, Phys. Rev. Lett. **68**, 580 (1992).

[63] V. Belavkin, A quantum stochastic calculus in fock space of input and output nondemolition processes, J. Sov. Math. v, 99 (1990).

[64] Convergence is exponential with the number of iterations and independent of the initial guess for $P(x)$, which we take arbitrarily.

[65] X. Cao, A. Tilloy, and A. D. Luca, Entanglement in a fermion chain under continuous monitoring, SciPost Phys. **7**, 024 (2019).

[66] X. Turkeshi, M. Dalmonte, R. Fazio, and M. Schirò, Entanglement transitions from stochastic resetting of non-Hermitian quasiparticles, Phys. Rev. B **105**, L241114 (2022).

[67] G. Salerno, H. M. Price, M. Lebrat, S. Häusler, T. Esslinger, L. Corman, J.-P. Brantut, and N. Goldman, Quantized Hall Conductance of a Single Atomic Wire: A Proposal Based on Synthetic Dimensions, Phys. Rev. X **9**, 041001 (2019).

[68] L. F. Livi, G. Cappellini, M. Diem, L. Franchi, C. Clivati, M. Frittelli, F. Levi, D. Calonico, J. Catani, M. Inguscio, and L. Fallani, Synthetic Dimensions and Spin-Orbit Coupling with an Optical Clock Transition, Phys. Rev. Lett. **117**, 220401 (2016).

[69] T. Ozawa, H. M. Price, N. Goldman, O. Zilberberg, and I. Carusotto, Synthetic dimensions in integrated photonics: From optical isolation to four-dimensional quantum hall physics, Phys. Rev. A **93**, 043827 (2016).

[70] S. Mittal, V. V. Orre, D. Leykam, Y. D. Chong, and M. Hafezi, Photonic Anomalous Quantum Hall Effect, Phys. Rev. Lett. **123**, 043201 (2019).

[71] R. A. Usmani, Inversion of a tridiagonal Jacobi matrix, Linear Algebra Appl. **212-213**, 413 (1994).

[72] Y. Meir and N. S. Wingreen, Landauer Formula for the Current Through an Interacting Electron Region, Phys. Rev. Lett. **68**, 2512 (1992).

3.4 Emergence of diffusion in integrability-broken Hamiltonians

In this last work, we continue to focus on inelastic processes and the emergence of diffusion, whilst shifting attention to interacting Hamiltonians. Unlike QSHs, a closed solution for self-energy with interactions is not known which adds a layer of complexity. To simplify, we resort to reservoirs in the Markovian limit that drive the system to an infinite temperature state, see Sec. 2.5.2.

We explore the effects of nearest-neighbor (NN) and next-to-nearest-neighbor (NNN) density-density interactions on a non-interacting chain. In the context of spins, these correspond to the XXZ model ⟦2⟧ with NNN magnetic interactions ⟦3⟧, with the mapping provided by the Jordan-Wigner transformation (2.79). At characteristic scales determined by Fermi's golden rule [136, 137], generic interactions (such as NNN interactions) are responsible for inelastic scattering processes that induce diffusion, lead to thermalization [138], and promote the emergence of quantum chaos [139]. This intuition breaks down for integrable models where the presence of an extensive number of conservation laws can prevent thermalization [140], and may suppress the emergence of diffusion [141]. The XXZ model is such a case, where the existence of quasi-particles that only scatter elastically [142] can lead to ballistic transport in the infinite size limit. All physical realizations of integrable models are, at best, almost integrable, posing the question of understanding transport in weak integrability-breaking setups.

The first model we investigate is a free chain in the presence of NNN interactions, a prototypical model of diffusion. Prior to our work, it had been suggested that the model supported an almost universal scaling of the ballistic-to-diffusive transition [143], see Fig. ⟦2⟧b where the curves for the current almost collapse with the scaling factor N/N^* ($N^* \sim V^{-2}$ is the scattering length estimated from Fermi's golden rule and V is the NNN interaction's strength). Our first result confirms that there is a true universal scaling, see Fig. ⟦3⟧, but the scaling factor must be modified to account for small system size deviations, see Eq. ⟦8⟧. The corrected scaling factor can be found by computing the particle current perturbatively in orders of the interaction ⟦6⟧. At the time, we employed the formalism of third-quantization [144, 145] to perform this perturbative expansion, but the same results could have been obtained from Keldysh field theory [55]. Third-quantization is a systematic procedure to diagonalize the Liouvillian in terms of creation and annihilation super-operators, akin to the diagonalization of Hamiltonian in second quantization, see Eq. ⟦5⟧. Obtaining the correct scaling factor is important since it allows for a more accurate determination of the system's diffusion constant from scaling arguments.

The majority of the work focuses on the role of weak NNN interactions on top of the XXZ chain in the ballistic regime, i.e. when the NN interactions are small Δ with respect to the hopping. Despite the current being ballistic for large systems, there is still a crossover length scale where the current decays from the non-interacting value

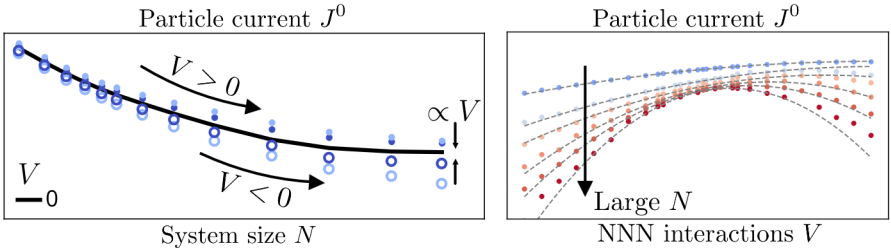

Figure 3.4: Adaptation from Figs. [[5,6]] of the paper. a) Current as a function of system size for weak NNN interactions, V. After a transition length, the current saturates to a quasi-ballistic regime with a renormalized current that depends linearly on V. b) Current as a function of NNN interactions. For small interactions, the current is fitted to a parabola with a linear term (dashed lines).

to the interacting one. The decay is expected since interactions tend to increase scattering and reduce the current. The presence of any NNN interaction is always expected to lead to diffusive physics after the scattering length N^*, and, in Fig. [[5]]a, we found some evidence that diffusive scaling $J^0 \sim N^{-1}$ does emerge for large systems. However, the presence of NNN terms modifies the current long before the onset of diffusion, see Fig. 3.4a. For weak NNN interactions and intermediate system sizes, the current may counter-intuitively increase upon adding NNN interactions, and depending on the sign, see Fig. 3.4b and Eq. [[10]]. In this limit, the current closely follows the current of the XXZ model ($V = 0$) up to a small correction linear in V, as if renormalized. This motivated us to coin a new transport regime, *quasi-ballisticity*.

The quasi-ballistic regime only exists in the limit of weak integrability breaking, $V \to 0$, and is characterized by a constant ballistic current, up to corrections of order V^2. It is important to estimate at which length scale, N_{QB}, the quadratic corrections destroy the quasi-ballistic regime. Expanding the current in orders of V

$$J^0 = (p_0(N) + p_1(N)V + p_2(N)V^2 + ...)\delta\mu + \mathcal{O}(\delta\mu^2) \,, \tag{3.3}$$

the coefficients $p_i(N)$ can be obtained by a polynomial fit to each curve in Fig. 3.4b, with the results presented in Fig. [[6]]. Only the second-order term diverges with the size, $p_2(N) \sim N$, while the others saturate at different values depending on the strength of the interaction. An estimate for N_{QB} is then given by the system size at which the second-order dominates over the first-order term, $p_2(N_{\text{QB}})V^2 \approx p_1(N_{\text{QB}})V \Rightarrow N_{\text{QB}} \sim |V|^{-1}$, which is much smaller than the scattering length $N^* \sim V^{-2}$ but still parametrically large.

In the work, we focus on characteristic length scales, but it's natural to hypothesize that there is also an associated time scale controlling this quasi-ballistic regime, t_{QB}, whose signatures should be present in the light-cone dynamics of quan-

tum quench protocols. Intriguingly, generalized hydrodynamics is not capable of capturing this regime since, being a coarse-grained approach, they always assume $N \to \infty$ before $V \to 0$.

Ballistic-to-diffusive transition in spin chains with broken integrability

João S. Ferreira and Michele Filippone
Department of Quantum Matter Physics, University of Geneva, 24 Quai Ernest-Ansermet, CH-1211 Geneva, Switzerland

(Received 26 June 2020; revised 28 September 2020; accepted 22 October 2020; published 9 November 2020; corrected 11 December 2020)

We study the ballistic-to-diffusive transition induced by the weak breaking of integrability in a boundary-driven XXZ spin chain. Studying the evolution of the spin current density $\mathcal{J}^s$ as a function of the system size L, we show that, accounting for boundary effects, the transition has a nontrivial universal behavior close to the XX limit. It is controlled by the scattering length $L^* \propto V^{-2}$, where V is the strength of the integrability-breaking term. In the XXZ model, the interplay of interactions controls the emergence of a transient "quasiballistic" regime at length scales much shorter than L^*. This parametrically large regime is characterized by a strong renormalization of the current which forbids a universal scaling, unlike the XX model. Our results are based on matrix product operator numerical simulations and agree with perturbative analytical calculations.

DOI: 10.1103/PhysRevB.102.184304

I. INTRODUCTION

A central assumption of statistical mechanics is that many-body interactions bring isolated out-of-equilibrium systems toward thermal equilibrium [1–4]. The phenomenon of thermalization in normal—metallic—conductors is generally associated with diffusion. Globally conserved quantities such as energy, charge, spin, or mass spread uniformly all over the system according to Fick's law,

$$\mathcal{J} = -D\nabla n, \tag{1}$$

in which the diffusion constant D relates the current density $\mathcal{J}$ to the application of a density gradient ∇n. Recently, it has been observed that in one dimension, quantum integrable systems defy thermalization [5]. This discovery has triggered an intense effort to understand the nontrivial dynamics of such systems under the recently developed framework of generalized hydrodynamics [6,7]. In particular, the presence of an extensive amount of conservation laws in integrable systems [8] generically leads to ballistic transport of conserved quantities [9]. An important case is spin transport in the XXZ model, which can show, for some choice of the model parameters, (super)diffusive behavior [10–18].

Unavoidable deviations from the realization of a perfect, fine-tuned integrable system lead to integrability breaking (IB). In that case, one typically expects the slow establishment of a chaotic-diffusive regime on timescales given by Fermi's golden rule (FGR) [19,20]. Nevertheless, the investigation on how IB triggers proper diffusive regimes for transport remains at a preliminary stage. Even though recent works [21–23] derived a generalized expression of FGR to describe diffusive hydrodynamics caused by integrability breaking, the onset of diffusion may still unveil highly nontrivial behavior [24,25]. Additionally, the onset of chaotic/diffusive behavior for fixed weak interactions is not controlled by Fermi's golden rule at small system sizes [26–28]. Recent works have also pointed out that the emergence of chaotic/diffusive behavior may not be fully related to the usual measurements of quantum chaos, such as level repulsion [29–31] or the eigenstate thermalization hypothesis [32].

Quantum quenches are a very efficient and widespread protocol used to study the relaxation dynamics of such many-body systems [17,33–40]. They are regularly performed in state-of-the-art cold-atom experiments [41–44] and can be efficiently simulated by numerical approaches [45–49]. Nevertheless, the description of the long-time dynamics driven by weak IB remains challenging for the available analytical and numerical studies.

We choose to address this issue from a different but complementary point of view. We investigate at which system *sizes* do weak IB interactions of strength V lead to a ballistic-to-diffusive transition in one-dimensional spin chains. V is compared to the spin-exchange strength J. We study the effect of next-nearest-neighbor interactions on the stationary current carried by a ballistic XXZ spin chain driven at its boundaries; see Fig. 1. The boundary terms induce a bias in the magnetization that in turn generates a spin current density, $\mathcal{J}^s$. This approach has the advantage of directly probing the stationary properties of highly excited many-body systems with large system sizes [13,50] and it has been recently formulated in terms of the local properties of the interacting region [51]. Different transport regimes are characterized by a unique scaling of current density with the system size L, $\mathcal{J}^s \propto L^{-\alpha}$. Here, we focus on the crossover from ballistic ($\alpha = 0$) to diffusive ($\alpha = 1$) as we approach the thermodynamic limit.

The presence of nonintegrable interactions in the Hamiltonian introduces a natural length scale to the problem: the scattering length $L^* \propto V^{-2}$, as suggested from perturbation theory and FGR. One could thus expect that the current scales as a universal function of L/L^*.

In this work, we show that the observation of such scaling is not trivial in the case of the XX chain in the presence of IB

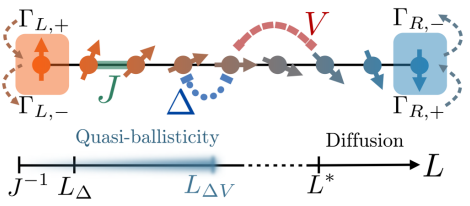

FIG. 1. Top: System under study: a spin current is induced via biased Lindblad jump operators at the edge of an XXZ spin chain described by Eqs. (2) and (3). Bottom: Schematic behavior of the steady-state current as a function of the system size L. The ballistic (size-independent) regime in the XXZ model sets in after the length scale L_Δ. Breaking integrability triggers diffusion beyond the scattering length L^*, given by Fermi's golden rule. The ballistic-to-diffusive crossover regime is controlled by the emerging length scale $L_{\Delta V} \ll L^*$, which defines a parametrically large "quasiballistic" regime.

perturbations. Our numerical calculations show that boundary effects strongly affect the ballistic-to-diffusive transition at short length scales, which are not controlled by the scattering length L^*. Nevertheless, relying on perturbation theory, we derive a nontrivial universal scaling of the current on the system size L. This scaling accounts for boundary corrections and it allows an accurate extrapolation of the results to the thermodynamic and $V \to 0$ limit. Our results are consistent with the establishment of a universal scaling as a function of L/L^* in this limit and also allow a good estimate of the diffusion constant D.

We then extend our work to the study of the integrable ballistic case in the presence of interactions ($|\Delta| < 1$). In this case, we show the emergence of *linear* corrections to the current in the IB strength V. These corrections control the emergence of a mesoscopic "quasiballistic" regime, in which the ballistic current is strongly renormalized before the onset of diffusion; see Fig. 1. More specifically, we show that, up to parametrically large systems $L < L_{\Delta V} \propto V^{-1} < L^*$, IB does not lead to current suppression. Instead the ballistic current is strongly renormalized and, for repulsive interactions ($V > 0$), it may even increase with respect to the integrable case.

The results in this paper are expected to manifest themselves in real experiments probing the transport [52–54] and relaxation properties of isolated interacting systems, close to integrable points.

Our paper is structured as follows. In Sec. II, we present the system, the Lindblad formalism, which allows us to describe a stationary state carrying a current and the numerical approach based on the time-dependent density matrix renormalization group (tDMRG) method. In Sec. III, we discuss the universal scaling induced by IB when perturbing the XX limit. Section IV discusses the effect of IB in the XXZ model. Section V is devoted to the discussion of our results and conclusions. The appendices incorporate details about the tDMRG implementation, perturbation theory, and complementary plots to our numerical analysis.

II. MODEL AND METHODS

We consider the anisotropic Heisenberg (XXZ) chain in one dimension [55],

$$H_{\mathrm{XXZ}} = J \sum_{i=1}^{L-1} \left(\sigma_i^x \sigma_{i+1}^x + \sigma_i^y \sigma_{i+1}^y\right) + \Delta \sum_{i=1}^{L-1} \sigma_i^z \sigma_{i+1}^z, \qquad (2)$$

in which $\sigma^{x,y,z}$ are the standard Pauli matrices and L the number of spins in the system. We set $J = 1$. The model (2) is integrable and its ground state is gapless for $\Delta \in [-1, 1]$ and gapped otherwise. Remarkably, it supports ballistic spin transport at finite energy density in the gapless phase [12], superdiffusion at the isotropic point $|\Delta| = 1$, and normal diffusion otherwise [11,13].

Transition to a diffusive regime is expected when breaking integrability. For the remainder of the paper, we explicitly break integrability by adding global next-nearest-neighbor (NNN) interactions,

$$H_{\mathrm{NNN}} = V \sum_{i=1}^{L-2} \sigma_i^z \sigma_{i+2}^z. \qquad (3)$$

We recall that V has units of the J coupling and, for the remainder of the paper, we consider weak ($V \ll 1$) and moderate ($V \approx 0.5$) interactions.

To study transport, we numerically mimic the experimentally relevant situation [52–54] in which the system is coupled at its two ends to a left (L) and a right (R) magnetization reservoir. If there is a small magnetization bias, it induces a nonequilibrium steady state (NESS) carrying spin current; see Fig. 1. Coupling to external (Markovian) reservoirs results in a nonunitary evolution of the system's density matrix ρ. We simulate this evolution with the Lindblad master equation $d\rho/dt = \hat{\mathcal{L}}(\rho)$ [56,57], where $\hat{\mathcal{L}}$ is the Liouvillian superoperator which describes the nonunitary dynamics of the system,

$$\hat{\mathcal{L}}(\rho) = -i[H, \rho] + \sum_{\substack{\alpha = L,R \\ \tau = \pm}} 2\Gamma_{\alpha\tau} \rho \Gamma_{\alpha\tau}^\dagger - \{\rho, \Gamma_{\alpha\tau}^\dagger \Gamma_{\alpha\tau}\}. \qquad (4)$$

The dissipative dynamics induced by the reservoirs is expressed in terms of the jump operators $\Gamma_{\alpha\tau} = \sqrt{\gamma(1 + \tau\mu_\alpha)}\sigma_\alpha^\tau$, where γ is the injection/loss rate and $\mu_L = -\mu_R = \frac{\delta\mu}{2}$, with $\delta\mu$ being the bias in magnetization; see also Fig. 1. To simplify the expressions, we fix $\gamma = 1$. Equation (4) effectively describes a system attached to weakly magnetized reservoirs which have a temperature much larger than the energy spectrum of the system [58,59]. This notion has been recently put on solid grounds in Ref. [51].

For small magnetization bias, $|\delta\mu| \ll 1$, the NESS induced by Eq. (4) is close to $\rho_\infty = \mathbb{I}^{\otimes L}/2^L$ [60]. It describes the infinite-temperature situation in which, irrespective of the system Hamiltonian, each spin is in a classical mixed state with the same 1/2 probability of being up or down. The stationary state carries a nonzero average spin current density $\mathcal{J}^s = 2\sum_i^L \langle \sigma_i^+ \sigma_{i+1}^- - \sigma_i^- \sigma_{i+1}^+ \rangle / L$.

The biased jump operators $\Gamma_{\alpha\tau}$ enforce different spin densities at the two ends of the chain [61] and allow for a direct investigation of the spin current. In particular, the dependence of the spin current $\mathcal{J}^s$ as a function of system size L allows

us to distinguish between ballistic and diffusive transport regimes. Ballistic regimes are not described by Fick's law (1) and they are characterized by a steady-state current that does not decay with system size L, whereas diffusive regimes are signaled by a current which decays inversely with L.

A. Numerical methods

To find the steady state of the master equation (4), we employ a time-dependent density matrix renormalization-group (tDMRG) method [45], implemented with the ITensor library [62]. For $\delta\mu = 0$, the steady state of Eq. (4) is the infinite-temperature state. We thus perform a real-time evolution of an initial density matrix $\rho(t=0) = \rho_\infty = \mathbb{I}^{\otimes L}/2^L$, which is written in a matrix product operator (MPO) form. Since the nonequilibrium steady state, $\rho_{\rm NESS} = \lim_{t\to\infty}\rho(t)$, is unique, it is well approximated by $\rho(t)$ for very large times and increasing bond dimensions. By numerically verifying convergence both in time and bond dimension, we are able to compute the NESS for system sizes up to 100 sites ($L = 100$). Our numerical simulations were carried out for a magnetization bias $\delta\mu = 0.1$, for which we verified that the current's response is linear in $\delta\mu$. The bond dimension is limited to $\chi = 160$ and the time step of the Trotter decomposition ranges from $dt = 0.05$ to $dt = 0.2$. The interested reader is directed to Appendix A, where we provide all the necessary details concerning our numerical simulations.

B. Analytical methods

To gain insight in the numerical results, we also rely on perturbation theory to compute the corrections to the spin current caused by weak interactions V, $\Delta \ll J$ in finite-sized systems. Similarly to conventional perturbation theory in the Hamiltonian language, the starting point is a fully diagonalized model. In our case, the reference model is the XX chain with boundary driving, which is a quadratic model and has been analytically solved relying on the third-quantization formalism [63,64]. The description of this formalism is rather technical and does not provide special physical insight. We give thus in Appendix B all the necessary details and describe here only the main steps. The procedure requires first to map the XX chain onto noninteracting fermions via the Jordan-Wigner transformation. In the absence of interactions ($\Delta = V = 0$), the generator of the dynamics, $\hat{\mathcal{L}}_{\rm XX}$, is quadratic in terms of L fermionic annihilation and creation operators. Nevertheless, the fact that the Liouvillian is a non-Hermitian superoperator acting on the density matrix requires working on an extended "third-quantization" basis of $2L \times 2L$ superoperators $\{\hat{c}_i, \hat{c}'_i\}$, which allows us to cast the Liouvillian in the diagonal form

$$\hat{\mathcal{L}}_{\rm XX}(\circ) = \sum_i^{2L} \alpha_i \hat{c}'_i \hat{c}_i(\circ), \tag{5}$$

in which the spectrum $\{\alpha_i\}$ can be calculated numerically, as detailed in Appendix B. In such basis, the NESS is expressed as a "vacuum" state ρ_0, for which $\hat{c}_i(\rho_0) = 0$, and the eigenstates of $\hat{\mathcal{L}}_{\rm XX}$ can be constructed from excitations on the vacuum state, $\rho_\mu = \sum_{\{\mu_i\}} \hat{c}'^{\mu_1}_1 \dots \hat{c}'^{\mu_{2L}}_{2L}(\rho_0)$.

The goal is to find a perturbative solution to the NESS of Eq. (4), in the form $\rho_{ss} = \sum_{m,n=0}^{\infty} V^m \Delta^n \rho_{m,n}$. We plug the perturbative ansatz in the steady-state condition, $\hat{\mathcal{L}}(\rho_{ss}) = 0$, and solve it order by order to find [65]

$$V^m \Delta^n \rho_{m,n} = i\hat{\mathcal{L}}^+_{\rm XX}\big([H_{\rm NNN}, \rho^{(m-1,n)}] + [H^{J=0}_{\rm XXZ}, \rho^{(m,n-1)}]\big), \tag{6}$$

where we introduced the Moore-Penrose pseudoinverse of the Liouvillian of the boundary-driven XX chain, $\hat{\mathcal{L}}^+_{\rm XX}(\circ) = \sum_{\alpha_i\neq 0} \alpha_i^{-1} \hat{c}'_i \hat{c}_i(\circ)$. Using the third-quantization formalism we thus find semianalytic expressions of ρ_{ss} and $\mathcal{J}^s$ up to second order in the interactions V and Δ, which are given in Appendix B.

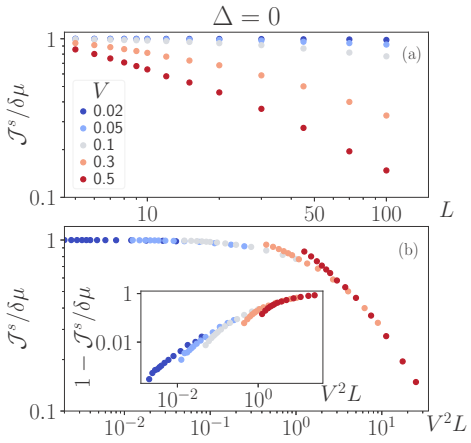

FIG. 2. Dependence of $\mathcal{J}^s$ in the XX model for different strengths V of the next-nearest-neighbor interaction (3) as a function of (a) system size L and (b) the scaling variable L/L^*. In the inset, the deviations from the value of the current in the ballistic limit are shown. Deviations from a universal scaling are observed in (b) for $L \lesssim 10$ at all strengths V.

III. IB AND XX MODEL ($\Delta = 0$): THE UNIVERSAL CROSSOVER TO DIFFUSION

For the XX chain ($\Delta = V = 0$), the MPO expression of the steady state of Eq. (4) has been derived in Refs. [66,67], and found to carry a ballistic spin current $\mathcal{J}^s = \delta\mu$ [68]. Interactions such as Eq. (3) induce inelastic scattering among free particles, which leads to a decay of the spin current and the onset of diffusion in the thermodynamic limit.

For finite but large systems, the ballistic-to-diffusive transition is marked by a sizable deviation from $\mathcal{J}^s = \delta\mu$ at a crossover length scale L^*. According to FGR, this scattering length is expected to scale as $L^* \sim V^{-2}$ in the $V \to 0$ limit.

We numerically compute the current, as a function of the system size L, for different strengths $V < J$ of the NNN interaction, Eq. (3); see Fig. 2(a). As expected, with increasing strength of the IB parameter V, the current decreases monotonically for a fixed length L and diffusion sets in at smaller L.

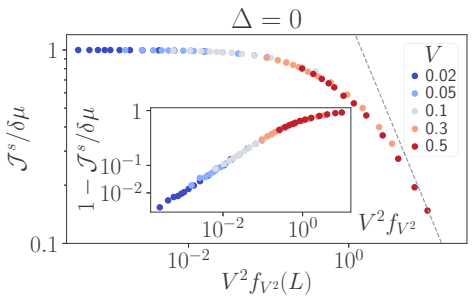

FIG. 3. Universal scaling dependence of $\mathcal{J}^s$ in the XX model for different strengths V of the next-nearest-neighbor interaction (3) as a function $V^2 f_{V^2}(L)$. The dashed gray line corresponds to the ansatz (8), valid for the diffusive regime. In the inset, the deviations from the value of the current in the ballistic limit are shown.

Assuming that the only characteristic length (beyond lattice spacing) is the scattering length, it is natural to expect a scaling hypothesis controlled by L^*, i.e., $\mathcal{J}^s/\delta\mu = \mathcal{F}(L/L^*) = \mathcal{F}(LV^2)$. However, such scaling ansatz does not allow a perfect collapse of all the numerical curves onto a unique function; see Fig. 2(b) and inset. We observe that for small systems, typically up to $L \sim 10$ sites, the current deviates significantly from the scaling for any value of V. The absence of a universal scaling is intriguing and also hinders the possibility to extrapolate numerical data to arbitrarily large system sizes. It is thus important to understand the deviations and possibly correct them.

Thus, we rely on perturbation theory, described in Sec. II B, to derive the correction to the current at finite sizes L. We find that the leading corrections to the current read

$$\mathcal{J}^s = [1 - V^2 f_{V^2}(L) + O(V^4)]\delta\mu. \tag{7}$$

Remarkably, the leading corrections to the current have a nontrivial dependence on the system size L, through the function $f_{V^2}(L)$, which is plotted in Fig. 8 in Appendix D. Apart from irrelevant corrections for short system sizes, f_{V^2} is as a linear function with a nonzero offset with respect to the origin, $f_{V^2}(L) \approx 0.40(L - 3.38)$. The divergence of the correction of order V^2 in Eq. (7) signals the transition to the diffusive regime in which the current is expected to scale as L^{-1}.

Surprisingly, a universal scaling of the numerical data is obtained when plotting the current as a function of the nontrivial parameter $V^2 f_{V^2}(L)$; see Fig. 3 and inset. The collapse of the curves is excellent up to large system sizes and up to moderate IB strengths, $V = 0.5$. This shows the importance of boundary effects in the ballistic-to-diffusive transition triggered by generic interaction on the XX model. The boundary corrections are encoded in the fact that the function $f_{V^2}(L)$ has an offset with respect to a straight line crossing the origin. Such offset becomes negligible for systems sizes $L \geqslant 10$.

The expression (7) is only valid as long as $V^2 f_{V^2}(L) \ll 1$ and, unluckily, we could not find a good expression fitting the whole curve in Fig. 3. Nevertheless, when approaching the diffusive regime, the numerics are consistent with the expression

$$\mathcal{J}^s = \frac{1.45}{V^2 f_{V^2}(L)}\delta\mu, \tag{8}$$

corresponding to the gray dashed lines in Fig. 3. For asymptotically large L, Eq. (8) acquires the form $\mathcal{J}^s = D^s_{\Delta=0}\delta\mu/2L$, in which $D^s_{\Delta=0} \approx 7.3/V^2$ is the spin diffusion constant. This value of the diffusion constant is derived by considering the equivalent of Fick's law (1) in the spin formulation of the problem, namely $\mathcal{J}^s = -D^s \nabla s^z = D^s\,\delta\mu/2L$, in which $s^z = \langle\sigma^z\rangle/2$ is the spin expectation value. We have verified numerically that $\nabla s^z = -\delta\mu/2L$ gives the correct estimate of the spin-density gradient in diffusive regimes; see Appendix C. One should notice that a precise evaluation of $D^s_{\Delta=0}$ for weak V would hardly be possible without considering the correct scaling parameter, as shown in Fig. 2.

This discussion concludes our analysis of the ballistic-to-diffusive transition induced by IB on the XX model. We showed that corrections caused by boundary effects affect the scaling of the current for short system sizes. Nevertheless, perturbation theory allows us to account for such finite-size corrections and derive a universal ballistic-to-diffusive crossover induced by IB on ballistic, noninteracting regimes. Our analytical calculation shows that boundary effects become negligible beyond systems of $L \sim 10$ sites, for which the ballistic-to-diffusive crossover is indeed nicely described by a universal function of L/L^*. It is important to stress that our analytical calculations are crucial to account for boundary corrections and thus allow an accurate extrapolation of the numerics to the thermodynamic and $V \to 0$ limit. Without perturbation theory, the universal nature of the scaling would have been difficult to establish based exclusively on numerical data.

We now extend our work to the interacting and integrable case, showing how nearest-neighbor interactions, of strength $0 < \Delta < 1$, strongly modify the effects of IB on the ballistic regime.

IV. IB AND XXZ MODEL WITH $|\Delta| < 1$

A. The ballistic, integrable regime

The sole presence of nearest-neighbor interactions does not hinder ballistic transport in the thermodynamic limit for $|\Delta| < 1$ [12,69,70]. For finite systems, the current depends nontrivially on the system size. For increasing L, the current decreases monotonically until it saturates to its ballistic (thermodynamic) value. This saturation occurs beyond a typical length scale L_Δ which depends on the strength Δ of the integrable nearest-neighbor interaction.

The behavior of $\mathcal{J}^s$ as a function of L is shown in Fig. 4, which reproduces the findings of Ref. [71] and that we display here for clarity. To our knowledge, the exact size dependence of the current is unknown. It is possible to obtain perturbatively the finite-size behavior of the current for $\Delta \to 0$:

$$\mathcal{J}^s = [1 - \Delta^2 f_{\Delta^2}(L) + O(\Delta^3)]\delta\mu, \tag{9}$$

where f_{Δ^2} is a linear function similar to f_{V^2}; see Appendix D. In analogy to the discussion of the previous section, Eq. (9) is only valid for system sizes $L < L_\Delta$, in which, for $\Delta \ll 1$, $L_\Delta \propto 1/\Delta^2$. Beyond L_Δ, the perturbative corrections diverge

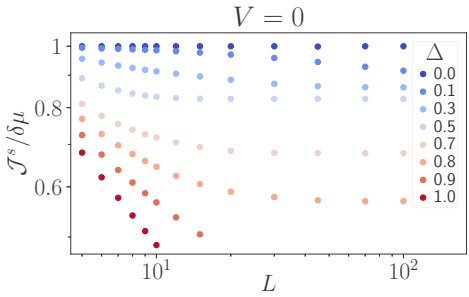

FIG. 4. Finite-size scaling of $\mathcal{J}^s$ in the ballistic regime of the XXZ model (2), for different $0 < \Delta < 1$. For $\Delta < 1$, the current always saturates to a constant value signaling the ballistic regime.

linearly in L and miss the saturation of the current which, to be derived, would require the resummation of the perturbation theory in Δ to all orders. It should be stressed that even though the expansions (7) and (9) look almost identical, their linear divergences do not signal analogous behaviors in the thermodynamic limit. In particular, in the nonintegrable case, one would find the diffusive current suppression described by Eq. (8).

B. Strong linear effects induced by IB

We now study the transition to the diffusive regime induced by the IB term (3) for $|\Delta| < 1$. In Fig. 5, we present the size dependence of the spin current for $\Delta = 0.3$ and different IB parameters. Figure 5(a) highlights the suppression of the current density for large systems and strong IB. The suppression is compatible with a diffusive scaling, marked by the dashed gray lines. However, the observation of a clear diffusive behavior lays beyond the available system sizes. Thus we cannot reach any conclusions about the Δ dependence of the diffusion constant [72].

Nevertheless, the most striking and visible effect in Fig. 5 is not the current suppression, but rather the strong sensitivity of $\mathcal{J}^s$ to the sign of the coupling constant V. This dependence is visible for any system size and any IB strength and it is absent in the noninteracting limit ($\Delta = 0$). Two features of such phenomenon deserve particular attention:

(i) The value of the current can even *increase* with respect to the integrable case after breaking integrability. This relative increase is more pronounced for small $V \ll 1$, see Fig. 5(b), but persists up to system sizes of the order of 50 sites for nonperturbative values of the IB strength $V \sim 0.1$; see Fig. 5(a). This is surprising, given the expectation that IB is supposed to trigger diffusion, and thus suppress the current as a function of the system size.

(ii) In the limit of $V \to 0$, the effects of IB appear to just renormalize the relaxation toward the ballistic regime and the saturation value of the current; see Fig. 5(b). Breaking of integrability marks a correction to the ballistic regime, long before the scattering length L^* and the related onset of diffusion. The curves for $|V| \leqslant 0.02$ also suggest that this effect reduces as

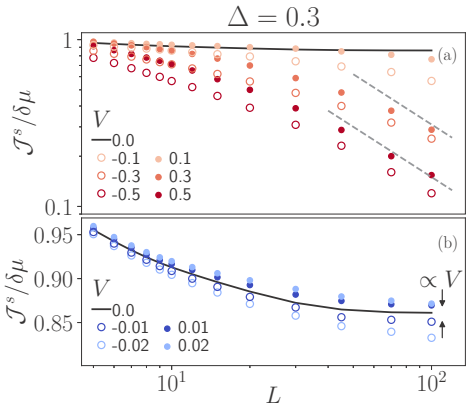

FIG. 5. System-size dependence of the XXZ current in the presence of nonintegrable interactions (3) and for different IB strengths V. In all cases, we compare to the integrable ballistic case for $\Delta = 0.3$ (solid black line). (a) For moderately strong IB ($|V| \geqslant 0.1$), at short system sizes, the stationary current is strongly sensitive to sign of the IB term V before the onset of diffusion, which is signaled by the dashed gray lines at larger system sizes. (b) Illustration of the quasiballistic regime in the $V \to 0$ limit. For weak IB, the ballistic regimes appears to be just renormalized by linear (sign-dependent) corrections in V.

$V \to 0$, while simultaneously persisting for larger systems. This effect has nothing to do with the boundary corrections discussed in Sec. III.

This strong sensitivity of the current to the sign of the IB term V hints at the existence of linear effects in V whose fate in the thermodynamic limit is intriguing—in particular, concerning the renormalization of the ballistic regime observed in Fig. 5(b). In the next section, we argue how linear corrections control the IB crossover to the diffusive regime, giving rise to an emergent mesoscopic "quasiballistic" regime.

C. The quasiballistic regime

The perturbation theory carried out in the previous sections provides some insight into the nature of the linear correction in V. It arises as a second-order term in ΔV when perturbing the current close to the XX limit:

$$\mathcal{J}^s \approx [1 - V^2 f_{V^2}(L) - \Delta^2 f_{\Delta^2}(L) + V\Delta f_{V\Delta}(L)]\delta\mu. \quad (10)$$

Similarly to the Δ^2 and V^2 corrections, $f_{V\Delta}$ also diverges linearly with the system size L; see Appendix D. The second-order nature (ΔV) of the linear corrections indicates that the effects discussed here only pertain the interplay between integrable and IB interactions. In the absence of nearest-neighbor interactions ($\Delta = 0$), the effects are trivially absent, as shown in Sec. III.

To understand the fate of the linear correction in the thermodynamic limit, we rely on a systematic study of the finite-size scaling of the current at finite Δ. We numerically

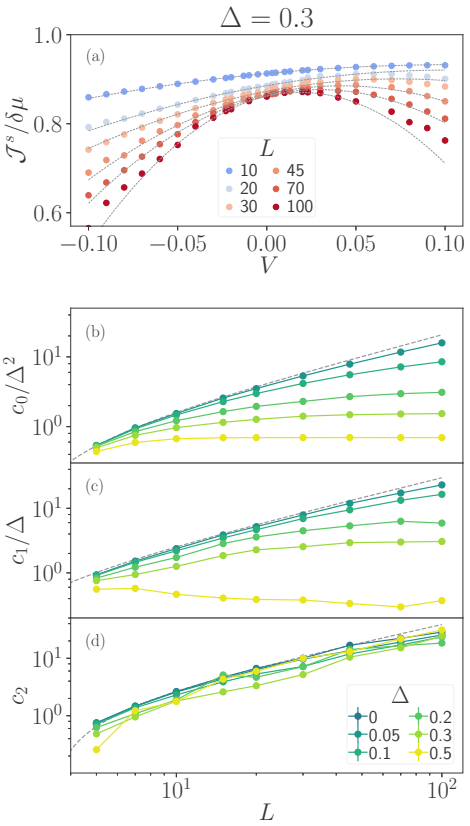

FIG. 6. (a) Dependence of $\mathcal{J}^s$ for $\Delta = 0.3$ and different system sizes, as a function of small IB parameters. Dashed lines represent the fitting functions of Eq. (11). (b)–(d) System-size dependence of the fitting parameters for different Δ parameters. The dashed gray lines correspond to the predictions from second-order perturbation theory. For small Δ, the results approach the perturbative predictions.

probe the $V \to 0$ limit by assuming a polynomial expansion of the current:

$$\frac{\mathcal{J}^s}{\delta\mu} = 1 - c_0(\Delta, L) + V c_1(\Delta, L) - V^2 c_2(\Delta, L) + O(V^3), \tag{11}$$

which extends Eq. (10) beyond the perturbative regime.

In Fig. 6(a), we depict the dependence of the spin current $\mathcal{J}^s$ on the IB perturbation strength V for finite $\Delta = 0.3$ and increasing system sizes L. For $V \ll \Delta$, all curves can be nicely fitted with expression (11), with c_i as free parameters. The asymmetry of the parabolic dependence on V is a clear indicator of the presence of linear corrections for $\Delta \neq 0$. In Figs. 6(b)–6(d), we show the obtained finite-size scaling of the coefficients c_i for different values of Δ. The dashed lines correspond to the analytic predictions derived with perturbation theory in Eq. (10). They show an excellent agreement with the numerics in the $\Delta \to 0$ limit [73].

Figure 6(c) clearly shows that the coefficient c_1, which controls the linear corrections in V, behaves analogously to c_0, and thus saturates to finite values at systems sizes of the order of L_Δ. The finite value of c_1 contributes to the strong sign dependence at moderately strong V in Fig. 5(a).

On the other hand, c_2, which controls the second-order corrections to $\mathcal{J}^s$ in V, increases linearly with L. Its divergence is only weakly affected by the presence of a finite Δ. The fact that only the terms of order $O(V^2)$ diverge suggests that the diffusive regime is established at the scattering length $L^* \sim 1/V^2$ [21–23].

The different size dependence of the coefficients c_1 and c_2 corresponds to strong quantitative effects of IB on integrable systems. First of all, the nonzero linear corrections in V signal that IB has prominent effects at system sizes much shorter than L^*. In contrast to the XX case, IB does not primarily lead to the inelastic scattering of quasiparticles and the onset of diffusion. Instead, IB leads to a transient and mesoscopic "quasiballistic" regime, in which the value of the ballistic current in the XXZ model is just renormalized by IB. Whether such corrections can be interpreted as a renormalization of the quasiparticle velocity is left for future investigation.

Additionally, such quasiballistic regime persists up to a novel and parametrically large length scale $L_{\Delta V}$, which controls the onset of diffusion and is much shorter than L^*. An estimate of $L_{\Delta V}$ can be obtained from Eq. (11). It is defined as the length scale at which the diverging term of order $O(V^2)$ dominates the linear correction of order $O(V)$. For $|V| \ll \Delta$, we can define such length scale as

$$L_{\Delta V} \sim \frac{1}{|V| c_1(\Delta, L \to \infty)} \ll L^* \sim \frac{1}{V^2}. \tag{12}$$

This emergent length scale marks the system sizes up to which IB acts as a renormalization of the ballistic current of the integrable XXZ model with $|\Delta| < 1$. For system sizes $L \simeq L_{\Delta V}$, the deviations from the ballistic regime become sizable, and the crossover to diffusion starts. Remarkably, such transient length scale does not emerge from generalized hydrodynamics approaches [21–23]. The reason is that generalized hydrodynamics is a "coarse-grained" approach, which considers the limit $L \to \infty$ before $V \to 0$. Our numerical and analytical predictions rely on the opposite order of limits, which will be relevant to study IB in real experiments. We expect our effects to appear on the transient timescales controlling the quantum evolution after quenches.

We conclude this section by stressing that the existence of such linear effects compromises the possibility to collapse the crossover to diffusion onto a unique, universal curve.

V. CONCLUSIONS

In this work, we studied and characterized the effects of integrability breaking on the spin current of a boundary-driven

chain. We have first considered integrability breaking of the noninteracting XX chain. We showed that the crossover to diffusion is indeed universal and controlled by a novel scaling parameter, $V^2 f_{V^2}(L)$, which we computed using perturbation theory and which accounts for boundary effects. The universal scaling found here allows us to show that the ballistic-to-diffusive crossover is controlled by the scattering length $L^* \sim V^{-2}$, consistently with FGR. Accounting for boundary effects was important to verify the universality of such transition based on numerical calculations.

Nevertheless, the fact that deviations from ballisticity in the XX model are controlled by second-order corrections in the IB strength V is not trivial. In Ref. [27], the evolution of eigenstates in the presence of IB terms was studied exactly for the same model. In that work, it was pointed out that, for fixed system sizes L, perturbation theory is expected to fail for systems sizes $\tilde{L} \propto V^{-1/2}$. Such an estimate is readily derived by noticing that NNN interactions have typical matrix elements of order V/L which couple $\rho \propto 1/L^3 \ln L$ states, because of total momentum conservation. Now, it is remarkable that the length scale $\tilde{L}$ does not appear at all in the finite-size scaling of the current during the onset of diffusion. The physical effects of such length scales pave the way to stimulating investigations concerning other effects of integrability breaking. It is also an interesting line of investigation to extend our approach to the regimes in which V is of the order of the spin exchange J, or larger.

We have then addressed the effects of IB in the ballistic regime of the XXZ model. Our observations are consistent with a diffusive regime in the thermodynamic limit, even though the precise determination of the diffusion constant in the presence of a finite $\Delta < 1$ and $V \to 0$ remains an interesting (and challenging) line of investigation [72]. Our main result, is that IB controls the ballistic-to-diffusive transition in a nontrivial way for interacting models at mesoscopic length scales. Unlike the noninteracting XX case, we showed that linear corrections in V influence transport long before the onset of diffusion. This is surprising given the expectation that IB would simply suppress the current as a function of size. The fact that the opposite may happen in the mesoscopic quasiballistic regime is a qualitatively new effect of interactions. As mentioned above, the physical meaning of such effect has to be clarified.

An interesting direction would be to compare and make the connection of our findings with the timescales describing the relaxation of nonintegrable quantum systems [29,30]—for instance, by studying the unitary evolution of a weakly polarized domain-wall state [6,7,13,39]. It would be important to understand the role of IB terms different from Eq. (3), such as disorder, single impurities [29,30,74], stochastic quantum noise [75–77], and also dephasing [78].

Future research directions could address the propagation of energy and spin [79] in the presence of IB—in particular, whether the Wiedemann-Franz law [80] is restored in the presence of IB terms, since it is notoriously violated in such systems at low temperatures [25,81–83]. An additional perspective is the investigation of different integrability perturbations and their effect on quantum ladder systems attached to reservoirs [84–86].

ACKNOWLEDGMENTS

J.S.F. and M.F. acknowledge several discussions with Dmitry A. Abanin, Vincenzo Alba, Christophe Berthod, Thierry Giamarchi, Tony Jin, and, in particular, with Marko Žnidaric during the whole realization of this work and support from FNS/SNF Ambizione Grant No. PZ00P2_174038. J.S.F. acknowledges Miles Stoudenmire and Matthew Fishman for helpful support with the ITensor library and thanks Michael Sonner and Sofia Azevedo for a careful reading of the manuscript.

APPENDIX A: NUMERICAL DETAILS

Except for the large coupling limit, $V \to \infty$, the models presented in the main text have a unique nonequilibrium steady state (NESS) in the thermodynamic limit. This condition ensures that we can reach the NESS via a real time evolution $\rho_\infty = \lim_{t\to\infty} \exp(\hat{\mathcal{L}}t)\rho(0)$ of any initial state $\rho(0)$. We initialize the state in the product state $\rho(t=0) = \mathbb{I}^{\otimes L}/2^n$.

For small systems, $L < 8$, we use exact diagonalization as baseline for other time-evolution methods. Beyond $L = 8$, we employ time-evolving block decimation (TEBD), which allows us to efficiently find the NESS of large spin chains, $L \lesssim 100$. The algorithm was first explored in Ref. [60] and consists of applying a Suzuki-Trotter decomposition of the Lindblad superoperator to the state ρ. In our case, we use a 4th-order decomposition introduced in Ref. [87]. At any time during the time evolution, the density matrix can be written in a matrix product operator form

$$\rho = \sum_{\{i\}} M_1^{i_1} M_2^{i_2} \dots M_L^{i_L} \left(\sigma_1^{i_1} \otimes \sigma_2^{i_2} \otimes \dots \otimes \sigma_3^{i_L}\right), \qquad \text{(A1)}$$

where we choose the local basis to be the Pauli matrices $\sigma^{0,1,2} = \sigma^{x,y,z}$ and $\sigma^3 = \mathbb{I}$ and $\dim(M_k^i) = \chi \times \chi$. In general, the application of nonunitary two-site gates leads to nonphysical states as it breaks the orthogonality condition assumed in TEBD. To avoid reorthogonalizing the MPO at every time step, we apply the gates sequentially instead [88]. We simulate the next-nearest interaction using the SWAP gate technique.

In the presence of interactions, the necessary bond dimension χ to simulate the NESS is expected to grow with the system size. We consider that the time-evolved state $\rho(t)$ correctly approximates the NESS if it satisfies three criteria: the current is homogeneous across the chain, the average current does not evolve in time, and the current converges as the bond dimension increases. Next, we present the algorithm used in this paper. The quantity $\bar{\mathcal{J}}$ represents the spatial average of the spin current

(1) Initialize with the product state $\rho(t=0) = \mathbb{I}^{\otimes L}/2^n$ ($\chi_0 = 1$).

(2) Increase the bond dimension by $\chi_i = \delta\chi + \chi_{i-1}$.

(3) Time-evolve the state until the current has saturated in time.

(a) Compute the time variance in the last $T = 10, 30$ time units (of hopping) $\sigma_T^2 = \sum_{i=1}^{T} [\bar{\mathcal{J}}(t-i) - \mu]^2/T$.

(b) Repeat step 3 until $|\sigma_{30}^2 - \sigma_{10}^2|/\sigma_{30}^2 < 1\%$.

(4) Check convergence

(a) Compute the spacial variance $\sigma^2(\mathcal{J}) = \sum_{i=2}^{L-1} (\mathcal{J}_i - \bar{\mathcal{J}})^2/(L-2)$.

(b) Compute the change with the bond dimension $\epsilon_\chi = \bar{\mathcal{J}}(\chi_i) - \bar{\mathcal{J}}(\chi_{i-1})$.

(c) Repeat steps 2, 3, and 4 until $|\sigma(\mathcal{J})/\bar{\mathcal{J}}| < 1\%$ and $|\epsilon_\chi/\bar{\mathcal{J}}| < 0.5\%$.

(5) Compute the final current and associated error $\epsilon_J = \max(\sigma(\mathcal{J}), \epsilon_\chi)$.

In most situations, we require a much stricter bond on the homogeneity condition, often requiring $|\sigma(\mathcal{J})/\bar{\mathcal{J}}| < 0.1\%$. The time step of the Trotter decomposition is variable along the algorithm. For small bond dimensions, we use a large time step, $dt = 0.2$, to quickly advance the simulation and reduce it when closer to convergence, up to $dt = 0.05$. Due to the convergence criterion employed, simulations can take weeks to converge or reach inaccessible bond dimensions. For this reason, if the criteria are not satisfied for $\chi \leqslant 160$, we consider that the system has not converged and do not show it.

The algorithm was implemented using the open-source ITensor library [62].

APPENDIX B: DIAGONALIZATION OF THE XX CHAIN

In this section, we provide a summary on how to diagonalize the noninteracting XX limit, $V = \Delta = 0$. We follow the protocol of Ref. [64] which reduces the diagonalization problem to finding the eigenbasis of a $2L \times 2L$ matrix. It is useful to work in the fermionic representation via the Jordan-Wigner transformation:

$$\begin{aligned}\sigma_j^+ &= e^{-i\pi\sum^{j-1} n_k} a_j^\dagger,\\ \sigma_j^- &= e^{i\pi\sum^{j-1} n_k} a_j,\\ \sigma_j^z &= 2a_j^\dagger a_j - 1.\end{aligned} \tag{B1}$$

In the fermionic representation, the Hamiltonian becomes

$$H_{\mathrm{XX}} = \sum_{i,j=1}^{L} h_{ij} a_i^\dagger a_j \tag{B2}$$

with $h_{i,j} = 2J\delta_{|i-j|,1}$. Since the $\{a_i, a_i^\dagger\}$ operators act left and right of the density matrix, it is useful to work in the Liouville space of superoperators. In the superoperator formalism, density matrices are mapped onto vectors in a vector space of dimensions $\mathbb{C}^{4^L} \times \mathbb{C}^{4^L}$ according to the mapping $\|M\rho N\rangle = M \otimes N^T \|\rho\rangle$, where $\|\rho\rangle$ is the row-vectorized form of the matrix ρ. We can now define a new set of $2L$ superoperators $\mathcal{B} = \{\hat{b}_i, \hat{b}_i^\dagger, \hat{b}_{L+i}, \hat{b}_{L+i}^\dagger\}_{i=1}^L$, which act on $\|\rho\rangle$ according to

$$\begin{aligned}\hat{b}_i\|\rho\rangle &= \|a_i\rho\rangle,\\ \hat{b}_i^\dagger\|\rho\rangle &= \|a_i^\dagger\rho\rangle,\\ \hat{b}_{L+i}\|\rho\rangle &= \|\hat{\mathcal{P}}(\rho a_i^\dagger)\rangle,\\ \hat{b}_{L+i}^\dagger\|\rho\rangle &= \|\hat{\mathcal{P}}(\rho) a_i\rangle,\end{aligned} \tag{B3}$$

where $\hat{\mathcal{P}} = e^{i\pi\sum n_i \otimes \mathbb{I} + \mathbb{I}\otimes n_i^T}$ is a superoperator string which imposes the necessary anticommutations relations $\{\hat{b}_i^\dagger, \hat{b}_j\} = \delta_{ij}$. In practice, the $\mathcal{B}$ basis acts as a complete set of creation and destruction operators in the occupation number basis of a lattice of size $2L$. Physically, $\hat{\mathcal{P}}$ is a parity operator with eigenvalues ± 1 and counts the number of excitations in the new fermionic system with $2L$ states. For reasons clear bellow, we will only be interested in $\hat{\mathcal{P}} = 1$. In the new $\mathcal{B}$ basis, the Lindblad superoperator reads

$$\begin{aligned}\hat{\mathcal{L}}_{\mathrm{XX}} = &-i\sum_{i,j=1}^{L}(h_{i,j}\hat{b}_i^\dagger\hat{b}_j - h_{ji}\hat{b}_{L+i}^\dagger\hat{b}_{L+j})\\ &+ \sum_{i=1,L}\Gamma(1+\mu_i)(2\hat{b}_i^\dagger\hat{b}_{L+i}^\dagger\hat{\mathcal{P}} - \hat{b}_{L+i}\hat{b}_{L+i}^\dagger - \hat{b}_i\hat{b}_i^\dagger)\\ &+ \sum_{i=1,L}\Gamma(1-\mu_i)(-2\hat{b}_i\hat{b}_{L+i}\hat{\mathcal{P}} - \hat{b}_{L+i}^\dagger\hat{b}_{L+i} - \hat{b}_i^\dagger\hat{b}_i).\end{aligned} \tag{B4}$$

Similarly to the diagonalization procedure of quadratic Hamiltonians, we are interested in finding a basis of $2L$ creation and annihilation superoperators $\mathcal{C} = \{\hat{c}_i', \hat{c}_i\}_{i=1}^{2L}$ that diagonalizes the unperturbed problem, $\hat{\hat{\mathcal{L}}}_{\mathrm{XX}} = \sum_{i=1}^{2L}\alpha_i\hat{c}_i'\hat{c}_i$. If such basis exists, the eigenstates of $\hat{\hat{\mathcal{L}}}_{\mathrm{XX}}$ can be constructed from excitations on the vacuum state of the c's operators, $\|\rho_\mu\rangle = \sum_{\{\mu_i\}}\hat{c}_1'^{\mu_1}\ldots\hat{c}_{2L}'^{\mu_{2L}}\|0\rangle$ and $\lambda_\mu = \sum_i^L(\mu_i\alpha_i + \mu_{L+i}\alpha_i^*)$. Trivially, the NESS is the vacuum state of the $\mathcal{C}$ basis.

Due to particle-hole symmetry, the values of α_i must come in conjugate pairs $\{\alpha, \alpha^*\}$ with $\mathrm{Re}(\alpha) \leqslant 0$. We fix $\alpha_i^* = \alpha_{L+i}$ in our notation. In general, the Lindblad superoperator is not Hermitian and neither are the $\hat{c}$'s superoperators; however, they still respect the fermionic anticommutation relations $\{\hat{c}_i, \hat{c}_j'\} = \delta_{i,j}$ and $\{\hat{c}_i, \hat{c}_j\} = \{\hat{c}_i', \hat{c}'_j\} = 0$. The $\hat{c}, \hat{c}'$ operators represent a linear superposition of particle and hole excitations acting both left and right of the density matrix and should be understood as the "normal modes" of the open system. The exact mapping between $\{\hat{c}_i, \hat{c}_i'\}$ and $\{\hat{b}_i, \hat{b}_i^\dagger\}$ operators can be found in Ref. [64] and is shown here for completeness:

$$\begin{bmatrix}\hat{b}_{1\to L}\\ \hat{b}^\dagger_{L+1\to 2L}\\ \hat{b}^\dagger_{1\to L}\\ \hat{b}_{L+1\to 2L}\end{bmatrix} = \begin{bmatrix}W & 0\\ 0 & -Y_L W^* Y_L\end{bmatrix}\begin{bmatrix}\hat{c}_{1\to L}\\ \hat{c}'_{L+1\to 2L}\\ \hat{c}'_{1\to L}\\ \hat{c}_{L+1\to 2L}\end{bmatrix}, \tag{B5}$$

where $Y_L = -i\left[\begin{smallmatrix}0 & \mathbb{I}_L\\ -\mathbb{I}_L & 0\end{smallmatrix}\right]$ and the columns of W are the right eigenvectors of a matrix M. In our work, M acquires a simple form

$$M = \frac{1}{2}\begin{bmatrix}-ih + \Lambda^+ - \Lambda^- & 2\Lambda^+\\ 2\Lambda^- & -ih - \Lambda^+ + \Lambda^-\end{bmatrix} \tag{B6}$$

with diagonal matrices $\Lambda_i^+ = (\delta_{i,1} + \delta_{i,L})\Gamma(1+\mu_i)$ and $\Lambda_i^- = (\delta_{i,1} + \delta_{i,L})\Gamma(1-\mu_i)$.

To our knowledge, there is no analytical solution for W as a function of L and so we resort to exact diagonalization. Once the mapping of Eq. (B5) is found, we can express any superoperator in the $\mathcal{C}$ basis.

APPENDIX C: UNIVERSAL SCALING

In this Appendix, we provide further details on the universality of the scaling discussed in Sec. III.

It follows from Fick's law that, when imposing a fixed bias, the magnetization profile interpolates linearly between

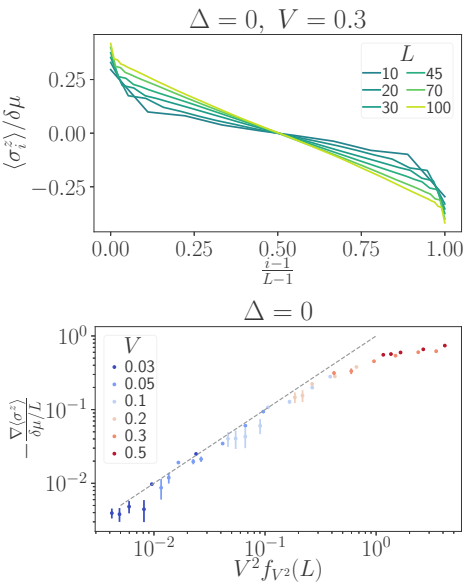

FIG. 7. Top: Magnetization profile close to the diffusive regime for different system sizes. Bottom: Rescaled slope of the magnetization for different IB parameters as a function of $V^2 f_{V^2}(L)$. System sizes range from $L = 15$ to $L = 100$. Analytic predictions close to the ballistic regime are depicted as dashed lines. In the diffusive regime $[V^2 f_{V^2}(L) \approx 1]$, the magnetization slope approaches $\delta\mu/L$ as expected.

the borders. However, this is only true in the thermodynamic limit, and finite systems present small deviations up to four sites into the chain's bulk. In Fig. 7 (top), we depict the magnetization profile of the XX model close to the diffusive regime for different system sizes. The effects of the border are visible up to very large systems, $L = 100$.

For consistency, we verify that the magnetization's gradient converges to $\nabla\langle\sigma^z\rangle = -\delta\mu/L$ in the diffusive regime, $V^2 f_{V^2}(L) \gg 1$, see Fig. 7 (bottom). There, we depict the rescaled gradient of σ^z obtained by a linear fit of the magnetization close to the middle of the chain. We find an overall scaling with $V^2 f_{V^2}(L)$ but, in contrast to Fig. 2, the finite-size effects in the magnetization profile lead to non-negligible deviations. Close to the ballistic regime, we find a moderate agreement with $\nabla\langle\sigma^z\rangle = -\frac{\delta\mu}{L} V^2 f_{V^2}(L)$, depicted as dashed gray line.

APPENDIX D: PERTURBATION THEORY

As mentioned in the main text, perturbation theory (PT) provides a benchmark and helpful insights on the numerical data in the limit of small interactions. In this section, we provide further details on the method.

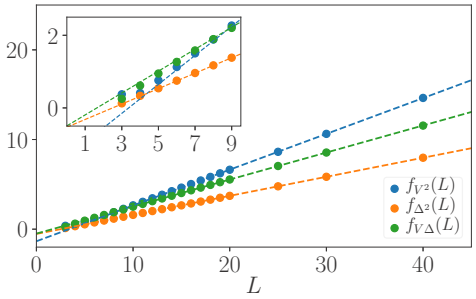

FIG. 8. System size dependence of the functions f_i in Eq. (D3). Dashed lines depict the linear fitting performed beyond $L = 6$. Inset: Highlight for very short systems, in which the deviations from perfect linear scaling can be appreciated.

The object of interest is the NESS of the system. It corresponds to the unique (in our case) zero eigenvalue of the nonunitary master equation (4). This equation can be written in terms of the Liouvillian super-operator $d_t\rho = \hat{\mathcal{L}}(\rho)$. Superoperators are denoted by a hat.

The first step in PT is to find the eigendecomposition of the unperturbed problem, i.e., the superoperator of the noninteracting boundary-driven XX model, $\hat{\mathcal{L}}_{\mathrm{XX}}$. As a direct consequence of the nonunitarity of general Lindblad evolutions, the Lindblad superoperator is described by a non-Hermitian matrix and thus has different left and right eigenvectors, $\tilde{\rho}_\mu$ and ρ_μ, respectively. They respect the normalization condition $\mathrm{Tr}(\tilde{\rho}_\mu \rho_\nu) = \delta_{\mu\nu}$ and share the same eigenvalue λ_μ, whose real part corresponds to the physical relaxation rate of ρ_μ.

The eigenstates of $\hat{\mathcal{L}}_{\mathrm{XX}}$ serve as the basis to perturbatively construct the eigenstates of the full problem. Since $\hat{\mathcal{L}}_{\mathrm{XX}}$ is a quadratic superoperator, it is useful to rely on the third-quantization formalism [63,64] to find its eigendecomposition. In Appendix B, we construct the 4^L eigenstates ρ_μ by consecutively acting with annihilation (creation) operators, $\hat{c}^{(\prime)}$, on a vacuum state of $2L$ particles, ρ_0. This approach allows us to diagonalize the Lindblad superoperator, which can be written as

$$\hat{\mathcal{L}}_{\mathrm{XX}}(\circ) = \sum_i^{2L} \alpha_i \hat{c}_i' \hat{c}_i(\circ) = \sum_\mu^{4^L} \lambda_\mu \rho_\mu \mathrm{Tr}(\tilde{\rho}_\mu \circ), \tag{D1}$$

where $\rho_\mu = \sum_{\{\mu_i\}} \hat{c}_1'^{\mu_1} \ldots \hat{c}_{2L}'^{\mu_{2L}}(\rho_0)$ and $\lambda_\mu = \sum_i^{2L} \mu_i \alpha_i$. All the models discussed here have a unique NESS that satisfies

TABLE I. Fitting parameters of the second-order corrections to the current.

	a	b
f_{V^2}	0.3992	−1.348
f_{Δ^2}	0.2124	−0.5307
$f_{V\Delta}$	0.3015	−0.4946

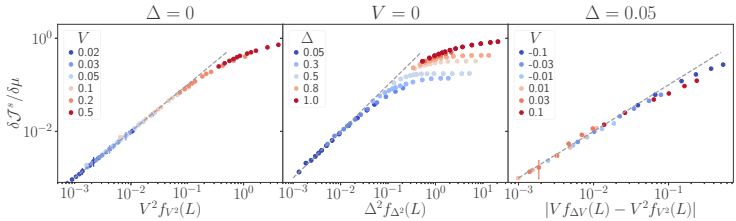

FIG. 9. Deviations from the ballistic current for small (next-to-)nearest-neighbor interactions. System sizes range from $L = 5$ to $L = 100$. The numerical data closely follow the analytic predictions of (D3) depicted as dashed lines.

$\lambda_0 = 0$ and $\tilde{\rho}_0 = \mathbb{I}$. The NESS of the XX model carries a finite current proportional to the bias, $\mathrm{Tr}[\hat{\mathcal{J}}^s\rho_0] = \delta\mu$. $\hat{\mathcal{J}}^s$ is the spin current density superoperator.

In the second step of PT, we look for a perturbative solution to the NESS of Eq. (4), in the form $\rho_{ss} = \sum_{m,n=0}^{\infty} V^m\Delta^n\rho^{(m,n)}$, where $\rho^{(0,0)} = \rho_0$ is the NESS of the XX model. Assuming orthonormality of left and right eigenvectors, the expansion terms can be computed order by order [65]:

$$V^m\Delta^n\rho_{m,n} = i\hat{\mathcal{L}}^{+}_{\mathrm{XX}}\big([H_{\mathrm{NNN}}, \rho^{(m-1,n)}] + \big[H^{J=0}_{\mathrm{XXZ}}, \rho^{(m,n-1)}\big]\big), \tag{D2}$$

where we introduced the Moore-Penrose pseudoinverse of the superoperator $\hat{\mathcal{L}}_{\mathrm{XX}}(\circ)$, $\hat{\mathcal{L}}^{+}_{\mathrm{XX}}(\circ) = \sum_{\mu>0}\lambda_\mu^{-1}\rho_\mu\mathrm{Tr}(\tilde{\rho}_\mu\circ)$. The above perturbation scheme ensures that at any truncation order, the density matrix remains Hermitian, positive-semidefinite, and with trace equal to 1 [89]. Equation (D2) leads to the same results of the variational approach in Ref. [71].

We analytically compute corrections to the bulk's spin current up to second order in perturbation theory. All the results are valid only in the linear response regime, $|\delta\mu| \ll 1$, and we discard higher-order corrections $O(\mu^2)$. Assuming $\gamma = J = 1$ in Eq. (4), we obtain

$$\begin{aligned}\mathcal{J}^s &= \sum_{m,n=0}^{\infty} V^m\Delta^n\mathrm{Tr}(\hat{\mathcal{J}}_s\rho^{(m,n)}) \\ &\approx [1 - V^2 f_{V^2}(L) - \Delta^2 f_{\Delta^2}(L) + V\Delta f_{V\Delta}(L)]\delta\mu. \end{aligned}\tag{D3}$$

The system size dependence of the functions $f_{V^2,\Delta^2,V\Delta}$ is shown in Fig. 8. Beyond $L \sim 5$, the scaling for all f_i is linear in L and the fitting functions $f_i = a_i L + b_i$ are depicted in corresponding dashed lines and reported in Table I.

Notice the linearity in V of the third term in Eq. (D3), which is responsible for the current enhancement. It is clear from Eq. (D3) that the large-L limit and the small-interaction limit do not commute. For instance, both the integral and nonintegrable corrections to the XX model lead to divergent contributions which do not capture the enforcement of ballistic or diffusive behavior at large system sizes.

We illustrate now the agreement with PT and our tDMRG simulations. In the main text, we compared the PT results against a polynomial fit of the current; see Fig. 6. We argued that Eq. (D3) correctly predicted the current in the limit of $\Delta \to 0$ but some small deviations were observed in the order $O(V^2)$ term. In Fig. 9, we present a complementary analysis of the data which does not rely on fitting polynomials. Figure 9 depicts the correction to the current, $\delta\mathcal{J}^s$, upon turning on interactions, respectively V, Δ, and V, for the left, center, and right plots. The x axis is rescaled according to (D3) and dashed gray lines depict the perturbation theory predictions.

We can observe that for small interactions (Δ and V), the current is indeed well described by Eq. (D3). As noted in the main text, the presence of a single next-nearest-neighbor interaction is characterized by a strong scaling of the current with the variable $V^2 f_{V^2}(L)$; Fig. 9 (left). This is qualitatively different from the nearest-neighbor interactions where the current converges to a value independent of L and a scaling with $\Delta^2 f_{\Delta^2}(L)$ is never possible; see Fig. 9 (center). Nevertheless, we can observe that for small $\Delta \leqslant 0.3$ an approximate scaling with $\Delta^2 f_{\Delta^2}(L)$ might be possible. In that situation, the current would saturate after a length of order $L_\Delta \sim 1/\Delta^2$. For stronger interactions, L_Δ appears to diverge close to $\Delta = 1$ but for $0.8 > \Delta > 0.3$ the current still saturates before $\Delta^2 f_{\Delta^2}(L) \lesssim 10$. Figure 9 (right) shows that, for small Δ, perturbation theory becomes exact and that the derivations seen in Fig. 6 are indeed an artifact of the fitting.

[1] J. M. Deutsch, Phys. Rev. A **43**, 2046 (1991).
[2] M. Srednicki, Phys. Rev. E **50**, 888 (1994).
[3] M. Rigol, V. Dunjko, and M. Olshanii, Nature (London) **452**, 854 (2008).
[4] L. D'Alessio, Y. Kafri, A. Polkovnikov, and M. Rigol, Adv. Phys. **65**, 239 (2016).
[5] T. Kinoshita, T. Wenger, and D. S. Weiss, Nature (London) **440**, 900 (2006).
[6] O. A. Castro-Alvaredo, B. Doyon, and T. Yoshimura, Phys. Rev. X **6**, 041065 (2016).
[7] B. Bertini, M. Collura, J. De Nardis, and M. Fagotti, Phys. Rev. Lett. **117**, 207201 (2016).
[8] M. Rigol, V. Dunjko, V. Yurovsky, and M. Olshanii, Phys. Rev. Lett. **98**, 050405 (2007).
[9] E. Ilievski and J. De Nardis, Phys. Rev. Lett. **119**, 020602 (2017).

[10] M. Ljubotina, M. Žnidarič, and T. Prosen, Phys. Rev. Lett. **122**, 210602 (2019).

[11] S. Gopalakrishnan and R. Vasseur, Phys. Rev. Lett. **122**, 127202 (2019).

[12] T. Prosen, Phys. Rev. Lett. **106**, 217206 (2011).

[13] M. Ljubotina, M. Žnidari, and T. Prosen, Nat. Commun. **8**, 16117 (2017).

[14] B. Bertini, F. Heidrich-Meisner, C. Karrasch, T. Prosen, R. Steinigeweg, and M. Znidaric, arXiv:2003.03334.

[15] E. Ilievski, J. De Nardis, M. Medenjak, and T. Prosen, Phys. Rev. Lett. **121**, 230602 (2018).

[16] J. De Nardis, S. Gopalakrishnan, E. Ilievski, and R. Vasseur, Phys. Rev. Lett. **125**, 070601 (2020).

[17] J. De Nardis, D. Bernard, and B. Doyon, Phys. Rev. Lett. **121**, 160603 (2018).

[18] A. Das, M. Kulkarni, H. Spohn, and A. Dhar, Phys. Rev. E **100**, 042116 (2019).

[19] Y. Tang, W. Kao, K.-Y. Li, S. Seo, K. Mallayya, M. Rigol, S. Gopalakrishnan, and B. L. Lev, Phys. Rev. X **8**, 021030 (2018).

[20] K. Mallayya, M. Rigol, and W. De Roeck, Phys. Rev. X **9**, 021027 (2019).

[21] A. J. Friedman, S. Gopalakrishnan, and R. Vasseur, Phys. Rev. B **101**, 180302(R) (2020).

[22] J. Durnin, M. J. Bhaseen, and B. Doyon, arXiv:2004.11030.

[23] F. Møller, C. Li, I. Mazets, H.-P. Stimming, T. Zhou, Z. Zhu, X. Chen, and J. Schmiedmayer, arXiv:2006.08577.

[24] P. Jung, R. W. Helmes, and A. Rosch, Phys. Rev. Lett. **96**, 067202 (2006).

[25] V. B. Bulchandani, C. Karrasch, and J. E. Moore, Proc. Natl. Acad. Sci. USA **117**, 12713 (2020).

[26] P. G. Silvestrov, Phys. Rev. E **58**, 5629 (1998).

[27] C. Neuenhahn and F. Marquardt, Phys. Rev. E **85**, 060101(R) (2012).

[28] M. Pandey, P. W. Claeys, D. K. Campbell, A. Polkovnikov, and D. Sels, Phys. Rev. X **10**, 041017 (2020).

[29] M. Brenes, E. Mascarenhas, M. Rigol, and J. Goold, Phys. Rev. B **98**, 235128 (2018).

[30] M. Brenes, T. LeBlond, J. Goold, and M. Rigol, Phys. Rev. Lett. **125**, 070605 (2020).

[31] M. Brenes, J. Goold, and M. Rigol, Phys. Rev. B **102**, 075127 (2020).

[32] D. J. Luitz and Y. Bar Lev, Phys. Rev. Lett. **117**, 170404 (2016).

[33] F. H. L. Essler and M. Fagotti, J. Stat. Mech.: Theory Exp. (2016) 064002.

[34] P. Calabrese and J. Cardy, J. Stat. Mech.: Theory Exp. (2016) 064003.

[35] D. Bernard and B. Doyon, J. Stat. Mech.: Theory Exp. (2016) 064005.

[36] A. Biella, M. Collura, D. Rossini, A. De Luca, and L. Mazza, Nat. Commun. **10**, 4820 (2019).

[37] C. W. von Keyserlingk, T. Rakovszky, F. Pollmann, and S. L. Sondhi, Phys. Rev. X **8**, 021013 (2018).

[38] V. Alba and P. Calabrese, Phys. Rev. B **100**, 115150 (2019).

[39] S. Jesenko and M. Žnidarič, Phys. Rev. B **84**, 174438 (2011).

[40] E. Ilievski, J. De Nardis, B. Wouters, J.-S. Caux, F. H. L. Essler, and T. Prosen, Phys. Rev. Lett. **115**, 157201 (2015).

[41] S. Trotzky, Y.-A. Chen, A. Flesch, I. P. McCulloch, U. Schollwöck, J. Eisert, and I. Bloch, Nat. Phys. **8**, 325 (2012).

[42] M. Gring, M. Kuhnert, T. Langen, T. Kitagawa, B. Rauer, M. Schreitl, I. Mazets, D. A. Smith, E. Demler, and J. Schmiedmayer, Science **337**, 1318 (2012).

[43] S. Hofferberth, I. Lesanovsky, B. Fischer, T. Schumm, and J. Schmiedmayer, Nature (London) **449**, 324 (2007).

[44] N. Jepsen, J. Amato-Grill, I. Dimitrova, W. W. Ho, E. Demler, and W. Ketterle, arXiv:2005.09549.

[45] U. Schollwöck, Rev. Mod. Phys. **77**, 259 (2005).

[46] S. R. White, Phys. Rev. Lett. **102**, 190601 (2009).

[47] S. R. White, Phys. Rev. Lett. **69**, 2863 (1992).

[48] D. Perez-Garcia, F. Verstraete, M. M. Wolf, and J. I. Cirac, Quantum Inf. Comput. **7**, 401 (2007).

[49] D. M. Kennes and C. Karrasch, Comput. Phys. Commun. **200**, 37 (2016).

[50] M. Žnidarič, Phys. Rev. B **99**, 035143 (2019).

[51] T. Jin, M. Filippone, and T. Giamarchi, arXiv:2008.11747.

[52] S. Krinner, D. Stadler, D. Husmann, J.-P. Brantut, and T. Esslinger, Nature (London) **517**, 64 (2015).

[53] J.-P. Brantut, C. Grenier, J. Meineke, D. Stadler, S. Krinner, C. Kollath, T. Esslinger, and A. Georges, Science **342**, 713 (2013).

[54] M. Lebrat, P. Grišins, D. Husmann, S. Häusler, L. Corman, T. Giamarchi, J.-P. Brantut, and T. Esslinger, Phys. Rev. X **8**, 011053 (2018).

[55] H. Bethe, Z. Phys. **71**, 205 (1931).

[56] V. Gorini, A. Kossakowski, and E. C. G. Sudarshan, J. Math. Phys. **17**, 821 (1976).

[57] G. Lindblad, Commun. Math. Phys. **48**, 119 (1976).

[58] H. P. Breuer and F. Petruccione, *The Theory of Open Quantum Systems* (Oxford University Press, 2002).

[59] C. Gardiner and P. Zoller, *Quantum Noise: A Handbook of Markovian and Non-Markovian Quantum Stochastic Methods with Applications to Quantum Optics*, Springer Series in Synergetics (Springer, 2000).

[60] T. Prosen and M. Žnidarič, J. Stat. Mech.: Theory Exp. (2009) P02035.

[61] If the boundary spins that are connected to the jump operators were to be isolated from the chain's bulk, their occupation would be $\mu_\alpha \leqslant 1$.

[62] M. Fishman, S. R. White, and E. M. Stoudenmire, arXiv:2007.14822.

[63] T. Prosen, New J. Phys. **10**, 043026 (2008).

[64] C. Guo and D. Poletti, Phys. Rev. A **95**, 052107 (2017).

[65] A. C. Li, F. Petruccione, and J. Koch, Sci. Rep. **4**, 4887 (2014).

[66] M. Žnidarič, J. Stat. Mech.: Theory Exp. (2010) L05002.

[67] M. Žnidarič, J. Phys. A: Math. Theor. **43**, 415004 (2010).

[68] The general expression for different injection rates $\gamma_{L/R} \neq 1$ on the left and on the right of the chain reads $\mathcal{J}^s = \delta\mu \cdot 4\gamma_L\gamma_R/[(1+\gamma_L\gamma_R)(\gamma_L+\gamma_R)]$ [67].

[69] X. Zotos, F. Naef, and P. Prelovsek, Phys. Rev. B **55**, 11029 (1997).

[70] X. Zotos, Phys. Rev. Lett. **82**, 1764 (1999).

[71] M. Žnidarič, Phys. Rev. Lett. **106**, 220601 (2011).

[72] R. J. Sánchez, V. K. Varma, and V. Oganesyan, Phys. Rev. B **98**, 054415 (2018).

[73] The parameter c_2 deviates slightly from PT results in the $\Delta \to 0$. This is an artifact of the fitting procedure as argued in Appendix D.

[74] M. Žnidarič, Phys. Rev. Lett. **125**, 180605 (2020).

[75] V. Eisler, J. Stat. Mech.: Theory Exp. (2011) P06007.
[76] M. Bauer, D. Bernard, and T. Jin, SciPost Phys. **3**, 033 (2017).
[77] D. Bernard, T. Jin, and O. Shpielberg, Europhys. Lett. **121**, 60006 (2018).
[78] M. Žnidarič and M. Horvat, Eur. Phys. J. B **86**, 67 (2013).
[79] J. J. Mendoza-Arenas, M. Žnidarič, V. K. Varma, J. Goold, S. R. Clark, and A. Scardicchio, Phys. Rev. B **99**, 094435 (2019).
[80] N. W. Ashcroft, *Solid State Physics* (Thomson Press, New Delhi, 2003).
[81] C. L. Kane and M. P. A. Fisher, Phys. Rev. Lett. **76**, 3192 (1996).
[82] R. Fazio, F. W. J. Hekking, and D. E. Khmelnitskii, Phys. Rev. Lett. **80**, 5611 (1998).
[83] M. Filippone, F. Hekking, and A. Minguzzi, Phys. Rev. A **93**, 011602(R) (2016).
[84] G. Salerno, H. M. Price, M. Lebrat, S. Häusler, T. Esslinger, L. Corman, J.-P. Brantut, and N. Goldman, Phys. Rev. X **9**, 041001 (2019).
[85] M. Filippone, C.-E. Bardyn, S. Greschner, and T. Giamarchi, Phys. Rev. Lett. **123**, 086803 (2019).
[86] S. Greschner, M. Filippone, and T. Giamarchi, Phys. Rev. Lett. **122**, 083402 (2019).
[87] T. Prosen and I. Pižorn, J. Phys. A: Math. Gen. **39**, 5957 (2006).
[88] A. J. Daley, Manipulation and simulation of cold atoms in optical lattices, Ph.D. thesis, Leopold-Franzens-Universitat Innsbruck, 2005, http://qo.pitt.edu/downloads/daleyphdthesis.pdf.
[89] This is not true in general and comes from the fact that we perturb by adding a Hamiltonian term.

Correction: Equation (2) contained a typographical error and has been fixed.

CHAPTER 4

Conclusions and Perspectives

This thesis reviews my work done over the past years directed at understanding transport in open systems. In particular, the role of interactions in the emergence of diffusion. Among the many possible tools available to tackle these problems, we chose to focus on the steady-state properties of boundary-driven systems. Such steady-states do not encompass a complete picture of out-of-equilibrium phenomena but, as explored in this thesis, they allow us to use a diversity of methods - numerical, analytic, or even empirical - to provide a comprehensive understanding from different angles. These methods are introduced in Chapter 2 with a special focus on Keldysh field theory applied to solving quantum stochastic Hamiltonians. We proved that a generic quadratic QSH supports an exact self-consistent expression for the self-energy. This extends the previously known solution of the dephasing model [34] to any spatially correlated noise. A closed expression for the self-energy allows us to compute any two-point correlation functions, which we explore in Chapter 3 to study the transport properties of QSHs.

The proposed solution allows explicit analytic expressions for the currents in small systems, enabling us to determine the operating limits of various quantum machines, as discussed in Sec. 3.1. This work stands out as one of the few comprehensive descriptions of quantum machines that does not require assumptions of weak coupling to the baths, weak driving, Lindblad reservoirs, or relies on other approximation schemes. Consequently, we are able to study the typically elusive intermediate regimes, signaled by peaks of the current when all energy scales are equivalent, and pinpoint the optimal operating regimes.

Some QSHs behave as quantum stochastic resistors and display emergent dif-

fusive behavior in the thermodynamic limit, which motivated us to develop a new theory of diffusive systems in Sec. 3.2. The $1/N$ expansion formalizes the intuitive idea that systems satisfying Fick's law ought to have a hydrodynamic length scale beyond which the microscopic details do not matter. At this scale, the hydrodynamic theory is governed by a single parameter, the diffusion constant, determined from the microscopic parameters. We relied on the exact solution of QSHs to design a real-space coarse-grain scheme to find the hydrodynamic theory and validate the $1/N$ expansion. We used it to successfully predict the emergence of Fick's law and the correct diffusion constant for different models.

In Sec. 3.3, we propose a semi-classical interpretation of the emergence of diffusion in quantum stochastic resistors. It re-interprets the stochastic noise as a semi-classical process where measurements randomly reset a particle's speed while fixing its position. This simple picture allows us to understand why, at low temperatures and in the diffusive regime, the conductance G is suppressed when the chemical potential is close to the band edges. It is also capable of predicting how the temperature in the baths modifies the conductance but not the diffusion constant.

In the concluding Sec. 3.4, we discuss the manifestation of diffusion arising from an integrability-breaking term in the Hamiltonian. Of particular interest, a new quasi-ballistic transport regime emerges at intermediate length scales. In this regime, the next-to-nearest neighbor interactions renormalize the ballistic current according to the relative sign between the interactions. As a consequence, the current may be increased with respect to the integrable current, which contradicts the intuition that interactions increase the scattering of particles and always decrease the current.

I would now like to analyze some of the possible future research directions spawned from each work and how they fit in the current research field.

Sec. 3.1 The use of measurements as a quantum resource for creating quantum engines/refrigerators is a relatively modern but very exciting idea [111]. A possible research direction would be to introduce unitary interactions, in particular studying the role of 3-body terms in the Hamiltonian and how to use them in our favor [146, 147]. I suggest starting from the measurement-induced cooling setup introduced in Sec. 3.1 and perturbatively adding a density-density interaction. Another possibility follows the research direction of Ref. [148]. The goal is to create a quantum machine that uses a thermal environment and non-reciprocity conditions as a resource to generate a current. The density measurement process already maps to a coupling of a bosonic infinite temperature bath. We would like to study the coupling to a finite-temperature bath. We expect that a high but finite temperature would retain much of the phenomena discussed in Sec. 3.1, but the question arises on how much lower in temperature can the extra bath go until no work can be extracted from it.

Sec. 3.2 In Sec. 3.2, we proposed the $1/N$ expansion to describe diffusive systems and successfully applied it to our class of QSHs. The success largely comes

from the fact that in these models our coarse-grain procedure exactly provides the correct effective action. However, for a generic interacting system, it's not so clear if our coarse grain gives the good action, and even if it does, how can we in practice compute it. Added to the difficulty, unitary interactions do not heat up the system to local infinite temperature state so it is not guaranteed that the effective action will remain diagonal. We would like to test the $1/N$ expansion in interacting systems, in particular, compare its predictions for the next-to-nearest neighbor interacting model of Sec. 3.4. Another important research direction stemming from the work is to better understand the ballistic-to-diffusive transition that occurs in the presence of long-range noise [149]. The first step would be to study how the transition changes with the rate γ, verify its critical exponents, and establish a link with similar transitions in Hamiltonian systems [150, 151]. It is unclear at this point if the transition belongs to some out-of-equilibrium universal class or even if it still exists below some critical γ value.

Sec. 3.3 In Sec. 3.3, we discussed noises that share the same current but correlate sites along the transverse direction differently. The natural question arises if there are other observables that can differentiate between these noises. We initiated a study program to understand the role of these noises in the Hall imbalance of fermionic ladders [152]. The Hall imbalance is the predecessor of Hall resistance for ladder setups and measures how the imbalance of occupancy in the transverse direction changes after applying an infinitesimal magnetic field. We already found promising results but we still need to understand better the topological aspects of the problem.

Sec. 3.4 Lastly, I would like to explore the dressed quasi-particle picture put forward to explain the quasi-ballistic regime in Sec. 3.4. The first step would be to numerically simulate a magnetization quench [53] and study the light cone at small times to find indications of a velocity that changes linearly with the integrability-breaking term. Then, it would be interesting to understand how to include this renormalization of velocity in the framework of quantum generalized hydrodynamics [28]. Part of this work was already developed in Ref. [153, 154].

The work developed during this thesis showcases the importance of studying models that allow for complete analytic tractability. We leverage the exact solution of the self-energy to first understand inelastic effects on transport through a single site and then extend this knowledge to motivate an effective transport description of diffusive systems. The insights and results merit by themselves further investigation from theory and from experiments alike, as discussed above. But most importantly, they provide a stepping stone to tackle two fundamental problems in quantum physics: the quantum impurity problem and the emergence of diffusion from unitary dynamics.

In parallel to the scientific work of this thesis, I have dedicated countless hours to demystifying the quantum world and bringing free educational content to students worldwide. I created, developed, designed, and distributed a new board game |Hop⟩ that explores quantum transport without the complex math found in this thesis, see Ref. [P5]. With the help of educational partners, |Hop⟩ is now used in Europe, the Americas, and Asia as a fun tool to spark students' interest in physics. As scientists, we bear an ethical responsibility to disseminate our knowledge to both professional peers and the broader public.

I hope the success of |Hop⟩ inspires you to disseminate science in your own unique way.

APPENDIX A

Grassmann numbers

Fermionic operators satisfy an anti-commuting algebra, $\{c_i, c_j^\dagger\} = \delta_{ij}$, which is best described in field theory by the use of Grassmann variables. In this notation, we denote two independent Grassmann variables that anti-commute with each other as ψ_i and $\bar{\psi}_i$

$$\{\psi_i, \psi_j\} = \{\bar{\psi}_i, \bar{\psi}_j\} = \{\psi_i, \bar{\psi}_j\} = 0 \,, \tag{A.1}$$

where $\psi_i^2 = 0 = \bar{\psi}_i^2$. An integration measure in the space of Grassmann variables can be constructed by requiring the primitive operator to be linear, which yields

$$\int d\psi = 0 \qquad\qquad \int d\psi\psi = 1 \,. \tag{A.2}$$

It is important to note that the order of the variables is crucial when evaluating integrals of multiple Grassmann numbers. Before using Eq. (A.2), the integration variables must be in the reverse order of those in the integrand. For example,

$$\int d\psi_1 \int d\psi_2 \psi_1 \psi_2 = -\int d\psi_1 \underbrace{\int d\psi_2 \psi_2}_{1} \psi_1 = -\int d\psi_1 \psi_1 = -1 \,. \tag{A.3}$$

Grassmann numbers play a crucial role in defining fermionic coherent states, which are eigenstates of fermionic creation and annihilation operators. These operators can be expressed as follows:

$$c\,|\psi\rangle = \psi\,|\psi\rangle\ , \qquad\qquad \langle\psi|\,c^\dagger = \langle\psi|\,\bar{\psi}\ . \tag{A.4}$$

For ease of reference, we use the barred variable to denote the eigenvalue of $c^\dagger$ but ψ and $\bar{\psi}$ remain independent Grassmann numbers. Employing the empty state $|0\rangle$ and occupied state $|1\rangle$ as basis vectors, the coherent states can be written as $|\psi\rangle = |0\rangle - \psi\,|1\rangle$ and $\langle\psi| = \langle 0| - \langle 1|\,\bar{\psi}$ and the overlap between these states can be expressed as

$$\langle\psi_i\,|\psi_j\rangle = \left(\langle 0| - \langle 1|\,\bar{\psi}_i\right)\left(|0\rangle - \psi_j\,|1\rangle\right) = 1 + \bar{\psi}_i\psi_j = e^{\bar{\psi}_i\psi_j}\ . \tag{A.5}$$

The completeness relation can be derived from this overlap as follows:

$$\mathbb{I} = \int d\bar{\psi}d\psi e^{-\bar{\psi}\psi}\,|\psi\rangle\,\langle\psi|\ . \tag{A.6}$$

Considering the relation

$$\begin{aligned}\mathrm{tr}\left[|\psi_i\rangle\,\langle\psi_j|\,X\right] &= \langle 0\,|\psi_i\rangle\,\langle\psi_j|\,X\,|0\rangle + \langle 1\,|\psi_i\rangle\,\langle\psi_j|\,X\,|1\rangle \\ &= \langle\psi_j|\,X\,|0\rangle - \psi_i\,\langle\psi_j|\,X\,|1\rangle \\ &= \langle\psi_j|\,X\,|0\rangle + \langle\psi_j|\,X\,|1\rangle\,\psi_i \\ &= \langle\psi_j|\,X\,|-\psi_j\rangle\ ,\end{aligned}$$

we can define the Grassmann integral representation of the trace operator:

$$\mathrm{tr}[\circ] = \int d\bar{\psi}d\psi e^{-\bar{\psi}\psi}\,\langle\psi|\circ|-\psi\rangle\ . \tag{A.7}$$

This minus sign is the reason why, in Sec. 2.3.2, the filed variables in the $-$ contour also have a minus sign. By combining this with the coherent state representation of a normal operator X,

$$\langle\psi|\,X[c^\dagger, c]\,|-\psi\rangle = e^{\bar{\psi}\psi}X[\bar{\psi}, -\psi] \tag{A.8}$$

we are set to develop a path integral formalism of fermionic systems.

APPENDIX B

Coupling to thermal baths

In this section, we discuss how a generic Lindblad master equation

$$\partial_t \rho = -i\,[H,\rho] + \gamma \sum_{\{Q\}} \left(Q\rho Q^\dagger + Q^\dagger \rho Q - \frac{1}{2}\left\{ QQ^\dagger + Q^\dagger Q, \rho \right\} \right) , \tag{B.1}$$

with quadratic operators Q and the associated action

$$S_\gamma = i\gamma \sum_{\{Q\}} \int dt (Q_t^{\dagger +} - Q_t^{\dagger -})(Q_t^+ - Q_t^-) \, , \tag{B.2}$$

emerges from the coupling to two thermal bosonic baths. This will justify why the action (B.2) is computed using the time-ordering procedure introduced in Sec. 2.3 where each individual operator Q and $Q^\dagger$ is evaluated at a time t and not their product.

Consider a single bosonic reservoir with the quadratic Hamiltonian $H_b = \sum_k \epsilon_k b_k^\dagger b_k$ and $[b_k, b_{k'}^\dagger] = \delta_{k,k'}$, coupled to the system via $H_c = \sum_k (b_k Q + b_k^\dagger Q^\dagger)$. The Keldysh action is obtained in a similar fashion to the fermionic counterpart but the standard rotation of the bosonic fields now introduces the classical, ϕ^c, and quantum, ϕ^q, components

$$\phi^c = \frac{\phi^+ + \phi^-}{\sqrt{2}} \qquad\qquad \phi^q = \frac{\phi^+ - \phi^-}{\sqrt{2}} \, , \tag{B.3}$$

whose conjugate fields rotate in the same way. The action of the bath and coupling reads

$$\begin{aligned} S_{\text{bath}} = &\sum_k \int dt dt' \begin{pmatrix} \bar{\phi}_k^c & \bar{\phi}_k^q \end{pmatrix}_t \begin{pmatrix} g^K_{b,kk} & g^R_{b,kk} \\ g^A_{b,kk} & 0 \end{pmatrix}^{-1} (t-t') \begin{pmatrix} \phi_k^c \\ \phi_k^q \end{pmatrix}_{t'} \\ &- \frac{1}{\sqrt{2}} \int dt \begin{pmatrix} \bar{\phi}_k^c & \bar{\phi}_k^q \end{pmatrix}_t \begin{pmatrix} Q_t^{\dagger +} - Q_t^{\dagger -} \\ Q_t^{\dagger +} + Q_t^{\dagger -} \end{pmatrix} \\ &- \frac{1}{\sqrt{2}} \int dt \begin{pmatrix} Q_t^+ - Q_t^- & Q_t^+ + Q_t^- \end{pmatrix} \begin{pmatrix} \phi_k^c \\ \phi_k^q \end{pmatrix}_t , \end{aligned} \tag{B.4}$$

where Q and $Q^\dagger$ and not the product $Q^\dagger Q$ is evaluated at a given time. $\boldsymbol{g}_b$ is the Green's function of the isolated bath whose components read

$$\begin{aligned} g^R_{b,kk'}(t-t') &= -i\theta(t-t')\delta_{kk'} e^{-i\epsilon_k (t-t')} \\ g^K_{b,kk'}(t-t') &= -i\delta_{kk'} \coth\left(\frac{\epsilon_k - \mu_b}{2T_b}\right) e^{-i\epsilon_k (t-t')} , \end{aligned} \tag{B.5}$$

where μ_b and T_b are the chemical potential and temperature of the bath respectively. The $\coth$ appears instead of the $\tanh$ since bosons follow the Bose-Einstein statistics. The integration of the bath's degrees of freedom can be done with the help of the Gaussian integral and yields

$$S_b = \frac{1}{2} \int dt dt' \begin{pmatrix} Q_t^+ - Q_t^- & Q_t^+ + Q_t^- \end{pmatrix} \sum_k \begin{pmatrix} g^K_{b,kk} & g^R_{b,kk} \\ g^A_{b,kk} & 0 \end{pmatrix} (t-t') \begin{pmatrix} Q_{t'}^{\dagger +} - Q_{t'}^{\dagger -} \\ Q_{t'}^{\dagger +} + Q_{t'}^{\dagger -} \end{pmatrix} . \tag{B.6}$$

The action (B.6) does not reduce to the Lindblad action (B.2) in any limit due to the retarded and advanced components. To recover Eq. (B.1) is it necessary to couple the system to a second bath with the exact same structure $H'_b = \sum_k \epsilon_k b'^\dagger_k b'_k$ via the conjugate coupling operator $H'_c = \sum_k (b'_k Q^\dagger + b'^\dagger_k Q)$. The total action is thus the sum of the two baths

$$\begin{aligned} S_{b+b'} = \frac{1}{2} \sum_k \int dt dt' &(Q_t^+ - Q_t^-) g^K_{b,kk}(t-t') (Q_{t'}^{\dagger +} - Q_{t'}^{\dagger -}) \\ &+ (Q_t^{\dagger +} - Q_t^{\dagger -}) g^K_{b,kk}(t-t') (Q_{t'}^+ - Q_{t'}^-) \\ &+ (Q_t^+ - Q_t^-)(g^R_{b,kk}(t-t') + g^A_{b,kk}(t'-t))(Q_{t'}^{\dagger +} + Q_{t'}^{\dagger -}) \\ &+ (Q_t^{\dagger +} - Q_t^{\dagger -})(g^R_{b,kk}(t-t') + g^A_{b,kk}(t'-t))(Q_{t'}^+ + Q_{t'}^-) \end{aligned} \tag{B.7}$$

where we swapped the dummy time variables in the advanced components. The last two terms are proportional to

$$\sum_k g^R_{b,kk}(t-t') + g^A_{b,kk}(t'-t) = -i\theta(t-t')\int d\omega\nu(\omega)(e^{-i\omega(t-t')} - e^{i\omega(t-t')}) \tag{B.8}$$

and so they vanish when we take the limit of constant density of states $\nu(\omega) \to \nu$. The Keldysh term however remains constant in the same limit

$$\sum_k g^K_{b,kk}(t-t') = -i\nu\int d\omega \coth\left(\frac{\omega-\mu_b}{2T_b}\right) e^{-i\omega(t-t')} , \tag{B.9}$$

and taking the limit where both μ_b and T_b diverge with a fixed ratio, $\mu_b/T_b = c^{st}$, we can neglect the frequency dependence in the coth to obtain $\sum_k g^K_{b,kk}(t-t') = 2\pi i\nu \coth\left(\frac{\mu_b}{2T_b}\right)\delta(t-t')$, which is exactly the Markovian limit. If we identify

$$\gamma = 2\pi\nu \coth\left(\frac{\mu_b}{2T_b}\right) , \tag{B.10}$$

the final action reads

$$S_{b+b'} = -i\frac{\gamma}{2}\sum_k \int dt(Q^-_t - Q^+_t)(Q^{\dagger+}_t - Q^{\dagger-}_t) + (Q^{\dagger-}_t - Q^{\dagger+}_t)(Q^+_t - Q^-_t) , \tag{B.11}$$

which is exactly the action associated with two jump operators, $L = Q$ and $L = Q^\dagger$, when we follow the prescription discussed in Sec. 2.3. Notice we did not have to explicitly take the Born and Markov approximations to obtain the Lindblad dynamics, a constant density of states of infinite reservoirs suffices.

APPENDIX C

Continuous measurement processes

We would now like to discuss the link between continuous measurement processes and the QSHs presented in Sec. 2.4. Consider we perform a positive-operator-valued measurement (POVM) on the system of interest as now detailed. In particular, we consider the class of POVMs characterized by its set of Kraus operators L_α, which are positive semi-definite matrices that satisfy the closure relation $\sum_\alpha L_\alpha^\dagger L_\alpha = \mathbb{I}$ in the Hilbert space [155]. Upon carrying out POVM, a given state ρ is updated with probability $p_\alpha = \text{tr}\left(L_\alpha^\dagger L_\alpha \rho\right)$ to the new state $\rho_\alpha = \frac{1}{p_\alpha} L_\alpha \rho L_\alpha^\dagger$.

As a result, the final density matrix describing all possible measurement outcomes is given by

$$\rho' = \mathcal{E}(\rho) = \sum_\alpha p_\alpha \rho_\alpha = \sum_\alpha L_\alpha \rho L_\alpha^\dagger \,, \tag{C.1}$$

where $\mathcal{E}$ is a linear, trace-preserving, and completely positive map. It is worth noting that by averaging over all possible measurement outcomes, we effectively discard all information acquired during the measurement process, while still modifying the system's dynamics.

To investigate the effect of multiple consecutive measurements at a given rate γ, we assume each measurement to be independent and instantaneous. The number of measurement events in a given time interval t follows a Poisson distribution $p_\gamma = \gamma t e^{-\gamma t}$. In between each pair of measurements, the system evolves according to the unitary operator

$$\rho(t) = \mathcal{U}(t,s)\rho(s) = e^{-iH(t-s)}\rho(s)e^{iH(t-s)} \,, \tag{C.2}$$

such that the full evolution is given by the time-ordered integral

$$\begin{aligned}\rho(t) &= \sum_{n=0}^{\infty} e^{-\gamma t}\gamma^n \int_0^t dt_n ... \int_0^{t_2} dt_1 \mathcal{U}(t,t_n)\mathcal{E}\mathcal{U}(t_n,t_{n-1})...\mathcal{E}\mathcal{U}(t_1,t_0)\rho(0) \\ &= \mathcal{M}(t,0)\rho(0) \\ &= e^{-\gamma t}\left(\mathcal{U}(t,0) + \gamma\int_0^t dt'\mathcal{U}(t,t')\mathcal{E}\mathcal{M}(t',0)\right)\rho(0)\ , \end{aligned} \tag{C.3}$$

where $t > t_n > ... > t_0 = 0$. To obtain the final Lindblad form it is enough to take the derivative with respect to t to show that

$$\begin{aligned}\partial_t\rho(t) &= -i[H,\rho(t)] - \gamma\rho(t) + \gamma\mathcal{U}(t,t)\mathcal{E}\mathcal{M}(t,t_0)\rho(t_0) \\ &= -i[H,\rho(t)] - \gamma\rho(t) + \gamma\mathcal{E}\rho(t) \\ &= -i[H,\rho(t)] + \gamma\sum_\alpha\left(L_\alpha\rho(t)L_\alpha^\dagger - \frac{1}{2}\left\{L_\alpha^\dagger L_\alpha,\rho(t)\right\}\right)\ . \end{aligned} \tag{C.4}$$

which is a specific case of Eq. (2.2), where the rate γ is the same for all the jump operators. This proof establishes continuous measurement processes as a possible unraveling of the Lindblad equation, a link we explore in Sec. 3.1 and Sec. 3.3. The evolution under continuous measurement is not only non-unitary but encodes non-gaussian correlations, making the QSH the preferred unraveling.

APPENDIX D

Numerical considerations of QSHs

In Sec. 3.2, we discuss extensive systems where analytically solving Eq. (2.76) is beyond reach and must be done numerically. While a numerical solution only requires the evaluation of a polynomial number of integrals, they can suffer from numerical instabilities. In this section, we discuss some of the numerical techniques employed to find a solution to Eq. (2.76) when reservoirs are taken in the wide-band limit, i.e. $\Sigma^R(\omega) = \Sigma^R$.

The main objects of interest are the Green's functions. It is advantageous to work on the eigenbasis of the retarded/advanced Green's function. Diagonalizing $\mathcal{G}_R$ resorts to finding the left and right eigenvalues of $M = H - \Sigma^R$, respectively $|l_\lambda\rangle$ and $\langle r_\lambda|$. In the eigenbasis, one has

$$\mathcal{G}^R(\omega) = (\omega\mathbb{I} - M)^{-1} = \sum_\lambda \frac{|l_\lambda\rangle \langle r_\lambda|}{\omega - \lambda} = [\mathcal{G}^A(\omega)]^\dagger \,, \tag{D.1}$$

where λ are the eigenvalues and always $\mathrm{Im}\lambda < 0$. Recall that we assume the wide-band limit where Σ^R does not depend on frequency. Since $\mathcal{G}^R$ is not a Hermitian matrix, its left and right eigenvectors are distinct but must remain orthonormal at all times, $\langle r_\lambda \, | l_{\lambda'} \rangle = \delta_{\lambda'\lambda}$. The matrix of left L and right R eigenvectors satisfy the normal eigenequations $LM = \Lambda L$ and $MR = R\Lambda$ with Λ the diagonal matrix of eigenvalues. These can be computed with standard linalg libraries [1] but the resulting vectors are not orthonormal $LR = C \neq \mathbb{I}$. To orthonormalize them we can do the

[1] Most linalg libraries order the eigenvalues by norm or the real/imaginary part which might be shared by different eigenvalues. We recommend using a non-linear ordering function, e.g. $\tanh(\tanh(\mathrm{Re}\lambda) + \tanh(\pi\mathrm{Im}\lambda))$.

rotation $L' = (PC_L)^{-1}L$ and $R' = RC_U^{-1}$ where $C = PC_LC_U$ is the lower-upper decomposition with partial pivoting P of the matrix C. In the rotated basis, the eigenvectors are now orthonormal $L'R' = \mathbb{I}$.

Having found the eigenvectors, we must perform the resulting energy integrals in the eigenbasis. All the integrals in Eq. (2.76) and (2.77) take the generic form

$$\int d\omega f^{\zeta}(\omega)\mathrm{tr}[\mathcal{G}^R(\omega)B\mathcal{G}^A(\omega)] = \sum_{\lambda,\lambda'} \langle r_\lambda | B | r^*_{\lambda'}\rangle \langle l^*_\lambda | l_\lambda\rangle \int d\omega \frac{f^{\zeta}(\omega)}{(\omega-\lambda)(\omega-\lambda'^*)} , \tag{D.2}$$

with B a generic matrix, $\zeta = \{0,1\}$ and f the Fermi function. The integral with $\zeta = 1$ can be computed using the following derivation

$$\begin{aligned}\int \frac{d\omega}{2\pi}\frac{\tanh(\frac{\omega-\mu}{T})}{(\omega-\lambda)(\omega-\lambda'^*)} &= \frac{8}{T}\sum_{k=1}^{\infty}\int \frac{d\omega}{2\pi}\frac{\omega}{(1-2k)^2\pi^2+4\omega^2}\frac{1}{(\omega-\frac{\lambda-\mu}{T})^2(\omega-\frac{\lambda'^*-\mu}{T})^2} \\ &= \frac{8i}{T}\sum_{k=1}^{\infty}\sum_{\text{top}}\mathrm{Res}\frac{\omega}{(\omega-i\frac{\pi}{2}|1-2k|)(\omega+i\frac{\pi}{2}|1-2k|)}\frac{1}{(\omega-\frac{\lambda-\mu}{T})^2(\omega-\frac{\lambda'^*-\mu}{T})^2} \\ &= \frac{i}{(\lambda'^*-\lambda)\pi^2}\left(\psi^{(1)}\left(\frac{1}{2}+\frac{i}{\pi}\frac{\lambda-\mu}{T}\right)+\psi^{(1)}\left(\frac{1}{2}-\frac{i}{\pi}\frac{\lambda'^*-\mu}{T}\right)\right) ,\end{aligned} \tag{D.3}$$

where the sum $\sum_{\text{top}}$ is performed over the poles in the upper half of the complex plane and $\psi^{(1)}$ is the trigamma function.

Personal works

[P1] J. S. Ferreira, T. Jin, J. Mannhart, T. Giamarchi, and M. Filippone. Exact description of transport and non-reciprocity in monitored quantum devices. *arXiv*, 2306.16452, 2023.

[P2] T. Jin, J. S. Ferreira, M. Filippone, and T. Giamarchi. Exact description of quantum stochastic models as quantum resistors. *Physical Review Research*, 4:013109, February 2022.

[P3] T. Jin, J. S. Ferreira, M. Bauer, M. Filippone, and T. Giamarchi. Semiclassical theory of quantum stochastic resistors. *Physical Review Research*, 5:013033, January 2023.

[P4] J. S. Ferreira and M. Filippone. Ballistic-to-diffusive transition in spin chains with broken integrability. *Physical Review B*, 102(18), November 2020.

[P5] J. S. Ferreira. $|\text{Hop}\rangle\langle\text{Quantum Game}|$: Exploring quantum and statistical physics through game mechanics. *arXiv*, 2401.xxxx, 2024.

Bibliography

[1] E. Shuryak. Strongly coupled quark-gluon plasma in heavy ion collisions. *Reviews of Modern Physics*, 89(3):5001, July 2017.

[2] L. Tesfatsion and K. L. Judd. Handbook of computational economics: agent-based computational economics. *Elsevier*, May 2006.

[3] J. Berges. Introduction to Nonequilibrium Quantum Field Theory. *AIP Conference Proceedings*, 739(1), December 2004.

[4] T. Markkanen, A. Rajantie, and S. Stopyra. Cosmological Aspects of Higgs Vacuum Metastability. *Frontiers in Astronomy and Space Sciences*, 5, December 2018.

[5] G. Grosso and G. P. Parravicini. Solid state physics. *Academic press*, August 1988.

[6] L. Talirz *et al.* Materials Cloud a platform for open computational science. *Scientific data*, 7(1):299, September 2020.

[7] C. Berthod. Spectroscopic Probes of Quantum Matter. *IOP Publishing*, November 2018.

[8] A. L. Cavalieri *et al.* Attosecond spectroscopy in condensed matter. *Nature*, 449(7165):1029–1032, October 2007.

[9] P. Vasa *et al.* Ultra-fast nano-optics. *Laser and Photonics Review*, 3(6):483–507, November 2009.

[10] A. Horn. Ultra-fast material metrology. *John Wiley & Sons*, July 2009.

[11] J. T. Barreiro *et al.* An open-system quantum simulator with trapped ions. *Nature*, 470(7335):486–491, February 2011.

[12] T. Langen, R. Geiger, and J. Schmiedmayer. Ultracold Atoms Out of Equilibrium. *Annual Review of Condensed Matter Physics*, 6(1):201–217, March 2015.

[13] C. Gross and I. Bloch. Quantum simulations with ultracold atoms in optical lattices. *Science*, 357(6355):995–1001, September 2017.

[14] I. Bloch, J. Dalibard, and W. Zwerger. Many-body physics with ultracold gases. *Reviews of Modern Physics*, 80(3):885–964, July 2008.

[15] J. Eisert, M. Friesdorf, and C. Gogolin. Quantum many-body systems out of equilibrium. *Nature Physics*, 11(2):124–130, February 2015.

[16] A. Kyprianidis *et al.* Observation of a prethermal discrete time crystal. *Science*, 372(6547):1192–1196, June 2021.

[17] S. Gopalakrishnan and R. Vasseur. Anomalous transport from hot quasiparticles in interacting spin chains. *Reports on Progress in Physics*, 86(3):036502, February 2023.

[18] D. A. Abanin and Z. Papić. Recent progress in many-body localization. *Annalen der Physik*, 529(7):1700169, July 2017.

[19] H. Spohn. Large Scale Dynamics of Interacting Particles. *Springer*, December 1991.

[20] L. D'Alessio, Y. Kafri, A. Polkovnikov, and M. Rigol. From quantum chaos and eigenstate thermalization to statistical mechanics and thermodynamics . *Advances in Physics*, 65(3):239–362, May 2016.

[21] A. Fick. On liquid diffusion. *The London, Edinburgh, and Dublin Philosophical Magazine and Journal of Science*, 10(63):30–39, July 1855.

[22] A. Fick. Ueber Diffusion. *Annalen der Physik und Chemie*, 170(1):59–86, July 1855.

[23] D. E. Steinmeyer and M. Chesterfield. Transport Phenomena, Revised 2nd Edition. *John Wiley & Sons*, 2008.

[24] B. Bertini *et al.* Finite-temperature transport in one-dimensional quantum lattice models. *Reviews of Modern Physics*, 93(2):025003, May 2021.

[25] I. Rotter and J. P. Bird. A review of progress in the physics of open quantum systems: theory and experiment. *Reports on Progress in Physics*, 78(11):4001, October 2015.

[26] G. T. Landi, D. Poletti, and G. Schaller. Nonequilibrium boundary-driven quantum systems: Models methods and properties. *Reviews of Modern Physics*, 94(4):5006, December 2022.

[27] R. Kubo. Statistical-Mechanical Theory of Irreversible Processes. I. General Theory and Simple Applications to Magnetic and Conduction Problems. *Journal of the Physical Society of Japan*, 12(6):570–586, June 1957.

[28] P. Ruggiero *et al.* Quantum Generalized Hydrodynamics. *Physical Review Letters*, 124(14):0603, April 2020.

[29] D. Bernard and T. Jin. Open Quantum Symmetric Simple Exclusion Process. *Physical Review Letters*, 123(8):0601, August 2019.

[30] M. Esposito and P. Gaspard. Exactly Solvable Model of Quantum Diffusion. *Journal of Statistical Physics*, 121(3-4):463–496, November 2005.

[31] M. Žnidarič. Exact solution for a diffusive nonequilibrium steady state of an open quantum chain. *Journal of Statistical Mechanics: Theory and Experiment*, (05):002, May 2010.

[32] M. V. Medvedyeva, F. H. L. Essler, and T. Prosen. Exact Bethe Ansatz Spectrum of a Tight-Binding Chain with Dephasing Noise. *Physical Review Letters*, 117:137202, September 2016.

[33] Y. Sung *et al.* Non-Gaussian noise spectroscopy with a superconducting qubit sensor. *Nature Communications*, 10(1):3715, September 2019.

[34] P. E. Dolgirev *et al.* Non-Gaussian correlations imprinted by local dephasing in fermionic wires. *Physical Review B*, 102(10):0301, September 2020.

[35] I. de Vega and D. Alonso. Dynamics of non-Markovian open quantum systems. *Reviews of Modern Physics*, 89(1):5001, January 2017.

[36] G. Lindblad. On the generators of quantum dynamical semigroups. *Communications in Mathematical Physics*, 48:119–130, June 1976.

[37] V. Gorini. Completely positive dynamical semigroups of N-level systems. *Journal of Mathematical Physics*, 17(5):821, May 1976.

[38] H.-P. Breuer and F. Petruccione. The Theory of Open Quantum Systems. *Oxford University Press*, January 2007.

[39] Y. Imry. Introduction to mesoscopic physics. *Oxford university press*, June 2002.

[40] S. Krinner, T. Esslinger, and J.-P. Brantut. Two-terminal transport measurements with cold atoms. *Journal of Physics: Condensed Matter*, 29(34):3003, July 2017.

[41] P. Drude. Zur Elektronentheorie der Metalle. *Annalen der Physik*, 306(3):566–613, 1900.

[42] P. Drude. Zur Elektronentheorie der Metalle II. Teil. Galvanomagnetische und thermomagnetische Effecte. *Annalen der Physik*, 308(11):369–402, 1900.

[43] G. Ódor. Universality classes in nonequilibrium lattice systems. *Reviews of Modern Physics*, 76(3):663–724, August 2004.

[44] T. Prosen and M. Žnidarič. Matrix product simulations of non-equilibrium steady states of quantum spin chains. *Journal of Statistical Mechanics: Theory and Experiment*, 2009(02):2035, February 2009.

[45] P. W. Anderson. Absence of Diffusion in Certain Random Lattices. *Physical Review*, 109(5):1492–1505, March 1958.

[46] R. Steinigeweg, J. Gemmer, and W. Brenig. Spin-Current Autocorrelations from Single Pure-State Propagation. *Physical Review Letters*, 112(12):0601, March 2014.

[47] J. Ziman. Electrons and Phonons. *Oxford University Press*, February 2001.

[48] M. Žnidarič. Nonequilibrium steady-state Kubo formula: Equality of transport coefficients. *Physical Review B*, 99(3):5143, January 2019.

[49] T. Heitmann *et al.* The spin-1/2 XXZ chain coupled to two Lindblad baths: Constructing nonequilibrium steady states from equilibrium correlation functions. *arXiv*, 2303.00430, March 2023.

[50] W. Götze and P. Wölfle. Homogeneous Dynamical Conductivity of Simple Metals. *Physical Review B*, 6(4):1226–1238, August 1972.

[51] T. Giamarchi. Umklapp process and resistivity in one-dimensional fermion systems. *Physical Review B*, 44(7):2905–2913, August 1991.

[52] G. Mahan. Quantum transport equation for electric and magnetic fields. *Physics Reports*, 145(5):251–318, January 1987.

[53] A. Biella *et al.* Ballistic transport and boundary resistances in inhomogeneous quantum spin chains. *Nature Communications*, 10(1):4820, October 2019.

[54] J. Thoenniss *et al.* Efficient method for quantum impurity problems out of equilibrium. *Physical Review B*, 107(20):1115, May 2023.

[55] A. McDonald and A. A. Clerk. Third quantization of open quantum systems: new dissipative symmetries and connections to phase-space and Keldysh field theory formulations. *arXiv*, 2302.14047, February 2023.

[56] J. Schwinger. On the Greens functions of quantized fields. I. *Proceedings of the National Academy of Sciences*, 37(7):452–455, July 1951.

[57] O. Konstantinov and V. Perel. A graphical technique for computation of kinetic quantities. *Zhurnal Eksperimentalnoi i Teoreticheskoi Fiziki*, 39, July 1960.

[58] L. P. Kadanoff. Quantum statistical mechanics. *CRC Press*, 1989.

[59] L. Keldysh. Diagram technique for nonequilibrium processes. *Zhurnal Eksperimentalnoi i Teoreticheskoi Fiziki*, 47:1515, October 1964.

[60] A. Kamenev. Field Theory of Non-Equilibrium Systems. *Cambridge University Press*, September 2011.

[61] L. M. Sieberer, M. Buchhold, and S. Diehl. Keldysh field theory for driven open quantum systems. *Reports on Progress in Physics*, 79(9):6001, August 2016.

[62] F. Thompson and A. Kamenev. Field theory of many-body Lindbladian dynamics. *Annals of Physics*, 455:169385, August 2023.

[63] H. F. Trotter. On the product of semi-groups of operators. *Proceedings of the American Mathematical Society*, 10(4):545–551, August 1959.

[64] M. Suzuki. Generalized Trotter formula and systematic approximants of exponential operators and inner derivations with applications to many-body problems. *Communications in Mathematical Physics*, 51(2):183–190, June 1976.

[65] A. Larkin and Y. Ovchinnikov. Nonlinear conductivity of superconductors in the mixed state. *Sov. Phys. JETP*, 41(5):960–965, July 1975.

[66] X. Turkeshi and M. Schiró. Diffusion and thermalization in a boundary-driven dephasing model. *Physical Review B*, 104(14):144301, October 2021.

[67] B. Derrida. Non-equilibrium steady states: fluctuations and large deviations of the density and of the current. *Journal of Statistical Mechanics: Theory and Experiment*, 2007(07):023, July 2007.

[68] L. Bertini *et al.* Macroscopic fluctuation theory. *Reviews of Modern Physics*, 87(2):593–636, June 2015.

[69] D. Bernard, T. Jin, and O. Shpielberg. Transport in quantum chains under strong monitoring. *Europhysics Letters*, 121(6):60006, March 2018.

[70] T. Müller, S. Diehl, and M. Buchhold. Measurement-Induced Dark State Phase Transitions in Long-Ranged Fermion Systems. *Physical Review Letters*, 128(1):010605, January 2022.

[71] J. Robertson and F. H. L. Essler. Exact solution of a quantum asymmetric exclusion process with particle creation and annihilation. *Journal of Statistical Mechanics: Theory and Experiment*, 2021(10):103102, October 2021.

[72] S. Datta. Electronic Transport in Mesoscopic Systems. *Cambridge University Press*, September 1995.

[73] T. Jin, M. Filippone, and T. Giamarchi. Generic transport formula for a system driven by Markovian reservoirs. *Physical Review B*, 102(20):5131, November 2020.

[74] M. Büttiker, A. Prêtre, and H. Thomas. Dynamic conductance and the scattering matrix of small conductors. *Physical Review Letters*, 70(26):4114–4117, June 1993.

[75] M. L. Polianski and P. W. Brouwer. Scattering matrix ensemble for time-dependent transport through a chaotic quantum dot. *Journal of Physics A: Mathematical and General*, 36(12):3215–3236, March 2003.

[76] Y. Meir and N. S. Wingreen. Landauer formula for the current through an interacting electron region. *Physical Review Letters*, 68(16):2512–2515, April 1992.

[77] H. M. Pastawski. Classical and quantum transport from generalized Landauer-Büttiker equations. *Physical Review B*, 44(12):6329–6339, September 1991.

[78] R. Landauer. Spatial Variation of Currents and Fields Due to Localized Scatterers in Metallic Conduction. *IBM Journal of Research and Development*, 1(3):223–231, July 1957.

[79] T. Prosen. Open XXZ Spin Chain: Nonequilibrium Steady State and a Strict Bound on Ballistic Transport . *Physical Review Letters*, 106(21):7206, May 2011.

[80] S. R. White. Density matrix formulation for quantum renormalization groups. *Physical Review Letters*, 69(19):2863–2866, November 1992.

[81] U. Schollwöck. The density-matrix renormalization group in the age of matrix product states. *Annals of Physics*, 326(1):96–192, January 2011.

[82] S. R. White and A. E. Feiguin. Real-Time Evolution Using the Density Matrix Renormalization Group. *Physical Review Letters*, 93(7), August 2004.

[83] P. Jordan and E. Wigner. Uber das Paulische Equivalenzverbot. *Zeitschrift fur Physik*, 47(9-10):631–651, September 1928.

[84] R. Orús. A practical introduction to tensor networks: Matrix product states and projected entangled pair states. *Annals of Physics*, 349:117–158, October 2014.

[85] J. Hauschild and F. Pollmann. Efficient numerical simulations with Tensor Networks: Tensor Network Python (TeNPy). *SciPost Physics Lecture Notes*, October 2018.

[86] J. I. Cirac, D. Pérez-García, N. Schuch, and F. Verstraete. Matrix product states and projected entangled pair states: Concepts, symmetries, theorems . *Reviews of Modern Physics*, 93(4), December 2021.

[87] J. Eisert. Entanglement and tensor network states. *arXiv*, 1308.3318, August 2013.

[88] G. Vidal *et al.* Entanglement in quantum critical phenomena. *Physical Review Letters*, 90(22):227902, June 2003.

[89] B. Bauer and C. Nayak. Area laws in a many-body localized state and its implications for topological order . *Journal of Statistical Mechanics: Theory and Experiment*, 2013(09):005, September 2013.

[90] F. Verstraete, J. J. García-Ripoll, and J. I. Cirac. Matrix Product Density Operators: Simulation of Finite-Temperature and Dissipative Systems. *Physical Review Letters*, 93(20), November 2004.

[91] A. J. Daley. *Manipulation and Simulation of Cold Atoms in Optical Lattices*. PhD thesis, Leopold-Franzens-Universitat Innsbruck, July 2005.

[92] T. Prosen and I. Pižorn. Operator space entanglement entropy in a transverse Ising chain. *Physical Review A*, 76(3):2316, September 2007.

[93] D. Wellnitz *et al.* Rise and Fall and Slow Rise Again of Operator Entanglement under Dephasing. *Physical Review Letters*, 129(17):0401, October 2022.

[94] A. J. Daley, C. Kollath, U. Schollwöck, and G. Vidal. Time-dependent density-matrix renormalization-group using adaptive effective Hilbert spaces . *Journal of Statistical Mechanics: Theory and Experiment*, 2004(04):4005, April 2004.

[95] N. Hatano and M. Suzuki. Finding Exponential Product Formulas of Higher Orders. In *Quantum Annealing and Other Optimization Methods*, pages 37–68. Springer Berlin Heidelberg, November 2005.

[96] S. Blanes, F. Casas, and A. Escorihuela-Tomàs. Applying splitting methods with complex coefficients to the numerical integration of unitary problems. *Journal of Computational Dynamics*, 9(2):85, April 2022.

[97] J. S. Ferreira. MPDO ITensor library. *Github*, 2020.

[98] M. Fishman, S. R. White, and E. M. Stoudenmire. The ITensor Software Library for Tensor Network Calculations. *SciPost Physics Codebases*, page 4, August 2022.

[99] P. W. Anderson. Localized Magnetic States in Metals. *Physical Review*, 124(1):41–53, October 1961.

[100] I. Affleck. Quantum Impurity Problems in Condensed Matter Physics. *arXiv*, 0809.3474, September 2009.

[101] Irreversibility and Heat Generation in the Computing Process | IBM Journals & Magazine | IEEE Xplore . *IBM Journal of Research and Development*, 5(3), July 1961.

[102] A. Bérut *et al.* Experimental verification of Landauer's principle linking information and thermodynamics. *Nature*, 483(7388):187–189, March 2012.

[103] R. Kosloff. Quantum Thermodynamics: A Dynamical Viewpoint. *Entropy*, 15(12):2100–2128, may 2013.

[104] J. M. R. Parrondo, J. M. Horowitz, and T. Sagawa. Thermodynamics of information. *Nature Physics*, 11(2):131–139, February 2015.

[105] B. Sothmann, R. Sánchez, and A. N. Jordan. Thermoelectric energy harvesting with quantum dots. *Nanotechnology*, 26(3):032001, December 2014.

[106] C. Elouard *et al.* Extracting work from quantum measurement in Maxwell demon engines. *Physical Review Letters*, 118(26):260603, June 2017.

[107] C. Elouard and A. N. Jordan. Efficient Quantum Measurement Engines. *Physical Review Letters*, 120(26):0601, June 2018.

[108] G. Benenti *et al.* Fundamental aspects of steady-state conversion of heat to work at the nanoscale. *Physics Reports*, 694:1–124, June 2017.

[109] J. Mannhart, H. Boschker, and P. Bredol. Non-unitary quantum electronics: Novel functions from the edge of the quantum world. *Nano Express*, 2(1):014008, March 2021.

[110] P. Bredol *et al.* Decoherence effects break reciprocity in matter transport. *Physical Review B*, 104(11):5413, September 2021.

[111] R. Kosloff and A. Levy. Quantum Heat Engines and Refrigerators: Continuous Devices. *Annual Review of Physical Chemistry*, 65(1):365–393, April 2014.

[112] A. Levy and R. Kosloff. The local approach to quantum transport may violate the second law of thermodynamics. *Europhysics Letters*, 107(2):20004, July 2014.

[113] P. P. Hofer *et al.* Markovian master equations for quantum thermal machines: local versus global approach. *New Journal of Physics*, 19(12):123037, December 2017.

[114] L. P. Kouwenhoven *et al.* Photon-assisted tunneling through a quantum dot. *Physical Review B*, 50(3):2019–2022, July 1994.

[115] R. Wang, C. Wang, J. Lu, and J.-H. Jiang. Inelastic thermoelectric transport and fluctuations in mesoscopic systems. *Advances in Physics: X*, 7(1), June 2022.

[116] L. P. Bettmann, M. J. Kewming, and J. Goold. Thermodynamics of a continuously monitored double-quantum-dot heat engine in the repeated interactions framework . *Physical Review E*, 107(4):4102, April 2023.

[117] Y. Dubi and M. D. Ventra. Colloquium: Heat flow and thermoelectricity in atomic and molecular junctions. *Reviews of Modern Physics*, 83(1):131–155, March 2011.

[118] H. E. D. Scovil and E. O. Schulz-DuBois. Three-Level Masers as Heat Engines. *Physical Review Letters*, 2(6):262–263, March 1959.

[119] L. Buffoni *et al.* Quantum Measurement Cooling. *Physical Review Letters*, 122(7):0603, February 2019.

[120] A. Mari and J. Eisert. Cooling by Heating: Very Hot Thermal Light Can Significantly Cool Quantum Systems. *Physical Review Letters*, 108:120602, March 2012.

[121] B. Cleuren, B. Rutten, and C. Van den Broeck. Cooling by Heating: Refrigeration Powered by Photons. *Physical Review Letters*, 108:120603, March 2012.

[122] J. D. Nardis, D. Bernard, and B. Doyon. Diffusion in generalized hydrodynamics and quasiparticle scattering. *SciPost Physics*, 6(4):049, April 2019.

[123] A. J. Friedman, S. Gopalakrishnan, and R. Vasseur. Diffusive hydrodynamics from integrability breaking. *Physical Review B*, 101(18):0302, May 2020.

[124] M. Bauer, D. Bernard, and T. Jin. Equilibrium fluctuations in maximally noisy extended quantum systems. *SciPost Physics*, 6(4), April 2019.

[125] J. F. Wienand *et al.* Emergence of fluctuating hydrodynamics in chaotic quantum systems. *arXiv*, 2306.11457, 2023.

[126] X. Cao, A. Tilloy, and A. D. Luca. Entanglement in a fermion chain under continuous monitoring. *SciPost Physics*, 7(2), August 2019.

[127] B. Vacchini and K. Hornberger. Quantum linear Boltzmann equation. *Physics Reports*, 478(4-6):71–120, July 2009.

[128] B. Doyon. Lecture notes on Generalised Hydrodynamics. *SciPost Physics Lecture Notes*, August 2020.

[129] J. Dalibard, Y. Castin, and K. Molmer. Wave-function approach to dissipative processes in quantum optics. *Physical Review Letters*, 68:580–583, February 1992.

[130] T. Ozawa and H. M. Price. Topological quantum matter in synthetic dimensions. *Nature Reviews Physics*, 1(5):349–357, April 2019.

[131] G. Salerno *et al.* Quantized Hall Conductance of a Single Atomic Wire: A Proposal Based on Synthetic Dimensions. *Physical Review X*, 9(4):1001, October 2019.

[132] M. Mancini *et al.* Observation of chiral edge states with neutral fermions in synthetic Hall ribbons. *Science*, 349(6255):1510–1513, September 2015.

[133] L. Yuan, Q. Lin, M. Xiao, and S. Fan. Synthetic dimension in photonics. *Optica*, 5(11):1396, October 2018.

[134] T. Ozawa *et al.* Synthetic dimensions in integrated photonics: From optical isolation to four-dimensional quantum Hall physics. *Physical Review A*, 93(4):3827, April 2016.

[135] X. Turkeshi *et al.* Entanglement transitions from stochastic resetting of non-Hermitian quasiparticles. *Physical Review B*, 105(24):1114, June 2022.

[136] Y. Tang *et al.* Thermalization near Integrability in a Dipolar Quantum Newtons Cradle. *Physical Review X*, 8(2):1030, May 2018.

[137] K. Mallayya, M. Rigol, and W. D. Roeck. Prethermalization and Thermalization in Isolated Quantum Systems. *Physical Review X*, 9(2):1027, May 2019.

[138] M. Srednicki. Thermal fluctuations in quantized chaotic systems. *Journal of Physics A: Mathematical and General*, 29(4):L75–l79, February 1996.

[139] L. D'Alessio *et al.* From quantum chaos and eigenstate thermalization to statistical mechanics and thermodynamics. *Advances in Physics*, 65(3):239–362, May 2016.

[140] L. Vidmar and M. Rigol. Generalized Gibbs ensemble in integrable lattice models. *Journal of Statistical Mechanics: Theory and Experiment*, 2016(6):4007, June 2016.

[141] E. Ilievski and J. D. Nardis. Microscopic Origin of Ideal Conductivity in Integrable Quantum Models. *Physical Review Letters*, 119(2):0602, July 2017.

[142] L. Bonnes, F. H. Essler, and A. M. Läuchli. Light-Cone Dynamics After Quantum Quenches in Spin Chains. *Physical Review Letters*, 113(18):7203, October 2014.

[143] M. Žnidarič. Magnetization transport in spin ladders and next-nearest-neighbor chains. *Physical Review B*, 88(20):5135, November 2013.

[144] T. Prosen. Third quantization: a general method to solve master equations for quadratic open Fermi systems. *New Journal of Physics*, 10(4):3026, April 2008.

[145] C. Guo and D. Poletti. Solutions for bosonic and fermionic dissipative quadratic open systems. *Physical Review A*, 95(5), May 2017.

[146] N. Linden, S. Popescu, and P. Skrzypczyk. How Small Can Thermal Machines Be? The Smallest Possible Refrigerator. *Physical Review Letters*, 105(13):0401, September 2010.

[147] A. Levy and R. Kosloff. Quantum Absorption Refrigerator. *Physical Review Letters*, 108(7), February 2012.

[148] P. Bredol. Nonreciprocity of the wave-packet scattering delay in ballistic two-terminal devices. *Physical Review B*, 103(3):5404, January 2021.

[149] F. Carollo, J. P. Garrahan, and I. Lesanovsky. Current fluctuations in boundary-driven quantum spin chains. *Physical Review B*, 98(9):4301, September 2018.

[150] L. S. Levitov. Absence of Localization of Vibrational Modes Due to Dipole-Dipole Interaction. *Europhysics Letters*, 9(1):83–86, May 1989.

[151] M. Saha, A. Purkayastha, and S. K. Maiti. More current with less particles due to power-law hopping. *Journal of Physics: Condensed Matter*, 32(2):5303, October 2019.

[152] S. Greschner, M. Filippone, and T. Giamarchi. Universal Hall Response in Interacting Quantum Systems. *Physical Review Letters*, 122(8):3402, February 2019.

[153] P. Orlov *et al.* Adiabatic eigenstate deformations and weak integrability breaking of Heisenberg chain. *Physical Review B*, 107(18), May 2023.

[154] F. M. Surace and O. Motrunich. Weak integrability breaking perturbations of integrable models. *arXiv*, 2302.12804, February 2023.

[155] J. Preskill. Lecture Notes for Physics 229: Quantum Information and Computation. September 1997.